

**Phytochemical and antibacterial  
studies on the genus *Hypericum*, with  
synthesis of antibacterial  
acylphloroglucinol derivatives**

Thesis presented by  
Ka Po Winnie Shiu  
for the degree of  
Doctor of Philosophy

Centre for Pharmacognosy and Phytotherapy  
The School of Pharmacy  
University of London

2008



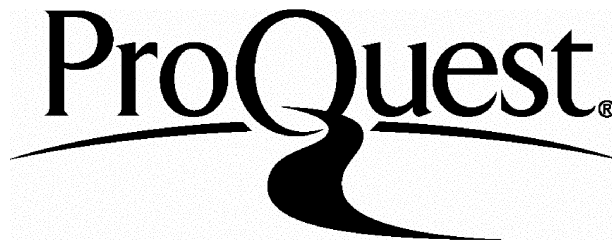
ProQuest Number: 10105103

All rights reserved

INFORMATION TO ALL USERS

The quality of this reproduction is dependent upon the quality of the copy submitted.

In the unlikely event that the author did not send a complete manuscript and there are missing pages, these will be noted. Also, if material had to be removed, a note will indicate the deletion.



ProQuest 10105103

Published by ProQuest LLC(2016). Copyright of the Dissertation is held by the Author.

All rights reserved.

This work is protected against unauthorized copying under Title 17, United States Code.  
Microform Edition © ProQuest LLC.

ProQuest LLC  
789 East Eisenhower Parkway  
P.O. Box 1346  
Ann Arbor, MI 48106-1346

THE SCHOOL OF PHARMACY  
University of London

**Plagiarism statement in thesis**

Thesis title: Phytochemical and antibacterial studies on the genus *Hypericum*  
Candidate: Ka Po Winnie Shiu

This thesis describes research conducted in the School of Pharmacy, University of London between 2004 and 2007 under the supervision of Professor Simon Gibbons. I certify that the research described is original and that any parts of the work that have been conducted by collaboration are clearly indicated. I also certify that I have written all the text herein and have clearly indicated by suitable citation any part of this dissertation that has already appeared in publication.



Signature

18-6-08

Date

## ABSTRACT

This thesis is part of an ongoing project to characterize the antibacterial constituents of the genus *Hypericum* and to investigate their antibacterial activity. Bioassay-guided fractionation using various chromatography techniques was carried out on six plants in this study. Fifteen natural products were isolated. Their structures were characterized by extensive 1- and 2-dimensional NMR experiments. A panel of *Staphylococcus aureus* strains was used in minimum inhibitory concentration (MIC) assays to evaluate the antibacterial properties of the plant extracts and isolated compounds.

2,5-dihydroxy-1-methoxyxanthone was isolated from the dichloromethane (DCM) extract of *H. forrestii*. Fractionation of the DCM extract of *H. moserianum* and *H. revolutum ssp. revolutum* yielded 1,7-dihydroxyxanthone and the new 3-hydroxy-1,4,7-trimethoxydibenzofuran respectively. All three compounds were active against various *S. aureus* strains with MIC values ranging from 128 to 256 µg/ml.

Stigmasterol was isolated from the hexane extract of *H. beanii*. Fractionation of the DCM extract of this plant led to the isolation of 1,7-dihydroxyxanthone and a mixture of two new acylphloroglucinols. (+)-catechin and (-)-shikimic acid were isolated from the methanol extract. The acylphloroglucinol mixture showed MIC values of 16-32 µg/ml. Stigmasterol, (+)-catechin and (-)-shikimic acid were inactive at 512 µg/ml.

Fractionation of the hexane extract of *H. olympicum L. cf. uniflorum* yielded β-sitosterol (inactive at 512 µg/ml) and a new acylphloroglucinol (WS-09; MIC = 0.5 to 1 µg/ml). Fractionation of the DCM extract of this plant yielded four other closely related acylphloroglucinols, with MIC values ranging from 64 to 128 µg/ml.

A new pyranone and lupeol were isolated from the hexane and DCM extracts of *H. choisianum* respectively. Both compounds were inactive at 512 µg/ml.

Due to the excellent activity of WS-09, a four-step synthesis method was designed and patented. Twenty-five compounds were synthesized and the structure-activity relationship of various acylphloroglucinol derivatives was investigated.

## TABLE OF CONTENTS

PLAGIARISM STATEMENT	2
ABSTRACT	3
TABLE OF CONTENTS	4
LIST OF FIGURES	9
LIST OF TABLES	13
LIST OF ABBREVIATIONS	15
ACKNOWLEDGEMENTS	17
CHAPTER ONE	18
1 INTRODUCTION	18
1.1 Aims and objectives	19
1.2 Current treatment for MRSA infections	20
1.3 Problems of antibiotic resistance	22
1.4 Mechanisms of antibiotic action and resistance in <i>Staphylococcus aureus</i>	24
1.4.1 $\beta$ -lactams	25
1.4.2 Aminoglycosides	26
1.4.3 Quinolones	26
1.4.4 Macrolides	27
1.4.5 Tetracyclines	29
1.4.6 Glycopeptides	29
1.5 Plants as a source of drugs	31
1.6 The genus <i>Hypericum</i>	33
1.7 Phytochemistry and antibacterial activity of <i>Hypericum</i> species	36
1.7.1 Acylphloroglucinol derivatives and related compounds	36
1.7.1.1 <i>H. perforatum</i>	37
1.7.1.2 <i>H. japonicum</i>	40
1.7.1.3 <i>H. drummondii</i>	42
1.7.1.4 <i>H. uliginosum</i>	44
1.7.1.5 <i>H. brasiliense</i>	44
1.7.1.6 <i>H. foliosum</i>	45
1.7.1.7 <i>H. sampsonii</i>	46
1.7.1.8 <i>H. sinaicum</i>	49
1.7.1.9 <i>H. revolutum</i>	49
1.7.1.10 <i>H. polyanthemum</i>	50
1.7.2 Xanthones	51
1.7.2.1 Simple oxygenated xanthones	51
1.7.2.2 Prenylated xanthones	52
1.7.2.3 Xanthone glycosides	53
1.7.2.4 Xanthonolignoids	54
1.7.3 Hypericins	55
1.7.4 Flavonoids	56
1.7.5 Tannins	58

CHAPTER TWO	60
2 MATERIALS AND METHODS	60
2.1 Plant material	60
2.2 Extraction	61
2.2.1 Small-scale extraction	61
2.2.2 Large-scale extraction	61
2.3 Chromatographic techniques	62
2.3.1 Vacuum liquid chromatography	64
2.3.2 Thin-layer chromatography	66
2.3.3 Solid-phase extraction	68
2.3.4 Size exclusion chromatography	70
2.3.5 High-performance liquid chromatography	71
2.4 Spectroscopic methods	73
2.4.1 Nuclear magnetic resonance	74
2.4.1.1 Proton ( <sup>1</sup> H) NMR	78
2.4.1.2 Carbon ( <sup>13</sup> C) NMR	79
2.4.1.3 Distortionless enhancement by polarization transfer	80
2.4.1.4 Correlation spectroscopy	82
2.4.1.5 Nuclear Overhauser effect spectroscopy	83
2.4.1.6 Heteronuclear multiple quantum coherence spectroscopy	84
2.4.1.7 Heteronuclear multiple bond coherence spectroscopy	85
2.5 Bioassays	87
2.5.1 Bacterial strains	87
2.5.2 Disk diffusion assay	88
2.5.3 Minimum inhibitory concentration assay	88
2.6 Synthesis	92
2.6.1 Synthesis of <b>WS-09</b>	92
2.6.1.1 Step 1: Conversion of ( <i>S</i> )-2-methylbutanoic acid to ( <i>S</i> )-2-methylbutanoyl chloride	94
2.6.1.2 Step 2: Friedel-Crafts acylation of phloroglucinol	95
2.6.1.3 Step 3: Protection of two hydroxyl groups	95
2.6.1.3.1 Using methoxymethyl chloride (MOM-Cl) as the protecting group	95
2.6.1.3.2 Using <i>tert</i> -butyldimethylsilyl chloride (TBDMS-Cl) as the protecting group	96
2.6.1.4 Step 4: Alkylation and deprotection	96
2.6.1.4.1 MOM-protected phloroglucinol	96
2.6.1.4.2 TBDMS-protected phloroglucinol	97
2.6.2 Synthesis of 2-methylbutanoyl phloroglucinol derivatives	97
2.6.3 Synthesis of acetylphloroglucinol derivatives	98

CHAPTER THREE	100
3 RESULTS AND DISCUSSION	100
3.1 Isolation of natural products	100
3.1.1 <i>H. forrestii</i>	100
3.1.2 <i>H. moserianum</i>	101
3.1.3 <i>H. beanii</i>	102
3.1.4 <i>H. revolutum ssp. revolutum</i>	107
3.1.5 <i>H. olympicum L. cf. uniflorum</i>	109
3.1.6 <i>H. choisianum</i>	111
3.2 Characterization of natural products	115
3.2.1 Characterization of <b>WS-01</b> as 2,5-dihydroxy-1-methoxy-xanthone	115
3.2.2 Characterization of <b>WS-02</b> as 1,7-dihydroxyxanthone (euxanthone)	120
3.2.3 Characterization of <b>WS-03</b> as a mixture of stigmasterol and $\beta$ -sitosterol	124
3.2.4 Characterization of <b>WS-04</b> as a mixture of 2,4-dihydroxy-6-methoxy-3-methyl-1-(2'-methylpropionyl)-benzene ( <b>WS-04a</b> ) and 2,4-dihydroxy-6-methoxy-3-methyl-1-(2'-methylbutanoyl)-benzene ( <b>WS-04b</b> )	126
3.2.5 Characterization of <b>WS-05</b> as (-)-shikimic acid ((-)-(3 <i>R</i> , 4 <i>S</i> , 5 <i>R</i> )-3,4,5-trihydroxy-1-cyclohexenecarboxylic acid)	133
3.2.6 Characterization of <b>WS-06</b> as (+)-3,3',4',5,7-flavanpentol ((+)-catechin)	138
3.2.7 Characterization of <b>WS-07</b> as $\beta$ -sitosterol	143
3.2.8 Characterization of <b>WS-08</b> as 3-hydroxy-1,4,7-trimethoxy-dibenzofuran	145
3.2.9 Acylphloroglucinols isolated from <i>H. olympicum L. cf. uniflorum</i>	150
3.2.9.1 Characterization of <b>WS-09</b> as 4,6-dihydroxy-2- <i>O</i> -(3'',7''-dimethyl-2'',6''-octadienyl)-1-(2'-methylbutanoyl)-benzene	151
3.2.9.2 Characterization of <b>WS-10</b> as 4,6-dihydroxy-2- <i>O</i> -(7''-hydroxy-3'',7''-dimethyl-2'',5''-octadienyl)-1-(2'-methylbutanoyl)-benzene	157
3.2.9.3 Characterization of <b>WS-11</b> as 4,6-dihydroxy-2- <i>O</i> -(6''-hydroxy-3'',7''-dimethyl-2'',7''-octadienyl)-1-(2'-methylbutanoyl)-benzene	163
3.2.9.4 Characterization of <b>WS-12</b> as 4,6-dihydroxy-2- <i>O</i> -(6''-hydroperoxy-3'',7''-dimethyl-2'',7''-octadienyl)-1-(2'-methylbutanoyl)-benzene	169
3.2.9.5 Characterization of <b>WS-13</b> as 4,6-dihydroxy-2- <i>O</i> -(6'',7''-epoxy-3'',7''-dimethyl-oct-2''-enyl)-1-(2'-methylbutanoyl)-benzene	176
3.2.10 Characterization of <b>WS-14</b> as 4-(3- <i>O</i> -3'')-3''-methylbutenyl-6-phenyl-pyran-2-one	183
3.2.11 Characterization of <b>WS-15</b> as lupeol	189

3.3	Purification and characterization of synthetic compounds	192
3.3.1	Reaction product from Step 1: <b>WS-S-01</b>	193
3.3.2	Reaction product from Step 2: <b>WS-S-02</b>	194
3.3.3	Reaction product from Step 3 (MOM): <b>WS-S-03</b>	196
3.3.4	Reaction product from Step 3 (TBDMS): <b>WS-S-04</b>	198
3.3.5	Reaction product from Step 4: <b>WS-S-05</b>	200
3.3.6	2-Methylbutanoyl phloroglucinol derivatives	203
3.3.6.1	Characterization of <b>WS-S-06</b> as ( <i>S</i> )-2- <i>O</i> -prenyl-2'-methylbutanoyl phloroglucinol	205
3.3.6.2	Characterization of <b>WS-S-07</b> as ( <i>S</i> )-2- <i>O</i> -geranyl-2'-methylbutanoyl phloroglucinol	207
3.3.6.3	Characterization of <b>WS-S-08</b> as ( $\pm$ )-2- <i>O</i> -geranyl-2'-methylbutanoyl phloroglucinol	209
3.3.6.4	Characterization of <b>WS-S-09</b> as ( <i>S</i> )-2- <i>O</i> -farnesyl-2'-methylbutanoyl phloroglucinol	211
3.3.6.5	Characterization of <b>WS-S-10</b> as ( <i>S</i> )-2- <i>O</i> -(3''-methylbutyl)-2'-methylbutanoyl phloroglucinol	213
3.3.6.6	Characterization of <b>WS-S-11</b> as ( <i>S</i> )-2- <i>O</i> -(3'',7''-dimethyloctyl)-2'-methylbutanoyl phloroglucinol	215
3.3.7	Acetylphloroglucinol derivatives	217
3.3.7.1	Characterization of <b>WS-S-14</b> and <b>WS-S-15</b> as 2- <i>O</i> -geranyl-acetylphloroglucinol and 4- <i>O</i> -geranyl-acetylphloroglucinol	219
3.3.7.2	Characterization of <b>WS-S-12</b> and <b>WS-S-13</b> as 2- <i>O</i> -prenyl-acetylphloroglucinol and 4- <i>O</i> -prenyl-acetylphloroglucinol	222
3.3.7.3	Characterization of <b>WS-S-16</b> and <b>WS-S-17</b> as 2- <i>O</i> -farnesyl-acetylphloroglucinol and 4- <i>O</i> -farnesyl-acetylphloroglucinol	224
3.3.7.4	Characterization of <b>WS-S-18</b> and <b>WS-S-19</b> as 2- <i>O</i> -(3''-methylbutyl)-acetylphloroglucinol and 4- <i>O</i> -(3''-methyl-butyl)-acetylphloroglucinol	227
3.3.7.5	Characterization of <b>WS-S-20</b> and <b>WS-S-21</b> as 2- <i>O</i> -(3'',7''-dimethyloctyl)-acetylphloroglucinol and 4- <i>O</i> -(3'',7''-dimethyloctyl)-acetylphloroglucinol	229
3.3.7.6	Characterization of <b>WS-S-22</b> and <b>WS-S-23</b> as 2- <i>O</i> -pentyl-acetylphloroglucinol and 4- <i>O</i> -pentyl-acetylphloroglucinol	231
3.3.7.7	Characterization of <b>WS-S-24</b> and <b>WS-S-25</b> as 2- <i>O</i> -decyl-acetylphloroglucinol and 4- <i>O</i> -decyl-acetylphloroglucinol	233
3.4	Physical properties of compounds	235
3.5	Antibacterial activity of natural products	243
3.5.1	Antibacterial activity of extracts	243
3.5.2	Antibacterial activity of the compound isolated from <i>H. forrestii</i>	245

3.5.3	Antibacterial activity of the compound isolated from <i>H. moserianum</i>	245
3.5.4	Antibacterial activity of the compounds isolated from <i>H. beanii</i>	246
3.5.5	Antibacterial activity of the compounds isolated from <i>H. revolutum ssp. revolutum</i>	247
3.5.6	Antibacterial activity of the compounds isolated from <i>H. olympicum L. cf. uniflorum</i>	248
3.5.7	Antibacterial activity of the compounds isolated from <i>H. choisianum</i>	250
3.6	Structure-activity relationship of synthetic derivatives	251
3.6.1	Acylphloroglucinol derivatives synthesized using protecting groups	251
3.6.2	Acylphloroglucinol derivatives synthesized without using a protecting group	253
3.6.2.1	Acetylphloroglucinol derivatives with <i>ortho</i> -substituent	254
3.6.2.2	Acetylphloroglucinol derivatives with <i>para</i> -substituent	256
CHAPTER FOUR		259
4	CONCLUSION	259
5	REFERENCES	261
6	LIST OF PUBLICATIONS	280
7	LIST OF PRESENTATIONS	281

## LIST OF FIGURES

Fig. 1	Photos of some <i>Hypericum</i> species.	35
Fig. 2	Keto-enol tautomerism in some acylphloroglucinol derivatives.	37
Fig. 3	Xanthone nucleus and numbering scheme.	51
Fig. 4	Soxhlet apparatus.	62
Fig. 5	Terminologies used in describing the NMR spectrum.	76
Fig. 6	Chemical structure of <b>WS-09</b> .	78
Fig. 7	<sup>1</sup> H NMR spectrum of <b>WS-09</b> in chloroform- <i>d</i> recorded at 500 MHz.	79
Fig. 8	<sup>13</sup> C NMR spectrum of <b>WS-09</b> in chloroform- <i>d</i> recorded at 125 MHz.	80
Fig. 9	DEPT 135 spectrum of <b>WS-09</b> in chloroform- <i>d</i> recorded at 125 MHz.	81
Fig. 10	Selected COSY correlations and COSY spectrum of <b>WS-09</b> .	82
Fig. 11	Selected NOESY correlations and NOESY spectrum of <b>WS-09</b> .	84
Fig. 12	HMQC spectrum of <b>WS-09</b> .	85
Fig. 13	Selected HMBC correlations and HMBC spectrum of <b>WS-09</b> .	86
Fig. 14	Schematic diagram showing the determination of MIC of compound X using a 96-microtitre plate.	90
Fig. 15	Reduction reaction of MTT.	91
Fig. 16	Reactions involved in the synthesis of ( <i>S</i> )-2- <i>O</i> -geranyl-2'-methylbutanoyl phloroglucinol ( <b>WS-S-07</b> ) and other 2-methylbutanoyl derivatives.	93
Fig. 17	Isolation of <b>WS-01</b> from <i>H. forrestii</i> DCM extract.	101
Fig. 18	Isolation of <b>WS-02</b> from <i>H. moserianum</i> DCM extract.	102
Fig. 19	<i>H. beanii</i> hexane extract - TLC profile of the extract and VLC fractions.	103
Fig. 20	<i>H. beanii</i> hexane extract - TLC profile of active fraction HB1.	103
Fig. 21	Isolation of <b>WS-02</b> and <b>WS-04</b> from <i>H. beanii</i> DCM extract.	105
Fig. 22	Isolation of <b>WS-05</b> and <b>WS-06</b> from <i>H. beanii</i> methanol extract.	106
Fig. 23	<i>H. revolutum ssp. revolutum</i> DCM extract - TLC profile of Sephadex fractions.	107
Fig. 24	Isolation of <b>WS-07</b> and <b>WS-08</b> from <i>H. revolutum ssp. revolutum</i> DCM	108
Fig. 25	Isolation of <b>WS-03</b> and <b>WS-09</b> from <i>H. olympicum L. cf. uniflorum</i> hexane extract.	109
Fig. 26	<i>H. olympicum L. cf. uniflorum</i> DCM extract - TLC profile of Sephadex fractions and the original extract.	110
Fig. 27	Isolation of <b>WS-09</b> to <b>WS-13</b> from <i>H. olympicum L. cf. uniflorum</i> DCM extract.	111
Fig. 28	<i>H. choisianum</i> hexane extract - TLC profile of VLC fraction 4 and fractions from further RP SPE separations.	112
Fig. 29	Isolation of <b>WS-14</b> from <i>H. choisianum</i> hexane extract.	113
Fig. 30	Isolation of <b>WS-15</b> from <i>H. choisianum</i> DCM extract.	114
Fig. 31	Structure of <b>WS-01</b> .	115
Fig. 32	<sup>1</sup> H NMR spectrum of <b>WS-01</b> in methanol- <i>d</i> <sub>4</sub> recorded at 500 MHz.	115
Fig. 33	HMBC spectrum of <b>WS-01</b> .	116
Fig. 34	HMBC correlations for <b>WS-01</b> .	116
Fig. 35	COSY spectrum of <b>WS-01</b> .	117
Fig. 36	NOESY spectrum of <b>WS-01</b> .	117
Fig. 37	Structure of <b>WS-02</b> .	120
Fig. 38	<sup>1</sup> H NMR spectrum of <b>WS-02</b> in methanol- <i>d</i> <sub>4</sub> recorded at 500 MHz.	120
Fig. 39	HMBC spectrum of <b>WS-02</b> .	121
Fig. 40	HMBC correlations for <b>WS-02</b> .	121

Fig. 41	COSY spectrum of <b>WS-02</b> .	122
Fig. 42	NOESY spectrum of <b>WS-02</b> .	122
Fig. 43	Structures of stigmasterol and $\beta$ -sitosterol.	124
Fig. 44	$^1\text{H}$ NMR spectrum of <b>WS-03</b> and stigmasterol standard in chloroform- <i>d</i> recorded at 500 MHz.	124
Fig. 45	Structures of <b>WS-04a</b> and <b>WS-04b</b> .	126
Fig. 46	$^1\text{H}$ NMR spectrum of <b>WS-04</b> in methanol- <i>d</i> <sub>4</sub> recorded at 500 MHz.	126
Fig. 47	$^{13}\text{C}$ NMR spectrum of <b>WS-04</b> in methanol- <i>d</i> <sub>4</sub> recorded at 125 MHz.	127
Fig. 48	HMBC spectrum of <b>WS-04</b> .	127
Fig. 49	HMBC correlations for <b>WS-04a</b> and <b>WS-04b</b>	128
Fig. 50	NOESY spectrum of <b>WS-04</b> .	129
Fig. 51	COSY spectrum of <b>WS-04</b> .	129
Fig. 52	Structure of <b>WS-05</b> .	133
Fig. 53	$^1\text{H}$ NMR spectrum of <b>WS-05</b> and (-)-shikimic acid standard in methanol- <i>d</i> <sub>4</sub> recorded at 500 MHz.	133
Fig. 54	HMBC spectrum of <b>WS-05</b> .	135
Fig. 55	COSY spectrum of <b>WS-05</b> .	135
Fig. 56	NOESY spectrum of <b>WS-05</b> .	136
Fig. 57	Key NOE correlations for <b>WS-05</b> .	137
Fig. 58	Flavan-3-ol skeleton.	138
Fig. 59	Structure of <b>WS-06</b> .	138
Fig. 60	$^1\text{H}$ NMR spectrum of <b>WS-06</b> in methanol- <i>d</i> <sub>4</sub> recorded at 500 MHz.	139
Fig. 61	HMBC spectrum of <b>WS-06</b> .	140
Fig. 62	Key HMBC correlations for <b>WS-06</b> .	140
Fig. 63	COSY spectrum of <b>WS-06</b> .	141
Fig. 64	NOESY spectrum of <b>WS-06</b> .	141
Fig. 65	Structure of <b>WS-07</b> .	143
Fig. 66	$^1\text{H}$ NMR spectrum of <b>WS-07</b> and $\beta$ -sitosterol standard in chloroform- <i>d</i> recorded at 500 MHz.	143
Fig. 67	Structure of <b>WS-08</b> .	145
Fig. 68	$^1\text{H}$ NMR spectrum of <b>WS-08</b> in chloroform- <i>d</i> recorded at 500 MHz.	145
Fig. 69	HMBC spectrum of <b>WS-08</b> .	146
Fig. 70	NOESY spectrum of <b>WS-08</b> .	146
Fig. 71	HMBC and NOESY correlations for <b>WS-08</b> .	147
Fig. 72	Acylphloroglucinols isolated from <i>H. olympicum</i> L. cf. <i>uniflorum</i> .	150
Fig. 73	Structure of <b>WS-09</b> .	151
Fig. 74	$^1\text{H}$ NMR spectrum of <b>WS-09</b> in chloroform- <i>d</i> recorded at 500 MHz.	151
Fig. 75	HMBC spectrum of <b>WS-09</b> .	152
Fig. 76	COSY spectrum of <b>WS-09</b> .	152
Fig. 77	NOESY spectrum of <b>WS-09</b> .	153
Fig. 78	HMBC correlations for <b>WS-09</b> .	154
Fig. 79	Structure of <b>WS-10</b> .	157
Fig. 80	$^1\text{H}$ NMR spectrum of <b>WS-10</b> in chloroform- <i>d</i> recorded at 500 MHz.	157
Fig. 81	HMBC spectrum of <b>WS-10</b> .	158
Fig. 82	COSY spectrum of <b>WS-10</b> .	158
Fig. 83	NOESY spectrum of <b>WS-10</b> .	159
Fig. 84	HMBC correlations for <b>WS-10</b> .	160
Fig. 85	Structure of <b>WS-11</b> .	163
Fig. 86	$^1\text{H}$ NMR spectrum of <b>WS-11</b> in chloroform- <i>d</i> recorded at 500 MHz.	163

Fig. 87	HMBC spectrum of <b>WS-11</b> .	164
Fig. 88	COSY spectrum of <b>WS-11</b> .	164
Fig. 89	NOESY spectrum of <b>WS-11</b> .	165
Fig. 90	HMBC correlations for <b>WS-11</b> .	166
Fig. 91	Structure of <b>WS-12</b> .	169
Fig. 92	<sup>1</sup> H NMR spectrum of <b>WS-12</b> in chloroform- <i>d</i> recorded at 500 MHz.	169
Fig. 93	HMBC spectrum of <b>WS-12</b> .	170
Fig. 94	COSY spectrum of <b>WS-12</b> .	170
Fig. 95	NOESY spectrum of <b>WS-12</b> .	171
Fig. 96	HMBC correlations for <b>WS-12</b> .	172
Fig. 97	Structure of 3-chloroperoxybenzoic acid.	174
Fig. 98	Structure of <b>WS-13</b> .	176
Fig. 99	<sup>1</sup> H NMR spectrum of <b>WS-13</b> in chloroform- <i>d</i> recorded at 500 MHz.	176
Fig. 100	Expansion of <sup>1</sup> H NMR spectrum of <b>WS-13</b> .	177
Fig. 101	HMBC spectrum of <b>WS-13</b> .	178
Fig. 102	COSY spectrum of <b>WS-13</b> .	179
Fig. 103	NOESY spectrum of <b>WS-13</b> .	179
Fig. 104	HMBC correlations for <b>WS-13</b> .	180
Fig. 105	Structure of <b>WS-14</b> .	183
Fig. 106	<sup>1</sup> H NMR spectrum of <b>WS-14</b> in chloroform- <i>d</i> recorded at 500 MHz.	183
Fig. 107	HMBC spectrum of <b>WS-14</b> .	185
Fig. 108	Key HMBC correlations for <b>WS-14</b> .	185
Fig. 109	COSY spectrum of <b>WS-14</b> .	186
Fig. 110	NOESY spectrum of <b>WS-14</b> .	186
Fig. 111	NOESY correlations for <b>WS-14</b> .	187
Fig. 112	Structure of <b>WS-15</b> .	189
Fig. 113	<sup>1</sup> H NMR spectrum of <b>WS-15</b> in chloroform- <i>d</i> recorded at 500 MHz.	189
Fig. 114	HMBC spectrum of <b>WS-15</b> .	190
Fig. 115	<sup>1</sup> H NMR spectrum of <b>WS-S-01</b> in chloroform- <i>d</i> recorded at 500 MHz.	193
Fig. 116	<sup>1</sup> H NMR spectrum of ( <i>S</i> )-2-methylbutyric acid in chloroform- <i>d</i> recorded at 500 MHz.	193
Fig. 117	Structure of <b>WS-S-01</b> .	194
Fig. 118	Structure of <b>WS-S-02</b> .	195
Fig. 119	<sup>1</sup> H NMR spectrum of <b>WS-S-02</b> in methanol- <i>d</i> <sub>4</sub> recorded at 500 MHz.	195
Fig. 120	Structure of <b>WS-S-03</b> .	197
Fig. 121	<sup>1</sup> H NMR spectrum of <b>WS-S-03</b> in chloroform- <i>d</i> recorded at 500 MHz.	197
Fig. 122	Structure of <b>WS-S-04</b> .	199
Fig. 123	<sup>1</sup> H NMR spectrum of <b>WS-S-04</b> in chloroform- <i>d</i> recorded at 500 MHz.	199
Fig. 124	Structure of <b>WS-S-05</b> .	201
Fig. 125	<sup>1</sup> H NMR spectrum of <b>WS-S-05</b> in chloroform- <i>d</i> recorded at 500 MHz.	202
Fig. 126	Structure of <b>WS-S-06</b> .	205
Fig. 127	<sup>1</sup> H NMR spectrum of <b>WS-S-06</b> in methanol- <i>d</i> <sub>4</sub> recorded at 500 MHz.	205
Fig. 128	Structure of <b>WS-S-07</b> .	207
Fig. 129	<sup>1</sup> H NMR spectrum of <b>WS-S-07</b> in chloroform- <i>d</i> recorded at 500 MHz.	207
Fig. 130	Structure of <b>WS-S-08</b> .	209
Fig. 131	<sup>1</sup> H NMR spectrum of <b>WS-S-08</b> in chloroform- <i>d</i> recorded at 500 MHz.	209
Fig. 132	Structure of <b>WS-S-09</b> .	211
Fig. 133	<sup>1</sup> H NMR spectrum of <b>WS-S-09</b> in chloroform- <i>d</i> recorded at 500 MHz.	211
Fig. 134	Structure of <b>WS-S-10</b> .	213

Fig. 135	<sup>1</sup> H NMR spectrum of <b>WS-S-10</b> in chloroform- <i>d</i> recorded at 500 MHz.	213
Fig. 136	Structure of <b>WS-S-11</b> .	215
Fig. 137	<sup>1</sup> H NMR spectrum of <b>WS-S-11</b> in DMSO- <i>d</i> <sub>6</sub> recorded at 500 MHz.	215
Fig. 138	Structures of <b>WS-S-14</b> and <b>WS-S-15</b> .	219
Fig. 139	<sup>1</sup> H NMR spectrum of <b>WS-S-14</b> in chloroform- <i>d</i> recorded at 500 MHz.	219
Fig. 140	<sup>1</sup> H NMR spectrum of <b>WS-S-15</b> in chloroform- <i>d</i> recorded at 500 MHz.	219
Fig. 141	Plane of symmetry in <i>para</i> - substituted acylphloroglucinol.	221
Fig. 142	Structures of <b>WS-S-12</b> and <b>WS-S-13</b> .	222
Fig. 143	<sup>1</sup> H NMR spectrum of <b>WS-S-12</b> in methanol- <i>d</i> <sub>4</sub> recorded at 400 MHz.	222
Fig. 144	<sup>1</sup> H NMR spectrum of <b>WS-S-13</b> in chloroform- <i>d</i> recorded at 400 MHz.	222
Fig. 145	Structures of <b>WS-S-16</b> and <b>WS-S-17</b> .	224
Fig. 146	<sup>1</sup> H NMR spectrum of <b>WS-S-16</b> in chloroform- <i>d</i> recorded at 400 MHz.	224
Fig. 147	<sup>1</sup> H NMR spectrum of <b>WS-S-17</b> in chloroform- <i>d</i> recorded at 400 MHz.	224
Fig. 148	Structures of <b>WS-S-18</b> and <b>WS-S-19</b> .	227
Fig. 149	<sup>1</sup> H NMR spectrum of <b>WS-S-18</b> in methanol- <i>d</i> <sub>4</sub> recorded at 500 MHz.	227
Fig. 150	<sup>1</sup> H NMR spectrum of <b>WS-S-19</b> in methanol- <i>d</i> <sub>4</sub> recorded at 500 MHz.	227
Fig. 151	Structures of <b>WS-S-20</b> and <b>WS-S-21</b> .	229
Fig. 152	<sup>1</sup> H NMR spectrum of <b>WS-S-20</b> in chloroform- <i>d</i> recorded at 500 MHz.	229
Fig. 153	<sup>1</sup> H NMR spectrum of <b>WS-S-21</b> in chloroform- <i>d</i> recorded at 500 MHz.	229
Fig. 154	Structures of <b>WS-S-22</b> and <b>WS-S-23</b> .	231
Fig. 155	<sup>1</sup> H NMR spectrum of <b>WS-S-22</b> in chloroform- <i>d</i> recorded at 500 MHz.	231
Fig. 156	<sup>1</sup> H NMR spectrum of <b>WS-S-23</b> in chloroform- <i>d</i> recorded at 500 MHz.	231
Fig. 157	Structures of <b>WS-S-24</b> and <b>WS-S-25</b> .	233
Fig. 158	<sup>1</sup> H NMR spectrum of <b>WS-S-24</b> in chloroform- <i>d</i> recorded at 500 MHz.	233
Fig. 159	<sup>1</sup> H NMR spectrum of <b>WS-S-25</b> in chloroform- <i>d</i> recorded at 500 MHz.	233

## LIST OF TABLES

Table 1	Examples of simple xanthenes isolated from <i>Hypericum species</i> .	52
Table 2	Quantity of plant material used in large-scale extraction and their accession numbers.	60
Table 3	Chemical shifts of deuterated solvents used.	77
Table 4	Different types of carbon signals on a DEPT NMR spectrum.	81
Table 5	A summary of the resistance mechanisms and sources of bacterial strains used.	87
Table 6	Chemical structures of synthetic compounds.	94
Table 7	Amount of reagents used in the synthesis (step 4) of 2-methylbutanoyl phloroglucinol derivatives.	98
Table 8	Amount of reagents used in the synthesis of acetylphloroglucinol derivatives.	99
Table 9	<sup>1</sup> H (500 MHz) and <sup>13</sup> C NMR (125 MHz) spectral data and <sup>1</sup> H- <sup>13</sup> C long-range correlations of <b>WS-01</b> recorded in methanol- <i>d</i> <sub>4</sub> .	119
Table 10	<sup>1</sup> H (500 MHz) and <sup>13</sup> C NMR (125 MHz) spectral data and <sup>1</sup> H- <sup>13</sup> C long-range correlations of <b>WS-02</b> recorded in methanol- <i>d</i> <sub>4</sub> .	123
Table 11	<sup>1</sup> H (500 MHz) and <sup>13</sup> C NMR (125 MHz) spectral data of <b>WS-03</b> recorded in chloroform- <i>d</i> .	125
Table 12	<sup>1</sup> H (500 MHz) and <sup>13</sup> C NMR (125 MHz) spectral data and <sup>1</sup> H- <sup>13</sup> C long-range correlations of <b>WS-4a</b> recorded in methanol- <i>d</i> <sub>4</sub> .	131
Table 13	<sup>1</sup> H (500 MHz) and <sup>13</sup> C NMR (125 MHz) spectral data and <sup>1</sup> H- <sup>13</sup> C long-range correlations of <b>WS-04b</b> recorded in methanol- <i>d</i> <sub>4</sub> .	132
Table 14	<sup>1</sup> H (500 MHz) and <sup>13</sup> C NMR (125 MHz) spectral data and <sup>1</sup> H- <sup>13</sup> C long-range correlations of <b>WS-05</b> recorded in methanol- <i>d</i> <sub>4</sub> .	137
Table 15	<sup>1</sup> H (500 MHz) and <sup>13</sup> C NMR (125 MHz) spectral data and <sup>1</sup> H- <sup>13</sup> C long-range correlations of <b>WS-06</b> recorded in methanol- <i>d</i> <sub>4</sub> .	142
Table 16	<sup>13</sup> C NMR (125 MHz) spectral data of <b>WS-07</b> recorded in chloroform- <i>d</i> .	144
Table 17	<sup>1</sup> H (500 MHz) and <sup>13</sup> C NMR (125 MHz) spectral data and <sup>1</sup> H- <sup>13</sup> C long-range correlations of <b>WS-08</b> recorded in chloroform- <i>d</i> .	149
Table 18	<sup>1</sup> H (500 MHz) and <sup>13</sup> C NMR (125 MHz) spectral data and <sup>1</sup> H- <sup>13</sup> C long-range correlations of <b>WS-09</b> recorded in chloroform- <i>d</i> .	156
Table 19	<sup>1</sup> H (500 MHz) and <sup>13</sup> C NMR (125 MHz) spectral data and <sup>1</sup> H- <sup>13</sup> C long-range correlations of <b>WS-10</b> recorded in chloroform- <i>d</i> .	162
Table 20	<sup>1</sup> H (500 MHz) and <sup>13</sup> C NMR (125 MHz) spectral data and <sup>1</sup> H- <sup>13</sup> C long-range correlations of <b>WS-11</b> recorded in chloroform- <i>d</i> .	168
Table 21	<sup>1</sup> H (500 MHz) and <sup>13</sup> C NMR (125 MHz) spectral data and <sup>1</sup> H- <sup>13</sup> C long-range correlations of <b>WS-12</b> recorded in chloroform- <i>d</i> .	175
Table 22	<sup>1</sup> H (500 MHz) and <sup>13</sup> C NMR (125 MHz) spectral data and <sup>1</sup> H- <sup>13</sup> C long-range correlations of <b>WS-13</b> recorded in chloroform- <i>d</i> .	182
Table 23	<sup>1</sup> H (500 MHz) and <sup>13</sup> C NMR (125 MHz) spectral data and <sup>1</sup> H- <sup>13</sup> C long-range correlations of <b>WS-14</b> recorded in chloroform- <i>d</i> .	188
Table 24	<sup>1</sup> H (500 MHz) and <sup>13</sup> C NMR (125 MHz) spectral data of <b>WS-15</b> recorded in chloroform- <i>d</i> .	191
Table 25	Chemical structures of synthetic compounds.	192
Table 26	<sup>1</sup> H (500 MHz) and <sup>13</sup> C NMR (125 MHz) spectral data of <b>WS-S-01</b> recorded in chloroform- <i>d</i> .	194

Table 27	<sup>1</sup> H (500 MHz) and <sup>13</sup> C NMR (125 MHz) spectral data of <b>WS-S-02</b> recorded in methanol- <i>d</i> <sub>4</sub> .	196
Table 28	<sup>1</sup> H (500 MHz) and <sup>13</sup> C NMR (125 MHz) spectral data of <b>WS-S-03</b> recorded in chloroform- <i>d</i> .	198
Table 29	<sup>1</sup> H (500 MHz) and <sup>13</sup> C NMR (125 MHz) spectral data of <b>WS-S-04</b> recorded in chloroform- <i>d</i> .	200
Table 30	<sup>1</sup> H (500 MHz) and <sup>13</sup> C NMR (125 MHz) spectral data of <b>WS-S-05</b> recorded in chloroform- <i>d</i> .	202
Table 31	Yield of 2-methylbutanoyl phloroglucinol derivatives.	204
Table 32	<sup>1</sup> H (500 MHz) and <sup>13</sup> C NMR (125 MHz) spectral data of <b>WS-S-06</b> recorded in methanol- <i>d</i> <sub>4</sub> .	206
Table 33	<sup>1</sup> H (500 MHz) and <sup>13</sup> C NMR (125 MHz) spectral data of <b>WS-S-07</b> recorded in chloroform- <i>d</i> .	208
Table 34	<sup>1</sup> H (500 MHz) and <sup>13</sup> C NMR (125 MHz) spectral data of <b>WS-S-08</b> recorded in chloroform- <i>d</i> .	210
Table 35	<sup>1</sup> H (500 MHz) and <sup>13</sup> C NMR (125 MHz) spectral data of <b>WS-S-09</b> recorded in chloroform- <i>d</i> .	212
Table 36	<sup>1</sup> H (500 MHz) and <sup>13</sup> C NMR (125 MHz) spectral data of <b>WS-S-10</b> recorded in chloroform- <i>d</i> .	214
Table 37	<sup>1</sup> H (500 MHz) and <sup>13</sup> C NMR (125 MHz) spectral data of <b>WS-S-11</b> recorded in DMSO- <i>d</i> <sub>6</sub> .	216
Table 38	Yield of acetylphloroglucinol derivatives.	217
Table 39	<sup>1</sup> H (500 MHz) and <sup>13</sup> C NMR (125 MHz) spectral data of <b>WS-S-14</b> and <b>WS-S-15</b> recorded in chloroform- <i>d</i> .	221
Table 40	<sup>1</sup> H (400 MHz) and <sup>13</sup> C NMR (100 MHz) spectral data of <b>WS-S-12</b> and <b>WS-S-13</b> recorded in methanol- <i>d</i> <sub>4</sub> and chloroform- <i>d</i> .	223
Table 41	<sup>1</sup> H (400 MHz) and <sup>13</sup> C NMR (100 MHz) spectral data of <b>WS-S-16</b> and <b>WS-S-17</b> recorded in chloroform- <i>d</i> .	226
Table 42	<sup>1</sup> H (500 MHz) and <sup>13</sup> C NMR (125 MHz) spectral data of <b>WS-S-18</b> and <b>WS-S-19</b> recorded in methanol- <i>d</i> <sub>4</sub> .	228
Table 43	<sup>1</sup> H (500 MHz) and <sup>13</sup> C NMR (125 MHz) spectral data of <b>WS-S-20</b> and <b>WS-S-21</b> recorded in chloroform- <i>d</i> .	230
Table 44	<sup>1</sup> H (500 MHz) and <sup>13</sup> C NMR (125 MHz) spectral data of <b>WS-S-22</b> and <b>WS-S-23</b> recorded in chloroform- <i>d</i> .	232
Table 45	<sup>1</sup> H (500 MHz) and <sup>13</sup> C NMR (125 MHz) spectral data of <b>WS-S-24</b> and <b>WS-S-25</b> recorded in chloroform- <i>d</i> .	234
Table 46	Antibacterial activity of <i>Hypericum</i> extracts against SA-1199B.	243
Table 47	MICs (μg/ml) of compounds isolated in this study.	244
Table 48	MICs (μg/ml) of <b>WS-09</b> against <i>Mycobacterium</i> strains, <i>P. aeruginosa</i> and <i>S. typhimurium</i> .	249
Table 49	MICs (μg/ml) of 2-methylbutanoyl phloroglucinol derivatives.	251
Table 50	MICs (μg/ml) of acetylphloroglucinol derivatives.	254

## LIST OF ABBREVIATIONS

ATP	Adenosine triphosphate
COSY	Correlation spectroscopy
CW	Continuous wave
DCM	Dichloromethane
DEPT	Distortionless enhancement by polarization transfer
DIPEA	Diisopropylethylamine
DMF	Dimethylformamide
DMSO	Dimethylsulphoxide
DNA	Deoxyribonucleic acid
EMRSA	Epidemic methicillin-resistant <i>Staphylococcus aureus</i>
FAS	Fatty acid synthase
FT	Fourier transformation
HMBC	Heteronuclear multiple bond coherence
HMQC	Heteronuclear multiple quantum coherence
HPLC	High-performance liquid chromatography
HR ESI-MS	High-resolution electrospray ionisation mass spectrometry
IR	Infra-red
MDR	Multi-drug resistant
MHB	Mueller-Hinton broth
MIC	Minimum inhibitory concentration
MOM	Methoxymethyl
MOM-Cl	Methoxymethyl chloride
MRSA	Methicillin-resistant <i>Staphylococcus aureus</i>
MS	Mass spectrometry
MTT	3-(3,4-dimethylthiazol-2-yl)-2,5-diphenyltetrazolium bromide
NCTC	The National Collection of Type Cultures
NMR	Nuclear magnetic resonance
NOE	Nuclear Overhauser effect
NOESY	Nuclear Overhauser effect spectroscopy
NP	Normal-phase
ODS	Octadecasilyl

p-HPLC	Preparative high-performance liquid chromatography
p-TLC	Preparative thin-layer chromatography
PBP	Penicillin-binding protein
PDA	Photodiode array
ppm	Parts per million
RNA	Ribonucleic acid
RP	Reverse-phase
rRNA	Ribosomal ribonucleic acid
SPE	Solid-phase extraction
SS- <i>Cmec</i>	Staphylococcal cassette chromosome <i>mec</i>
TBDMS	Tert-butyldimethylsilyl
TBDMS-Cl	Tert-butyldimethylsilyl chloride
TLC	Thin-layer chromatography
TMS	Tetramethylsilane
tRNA	Transfer ribonucleic acid
UV	Ultra-violet
VLC	Vacuum liquid chromatography

## ACKNOWLEDGEMENTS

I would like to acknowledge and thank the following people for all the help, advice and support they provided during my PhD:

My supervisor, Professor Simon Gibbons, who offered me the opportunity to work on the ongoing *Hypericum* project. I would also like to thank him for his help, encouragement, and sharing his knowledge and expertise in the phytochemistry field.

My second supervisors, Dr Joanne Barnes and Dr Jose Prieto-Garcia, for their support during my PhD.

Dr John Malkinson for his help and advice on the synthesis work.

Dr Mire Zloh for the general discussions on NMR.

Mr Emmanuel Samuel and Mr Trevor Gibson for performing mass spectrometry analysis.

Colleagues and friends at the Centre for Pharmacognosy and Phytotherapy.

My parents and my fiancé for their encouragement throughout my PhD.

The School of Pharmacy and EPSRC for my PhD Studentship.

# CHAPTER ONE

## 1 INTRODUCTION

The work presented in this thesis is part of an on-going project at the Centre of Pharmacognosy and Phytotherapy, The School of Pharmacy, University of London, to investigate the phytochemistry and antibacterial properties of the *Hypericum* genus, focusing on the activity against *Staphylococcus aureus* (Gibbons *et al.*, 2002). In that study, it was found that 33 out of 34 chloroform extracts of different *Hypericum* species and varieties showed significant activity in a disk diffusion assay and five extracts had minimum inhibition concentrations of 64 µg/ml against the methicillin-resistant *S. aureus* (MRSA) strain XU212. This demonstrated the potential of this genus to produce antibacterial compounds, which could be further developed into antibiotics to combat the problem of MRSA infection.

*S. aureus* is a Gram-positive bacterium which is commonly found on the moist skin and nasal cavity of healthy individuals and usually poses no threat to health. However, these organisms can become pathogenic in more vulnerable people, especially hospital in-patients receiving treatments or undergoing investigations. *S. aureus* infections can range from local cellulitis and impetigo on the skin to systemic septicaemia, pneumonia and endocarditis. Penicillin was the first antibiotic launched in the 1940s to treat staphylococcal infections. The discovery was made by Alexander Fleming who observed an inhibition of bacterial growth around a contaminant mould (*Penicillium notatum*) on a staphylococcal culture. Resistance to penicillin emerged quickly owing to the ability of the bacteria to produce β-lactamase, an enzyme that hydrolyzes the β-lactam ring in penicillin

(Barber *et al.*, 1948). In 1960, the semi-synthetic  $\beta$ -lactamase stable methicillin was introduced but MRSA emerged in 1961 (Jevons, 1961). As we now know, the rapid increase in antibiotic resistance was largely due to inappropriate antibiotic use. Since then, new classes of antibiotics were discovered and developed, including macrolides, tetracyclines, aminoglycosides and cephalosporins. Even these antibiotics did not overcome the problem of antibiotic resistance. Antibiotic resistance in *S. aureus*, particularly MRSA, therefore presents a big challenge to healthcare professionals and research scientists. MRSA strains resistant to different classes of antibiotics have been isolated, with many showing multi-drug resistance. Therefore, apart from restricting the use of antibiotics and preventing MRSA spread with strict hygiene measures, there is an urgent need to develop new therapeutic agents to overcome antibiotic resistance.

### **Aims and objectives**

The aim of this PhD project was to investigate the phytochemistry and antibacterial activity of plants from the *Hypericum* genus. The objectives were as follows:

- Isolate and purify antibacterial compounds from selected plants using bioassay-guided fractionation.
- Characterize the compounds using various spectroscopic techniques.
- Test the compounds for antibacterial activity against *S. aureus* strains.
- Design a synthetic route for **WS-09** which showed potent activity.
- Synthesize derivatives of **WS-09** to study the structure-activity relationship of the compounds.

## 1.2 Current treatment for MRSA infections

The current treatment reserved for MRSA infections in the UK includes the glycopeptides vancomycin (Vancocin®) and teicoplanin (Targocid®), the oxazolidinone linezolid (Zyvox®), and a combination of the streptogramins, quinupristin and dalfopristin (Synercid®) (British National Formulary, 2007). Daptomycin (Cubicin®), a lipopeptide, and telithromycin (Ketek®), a ketolide derived from clarithromycin, have recently been licensed to treat complicated skin and soft-tissue infections caused by MRSA in the UK (British National Formulary, 2007). Glycopeptides act as inhibitors of bacterial cell wall synthesis (Allen and Nicas, 2003). Oxazolidinones interfere with the binding of messenger ribonucleic acid (mRNA) to ribosomes at the initiation phase of translation in protein synthesis (Shinabarger *et al.*, 1997). Each of the individual streptogramin components is bacteriostatic, but together they demonstrate synergistic bactericidal activity to block protein synthesis in bacteria, leading to cell death (Johnston *et al.*, 2002). Daptomycin interacts with the bacterial cell membrane and disrupts its normal function, followed by the arrest of deoxyribonucleic acid (DNA), ribonucleic acid (RNA) and protein synthesis (Canepari *et al.*, 1990). Ketolide belongs to the new distinct class of 14-membered macrolides, in which the cladinose moiety of erythromycin is replaced with a 3-keto function group (Griesgraber *et al.*, 1996).

In Japan,  $\beta$ -lactams, mainly imipenem, cefmetazole and flomoxef, were used in combination with fosfomycin in the treatment of MRSA (Otsuka *et al.*, 1994). Fosfomycin was suggested to block the induction of penicillin-binding protein 2' (PBP2'), the additional protein expressed in MRSA, allowing the  $\beta$ -lactam to

retain its activity. The aminoglycoside, arbekacin, has also been used since the 1990s (Kobayashi *et al.*, 1995). Arbekacin was found to be highly stable in the presence of inactivating enzymes including 2''-aminoglycoside phosphotransferase, 4''-aminoglycoside adenylyltransferase and 3''-aminoglycoside phosphotransferase (Ubukata *et al.*, 1984, Kondo *et al.*, 1984). It has been reported later that although arbekacin can be acetylated by aminoglycoside acetyltransferases, the acetylated product retains up to 60 % of the antibiotic activity to inhibit bacterial growth (Hotta *et al.*, 2000).

Apart from the above drugs which are already licensed for clinical use, many potential antibiotics are being investigated and undergoing clinical trials. They include the glycopeptides oritavancin, telavancin and dalbavancin (Van Bambeke, 2004). Additionally, two cephalosporins (ceftobiprole and PPI-0903) and one carbapenem (RO4908463) are in advanced clinical development, with ceftobiprole recently completed the first Phase III clinical trial (Page, 2006). It has been shown these three antibiotics have high affinity for PBP 2' and act as an inhibitor of PBP 2' (Hebeisen *et al.*, 2001; Andes and Craig, 2006; Kawamoto *et al.*, 2003). These studies have also shown that ceftobiprole is stable to hydrolysis by  $\beta$ -lactamases, whereas PPI-0903 and RO4908463 are hydrolyzed by class C  $\beta$ -lactamases.

### 1.3 Problems of antibiotic resistance

The occurrence of antibiotic resistance dated back to the 1940s when penicillin was first introduced. Previous studies have shown that about 6 % of *S. aureus* isolated in hospital were resistant to penicillin by 1946 (Barber *et al.*, 1948). In the same publication, the authors also documented that this figure increased dramatically to 50 % by 1948. A more recent study in 2000 showed that 84 % of methicillin-susceptible *S. aureus* isolated from hospitals in the UK were resistant to penicillin at that time (Henwood *et al.*, 2000).

The problem of antibiotic resistance was intensified by the emergence of multi-drug resistant (MDR) strains of *S. aureus*. As the name implies, MDR strains are not only resistant to one antibiotic, but show resistance to a wide range of chemicals, including clinically irrelevant substances. A good example of an MDR strain of *S. aureus* is SA-1199B, which will be used in the bioassay-guided fractionation of extracts in this project. This strain is sensitive to methicillin, but it overexpresses the NorA transporter protein, which is responsible for effluxing certain fluoroquinolones and quaternary ammonium compounds (Markham *et al.*, 1999).

Epidemic MRSA (EMRSA) strains have also caused substantial threat to the health of the population in the UK. The first EMRSA strain (EMRSA-1), which emerged in the mid-1980s, was an MDR strain resistant to penicillin, tetracycline, erythromycin and streptomycin (Marples *et al.*, 1986). Up until now, 17 EMRSA strains have been isolated and characterized, all of which are multi-drug resistant (Aucken *et al.*, 2002). EMRSA-15 and 16 are especially of clinical significance.

EMRSA-15 is resistant to  $\beta$ -lactams, ciprofloxacin and is variably resistant to erythromycin, whereas EMRSA-16 is resistant to  $\beta$ -lactams, ciprofloxacin, erythromycin, kanamycin, neomycin and occasionally resistant to gentamycin (Aucken *et al.*, 2002). Their emergence has coincided with a substantial increase in the incidence of MRSA infection over five years in the 1990s, from 1-2 % to 40 % of all *S. aureus* infections in UK hospitals (Reacher *et al.*, 2000). It was also estimated that EMRSA-15 and 16 accounted for > 95 % of MRSA bacteraemias in the UK in 2001 (Johnson *et al.*, 2001). It was apparent that these two strains are particularly adapted to cause problems in hospitals compared with other EMRSA strains. However, the reason for this is not clear. EMRSA-15 and 16 are among the six *S. aureus* strains used in MIC assays in this project.

Despite the new advances in antibiotic development, community- and hospital-acquired MRSA infections remain to be a big concern due to the possibility of resistance to these new drugs. Vancomycin-intermediately-susceptible *S. aureus* (defined as MIC values > 4  $\mu\text{g/ml}$  and < 32  $\mu\text{g/ml}$ ; NCCLS, 1997) was first isolated in 1997 (Hiramatsu *et al.*, 1997). In 2002, MRSA strains fully resistant to vancomycin were isolated in the US (Morbidity Mortality Weekly Report 2002, 2002a). Resistance to linezolid has also been reported in some patients followed by prolonged antibiotic treatment in the US (Peeters and Sarria, 2005). Resistance to daptomycin has been developed in patients while on treatment of MRSA infection, leading to clinical failure (Skiest, 2006; Marty *et al.*, 2006). The most recent report from the UK National Statistics (UK National Statistics 2005) showed that death certificates with MRSA as the underlying cause rose from 51 to 1629 between 1993 and 2005. However, the data from the period of

2005 to 2007 have not been published. Although an encouraging fall in the cases of MRSA bacteraemia from 1742 (Apr to Jun 2006) to 1072 (Jul to Sep 2007) was reported under the mandatory surveillance scheme in England (Health Protection Agency, 2008), the problem of antibiotic resistance in *S. aureus* must not be neglected. The need to discover and develop new drug leads is urgent in order to overcome the anticipated drug resistance in the future.

#### **1.4 Mechanisms of antibiotic action and resistance in *Staphylococcus aureus***

To understand the mechanism of antibiotic resistance, it is important to know how the antibiotics work in the first place. The commonly used antibiotics to treat *S. aureus* infections act by inhibiting cell growth processes in bacteria, such as cell wall synthesis, protein synthesis and DNA synthesis. Antibiotic resistance arises when the inhibition of these processes fail, thereby rendering the antibiotic ineffective. The main mechanisms of antibiotic resistance include:

- Inactivation or destruction of the antibiotic by bacterial enzymes
- Alteration of the target site in bacteria
- Antibiotic efflux mechanism

The mode of action of the commonly used antibiotics in *S. aureus* infections and the mechanisms of resistance to these antibiotics are described below.

### 1.4.1 $\beta$ -lactams

$\beta$ -lactam antibiotics inhibit bacterial cell wall synthesis by binding to the penicillin binding proteins (PBPs). The primary mechanism of resistance to penicillins in *S. aureus* is by producing  $\beta$ -lactamase, an enzyme which hydrolyzes and therefore inactivates the  $\beta$ -lactam ring in this class of antibiotics.

Methicillin and its analogues, nafcillin and oxacillin, act by binding and inactivating the PBP involved in cell wall synthesis. These compounds have bulky 6' acyl groups which sterically hinder the attack on the  $\beta$ -lactam ring, thus allowing activity to be retained against penicillinase-producing *S. aureus* (Livermore and Williams, 1996). Low-level resistance is caused by  $\beta$ -lactamase over-production, increased levels of intrinsic PBPs or reduction of their binding affinity (Barg *et al.*, 1991). High-level resistance, on the other hand, is dependent on the expression of an alternative PBP (PBP 2a or 2') encoded by the *mecA* gene, which has low affinity for most  $\beta$ -lactam antibiotics (Berger-Bächi, 1994). The *mecA* gene is located on the chromosome. It is carried by large (32-60kb) sections of chromosomally inserted DNA, which have been termed staphylococcal cassette chromosome *mec* (SS-*Cmec*) (Hiramatsu *et al.*, 1999). Expression of *mecA* is either constitutive or inducible by some  $\beta$ -lactam antibiotics (excluding methicillin and oxacillin), or heterogeneous, with only a few cells in a population expressing the gene (Berger-Bächi, 1994).

#### 1.4.2 Aminoglycosides

Aminoglycoside antibiotics are inhibitors of protein synthesis and interfere with bacterial translation. Bacterial resistance to aminoglycosides is primarily mediated by the expression of enzymes which covalently modify the antibiotics by acetylation, phosphorylation or adenylation (Wright, 1999). The enzymes involved are *N*-acetyltransferases, *O*-phosphoryltransferases and *O*-adenyltransferases respectively. This modification interferes with the binding to the target 16S ribosomal RNA (rRNA) in the decoding region of the A-site of the ribosome (Llano-Sotelo *et al.*, 2002). This leads to inhibition of protein synthesis and loss of cell functions.

#### 1.4.3 Quinolones

Quinolones are inhibitors of nucleic acid synthesis. Fluoroquinolones have been shown to have two intracellular targets within bacteria, namely DNA gyrase (encoded by *gyr*) and DNA topoisomerase IV (encoded by *par*) (O'Grady *et al.*, 1997). It has been proposed that the primary target of quinolones is DNA topoisomerase IV in Gram-positive bacteria like *S. aureus*, whereas DNA gyrase is the primary target in Gram-negative bacteria like *Escherichia coli* (Piddock, 1998). Both enzymes act on double-stranded DNA. DNA gyrase catalyzes the ATP-dependent supercoiling activity of relaxed covalently closed circular DNA, and topoisomerase IV catalyzes the ATP-dependent decatenation activity of catenated DNA (Yoshida *et al.*, 1993). Quinolones act on topoisomerase IV by stabilizing an enzyme reaction intermediate in which both DNA strands are

cleaved and covalently linked to the breakage-reunion subunits (Nakamura, 1997). The resultant quinolone-DNA-enzyme complex then initiates a series of events that lead to cell death.

Three main mechanisms of quinolone resistance have been shown in *S. aureus*: (1) DNA gyrase gene mutation (Nakamura, 1997), (2) topoisomerase IV gene mutation (Ferrero *et al.*, 1994) and (3) an active efflux pump (Kaatz *et al.*, 1993).

One of the MDR pumps responsible for quinolone resistance is NorA, a chromosomally encoded pump that confers resistance upon overexpression (Neyfakh *et al.*, 1993). NorA promotes the active efflux of a variety of compounds, including ethidium bromide, benzalkonium and fluoroquinolones. This efflux pump belongs to the major facilitator superfamily transporter, also known as the uniporter-symporter-antiporter family, and uses proton-motive force as the driving force for efflux (Pao *et al.*, 1998).

#### **1.4.4 Macrolides**

Erythromycin is one of first generation macrolides in clinical use. The major side-effect of erythromycin is gastrointestinal discomfort, which is overcome by second generation macrolides including clarithromycin and azithromycin. This group of antibiotics are protein synthesis inhibitors. They stimulate the dissociation of peptidyl-transfer RNA (tRNA) from ribosomes by binding to the bacterial 50S ribosomal subunit (Russell and Chopra, 1996).

Resistance to macrolides is caused by three main mechanisms. The predominant mechanism is the target site modification mediated by one or more *erm* genes (*ermA*, *ermB* and *ermC*) encoding a 23S ribosomal RNA (rRNA) methylase (Leclercq and Courvalin, 1991). This enzyme alters the binding sites of macrolides, lincosamides and streptogramin B antibiotics. The addition of two methyl residues to a highly conserved adenine residue in domain V, the peptidyl transferase centre of 23S rRNA, leads to a conformational change in the ribosome, rendering the strain resistant to most macrolides, lincosamides and streptogramin B compounds. This resistance pattern is known as MLS<sub>B</sub> resistance. The second mechanism of resistance to MLS antibiotics arises from the presence of macrolide efflux pumps encoded by *msrA* or *msrB* (Ross *et al.*, 1989). Ross *et al.* found that the *msrA* gene is a sequence of a 488-amino-acid protein and has two potential ATP-binding domains. The resistance is mediated by the plasmid-borne ABC-transporter protein *msrA* and is dependent on additional chromosomally encoded transmembrane domains. One of the *S. aureus* strains containing the *msrA* gene is RN4220, which was used in antibacterial assays in this project. Enzymatic inactivation of macrolides by *S. aureus* has been reported more recently. This involves two enzymes (EreA and EreB) that hydrolyze the lactone ring of the macrolide nucleus and phosphotransferases that inactivate macrolides by introducing a phosphate on the 2'-hydroxyl group of the amino sugar (Wondrack and Sutcliffe, 1996).

#### 1.4.5 Tetracyclines

Like macrolides, tetracyclines are protein synthesis inhibitors. Two main mechanisms exist for tetracycline resistance in *Staphylococci*: (1) active efflux that emerges with the acquisition of plasmid-based genes such as *TetK* and *TetL*; and (2) ribosomal protection mediated by transposon- or chromosome-located *TetM* and *TetO* determinants (Fluit *et al.*, 2001). Bismuth *et al.* (1990) found that *S. aureus* strains carrying only *TetK* were resistant to tetracycline, but susceptible to minocycline. The authors also had the following findings: (1) The *TetM* gene is believed to confer resistance to all tetracyclines; (2) Most *TetM*-positive isolates also carry the *TetK* gene and MRSA isolates are typically of *TetM* or *TetKM* genotype and (3) The *TetL* gene has been found only in *S. aureus* isolates carrying the *TetM* gene.

*TetK* gene encodes for a hydrophobic, 50.6 kDa membrane bound protein that actively efflux tetracycline and is thought to confer resistance to this agent (Guay *et al.*, 1993). The tetracycline resistance efflux protein TetK is composed of 14 transmembrane segment and can mediate net potassium ion uptake (Guay *et al.*, 1993). XU212, an MRSA strain with TetK efflux pump, was used in antibacterial assays in this project.

#### 1.4.6 Glycopeptides

Glycopeptide antibiotics, such as vancomycin and teicoplanin, are inhibitors of cell wall synthesis. They act by binding to the terminal D-Ala-D-Ala dipeptide of

bacterial peptidoglycan in the cell wall of Gram-positive bacteria. Since Gram-negative bacteria have an additional lipopolysaccharide outer membrane, the target site of glycopeptides is inaccessible. Formation of the glycopeptide-peptidoglycan complex results in inhibition of the cell wall transpeptidase that maintains cell wall integrity and thus prevents cell wall synthesis, blocking cell division and growth (Barna and Williams, 1984).

One mechanism of resistance to glycopeptides in *S. aureus* is by producing excessive amount of cell wall precursors. Consequently, glycopeptide-resistant *S. aureus* has a thickened cell wall which has been suggested to trap the glycopeptide molecules, thereby preventing them from reaching their target site (Hiramatsu, 1998).

## 1.5 Plants as a source of drugs

The use of plants as medicines to heal wounds and fight diseases dated back to the ancient times. Even nowadays, plants are an attractive and powerful source for the discovery of new drug leads. In fact, many drugs in clinical use are derived from a plant source. The best-known example is aspirin (acetylsalicylic acid), which is derived from salicin isolated from willow bark. At one time, patients were advised to take the powdered willow bark to reduce fever and inflammation. In the modern world, aspirin still plays an important role as an anti-pyretic, anti-inflammatory and anti-platelet medicine. Other drugs in clinical use that are derived from plants include the cardiac glycoside digoxin from the *Digitalis* species, the anti-muscarinic atropine from *Atropa belladonna* and the alkaloid analgesic morphine from *Papaver somniferum*.

The reason for the success of natural products is their ability to produce a great diversity of secondary metabolites which possess a variety of biological activities. These compounds can potentially be purified, characterized, optimized and developed as drug leads. They can also be synthetically modified to provide a further range of compounds of interest. It has been estimated that approximately 60 % of the anti-tumour and anti-infective drugs commercially available or under clinical trials are from a natural origin (Cragg *et al.*, 1997). Additionally, natural herbal remedies have also gained popularity from the public over the past few decades. This is due to the common belief that natural products are 'safe' and free from side-effects, whereas the commercially available synthetic drugs are 'unnatural' and have many undesirable effects. While this is not necessarily true, a report has indicated that the herbal remedy St

John's wort (*Hypericum perforatum*) was the most frequently drug prescribed for mild to moderate depression in Germany in 1998 (Brevoort, 1998). It was reported in the same article that the sales of this preparation increased by 2800 % between 1997 and 1998 in USA.

Research has been conducted to investigate the potential of developing new anti-staphylococcal antibiotics using plants as a source. Examples of pure compounds isolated from plants showing anti-staphylococcal activity have been documented in a review (Gibbons, 2004). The rationale behind the search of antibiotics from plant sources is that higher plants have evolved biochemical defence mechanisms in response to environmental stress, predators and invasive micro-organisms. It is therefore likely that plants produce antimicrobial agents as secondary metabolites.

Although plants provide a promising source of drug leads, the activity of natural product research has been downsized in the pharmaceutical industry. This is due to the development of new and versatile technologies being favoured in the drug discovery process, such as combinatorial chemistry and high-throughput screening. While these methods are highly efficient in optimizing drug molecules and identifying the active compounds, the major drawback is that the compounds generated using combinatorial chemistry often lack chirality and rigidity, which are two important properties of a drug molecule (Feher and Schmidt, 2003). Because of the structural diversity of natural products, it is likely that when these technologies are supplemented with natural product research, both the quantity and the diversity of compounds in the chemical library will be enhanced, therefore making the screening process more effective.

## 1.6 The genus *Hypericum*

*Hypericum* belongs to the Guttiferae (alternative name Clusiaceae) family. It is a genus of approximately 450 species and occurs in all temperate parts of the world (Robson, 2003). The latin name *Hypericum* originated from the Greek words *hyper* (meaning over) and *eikon* (meaning image). It was thought that *Hypericum* species were hung around houses to ward off evil spirits due to the plants' strong aroma. It was, however, not documented which species were used. *Hypericum* species appear as herbs or shrubs and have impressive yellow flowers. Fig. 1 shows the images of some *Hypericum* species taken from Royal Botanical Garden at Wakehurst Place, Surrey.

*Hypericum perforatum* (more commonly known as St John's Wort) is the most widely investigated species of the genus and has been used as a medicinal plant for centuries. It is a perennial herb indigenous to Europe, western Asia and northern Africa (Physicians' Desk Reference 2006). Traditionally, oily preparations of *H. perforatum* were applied externally to treat minor burns, wounds and inflammation of the skin (Edzard, 2003). Extracts of *H. perforatum* were also taken internally for the treatment of excitability, depression, anxiety and as a nerve tonic (Newall *et al.*, 1996; Physicians' Desk Reference 2006). St John's wort was first licensed in Germany for use in anxiety, depression and sleep disorders in the 1980s.

*H. perforatum* is also probably one of the most extensively studied medicinal plants to date. Much research was carried out to characterize the plant's active constituents, chemistry, pharmacology and toxicology, which were documented in several reviews (Barnes *et al.*, 2001; Greeson *et al.*, 2001; Medina *et al.*, 2006;

Caccia, 2005). The antidepressant activity was initially attributed to the naphthodianthrone hypericin (Meruelo *et al.*, 1988). However, the prenylated acylphloroglucinol hyperforin emerged more recently as one of the principal constituents responsible for antidepressant activity, which acts as a synaptic re-uptake inhibitor of various neurotransmitters (Laakmann *et al.*, 1998).

The widespread interest in the use of *H. perforatum* in depression has attracted much attention in investigating the bioactive metabolites from other species in this genus. Extracts from various *Hypericum* species have been shown to possess antibacterial (Rocha *et al.*, 1995), anti-MRSA (Gibbons *et al.*, 2005), antiviral (Weber *et al.*, 1994), anti-inflammatory (Trovato *et al.*, 2001) and analgesic (Trovato *et al.*, 2001) activities.

Six *Hypericum* species were used in the phytochemical and antibacterial studies in this project, including *H. forrestii* N. Robson, *H. moserianum* André, *H. revolutum ssp. revolutum* Vahl, *H. beanii* N. Robson, *H. olympicum* L. *cf. uniflorum* N. Robson and *H. choisianum* Wall. ex Robson. *H. forrestii*, *H. moserianum*, *H. beanii* and *H. choisianum* are classified under the section *Ascyreia* and are distributed in Turkey and South Bulgaria, Pakistan, India and Ceylon to East China and south to Lombok and Celebes (Robson, 1977). *H. revolutum ssp. revolutum* is classified under the section *Campylosporus* and is distributed in tropical and South East Africa, Socotra, Yemen, Arabia, Madagascar, Guatemala and Mexico (Robson, 1977). *H. olympicum* L. *cf. uniflorum* is one of the two species classified under the section *Olympia* and is distributed in South Balkan Peninsula and Western Turkey (Robson, 1977). Extensive literature and internet searches indicate that the medicinal and traditional uses of these specific species are unknown.



*H. olympicum L. cf. uniflorum*



*H. beanii*



*H. pseudohenryi*



*H. moserianum*



*H. foliosum*



*H. forrestii*



*H. kouytchense*



*H. maclarenii*

Fig. 1. Photos of some *Hypericum* species. Royal Botanical Gardens, Wakehurst Place, Surrey

## 1.7 **Phytochemistry and antibacterial activity of *Hypericum* species**

The genus *Hypericum* produces a wide range of natural products. The best known examples of metabolites which represent this genus are the hypericins (hypericin and pseudohypericin). Other classes of compounds that are typical of this genus include xanthenes, flavonoids, procyanidins and tannins. Prenylated acylphloroglucinols such as hyperforin are also common and are of particular interest since many of them show antibacterial activity. Examples of each class of compound will be given below, with a focus on the acylphloroglucinol derivatives.

### 1.7.1 **Acylphloroglucinol derivatives and related compounds**

Acylphloroglucinol derivatives are natural products based on an acylated phloroglucinol (1,3,5-trihydroxybenzene) (1). In many cases the acylphloroglucinol has a keto-enol form, which can undergo keto-enol tautomerism (Fig. 2). Apart from the occurrence in *Hypericum*, these natural products have also been isolated from other genera, including *Eucalyptus* (Ghisalberti, 1996), *Helichrysum* (Jakupovic *et al.*, 1989) and *Garcinia* (Hamed *et al.*, 2006, Weng *et al.*, 2004) and *Humulus* (Bohr *et al.*, 2005). Due to the commercial interest of St John's wort as an antidepressant, an increasing amount of phytochemical studies on various *Hypericum* species has been conducted over the past 20 years, leading to the discovery of many new acylphloroglucinol derivatives.

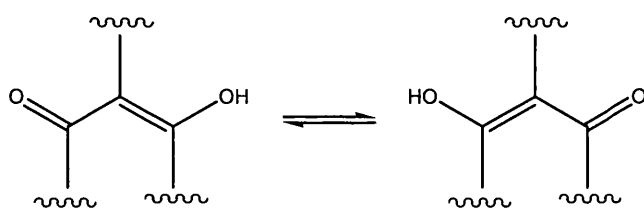
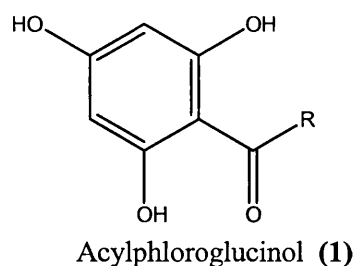
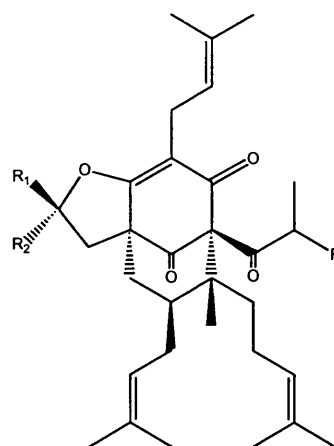
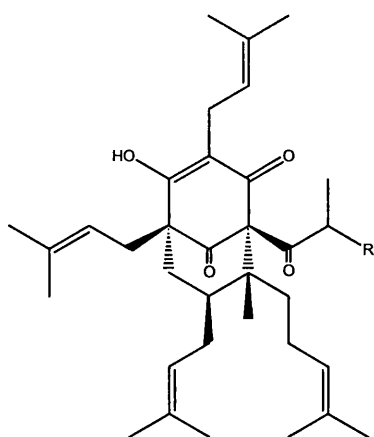


Fig. 2. Keto-enol tautomerism in some acylphloroglucinol derivatives

### 1.7.1.1 *H. perforatum*

Antibacterial properties of *H. perforatum* were first reported in 1959 (Gaind and Ganjoo, 1959). Later, it was found that the major antibacterial constituent was hyperforin (**2**) (Bystrov *et al.*, 1975). Hyperforin is one of the best characterized constituents of *H. perforatum* in terms of its pharmacological properties. Apart from being an antibacterial agent, hyperforin was also shown to be an antidepressant, anti-inflammatory, anti-angiogenic and antitumour agent (Beerhues, 2006; Medina, 2006). Its ability to inhibit cytochrome P450 CYP3A4 activity makes St John's wort preparations prone to interact with many prescription drugs (Lee *et al.*, 2006, BNF 2007).

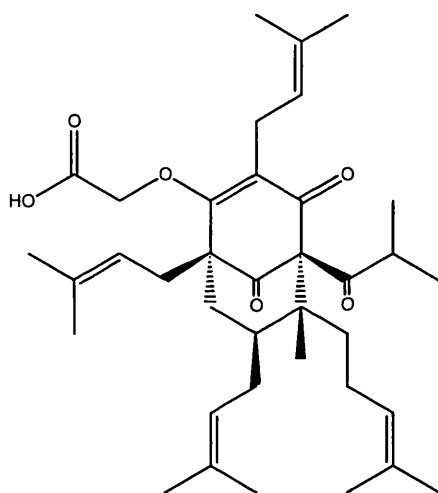


Hyperforin (**2**)     R = CH<sub>3</sub>  
 Adhyperforin (**3**)     R = CH<sub>2</sub>CH<sub>3</sub>

	R	R <sub>1</sub>	R <sub>2</sub>
Furohyperforin ( <b>4</b> )	CH <sub>3</sub>	C(CH <sub>3</sub> ) <sub>2</sub> OH	H
Furoadhyperforin ( <b>5</b> )	CH <sub>2</sub> CH <sub>3</sub>	C(CH <sub>3</sub> ) <sub>2</sub> OH	H
Furohyperforin A ( <b>6a</b> )	CH <sub>3</sub>	H	OH
( <b>6b</b> )	CH <sub>3</sub>	OH	H

Hyperforin is a bicyclic acylphloroglucinol substituted with lipophilic isoprene chains and a 2-methylpropionyl side-chain. It occurs as a mixture of interconverting tautomers in solution (Verotta *et al.*, 2000). Adhyperforin, which possesses a 2-methylbutanoyl side-chain was later isolated from *H. perforatum* (Maisenbacher and Kovar, 1992). Both hyperforin and adhyperforin are poorly stable when exposed to light and oxygen (Maisenbacher and Kovar, 1992). The major oxidation products of hyperforin and adhyperforin were characterized as furohyperforin and furoadhyperforin respectively (Trifunovic *et al.*, 1998; Verotta *et al.*, 1999). Upon oxidation, a cyclized ether is formed between the prenyl group and the enolic hydroxyl group. Furohyperforin A, which was a mixture of two stereo-isomers, was also identified as a further degradation product of hyperforin (Vajs *et al.*, 2003). It was suggested that the instability of hyperforin is due to the enolized  $\beta$ -dicarbonyl system, as natural analogues lacking this moiety are stable (Verotta *et al.*, 1999, 2000). This suggestion can

also be also supported by the results of a more recent study, in which a stable hyperforin derivative, aristoforin (*O*-(carboxymethyl)-hyperforin) (7), was synthesized (Gartner *et al.*, 2005). In aristoforin, the enolizable hydroxyl group is replaced by an *O*-carboxymethyl group. The study showed that aristoforin was (1) highly stable when exposed to light and oxygen, (2) more soluble in water than hyperforin and (3) able to retain the antitumour activity of hyperforin against MT-450 mammary tumour cells. These properties of aristoforin make it more suitable as a potential antitumour drug when compared with hyperforin.

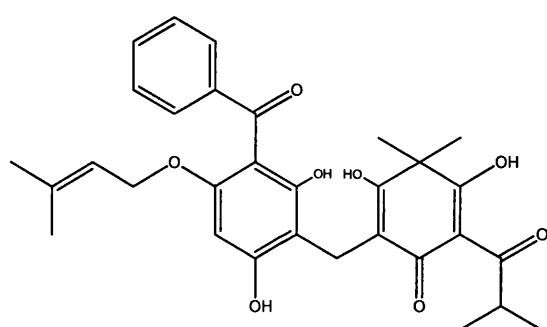


Aristoforin (7)

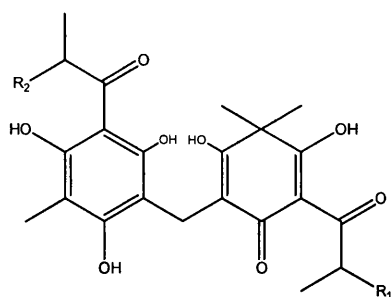
Hyperforin was shown to be active against *S. aureus* and MRSA at concentrations as low as 0.1  $\mu\text{g/ml}$  (Schempp *et al.*, 1999), whereas the antibacterial activity of adhyperforin was not documented. The degradation product furohyperforin A was found to be moderately active against *S. aureus* at an MIC of 50  $\mu\text{g/ml}$  (Vajs *et al.*, 2003). The antibacterial activity of the synthetic derivative aristoforin, however, has not been determined. It would be interesting to investigate whether the exceptional antibacterial activity of hyperforin is retained in aristoforin.

### 1.7.1.2 *H. japonicum*

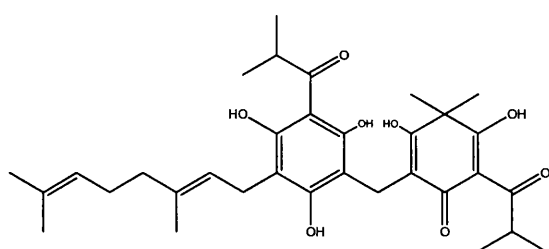
*H. japonicum* is a Chinese medicinal plant used for the treatment of infectious hepatitis, gastrointestinal disorders and some tumours (Ishiguro *et al.*, 1986). Acylphloroglucinol-filicinic acid derivatives have been isolated from the ether extracts of this plant, including sarothralin (**8**), saroaspidin A (**9**), B (**10**), C (**11**), sarothralen A (**12**), B (**13**), C (**14**) and D (**15**) (Ishiguro *et al.*, 1986, 1987, 1994). The chemical structure of these compounds was characterized by an acyl-substituted filicinic acid moiety linked to an acylphloroglucinol moiety *via* a methylene bridge. Saroaspidin A, B and C differ in the length of the acyl hydrocarbon chains (2-methylpropionyl or 2-methylbutanoyl). The structural isomers, sarothralen C and D, showed antibacterial activity against *S. aureus* with MIC values of 25 and 12.5  $\mu\text{g/ml}$  respectively (Ishiguro *et al.*, 1994). The antibacterial activity of compounds (**8**) to (**13**) and some synthetic phloroglucinol derivatives was studied by Yamaki *et al.* (1994). The natural products showed excellent activity against *S. aureus*, with MIC values ranging from 1.56  $\mu\text{g/ml}$  to 12.5  $\mu\text{g/ml}$  (Yamaki *et al.*, 1994). In the same publication, the authors concluded that the presence of both phloroglucinol and filicinic acid moieties was not always necessary for activity, but phloroglucinol with an enolizable  $\beta$ -dicarbonyl system was essential. The stereochemistry at the chiral centres of these compounds (marked with \*) was not determined by the authors.



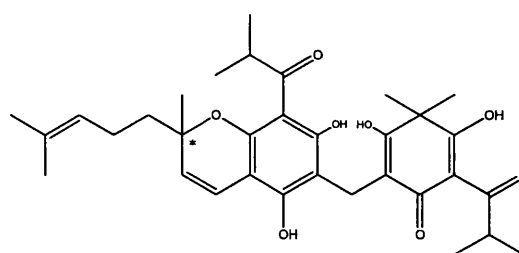
Sarothralin (**8**)



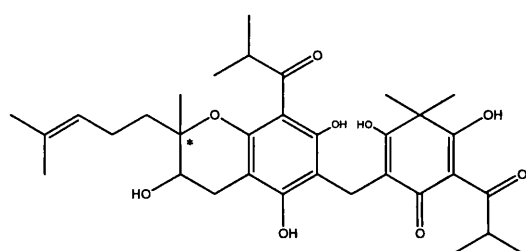
	R <sub>1</sub>	R <sub>2</sub>
Saroaspidin A (9)	CH <sub>3</sub>	CH <sub>3</sub>
Saroaspidin B (10)	CH <sub>3</sub>	CH <sub>2</sub> CH <sub>3</sub>
Saroaspidin C (11)	CH <sub>2</sub> CH <sub>3</sub>	CH <sub>2</sub> CH <sub>3</sub>



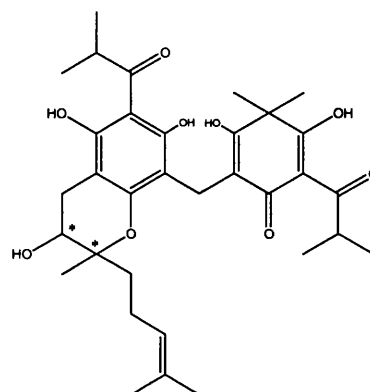
Sarothralen A (12)



Sarothralen B (13)

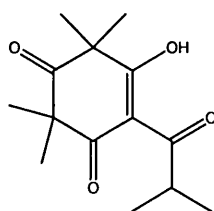


Sarothralen C (14)



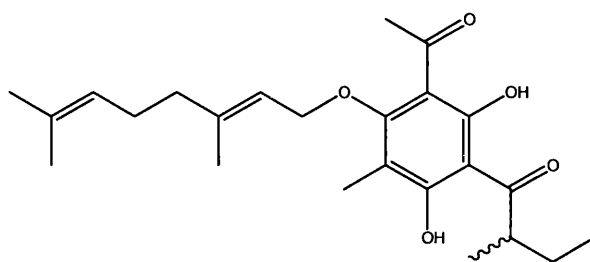
Sarothralen D (15)

Flavesone (16), an acyl-filicinic acid derivative, has been isolated from *H. japonicum* (Hu *et al.*, 2000). This compound was previously reported as the main antimicrobial component in the essential oil from *Leptospermum scoparium* (commonly known as Tea tree) (van Klink *et al.*, 1999).



Flavesone (16)

Hu *et al.* (2000) also isolated an *O*-geranylated acylphloroglucinol (**17**) from the same plant. Two acyl side-chains are present in this compound, including an acetyl group and a 2-methylbutanoyl group. The authors suggested that *O*-prenylation was less common than *C*-prenylation in natural products and it seemed that this acylphloroglucinol was the first metabolite with a geranyloxy group in *Hypericum* species.

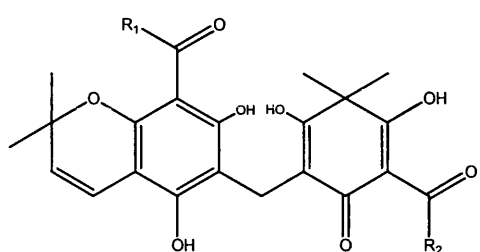


(17)

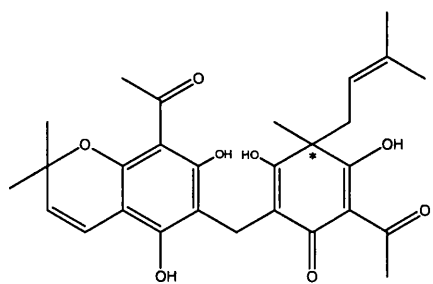
### 1.7.1.3 *H. drummondii*

Seven filicinic acid derivatives were isolated from the hexane extract of the aerial parts and roots of *H. drummondii*, namely drummondins A (**18**), B (**19**), C (**20**), D (**21**), E (**22**) and F (**23**), and isodrummondin D (**24**) (Jayasuriya *et al.*, 1989, 1991). These acylphloroglucinol derivatives show structural similarity to those isolated from *H. japonicum* (section 1.7.1.2). Drummondins A, B and C possess an acyl-filicinic acid moiety connected to a 2,2-dimethyl chromene *via* a methylene bridge. Drummondin D and isodrummondin D are structural isomers, differing in the position of cyclization in the chromene moiety. Drummondin E shows structural similarity with isodrummondin D. Instead of possessing a chromene moiety, a prenyl chain is attached to the phloroglucinol moiety *via* an ether linkage in drummondin E. Drummondin F possesses a modified filicinic

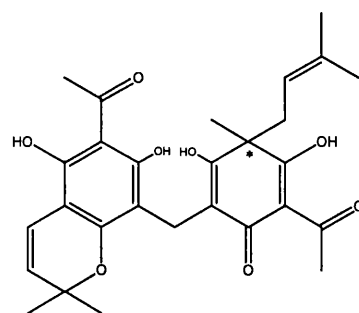
acid derivative connected to a *C*-prenylated phloroacetophenone *via* a methylene bridge. The stereochemistry of the chiral centres was not reported, however. Jayasuriya *et al.* (1989) found that all of the drummondins were highly active against *S. aureus*, *Bacillus subtilis* and *Mycobacterium smegmatis*, with MIC values ranging from 0.39 µg/ml to 6.25 µg/ml. They were, however, inactive against Gram-negative bacteria (*Escherichia coli* and *Pseudomonas aeruginosa*).



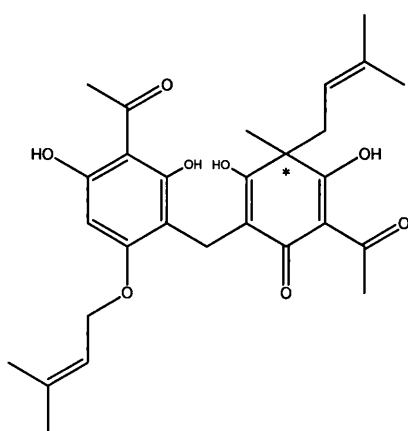
	R <sub>1</sub>	R <sub>2</sub>
Drummondin A (18)	CH <sub>2</sub> CH <sub>3</sub>	CH <sub>2</sub> CH <sub>3</sub>
Drummondin B (19)	CH <sub>3</sub>	CH <sub>2</sub> CH <sub>3</sub>
Drummondin C (20)	CH <sub>3</sub>	CH <sub>3</sub>



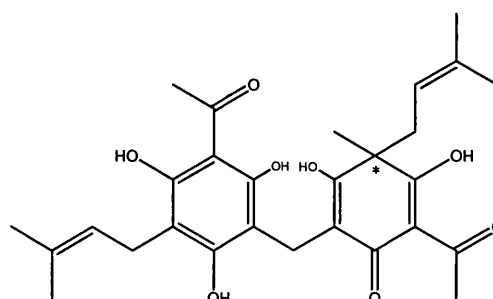
Drummondin D (21)



Isodrummondin D (24)



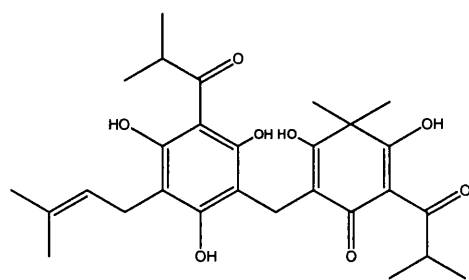
Drummondin E (22)



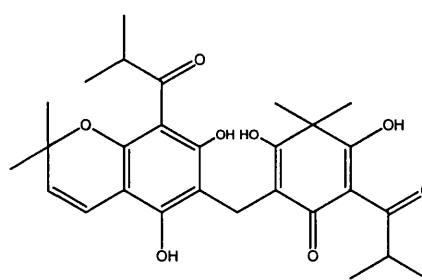
Drummondin F (23)

#### 1.7.1.4 *H. uliginosum*

Uliginosin A (**25**) and B (**26**) are two older acylphloroglucinols isolated from the genus *Hypericum* (Parker and Johnson, 1968). These two structurally related compounds were isolated from *H. uliginosum*, which is a medicinal plant used for the treatment of diarrhea in Mexico. Uliginosin A is a 2-methylpropionyl acylphloroglucinol substituted with a prenyl side-chain and an isopropionyl filicinic acid derivative bridged by a methylene group. In uliginosin B, the prenyl group undergoes cyclization with the hydroxyl group located between the prenyl and the acyl side-chain.



Uliginosin A (**25**)

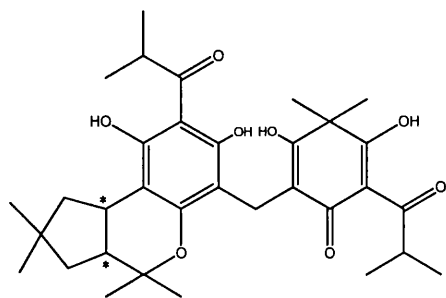


Uliginosin B (**26**)

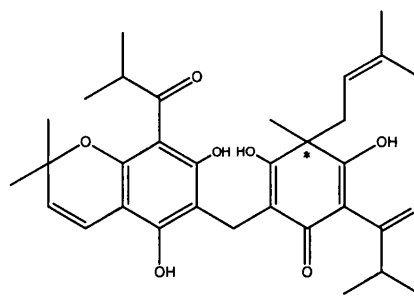
#### 1.7.1.5 *H. brasiliense*

Antibacterial acylphloroglucinol derivatives have been isolated from the petrol extract of the leaves and flowers of *H. brasiliense*, namely hyperbrasilols A (**27**), B (**28**) and C (**29**), together with isohyperbrasilol B (**30**) (Rocha *et al.*, 1995, 1996). The known compound uliginosin A (**25**), previously isolated from *H. uliginosum*, was also isolated. These compounds have a dimeric structure consisting of two acyl filicinic acid moieties linked by a methylene bridge. The stereochemistry at the chiral centres was not reported by the authors. The authors

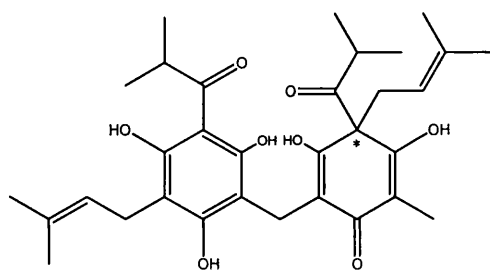
reported antibacterial activities of these four phloroglucinols against *Bacillus subtilis*. The minimum concentration required to inhibit bacterial growth in thin-layer chromatography bioassay ranged from 0.16 to 0.6 µg/ml.



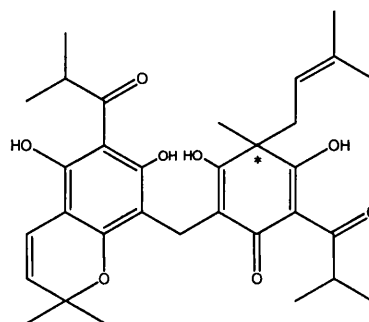
Hyperbrasilol A (27)



Hyperbrasilol B (28)



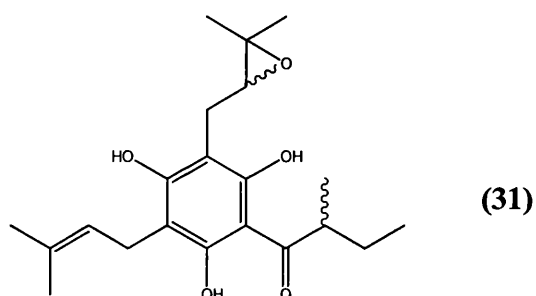
Hyperbrasilol C (29)



Isohyperbrasilol B (30)

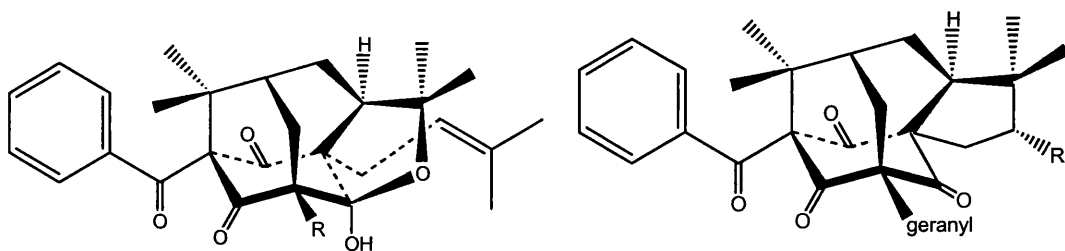
#### 1.7.1.6 *H. foliosum*

An acylphloroglucinol (31) was isolated by our group at the Centre for Pharmacognosy and Phytotherapy in 2005 (Gibbons *et al.*, 2005). It is a relatively simple molecule with a 2-methylbutanoyl side-chain, a *C*-substituted prenyl group and a *C*-substituted epoxidized prenyl group. It was active against a panel of *S. aureus* strains (ATCC 25923, SA-1199B, RN4220 and XU212) and MIC values ranged from 16 to 32 µg/ml.



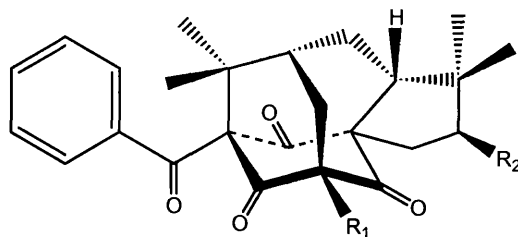
### 1.7.1.7 *H. sampsonii*

*H. sampsonii* is a Chinese herbal medicine used in the treatment of various disorders such as backache, burns, diarrhoea, snakebites and swellings (Hu and Sim, 1998). This is the first *Hypericum* species known to produce a series of complex, caged polyprenylated benzoylphloroglucinols (sampsoniones A to Q (32 to 48)). Sampsoniones A (32) and B (33) were identified to possess the novel 5-oxatetracyclo-skeleton arising from cyclizations of two prenyl substituents (Hu and Sim, 1998). Sampsoniones C to H (34 to 39) show an unusual carbotetracyclo-skeleton formed by complex cyclizations of three prenyl substituents (Hu and Sim, 1999). Sampsoniones I (40) and J (41) are polyprenylated benzoylphloroglucinols with an adamantanyl skeleton (Hu and Sim, 1999). Derivatives showing similar structures were later isolated from the same plant and characterized as sampsoniones K (42), L (43) and M (44) (Hu and Sim, 2000). Sampsoniones N to Q (45 to 48) were isolated more recently together with the known compound 7-epiclusianone (49) (Xiao *et al.*, 2007). Compounds (45) to (49) were tested for antibacterial activity in our research centre as part of my PhD work. Of these, only 7-epiclusianone was active against SA-1199B at an MIC of 4 µg/ml. The bioassay data were published in the same publication.

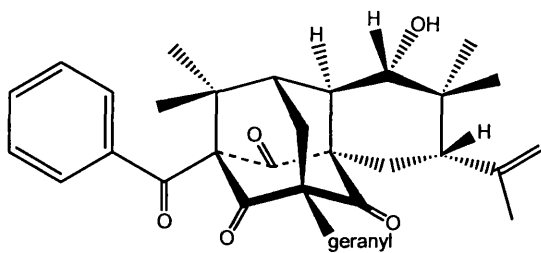


Sampsonione A (32) R = geranyl  
Sampsonione B (33) R = prenyl

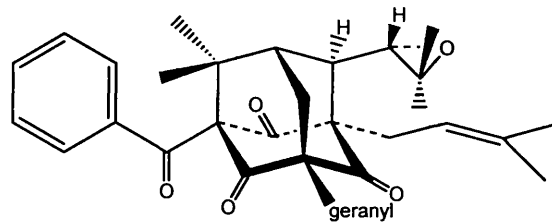
Sampsonione C (34) R = 1-hydroxy-isopropyl  
Sampsonione D (35) R = 1-methylvinyl  
Sampsonione E (36) R = O (ketone)



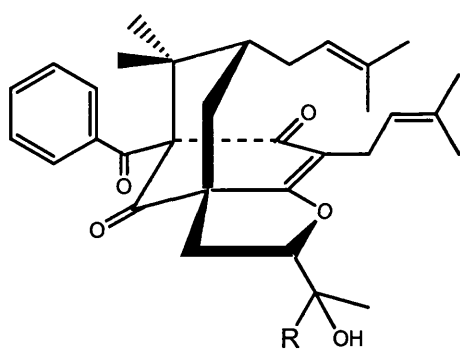
	R <sub>1</sub>	R <sub>2</sub>
Sampsonione F (37)	geranyl	1-hydroxy-isopropyl
Sampsonione G (38)	prenyl	1-hydroxy-isopropyl
Sampsonione H (39)	geranyl	H



Sampsonione I (40)

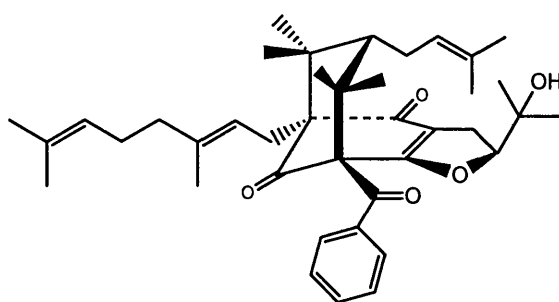
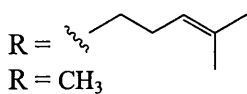


Sampsonione J (41)

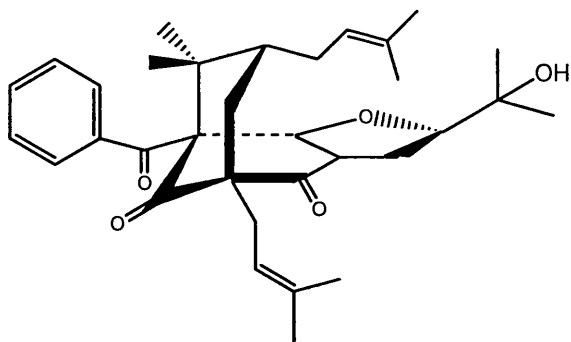


Sampsonione K (42)

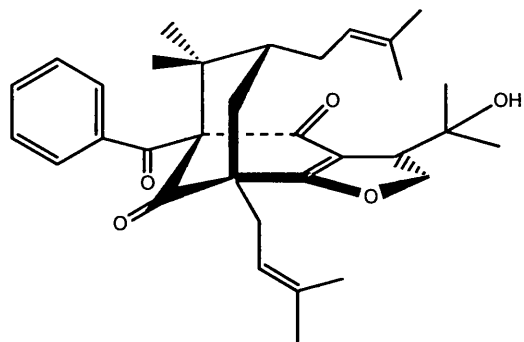
Sampsonione L (43)



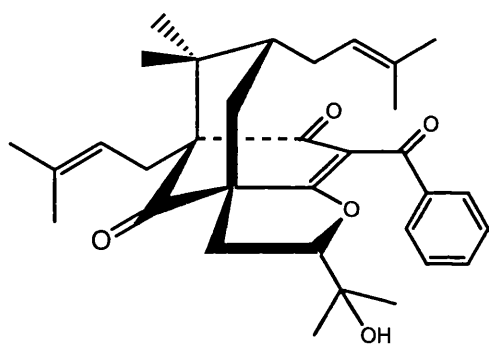
Sampsonione M (44)



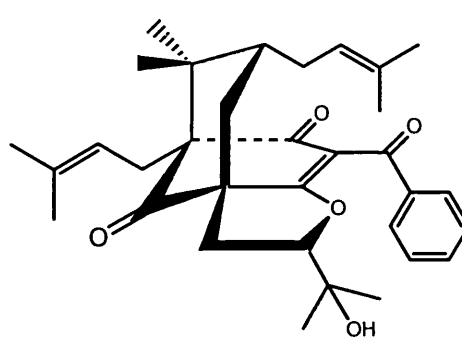
Sampsonione N (45)



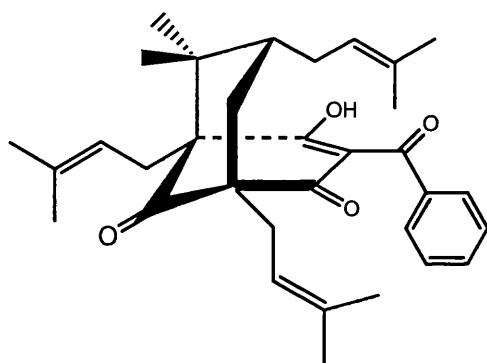
Sampsonione O (46)



Sampsonione P (47)



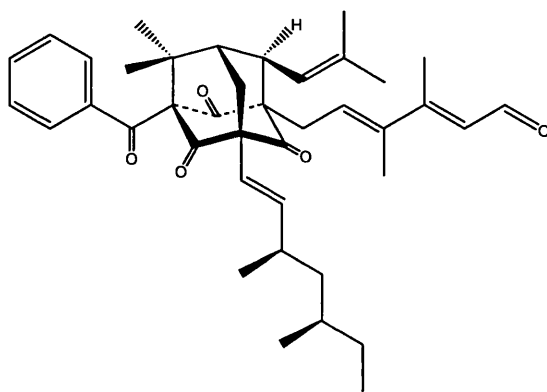
Sampsonione Q (48)



7-Epiclusianone (49)

### 1.7.1.8 *H. sinaicum*

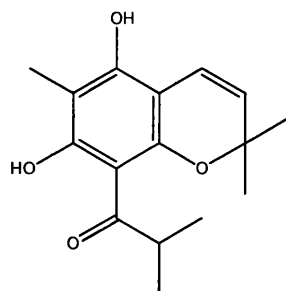
Sinaicinone (**50**), another complex adamantanyl derivative, was isolated from the ethanolic extract of *H. sinaicum* (Řezanka and Sigler, 2007). It is a triketone substituted with a benzoyl group and two unsaturated branched side-chains, one of which has an aldehyde functional group at the terminal. This is the second *Hypericum* species known to produce metabolites that possess the unusual adamantanyl core structure. The bioactivity of this compound, however, has not been studied.



Sinaicinone (**50**)

### 1.7.1.9 *H. revolutum*

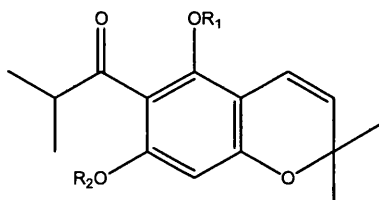
An antifungal benzopyran with a 2-methylpropionyl side-chain (**51**) was isolated from the ether extract of *H. revolutum* (Décosterd *et al.*, 1986). This compound has not been tested for antibacterial activity.



(**51**)

### 1.7.1.10 *H. polyanthemum*

Three benzopyrans (**52-54**) were isolated from *H. polyanthemum* using antibacterial bioassay-guided isolation (Dall'Agnol *et al.*, 2003). As with the benzopyran isolated from *H. revolutum*, these compounds have a 2-methylpropionyl side-chain. The antibacterial activity of these compounds was not reported by the authors.



	R <sub>1</sub>	R <sub>2</sub>
<b>(52)</b>	CH <sub>3</sub>	CH <sub>3</sub>
<b>(53)</b>	CH <sub>3</sub>	H
<b>(54)</b>	H	CH <sub>3</sub>

## 1.7.2 Xanthenes

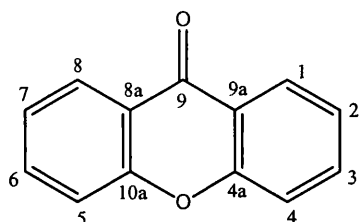


Fig. 3. Xanthone nucleus and numbering scheme.

Xanthenes are metabolites that are commonly found in the genus *Hypericum*. In fact, the majority of natural xanthenes are found in two families: Guttiferae and Gentianaceae (Sultanbawa, 1980). The occurrence of xanthenes isolated from the Guttiferae family was documented in a review by Bennett and Lee (1989), whereas the occurrence of tri-oxygenated and tetra-oxygenated xanthenes was documented in two reviews by Peres *et al.* (1997, 2000). According to these reviews, the most abundant natural sources of xanthenes in other genera from the Guttiferae family include *Calophyllum*, *Garcinia*, *Kielmeyera* and *Vismia*. The biological activities of xanthenes include antibacterial, anti-oxidant, antitumour, anti-inflammatory and antidepressant activity, and are published in a more recent review (Pinto *et al.*, 2005). The chemical structure of the xanthone nucleus and its numbering scheme is shown in Fig. 3. The main classes of xanthenes include simple oxygenated xanthenes, prenylated xanthenes, xanthone glycosides and xanthonolignoids. Examples of compounds isolated from *Hypericum* species are given below.

### 1.7.2.1 Simple oxygenated xanthenes

The majority of the xanthenes isolated from the genus *Hypericum* have simple chemical structures, with a xanthone nucleus substituted with hydroxyl and/or

methoxyl group(s) at various positions. Examples of simple xanthenes isolated from *Hypericum* species listed in the three reviews mentioned above are given in Table 1.

Table 1. Examples of simple xanthenes isolated from *Hypericum* species (Bennett and Lee, 1989; Peres *et al.*, 1997, 2000).

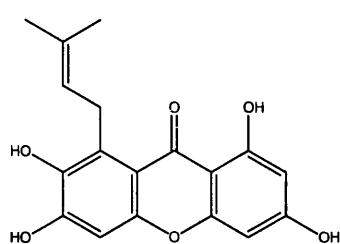
Compound	Source
2-hydroxyxanthone	<i>H. balearicum</i> , <i>H. canariensis</i> , <i>H. ericoides</i> , <i>H. mysorensense</i>
1,7-dihydroxyxanthone	<i>H. balearicum</i> , <i>H. canariensis</i> , <i>H. ericoides</i> , <i>H. mysorensense</i>
1-hydroxy-7-methoxyxanthone	<i>H. mysorensense</i>
2,5-dihydroxyxanthone	<i>H. canariensis</i>
2,3-dimethoxyxanthone	<i>H. mysorensense</i>
2-hydroxy-5-methoxyxanthone	<i>H. androsaemum</i>
3-hydroxy-2-methoxyxanthone	<i>H. androsaemum</i> , <i>H. balearicum</i>
2-hydroxy-3,4-dimethoxyxanthone	<i>H. canariensis</i> , <i>H. sampsonii</i>
2,3,4-trimethoxyxanthone	<i>H. ericoides</i>
3-hydroxy-2,5-dimethoxyxanthone	<i>H. androsaemum</i>
1,2,5-trihydroxyxanthone	<i>H. balearicum</i>
2,3,4-trimethoxyxanthone	<i>H. ericoides</i>
4-hydroxy-2,3,6-trimethoxyxanthone	<i>H. reflexum</i>
2,4-dihydroxy-3,6-dimethoxyxanthone	<i>H. reflexum</i>
1,3,5,6-tetrahydroxyxanthone	<i>H. androsaemum</i>
1,3,6,7-tetrahydroxyxanthone	<i>H. androsaemum</i>

### 1.7.2.2 Prenylated xanthenes

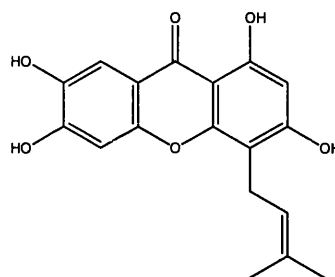
Prenylated xanthenes are also very common in *Hypericum* species. Many undergo oxidative coupling of prenyl side chains with the neighbouring hydroxyl group to give pyran ring systems as seen in some acylphloroglucinols.

Tetra-oxygenated xanthenes substituted with a prenyl group have been isolated from *H. androsaemum* (55) (Nielsen and Arends, 1979) and *H. japonicum* (56)

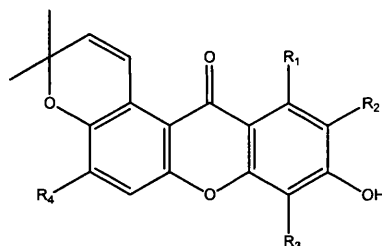
(Wu *et al.*, 1998). A series of xanthenes where the prenyl group at C-8 is coupled to the hydroxyl group at C-7 was isolated from *H. patulum*, namely hyperxanthone (57), toxyloxanthone B (58), paxanthone (59), garcinone B (60) and paxanthone B (61) (Ishiguro *et al.*, 1995, 1996, 1997). Additionally, toxyloxanthone B has also been isolated from *H. androsaemum*, *H. sampsonii* and *H. ascyron* (Hu and Sim, 1999; Nielsen and Arends, 1979).



(55)



(56)

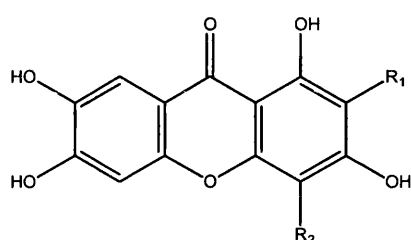


	R <sub>1</sub>	R <sub>2</sub>	R <sub>3</sub>	R <sub>4</sub>
Hyperxanthone (57)	H	H	H	OH
Toxyloxanthone B (58)	OH	H	H	OH
Paxanthone (59)	OH	H	H	OMe
Garcinone B (60)	OH	Prenyl	H	OH
Paxanthone B (61)	OH	H	Prenyl	OH

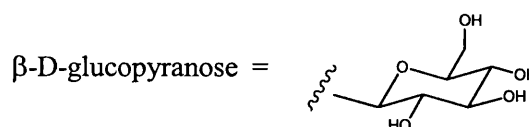
### 1.7.2.3 Xanthone glycosides

The xanthone glycosides, mangiferin (62) and isomangiferin (63) have been found in more than 30 species of *Hypericum*, including *H. perforatum*, *H. maculatum*, *H. calycinum* and *H. sampsonii* (Kitanov and Nedialkov, 1998). Kitanov and Nedialkov (1998) also found that both mangiferin and isomangiferin

were present in 26 out of 36 species under investigation. Mangiferin is identified to be the major component of mangoes (*Mangifera indica*) and its biological activity is widely studied. It is shown to be antidiabetic (Miura *et al.*, 2001), antioxidant (Dar *et al.*, 2005), anti-inflammatory (Garrido *et al.*, 2004), antitumour (Guha *et al.*, 1996), antiviral (Guha *et al.*, 1996) and immunomodulatory (Makare *et al.*, 2001).

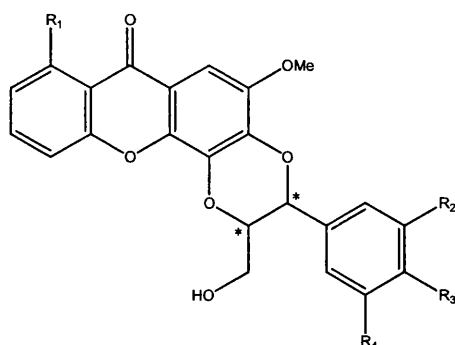


	R <sub>1</sub>	R <sub>2</sub>
Mangiferin (62)	H	β-D-glucopyranose
Isomangiferin (63)	β-D-glucopyranose	H



#### 1.7.2.4 Xanthonolignoids

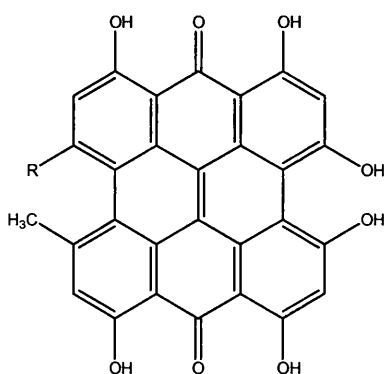
The less common xanthonolignoids are a class of compounds which are thought to be formed by the coupling of a cinnamyl alcohol with an *ortho*-dihydroxyxanthone (Bennett and Lee, 1989). Kielcorin (64) has been isolated from the several *Hypericum* species, including *H. henryi*, *H. androsaemum*, *H. calycinum*, *H. canariensis*, *H. maculatum* and *H. perforatum* (Nielsen and Arends, 1978; Wu *et al.*, 1998). Candensin A (65) has been isolated from *H. henryi* (Wu *et al.*, 1998), whereas candensin C (66) and D (67) have been isolated from *H. canariensis* (Cardona *et al.*, 1985). These xanthonolignoids exist as a mixture of stereoisomers at the chiral centres in nature.



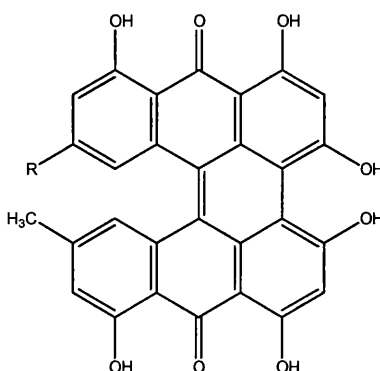
	R <sub>1</sub>	R <sub>2</sub>	R <sub>3</sub>	R <sub>4</sub>
Kielcorin ( <b>64</b> )	H	H	OH	OMe
Candensin A ( <b>65</b> )	OH	H	OMe	OH
Candensin C ( <b>66</b> )	OH	H	OMe	OMe
Candensin D ( <b>67</b> )	H	OMe	OH	OMe

### 1.7.3 Hypericins

Hypericins are natural products belonging to a group of compounds called naphthodianthrone and are mostly found in the genus *Hypericum* (Kitanov, 2001). The main hypericins present in this genus are hypericin (**68**) and pseudohypericin (**69**), which are converted from the precursors protohypericin (**70**) and protopseudohypericin (**71**) under light (Vanhaelen and Vanhaelen-Fastre, 1983).



(**68**) R=CH<sub>3</sub>, (**69**) R=CH<sub>2</sub>OH



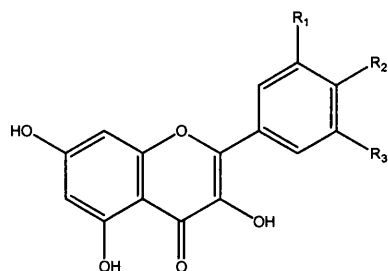
(**70**) R=CH<sub>3</sub>, (**71**) R=CH<sub>2</sub>OH

Hypericin and pseudohypericin are reddish-black pigments that can be found in glands on the leaves, stems and flowers in approximately two-thirds of all *Hypericum* species (Robson, 2003). Hypericin was reported to have anti-depressant, antibacterial, antiviral and anti-neoplastic properties (Duke *et al.*, 1985; Lavie *et al.*, 1995; Kubin *et al.*, 2005). The ability of hypericin to bind to lipoproteins and thereby disrupting bacterial membrane function might account for its antibacterial activity (Lavie *et al.*, 1995). Hypericin and pseudohypericin are photosensitizing agents which are believed to cause hypericism, a photosensitizing effect that causes skin erythema and edema (Giese, 1980).

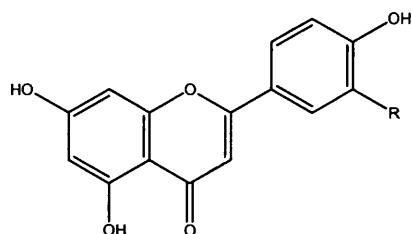
#### **1.7.4 Flavonoids**

Flavonoids are natural products based on the C<sub>6</sub>-C<sub>3</sub>-C<sub>6</sub> skeleton. They can be further divided into many classes, such as flavones, flavonols, dihydroflavonols, flavanones, chalcones and biflavonoids. This class of compounds is known to have a wide range of biological activity, including antibacterial (Alcaráz *et al.*, 2000), antiviral (Wang *et al.*, 1998), anti-oxidant (Škerget *et al.*, 2005), anti-inflammatory activity (Laughton *et al.*, 1991), antitumour (Fotsis *et al.*, 1997) and antithrombogenic (Gryglewski *et al.*, 1987). Flavonoids are almost ubiquitous in higher plants and are therefore very common in *Hypericum* species (Rocha *et al.*, 1995; Wu *et al.*, 1998; Crockett *et al.*, 2005). The major flavonoid aglycones found in *Hypericum* species are the flavonols quercetin (72), kaempferol (73), myricetin (74), and the flavones apigenin (75) and luteolin (76). Quercetin is the common aglycone of the flavonoid glycosides commonly isolated from the genus *Hypericum*. Quercetin glycosides include rutin (77), hyperoside (78), quercitrin

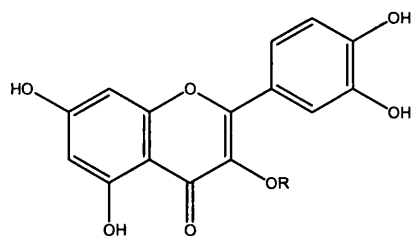
(79) and isoquercitrin (80). The biflavonoids I3, II8-biapigenin (81) and I3', II8-biapigenin (82) (also known as amentoflavone) are also common in this genus.



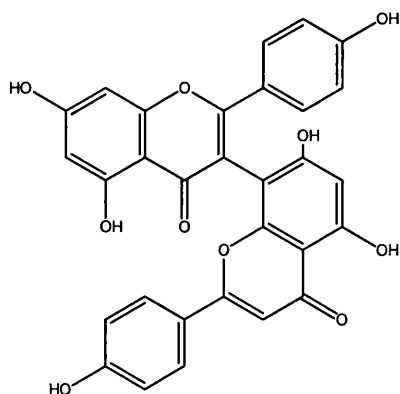
	R <sub>1</sub>	R <sub>2</sub>	R <sub>3</sub>
Quercetin (72)	H	OH	OH
Kaempferol (73)	H	OH	H
Myricetin (74)	OH	OH	OH



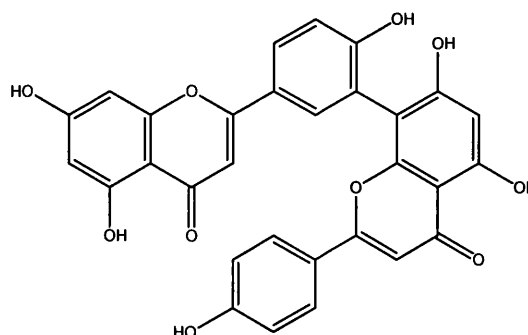
	R
Apigenin (75)	H
Luteolin (76)	OH



	R
Rutin (77)	β-rutinosyl
Hyperoside (78)	β-D-galactosyl
Quercitrin (79)	α-D-rhamnosyl
Isoquercitrin (80)	β-D-glucosyl



(81)

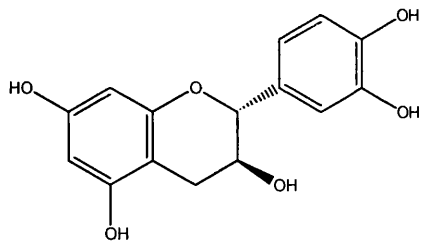


(82)

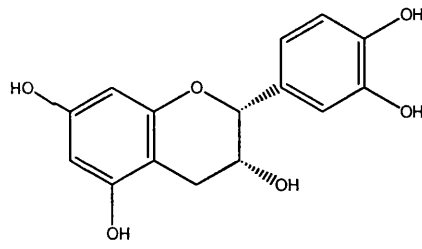
Flavonoids are known to be synthesized by plants in response to microbial infection as a defence mechanism (Dixon *et al.*, 1983). It is therefore not surprising that this group includes compounds which are broadly antibacterial. For example, the antibacterial activity of simple flavones, luteolin and apigenin, against methicillin-sensitive *S. aureus* and MRSA has been demonstrated by Sato *et al.* (2000). The authors found that apigenin (MIC = 3.9-15.6 µg/ml) was more potent than luteolin (MIC = 62.5-125 µg/ml) and that there were no differences in susceptibility to the two compounds in the methicillin-sensitive *S. aureus* and MRSA strains. The flavonols quercetin and rutin have been isolated from *H. brasiliense* (Abreu *et al.*, 2004). Quercetin and rutin exhibited MIC values of 16 µg/ml and 32 µg/ml against *S. aureus* respectively (Basile *et al.*, 2000).

### **1.7.5 Tannins**

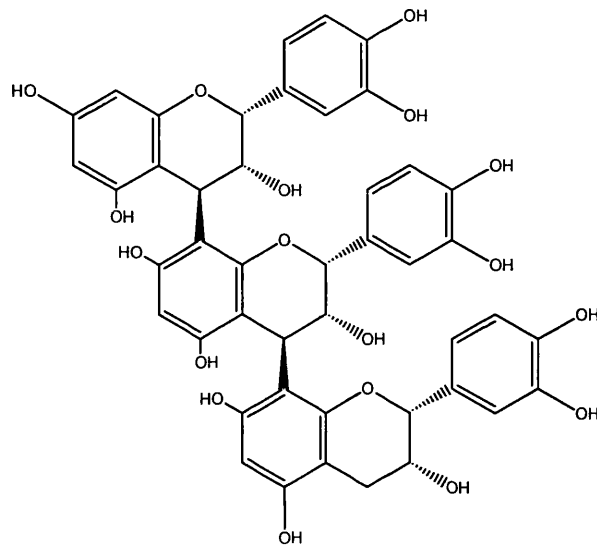
Tannins are polyphenols of high molecular weight (usually between 500 and 3000) and can be classified as condensed tannins (procyanidins) and hydrolysable tannins. Procyanidins are formed by condensation of flavanol units, such as (+)-catechin (**83**) and (-)-epicatechin (**84**). Hydrolyzable tannins, on the other hand, are esters of phenolic acids (such as gallic acid) and a polyol which is usually glucose. Tannins are known to have anti-oxidant and antimicrobial activity (Haslam, 1996; Scalbert, 1991). Condensed tannins have been reported in the aqueous extract of *H. perforatum*, including procyanidins A2, B1, B2, B3, B5, B7 and C1 (Ploss *et al.*, 2001). The chemical structure of procyanidin C1 (**85**) illustrates the structure of a procyanidin polymer (trimer in this case).



(+)-catechin (83)



(-)-epicatechin (84)



Procyanidin C1 (85)

## CHAPTER TWO

### 2 MATERIALS AND METHODS

#### 2.1 Plant material

The aerial parts of the plants used in this project were collected from the Royal Botanic Garden at Wakehurst place in Surrey, which forms part of the National *Hypericum* Collection. *H. beanii* N. Robson and *H. revolutum ssp. revolutum* Vahl were collected in August 2003. *H. olympicum L. cf. uniflorum* N. Robson, *H. forrestii* N. Robson, *H. moserianum* André and *H. choisianum* Wall. ex N. Robson were collected in August 2005. Voucher specimens were deposited at the Centre for Pharmacognosy and Phytotherapy, School of Pharmacy, University of London. The quantity of plant material used in large-scale extraction and accession numbers of the plants are summarized in Table 2.

Table 2. Quantity of plant material used in large-scale extraction and their accession numbers.

Species	Quantity (g)	Accession number
<i>H. forrestii</i> N. Robson	556	1969-34381
<i>H. moserianum</i> André	471	1969-34191
<i>H. revolutum ssp. revolutum</i> Vahl	495	1972-3163
<i>H. beanii</i> N. Robson	650	1988-8790
<i>H. olympicum L. cf. uniflorum</i> N. Robson	937	1969-31184
<i>H. choisianum</i> Wall. ex N. Robson	1018	1977-4670

## **2.2 Extraction**

### **2.2.1 Small-scale extraction**

All plants were air-dried and finely powdered prior to extraction. Small-scale extraction of each plant was initially carried out using approximately 10 g of material. Each plant was sequentially extracted with hexane, dichloromethane (DCM) and methanol (50 ml each) in a conical flask by sonication at room temperature. After 30 minutes of extraction with hexane, the extract was filtered and dried using a rotary evaporator. The process was then repeated with DCM and methanol. Once antibacterial activity was confirmed by disk diffusion assay and MIC assay using the SA-1199B strain (**section 2.5.3**), large-scale extraction of the plant was performed.

### **2.2.2 Large-scale extraction**

Large-scale extraction was carried out using a Soxhlet apparatus (Fig. 4). The dried and powdered material was extracted sequentially with solvents of increasing polarity (3.5 L of hexane, DCM and methanol). The plant material was placed in a thimble made of thick filter paper, which was then loaded into the main chamber of the Soxhlet apparatus. The apparatus was then placed onto a 5 L round-bottomed flask containing 3.5 L hexane and finally equipped with a reflux condenser. The flask was gently heated using a heating mantle, causing the reflux of the solvent which was collected in the chamber where extraction of the plant material took place. When the Soxhlet chamber was nearly full, the extract was emptied *via* a siphon side arm back into the round-bottomed flask.

This process was repeated and the solvent used in Soxhlet extraction was recycled. The duration of extraction with each solvent was usually for 5 days, when the solvent accumulated in the chamber became clear. The extract was then filtered, dried under vacuum and stored in a freezer. The extraction process was repeated with DCM and methanol, giving three extracts for each plant.



Fig. 4. Soxhlet apparatus.

### **2.3 Chromatographic techniques**

Chromatographic techniques were used extensively in this project to fractionate plant extracts and purify compounds of interest from a complex mixture of compounds. It involves the distribution and elution of compounds between a stationary phase and a mobile phase in a specific direction. Different compounds

have varying affinity towards these two phases and therefore have different retention times. In this project, liquid chromatography and size exclusion (gel permeation) chromatography were used to separate and isolate compounds from the plant extracts.

A wide range of stationary phase sorbents is available for liquid chromatography, including silica and bonded-phase silica (C<sub>8</sub>, C<sub>18</sub>, alumina). Because the nature of the compounds to be separated from the extracts was unknown, the commonly used silica and C<sub>18</sub> were used in normal- and reverse-phase chromatography respectively in this project. In normal-phase (NP) chromatography, a polar stationary phase is used and the column is eluted with non-polar solvents. As the sample passes through a normal-phase column, polar natural products adsorb to the stationary phase more strongly than non-polar natural products. This is due to hydrogen-bonding between the hydroxyl groups in the polar compounds and the silanol groups in silica. The non-polar compounds thus move more quickly and are eluted before the polar compounds. As the column is eluted with a more polar solvent (e.g. methanol), the solvent can competitively form hydrogen bonds with the stationary phase, therefore displacing and eluting the adsorbed polar compounds.

Reverse-phase (RP) chromatography is the reverse of normal-phase chromatography, i.e. a non-polar stationary phase is used and the column is eluted with polar solvents (water, methanol and acetonitrile). It utilizes the partition mechanism to achieve separation and relies on the relative solubility of the compounds in the hydrophobic stationary phase and the mobile phase

(Cannell, 1998). In C<sub>18</sub> stationary phase, the silanol groups in silica are reacted with a straight-chain C<sub>18</sub> alkyl unit, forming an octadecasilyl (ODS) phase. Non-polar constituents in a sample partition into the hydrophobic ODS phase, whereas the polar constituents partition into the aqueous phase. The non-polar constituents therefore have a longer retention time and the more polar compounds are eluted more quickly with the polar solvent.

Acidic compounds can cause streaking on thin-layer chromatography (TLC) plates and peak-tailing in high-performance liquid chromatography (HPLC) due to hydrogen-bonding between the compounds and the silanol groups in silica or the unreacted silanol groups in bonded-phase silica. This effect can be reduced by the addition of 1 % acetic acid to the mobile phase. On the other hand, basic compounds can also cause similar effects. This can be reduced by the addition of 1 % diethylamine to the mobile phase. The chromatography techniques used in this project are described below.

### **2.3.1 Vacuum liquid chromatography**

As the name implies, vacuum liquid chromatography (VLC) involves liquid chromatography where an analyte in solution is loaded onto the stationary phase and eluted with solvents with different polarity under vacuum. This technique allows a relatively large amount of material (about 10-15 g) to be loaded onto the column. VLC was generally used as the first step to fractionate a crude plant extract.

The set-up for VLC included a glass column (60 mm x 170 mm) with a fritted disk and a quick fit joint, an adapter with a side arm which was connected to the vacuum and a 250 ml round-bottomed flask. The packing material for the stationary phase was preparative TLC grade silica gel 60 PF<sub>254+366</sub> (Merck). To pack a VLC column, the silica powder was poured into the column and allowed to settle under vacuum so that the column was two-thirds filled with silica. The powder was compressed and the top of the column was made flat with a glass stopper, ensuring the stationary phase was tightly packed and the surface was even for good separation. Care must be taken to avoid cracks in the column, as this would lead to poor separation. Once the column is packed, it was washed with a non-polar solvent under vacuum, which was usually hexane. The column was allowed to run dry after the solvent was eluted.

Plant extracts to be fractionated were adsorbed onto an equal amount of silica which was then loaded evenly onto the column. For non-polar extracts (hexane and DCM), a step-gradient solvent system was used as the mobile phase, from 100 % hexane to 100 % ethyl acetate in 10 % increments. 200 ml fractions were collected in round-bottomed flasks and dried under vacuum. Methanol was used in a final wash to elute any material remaining on the column. For methanol extracts, a step-gradient system of 100 % chloroform to 100 % methanol was used.

### 2.3.2 Thin-layer chromatography

The first step to analyze the extracts and fractions was to run an analytical thin-layer chromatography (TLC) on TLC plates using different solvent systems. This technique can be used to determine the chemical complexity of a sample and to show whether a particular substance was present in the mixture by comparing with commercial standards.

TLC is a simple, quick and convenient way to separate a mixture of compounds. This technique involves the separation of compounds on a thin layer of sorbent which is backed with glass or aluminium. By running TLC plates in different solvent systems, different degrees of separation may be achieved. Silica gel and alumina plates (Merck; 20 x 20 mm, 0.2 mm, 60 F<sub>254</sub>) were used for normal-phase separation whereas RP-18 plates (Merck; 20 x 20 mm, 0.2 mm, 60 F<sub>254</sub>) were used for reverse-phase separation. For normal-phase TLC plates, non-polar solvents were used, for example, hexane, ethyl acetate, toluene, chloroform and DCM. For reverse-phase TLC plates, methanol, acetonitrile and water were commonly used. These solvents can be used on their own or in combination with varying concentrations to create different mobile phase systems.

TLC can be used as an analytical or preparative technique. In analytical TLC, the sample is dissolved in a minimal amount of solvent and applied as a spot or band 1.5 cm from the bottom of a small TLC plate using a capillary tube. After the solvent evaporates, the plate is placed in a small solvent tank containing the mobile phase. The depth of the mobile phase should be about 1 cm and should

not be able to touch the sample on the TLC plate. As the volatile mobile phase slowly rises to the top, separation of the compounds in the sample takes place. When the solvent front nearly reaches the top of the plate (about 2 cm from the top of the plate), the plate is removed and allowed to dry. The position of the solvent front should be marked so as to calculate the value of retention factor ( $R_f$ ). The  $R_f$  value of a compound is constant under a specific stationary phase and mobile phase and therefore can be useful in identifying a compound by comparing it with a standard. The  $R_f$  value is defined as:

$$R_f = \frac{\text{Distance travelled by the compound}}{\text{Distance travelled by the solvent front}}$$

The position of UV-active compounds can be identified by viewing the TLC plate under long- (366 nm) and short-wave (254 nm) UV light. The plate can also be sprayed with a reagent and dried under heat to detect non-UV-active compounds. Vanillin-sulphuric acid (4 %) is a commonly used universal spray reagent. It undergoes a colour reaction with many types of natural products and hence the position of compounds can be identified. Dragendorff's reagent was also used for the detection of alkaloids.

Analytical TLC can be scaled up to purify and isolate compounds by using plates of 20 x 20 cm in a large solvent tank, i.e. preparative TLC (pTLC). In this technique, the sample is applied on a TLC plate as a straight line (2 cm from the bottom and the edges of the plate). The maximum amount of sample that can be loaded onto one plate is about 20 mg and therefore usually a few plates are run simultaneously. After the plates are developed, they are allowed to dry. The

compound(s) of interest can be located by viewing the plate under UV light or using a spray agent. The sorbent on the TLC plates containing the compound is then scrapped off. The compound is eluted with suitable solvents from the sorbent using a small column.

### **2.3.3 Solid-phase extraction**

Solid-phase extraction (SPE) is a useful technique for sample cleanup and the separation of plant extracts and fractions. Two types of commercially available SPE columns were used: Strata SI-1 Silica 10 g/60 ml giga tubes (Phenomenex) and C<sub>18</sub>-E 10 g/60 ml giga tubes (Phenomenex) for normal-phase and reverse-phase separation respectively. Unlike VLC, only a maximum of about 500 mg can be loaded onto each SPE cartridge.

In this technique, the column was mounted on a manifold and equilibrated by eluting the first solvent system through the column under vacuum. The sample to be fractionated was dissolved in a minimal amount of solvent, which should be the same as the first eluting solvent. This was then applied onto the top of the column evenly by a pipette and loaded onto the column by applying vacuum. To achieve a good separation, the vacuum and flow-rate of the apparatus were adjusted so that the eluent was eluted slowly. If the flow-rate was too high, the sample would not have enough contact time to adsorb to the stationary phase of the cartridge. Better separation could be achieved by eluting at a slower rate.

For sample fractionation, the mobile phase used in a normal-phase SPE column was usually a step-gradient of 100 % hexane to 100 % ethyl acetate in 10 % increments and finally washed with methanol. With reverse-phase SPE columns, a step-gradient of 100 % water to 100 % methanol or acetonitrile in 10 % increments was used, with 100 % acetone and/or chloroform as a final wash. 50 ml fractions were collected. Separation of fractions containing compounds showing similar  $R_f$  values on TLC plates could be separated by eluting with solvents in isocratic mode using normal-phase or reverse-phase SPE cartridges. The column was allowed to run dry before eluting with another solvent system. Organic solvents were removed under vacuum, whereas water was removed by freeze-drying.

In the case of sample clean-up, the eluting solvents and the stationary phase were chosen so that the SPE cartridge either retains the compounds of interest or the undesired compounds such as fats and chlorophylls. For example, by eluting a sample through a reverse-phase column with methanol, the more polar compounds of interest could be collected and the unwanted fat and chlorophylls would be retained in the column. The unwanted material could be removed from the column by eluting with acetone and chloroform. These fractions were then analysed by analytical TLC to make sure that the undesired fraction only contained the unwanted substances before discarding.

#### **2.3.4 Size exclusion chromatography**

Sephadex was used as the stationary phase in size exclusion chromatography. It is a cross-linked polymer with pores of various sizes and therefore separates extracts and fractions according to molecular weights. Large molecules pass through the column more quickly whereas small molecules are trapped in the pores of Sephadex and are eluted more slowly. This technique is very useful in sample clean-up because natural products with high molecular weight like fatty acids and chlorophylls are eluted in the first few fractions.

Sephadex is manufactured from the cross-linking of dextran and is supplied in the form of dry beads. The more commonly used is the Sephadex G-series, e.g. Sephadex G-25. Sephadex LH-20 (Amersham Biosciences), which has porous beads with diameters ranging from 30-160  $\mu\text{m}$ , was used during the study. It was specifically developed for gel permeation of natural products and was prepared by the hydroxypropylation of G-25, thus adding lipophilicity to the matrix but also retaining its hydrophilicity.

The column was prepared by soaking approximately 150 g Sephadex LH-20 in 300 ml of a suitable solvent overnight, allowing the Sephadex beads to swell and form a gel. The solution was then poured into the column as a slurry. The Sephadex was allowed to settle in the column under gravity for about 1 h. The excess solvent was then removed from the column through the tap at the bottom. Columns of different sizes were used during the study, depending on whether a

fine separation was required for a simpler fraction, or a coarse separation was required for a crude extract or more complex fraction.

For the more non-polar samples, chloroform and DCM are suitable solvents as the mobile phase. Chloroform-methanol 1:1 was used for samples containing both non-polar and polar compounds and methanol was used for more polar samples. The samples were prepared by dissolving in 1-2 ml of the suitable solvent and were applied to the top of the column by a pipette and loaded onto the column by opening the tap. The mobile phase solvent was added slowly throughout the entire separation process. The first fraction collected in a conical flask was the void volume and contained any molecules that were too large to enter the pores of the polymer matrix. Further eluents were collected in test tubes or 50 ml beakers. Methanol was used as a final wash to elute compounds remaining on the column. Fractions showing similar TLC profile were then grouped together and dried under vacuum.

### **2.3.5 High-performance liquid chromatography**

Modern high-performance liquid chromatography (HPLC) is a versatile tool widely used in natural product chemistry with many applications including the analysis of plant extracts and fractions, purification and isolation of single compounds from a mixture, identification and quantification of compounds. The sample is injected through an injection port into a primed and equilibrated HPLC column. The solvents were pumped continuously in a gradient or isocratic mode into the column under high pressure. The elution of UV active compounds can

be detected by the photodiode array (PDA) detector which shows UV absorption between 190 and 800 nm. The PDA detector is coupled to a computer which shows the chromatogram of the sample as a series of peaks.

Analytical HPLC experiments in this project were performed on a Waters 600 Controller linked to a Waters 996 PDA detector. The column used was a Waters Nova-Pak C<sub>18</sub> column (8 x 10 mm, 4 μm). Samples used in analytical HPLC analysis were made up in a suitable solvent to give a 2 mg/ml solution. The injection volume was 30 μl. A gradient system from 5 % to 100 % acetonitrile or methanol in water or an isocratic system and a flow rate of 1 ml/min was used. Depending on the separation of the compounds as shown in the chromatogram, the solvent systems were modified to achieve better separations of the peaks. The optimized condition was then used in preparative HPLC (p-HPLC) to isolate the individual compounds.

The system used for p-HPLC in the project was a Waters Prep LC 4000 coupled to a Waters 996 PDA array detector. The column used was a Waters XTerra Prep C<sub>18</sub> column (19 x 300 mm, 10 μm). The injection volume was 1 ml and a maximum of 50 mg was loaded onto the column per injection.

## 2.4 Spectroscopic methods

Various spectroscopic methods were used in the study to aid the structural elucidation of natural products. The primary technique used was nuclear magnetic resonance (NMR) spectroscopy (section 2.4.1). Additional information on the compounds was provided by mass spectrometry (MS), ultra-violet (UV) spectroscopy, infra-red (IR) spectroscopy and specific optical rotation ( $[\alpha]_D$ ).

Low-resolution mass spectra were recorded on a Thermo Finnigan ThermoQuest Navigator. Accurate (high-resolution) mass data provided information on the molecular formulae of the purified compounds and were recorded on a Micromass Q-TOF Ultima Global Tandem Mass Spectrometer at London School of Pharmacy or a Bruker Microtof mass spectrometer at the BioCentre, University of Reading.

The presence or absence of chromophores in the isolated compounds was determined by UV spectra, which were recorded on a Thermo Electron Corporation Helios spectrophotometer. The samples were dissolved in approximately 1.2 ml of chloroform or methanol. The concentrations of the samples were recorded so that the molar extinction coefficient, or molar absorptivity, could be calculated according to the Beer-Lambert law:

$$A = \epsilon.c.l$$

where A is the absorbance,  $\epsilon$  is the molar extinction coefficient, c is the sample concentration (mol/l) and l is the path length (cm).

IR spectra reveal the presence of certain functional groups, e.g. hydroxyl group and carbonyl groups. Samples were dissolved in an appropriate solvent and applied as a thin-film on a Nicolet 360 FT-IR spectrometer.

The specific rotation,  $[\alpha]_D$ , was measured on a Perkin Elmer Polarimeter Model 343. Samples were dissolved in chloroform or methanol and the sample concentrations were recorded. The equation used to calculate the value of  $[\alpha]_D$  is given as:

$$[\alpha]_D^T = 100.\alpha / c.l$$

where  $[\alpha]_D$  is specific optical rotation, T is temperature ( $^{\circ}\text{C}$ ),  $\alpha$  is the measured optical rotation, c is concentration (g/100ml), l is the path length (dm).

A positive value denotes dextrorotary rotation whereas a negative value denotes levorotary rotation.

#### **2.4.1 Nuclear magnetic resonance**

Nuclear magnetic resonance (NMR) is a powerful tool used extensively by organic chemists in the structural elucidation of compounds. This technique was routinely used in this study to identify the chemical structures of the purified compounds isolated from plants and the synthetic derivatives. As the physics

and mathematics behind the theory of NMR can be quite complex, only a brief introduction of the principle is given below.

Some atomic nuclei exhibit mechanical spin phenomena which are associated with an angular momentum. This makes the nuclei behave like a bar magnet and is characterized by the spin number,  $I$ . When placed in an externally applied magnetic field, they can align themselves in  $2I+1$  orientations.  $^1\text{H}$  and  $^{13}\text{C}$  are the most common nuclei used in NMR applications and have a spin number of  $\frac{1}{2}$ . Therefore, they can take up one of the two orientations in an external magnetic field. The nuclei which are opposed to the applied field are in a higher energy state whereas those that align with the field are in a lower energy state. The lower energy orientation is more favourable and therefore a larger population of nuclei will be in this orientation.

By irradiating the nuclei with electromagnetic radiation of the correct frequency, the lower energy state will absorb the energy and get promoted to the higher energy state. This transition causes the nuclei to be in resonance with the applied magnetic field, hence the term 'nuclear magnetic resonance'. The nuclear transition can be recorded by the continuous wave (CW) method or Fourier transformation (FT) method and converted into an NMR spectrum.

NMR spectrum is a plot of absorption signals against a chemical shift ( $\delta$ ) scale. Chemical shift is expressed in parts per million (ppm) and is defined by the equation below:

$$\text{Chemical shift } (\delta) = \nu_s \text{ (Hz)} - \nu_{\text{TMS}} \text{ (Hz)} / \text{operating frequency}$$

where  $\nu_s$  is the frequency of the signal peak and  $\nu_{\text{TMS}}$  is the frequency of tetramethylsilane (TMS).

TMS is used as an internal standard and has a chemical shift of zero. The usual chemical scale for  $^1\text{H}$  and  $^{13}\text{C}$  NMR is 0-12 and 0-220 ppm respectively. The chemical shift of nuclei gives an indication of their chemical environment. Because of the difference in the electron density around the nuclei in a molecule, each nucleus is said to have different chemical environments and therefore different chemical shifts. Circulating electrons around a nucleus generate a small magnetic field which is opposed to the applied field. Nuclei in a high electron density environment (e.g. adjacent to electron-donating atoms) are shielded by the electrons. These nuclei experience a relatively weaker magnetic field and therefore require a higher field (low chemical shift, or upfield) to bring them into resonance. On the other hand, nuclei in a low electron density (e.g. adjacent to electron-withdrawing atoms) are deshielded and undergo transition at a lower field (high chemical shift, or downfield). These terminologies are commonly used in describing chemical shifts in NMR spectra and are summarized in Fig. 5.

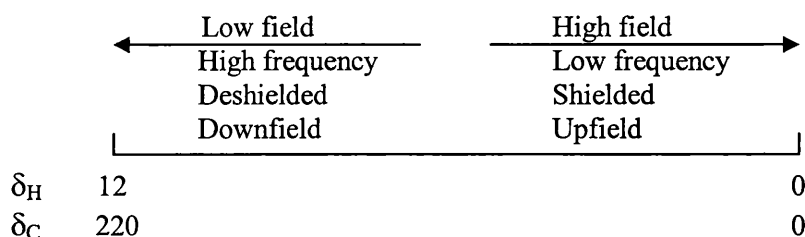


Fig. 5. Terminologies used in describing the NMR spectrum.

In this study, proton ( $^1\text{H}$ ) NMR spectra were obtained on a Bruker AVANCE 400 MHz NMR spectrometer for plant extracts and fractions to determine which types of compounds might be present to facilitate the separation process. For example, the presence of phytosterols and fatty acids can easily be recognized from the  $^1\text{H}$  NMR spectra and phenolics may be recognized from the presence of aromatic protons. It was also used to check the purity of an isolated compound. If the purity was satisfactory, a full set of NMR experiments was then carried out on a Bruker AVANCE 500 MHz NMR spectrometer to obtain spectra with signals of a better resolution. The various NMR experiments used in this study will be discussed in the next section and illustrated by the NMR spectra of **WS-09**. The chemical structure of **WS-09** is shown in Fig. 6. NMR solvents used in the experiments included deuterated chloroform, acetone, methanol and dimethylsulphoxide (DMSO). The chemical shifts of these solvents are shown in Table 3.

Table 3. Chemical shifts of deuterated solvents used.

Deuterated solvent	$\delta_{\text{H}}$ (ppm)	$\delta_{\text{C}}$ (ppm)
Chloroform- <i>d</i>	7.26	77.0
Acetone- <i>d</i> <sub>6</sub>	2.05	30.5, 205.1
Methanol- <i>d</i> <sub>4</sub>	3.31	49.0
DMSO- <i>d</i> <sub>6</sub>	2.50	39.5

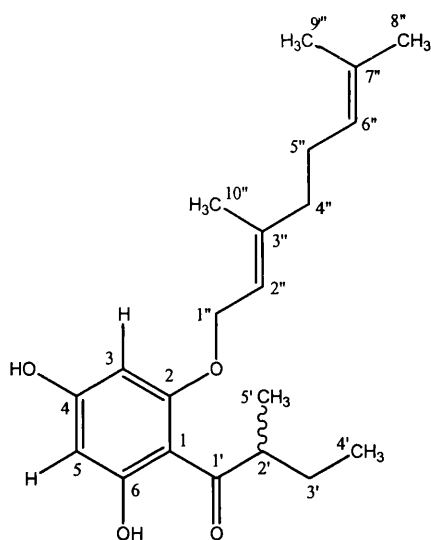


Fig. 6. Chemical structure of **WS-09**.

#### 2.4.1.1 Proton ( $^1\text{H}$ ) NMR

Nuclei in the same chemical environment are described as equivalent and they appear on  $^1\text{H}$  NMR as singlets at the same chemical shift. Nuclei in different environments are non-equivalent and have different chemical shifts. Non-equivalent nuclei that are close together (two to three bonds apart) exert an influence on the magnetic field of the neighbouring nuclei. This effect is known as spin-spin coupling and results in the splitting pattern of the  $^1\text{H}$  NMR spectrum. This phenomenon is extremely common in  $^1\text{H}$  NMR due to the high natural abundance of  $^1\text{H}$  (99.985%). In general, the multiplicity of a signal is  $n+1$ , where  $n$  is the number of non-equivalent protons within three bond lengths from the proton of interest. The distance between the split absorption lines is described as the coupling constant ( $J$ , in Hz) and is a measure of the magnetic interaction between the two nuclei. It is calculated as the difference in frequency between the split absorption lines. The number of protons that give rise to the signal is determined by the integration of the peak. Fig. 7 shows the  $^1\text{H}$  NMR spectrum of

WS-09, illustrating the splitting of signals, chemical shifts and integration of peaks.

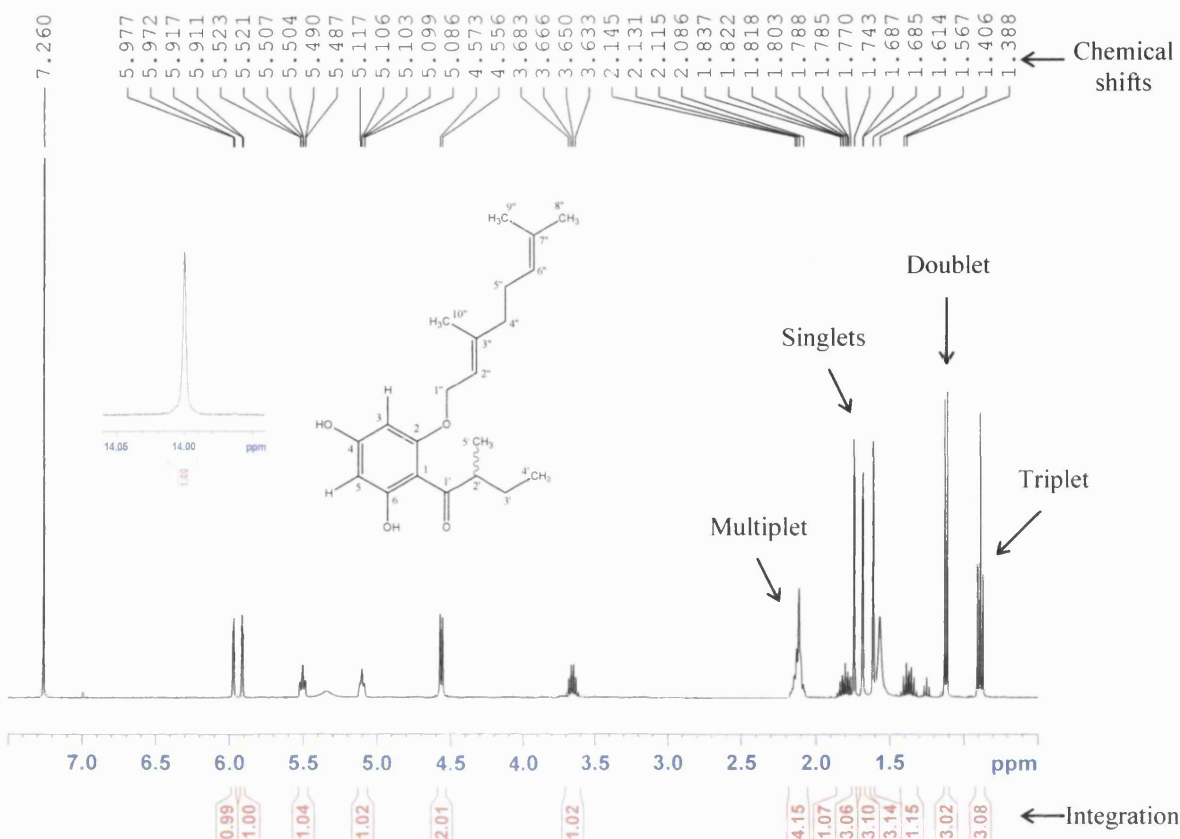


Fig. 7. <sup>1</sup>H NMR for WS-09 in chloroform-*d* recorded at 500 MHz.

#### 2.4.1.2 Carbon (<sup>13</sup>C) NMR

In this project, an external magnetic field of 100 MHz or 125MHz was used in recording <sup>13</sup>C and DEPT 135 NMR experiments. Carbon experiments are much less sensitive than proton experiments. This is because of the low abundance of <sup>13</sup>C (1.1%). The low natural abundance of <sup>13</sup>C also makes it unlikely that the two neighbouring nuclei in the same molecule are both <sup>13</sup>C, which would couple to each other. As a result, spin-coupling of <sup>13</sup>C nuclei is rarely observed. In addition, the <sup>13</sup>C NMR experiment is often proton-decoupled, in which the sample is irradiated with a second frequency which excites all the protons to the

high energy state. This process disallows the proton-carbon spin-coupling process. Unlike  $^1\text{H}$  NMR, overlapping of signals are not common with  $^{13}\text{C}$  NMR. This is because  $^{13}\text{C}$  nuclei come into resonance in a wider range of frequencies. As a result, the signals in the  $^{13}\text{C}$  NMR spectrum are commonly seen as discrete singlets. Fig. 8 shows the  $^{13}\text{C}$  NMR spectrum of **WS-09**.

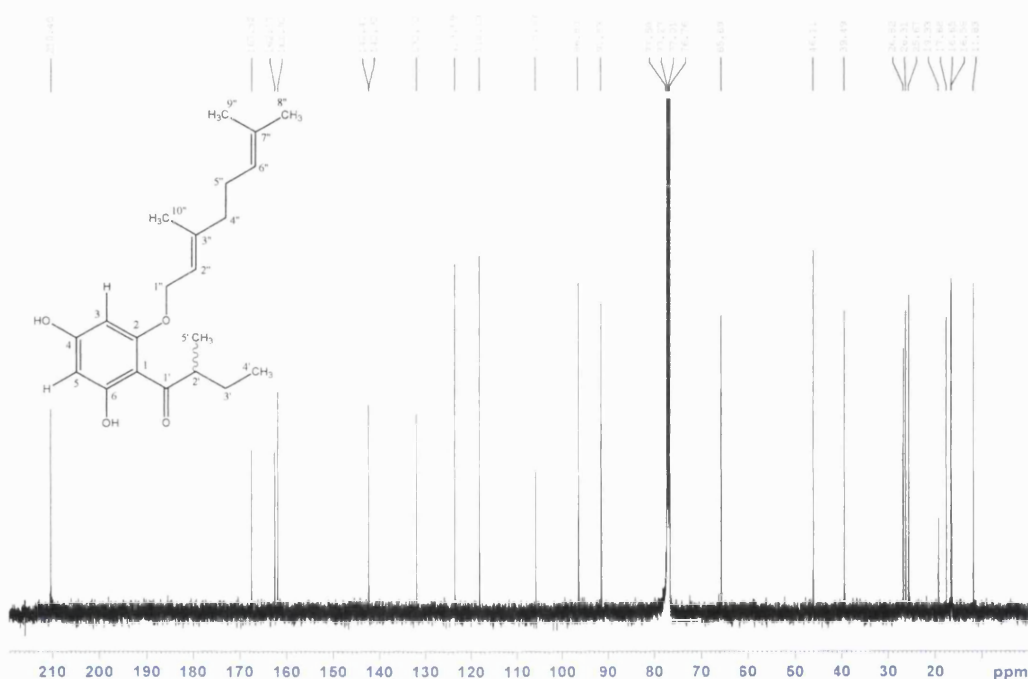


Fig. 8.  $^{13}\text{C}$  NMR for **WS-09** in chloroform-*d* recorded at 125 MHz.

#### 2.4.1.3 Distortionless Enhancement by Polarization Transfer (DEPT)

The distortionless enhancement by polarization transfer (DEPT) experiment utilizes polarization transfer from a proton to a carbon nucleus *via* one covalent bond to increase the signal strength of the carbon nucleus. By exciting the final  $^1\text{H}$  decoupler pulse at different angles ( $45^\circ$ ,  $90^\circ$  or  $145^\circ$ ), the multiplicity of the carbon nucleus may be determined. Table 4 shows the signals given by each type of carbon nucleus in experiments using different pulse angles. DEPT 135 experiments were used throughout this project. The signals for methine (CH)

and methyl (CH<sub>3</sub>) carbons are positive in the spectrum and those for methylene (CH<sub>2</sub>) carbons are negative. By comparing the DEPT 135 spectrum with the <sup>13</sup>C spectrum, quaternary carbons can be identified, as their signals appear on the <sup>13</sup>C spectrum but not on the DEPT 135 spectrum. The DEPT 135 spectrum of **WS-09** is shown in Fig. 9.

Table 4. Different types of carbon signals on a DEPT NMR spectrum

Pulse angle	Methine (CH)	Methylene (CH <sub>2</sub> )	Methyl (CH <sub>3</sub> )	Quaternary carbon
45°	Positive	Positive	Positive	Nil
90°	Positive	Nil	Nil	Nil
135°	Positive	Negative	Positive	Nil

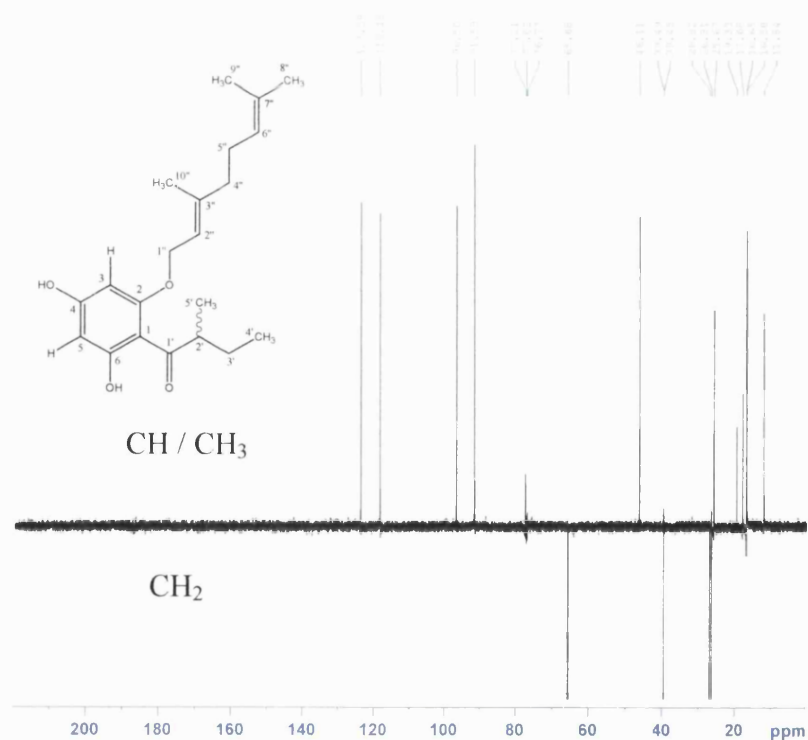


Fig. 9. DEPT 135 spectrum for **WS-09** in chloroform-*d* recorded at 125 MHz.

#### 2.4.1.4 CORRELATION SPECTROSCOPY (COSY)

Correlation spectroscopy (COSY) is a 2-dimensional (2D) NMR technique which shows the connectivity of spin-spin (scalar) coupled protons *via* two or three bonds. In a COSY spectrum, two proton chemical shift axes are plotted against each other at 90°. The diagonal contours are the signals corresponding to the peaks in the 1D  $^1\text{H}$  spectrum. Other cross-peaks which are symmetrically placed about the diagonal indicate mutually spin-spin coupled protons in the molecule. The COSY spectrum (Fig. 10) was used to connect the hydrogens in the 2-methylbutanoyl side-chain by examining the cross-peaks of the spectrum. This is demonstrated by cross-peaks between (1) the methyl doublet and the methine multiplet, (2) the methine multiplet and the methylene multiplets and (3) the methylene multiplets and the methyl triplet.

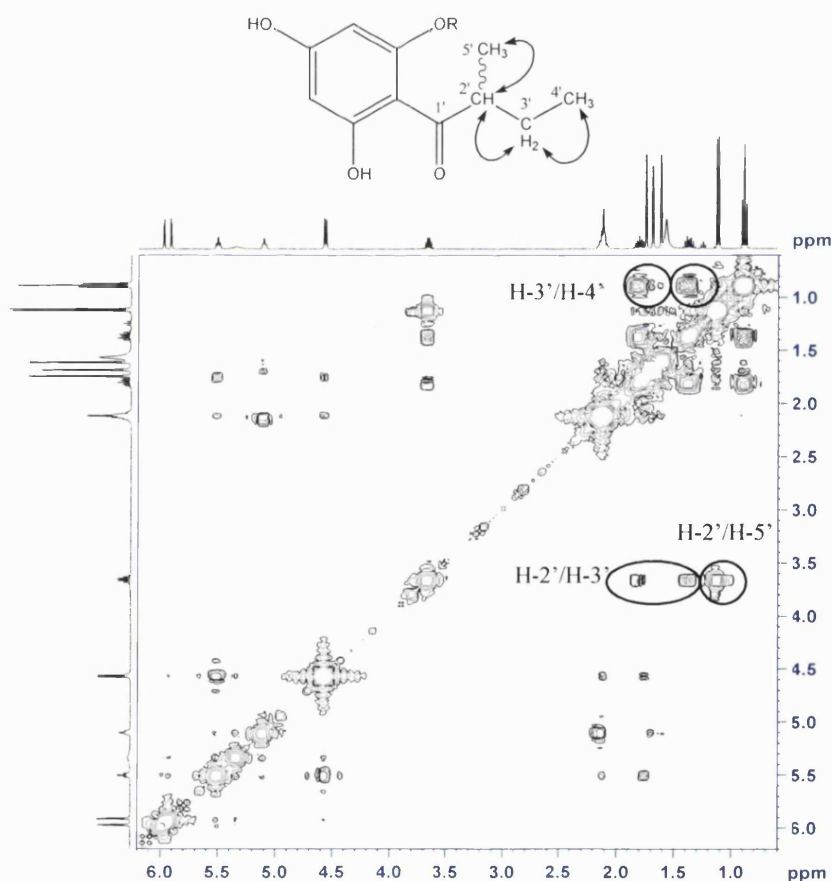


Fig. 10. Selected COSY correlations and COSY spectrum of **WS-09**.

#### 2.4.1.5 Nuclear Overhauser Effect Spectroscopy (NOESY)

Protons can interact with each other through space as well as through bonds. This interaction can be seen when one nucleus is irradiated at its resonance frequency and the other is detected as a more intense or weaker signal than usual (Williams and Fleming, 1995). This is known as the nuclear Overhauser effect (NOE). The magnitude of NOE is inversely proportional to the sixth power of the internuclear distance and is only observable over short distances (between 2 to 4 Å). The NOESY experiment utilizes this effect to provide information on proton-proton interaction through space, as opposed to through bond interaction in COSY. The cross-peaks on the spectrum therefore indicate protons close in proximity. This technique plays an important role in determining the stereochemistry of a molecule. As with the COSY spectrum, NOESY is a 2D experiment where two proton chemical shift axes are plotted against each other at 90°.

Fig. 11 shows some NOE correlations for **WS-09**. The oxymethylene protons (H-1'') show an NOE correlation to a methyl group (H-10'') and an aromatic proton (H-3), indicating that they are close in spatial proximity. The olefinic proton at  $\delta_{\text{H}}$  5.10 m (H-6'') showed an NOE correlation with a methyl singlet ( $\delta_{\text{H}}$  1.69, H-8''), indicating that they are in the *cis*-configuration. This olefinic proton does not show any NOE correlation with the methyl singlet at  $\delta_{\text{H}}$  1.62 (H-9'') which is in the *trans*-configuration.

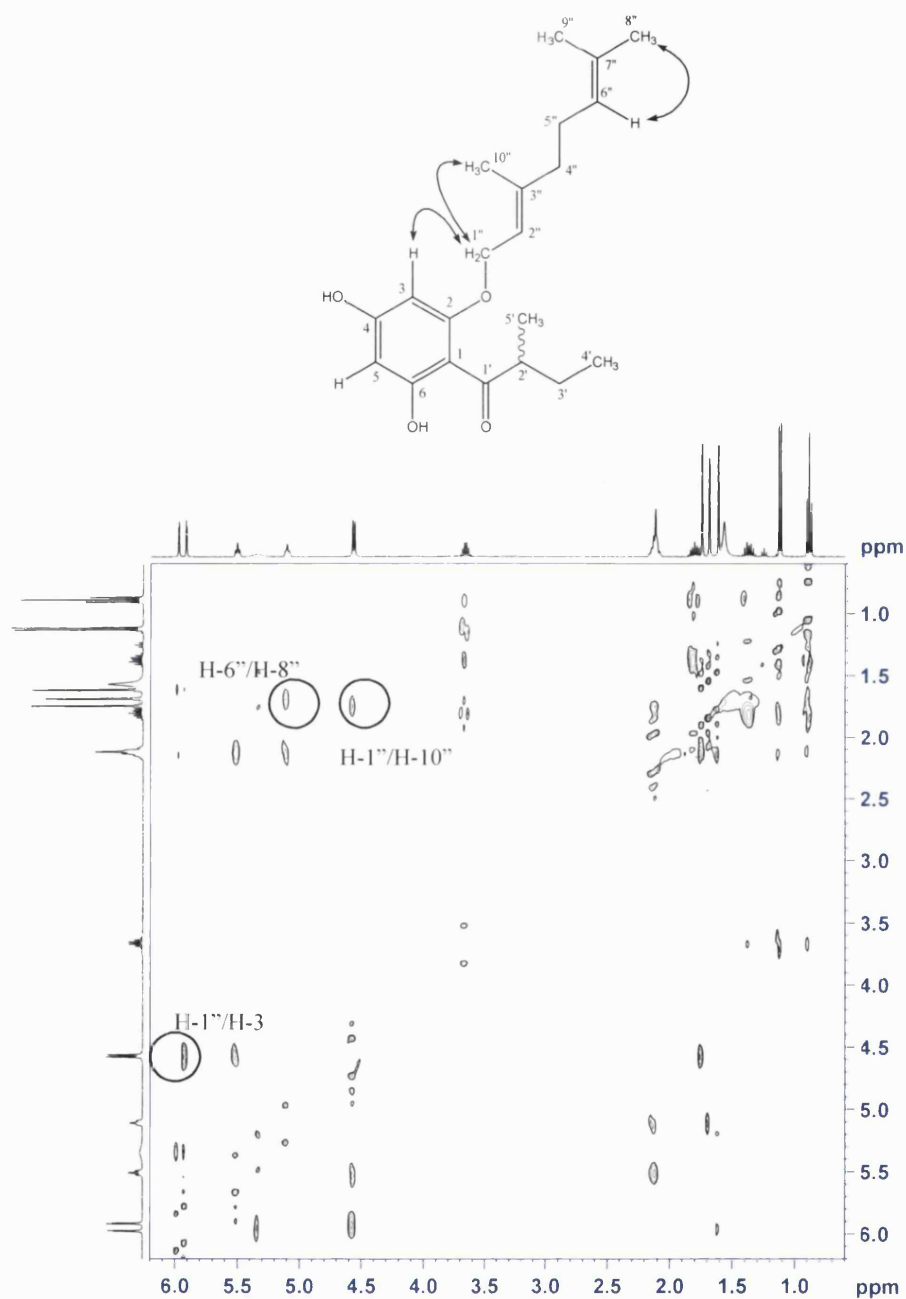


Fig. 11. Selected NOESY correlations and NOESY spectrum of **WS-09**.

#### 2.4.1.6 Heteronuclear Multiple Quantum Coherence (HMQC) Spectroscopy

The correlation between a carbon atom and a proton to which it is directly attached (i.e. one bond correlation) can be determined through an HMQC

spectrum. In the 2D HMQC spectrum, the  $^{13}\text{C}$  and  $^1\text{H}$  NMR spectra are plotted on the left and top axes respectively. The  $^1\text{H}$ - $^{13}\text{C}$  short-range correlations are shown as cross-peaks in the spectrum. Fig. 12 shows cross-peaks for direct coupling of protons to the carbons they are attached to.

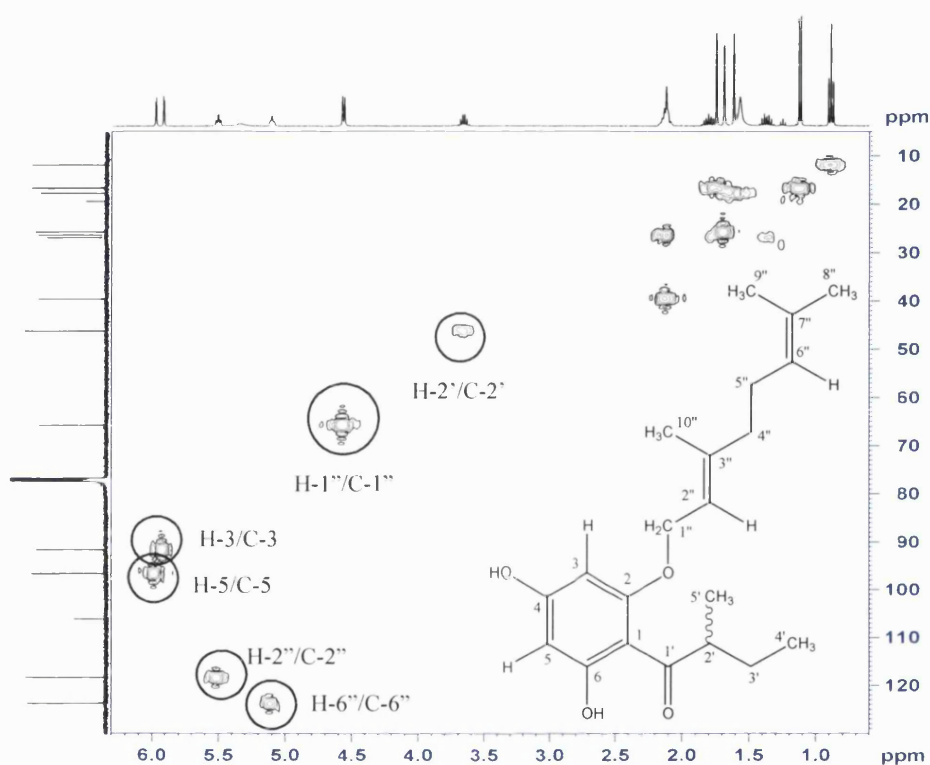


Fig. 12. HMQC spectrum of **WS-09**.

#### 2.4.1.7 Heteronuclear Multiple Bond Coherence (HMBC) spectroscopy

HMBC is similar to HMQC in that  $^1\text{H}$ - $^{13}\text{C}$  connectivity is observed. However, unlike HMQC, the cross-peaks on an HMBC spectrum represent long-range  $^1\text{H}$ - $^{13}\text{C}$  coupling *via* two (geminal,  $^2J$ ) and three (vicinal,  $^3J$ ) bonds.  $^1\text{H}$ - $^{13}\text{C}$  coupling *via* four bonds is also possible, but it is not common. The HMBC spectrum can therefore provide valuable information on the partial structure of a molecule. Fig. 13 shows the HMBC spectrum of **WS-09**. By examining the cross-peaks

between the hydrogen-bonded hydroxyl group signal at  $\delta_H$  14.02 and the three carbons (C-1, C-5 and C-6), it can be placed at C-6 ( $\delta_C$  167.5). Similarly, cross-peaks are observed between the oxymethylene group (H-1'') and three carbons (C-2, C-2'' and C-3''). The  $^3J$  correlation between this group and C-2 ( $\delta_C$  162.6) confirms the point of attachment of the geranyloxy group to the 2-methylbutanoyl phloroglucinol nucleus.

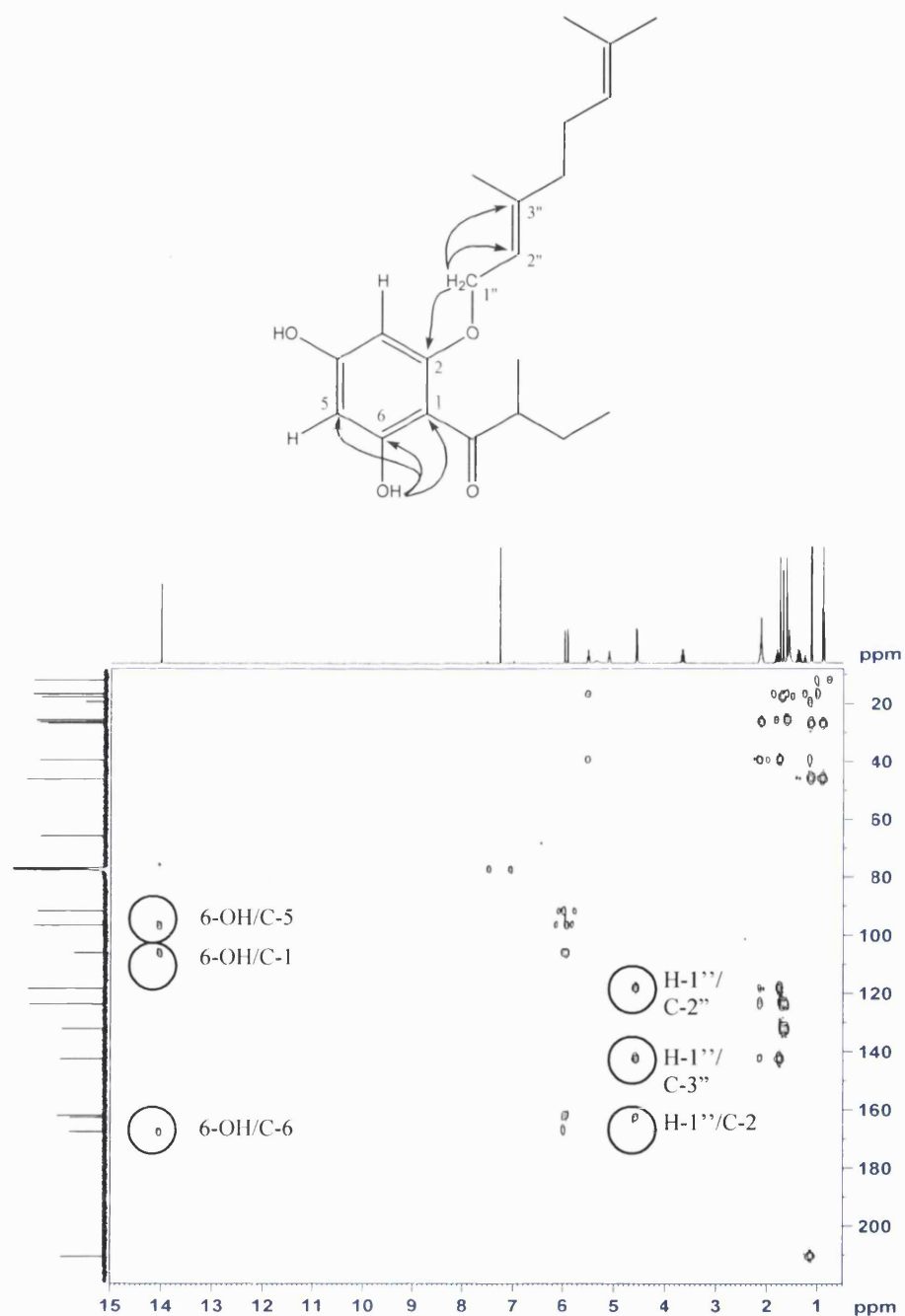


Fig. 13. Selected HMBC correlations and HMBC spectrum of **WS-09**.

## 2.5 Bioassays

### 2.5.1 Bacterial strains

The *S. aureus* strains used in this project included ATCC 25923, SA-1199B, RN4220, XU212, EMRSA-15 and EMRSA-16. Additionally, **WS-09**, which showed excellent anti-staphylococcal activity with MIC values of 0.5 to 1 µg/ml was also tested against various *Mycobacterium* strains and the Gram-negative bacteria *Pseudomonas aeruginosa* and *Salmonella typhimurium*. A summary of the bacterial strains and sources is shown in Table 5. Norfloxacin, tetracycline, erythromycin, oxacillin, rifampicin and ethambutol were used as control. All antibiotics were obtained from the Sigma Chemical Co.

Table 5. A summary of the resistance mechanisms and sources of bacterial strains used.

Strain	Description	Source
<b><i>S. aureus</i></b>		
ATCC 25923	Standard lab strain	E. Udo (Gibbons and Udo, 2000)
SA-1199B	Over-expresses NorA MDR efflux pump	G. Kaatz (Kaatz <i>et al.</i> , 1993)
RN4220	Possesses MsrA macrolide efflux protein	J. Cove (Ross <i>et al.</i> , 1989)
XU212	Kuwait hospital isolate; possesses TetK tetracycline efflux pump	E. Udo (Gibbons and Udo, 2000)
EMRSA-15	Epidemic strain, UK	P. Stapleton, ULSOP (Richardson <i>et al.</i> , 1993)
EMRSA-16	Epidemic strain, UK	P. Stapleton, ULSOP (Cox <i>et al.</i> , 1995)
<b><i>Mycobacterium</i> species</b>		
<i>M. smegmatis</i> ATCC14468	Fast-growing <i>Mycobacterium</i> species	The National Collection of Type Cultures (NCTC)
<i>M. fortuitum</i> ATCC6841	Fast-growing <i>Mycobacterium</i> species	NCTC
<i>M. smegmatis</i> MC <sup>2</sup> 2700	Possesses the <i>M. tuberculosis</i> fatty acid synthase I gene, ΔFas 1	O. Zimhony (Zimhony <i>et al.</i> , 2004)
<i>M. phlei</i> ATCC11758	Fast-growing <i>Mycobacterium</i> species	NCTC
<b><i>P. aeruginosa</i></b>		
K767	Wild type	NCTC
<b><i>S. typhimurium</i></b>		
L354	Wild type	NCTC

### **2.5.2 Disk diffusion assay**

The disk diffusion assay is a quick method of detecting antibacterial activity of a sample. Mueller-Hinton agar (Oxoid) in Petri dishes was inoculated with a bacterial suspension ( $10^7$  cfu/ml) and the excess suspension removed. Test samples were then added to blank disks (5 mm; Oxoid) at a concentration of 1 mg/disk, which were applied to the surface of the agar. The commercially available antibiotic control discs (vancomycin, 5 µg/disk) were also added onto the agar on the same Petri dish. The Petri dishes were incubated for 18 h at 37 °C. Inhibition of bacterial growth was shown as clear zones around the discs. Although the disk diffusion assay is quick and simple, one major drawback of it is that the diffusion of lipophilic extracts or compounds through the media may be impaired on the aqueous agar. This might lead to small zones of inhibition even though the sample being tested has good antibacterial activity. Crude plant extracts from small-scale extraction were tested against SA-1199B using this method in the initial screening. The MIC assay was used preferably to assess the antibacterial activity of fractions and pure compounds.

### **2.5.3 Minimum inhibitory concentration assay**

The minimum inhibitory concentration (MIC) assay is a very useful way to quantify the *in vitro* antibacterial activity of a sample with reference to a control antibiotic. It was used in this project to assist the bioassay-guided fractionation of plant extracts and to determine the activity of extracts, fractions, purified natural products and synthetic derivatives.

All MIC assays were carried out according to the NCCLS guidelines (NCCLS, 1997). All *S. aureus*, *P. aeruginosa* and *S. typhimurium* strains were cultured on nutrient agar (Oxoid) and incubated for 24 h at 37 °C prior to MIC determination. All *Mycobacterium* species were cultured on Columbia agar (Oxoid) supplemented with 7 % defibrinated horse blood (Oxoid). *M. fortuitum*, *M. smegmatis* and *M. phlei* were sub-cultured and incubated for 72 hours at 37 °C prior to the assay.

Mueller-Hinton broth (MHB, Oxoid) was adjusted to contain 20 mg/l and 10 mg/l of Ca<sup>2+</sup> and Mg<sup>2+</sup> respectively. The test samples (approximately 3 mg) were allowed to dissolve in dimethylsulphoxide (DMSO) prior to dilution into MHB, forming a stock solution with a concentration of 2048 µg/ml. This would result in a starting concentration of 512 µg/ml in the first well of the 96-well microtitre plate. For samples that were available in smaller quantities (e.g. 1-2 mg), a lower starting concentration was used (e.g. 128 µg/ml). Tetracycline, oxacillin and ethambutol were dissolved directly into MHB. Norfloxacin, erythromycin and isoniazid were first dissolved in DMSO before being diluted in MHB. Bacterial inocula equivalent to 1 x 10<sup>8</sup> cfu/ml was prepared in normal saline (0.9 % sodium chloride in purified water) by comparison with a 0.5 McFarland turbidity standard and then diluted in normal saline to give an approximate inoculum density of 5 x 10<sup>5</sup> cfu/ml.

MIC assay was carried out using a 96-well microtitre plate (Nunc, 0.3 ml per well). A schematic diagram of a 96-well microtitre plate is shown in Fig. 14. 125 µl of MHB was dispensed into wells 1 to 11 followed by the addition of 125

$\mu\text{l}$  of test solution (control or sample) to well 1. A serial dilution was carried out from well 1 to 10, with the last 125  $\mu\text{l}$  of solution dispensed into well 12. Well 12 was used as a sterile control as it only contained the test solution. 125  $\mu\text{l}$  of bacteria inoculum was then added to wells 1 to 11. Well 11 acted as a growth control as it contained MHB and bacteria only. All samples were tested in duplicate. A DMSO control (3.125 %) was included to show that DMSO did not inhibit any bacterial growth at this concentration and therefore did not interfere with the MIC assay. When more than one bacteria strain was tested, one plate was used for each strain to avoid cross-contamination. The plates were then incubated at 37 °C for the usual incubation time for the strains.

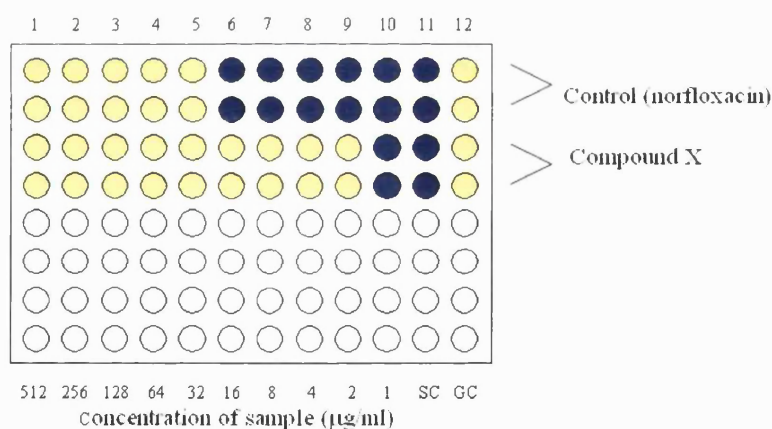


Fig. 14. Schematic diagram showing the determination of MIC of compound X using a 96-microtitre plate. SC: sterile control; GC: growth control

3-[4,5-dimethylthiazol-2-yl]-2,5-diphenyltetrazolium bromide (MTT; Lancaster Synthetics) was used as an indicator to determine bacterial growth. 20  $\mu\text{l}$  of a 5 mg/ml methanolic MTT solution (yellow) was added to each well of the 96-well plate and incubated 37 °C for 20 minutes. A dark blue coloration indicated bacterial growth, as the active mitochondrial reductase enzymes in viable cells caused the reduction of the yellow MTT to a dark blue formazan product (Fig.

15). The MIC was recorded as the lowest concentration at which no growth was observed. In the illustration in Fig. 14, where the starting concentration of the test compound is 512  $\mu\text{g/ml}$ , the MIC of the control antibiotic norfloxacin is 32  $\mu\text{g/ml}$  and that of compound X is 2  $\mu\text{g/ml}$ .

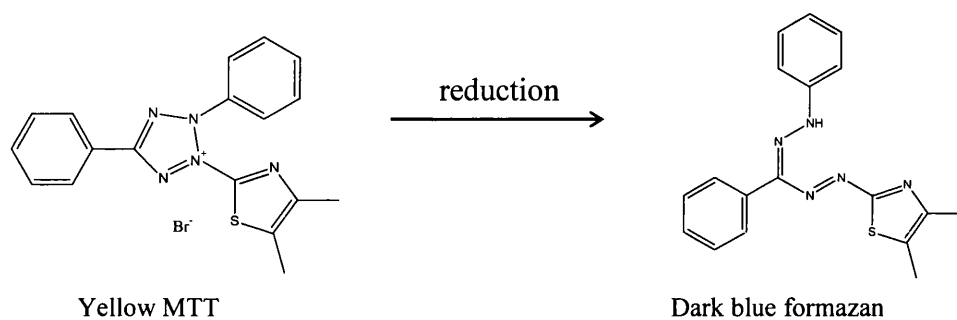
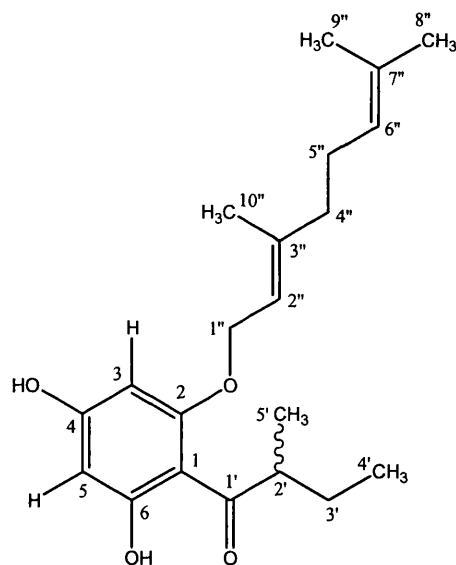


Fig. 15. Reduction of MTT

## 2.6 Synthesis

The acylphloroglucinol isolated from *H. olympicum L. cf. uniflorum*, **WS-09**, showed excellent anti-staphylococcal activity with an MIC at 0.5-1  $\mu\text{g/ml}$  against a panel of *S. aureus* strains. This compound can potentially be further developed and formulated into an antibacterial agent with clinical use. A synthesis method suitable for production of this compound on a large scale was therefore developed and a series of derivatives was synthesized to study the structure-activity relationship of the compounds.



**WS-09**

### 2.6.1 Synthesis of WS-09

A synthetic route of preparing **WS-09** was designed and summarized in Fig. 16. Reactions were initially carried out on a small scale using the commercially available racemic ( $\pm$ )-2-methylbutanoyl chloride (Sigma) as the starting material, giving a racemic ( $\pm$ )-2-*O*-geranyl-2'-methylbutanoyl phloroglucinol (**WS-S-08**).

The successful reactions which gave the desired products with a satisfactory yield were then scaled up using the same conditions. Since a pure enantiomer is often desired in a pharmaceutical product, the commercially available (*S*)-enantiomer of 2-methylbutanoic acid was used as the starting material in the synthesis on a larger scale.

Four steps were involved in the synthesis of (*S*)-2-*O*-geranyl-2'-methylbutanoyl phloroglucinol (**WS-S-07**) and other 2-methylbutanoyl phloroglucinol derivatives: (1) Conversion of (*S*)-methylbutanoic acid to (*S*)-2-methylbutanoyl chloride (Begley *et al.*, 1987); (2) Friedel-Crafts acylation of phloroglucinol (Crombie *et al.*, 1987); (3) Protection of two hydroxyl groups of acylphloroglucinol (Kumazawa *et al.*, 2000; Liu *et al.*, 1996); and (4) Alkylation and deprotection of the acylphloroglucinol (Kumazawa *et al.*, 2000). A summary of all synthesized compounds is shown in Table 6. The purification procedure, structural elucidation and yield of these compounds will be described in the results section (**section 3.3**).

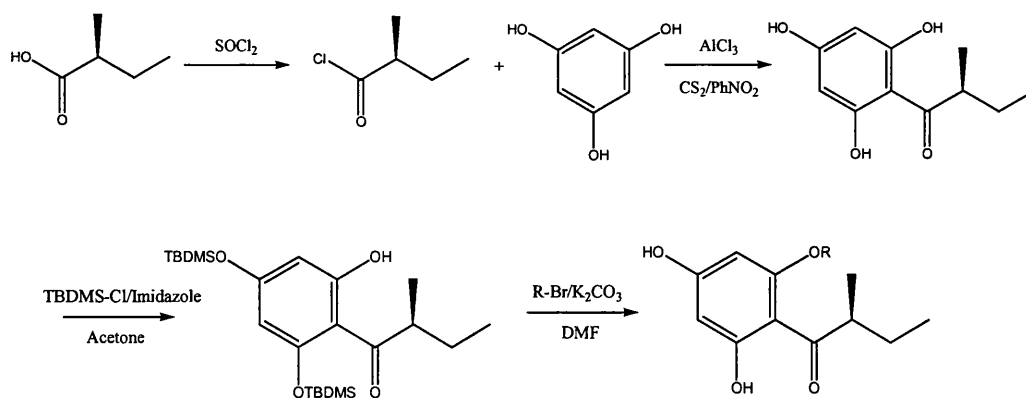


Fig. 16. Reactions involved in the synthesis of (*S*)-2-*O*-geranyl-2'-methylbutanoyl phloroglucinol (**WS-S-07**) and other 2-methylbutanoyl phloroglucinol derivatives.

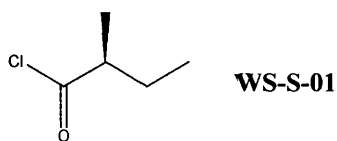


Table 6. Chemical structures of synthetic compounds.

		<b>R<sub>1</sub></b>	<b>R<sub>2</sub></b>	<b>R<sub>3</sub></b>
	<b>WS-S-03</b>	H	MOM	MOM
	<b>WS-S-05</b>	Geranyl	MOM	MOM
	<b>WS-S-08</b>	Geranyl	H	H
	<b>WS-S-02</b>	H	H	H
	<b>WS-S-04</b>	H	TBDMS	TBDMS
	<b>WS-S-06</b>	Prenyl	H	H
	<b>WS-S-07</b>	Geranyl	H	H
	<b>WS-S-09</b>	Farnesyl	H	H
	<b>WS-S-10</b>	3-Methylbutyl	H	H
	<b>WS-S-11</b>	3,7-Dimethyl-octyl	H	H
	<b>WS-S-12</b>	Prenyl	H	H
	<b>WS-S-13</b>	H	Prenyl	H
	<b>WS-S-14</b>	Geranyl	H	H
	<b>WS-S-15</b>	H	Geranyl	H
	<b>WS-S-16</b>	Farnesyl	H	H
	<b>WS-S-17</b>	H	Farnesyl	H
	<b>WS-S-18</b>	3-Methylbutyl	H	H
	<b>WS-S-19</b>	H	3-Methylbutyl	H
	<b>WS-S-20</b>	3,7-Dimethyl-octyl	H	H
	<b>WS-S-21</b>	H	3,7-Dimethyl-octyl	H
	<b>WS-S-22</b>	Pentyl	H	H
	<b>WS-S-23</b>	H	Pentyl	H
	<b>WS-S-24</b>	Decyl	H	H
	<b>WS-S-25</b>	H	Decyl	H

### 2.6.1.1 Step 1: Conversion of (*S*)-2-methylbutanoic acid to (*S*)-2-methylbutanoyl chloride

(*S*)-2-methylbutyric acid (10 g, 97.91 mmol) and thionyl chloride (10.71 ml, 146.9 mmol, 1.5 eq) were heated together at 80 °C under reflux for 2 hours. Purification of the mixture gave (*S*)-2-methylbutanoyl chloride (**WS-S-01**).

### 2.6.1.2 Step 2: Friedel-Crafts acylation of phloroglucinol

Aluminium trichloride (46.43 g, 351.8 mmol, 4.1 eq) was added to a stirring suspension of phloroglucinol (10.81 g, 85.8 mmol, 1 eq) in carbon disulphide (50 ml). Nitrobenzene (40 ml) was added to the solution over 30 min. The solution was then heated under reflux at 55 °C for 30 min. (*S*)-2-methylbutyryl chloride (10.34 g, 85.8 mmol) was dissolved in 5 ml nitrobenzene which was added to the reaction mixture over 30 min, and heated for another 30 min. Purification of the reaction mixture gave (*S*)-2-methylbutanoyl phloroglucinol (**WS-S-02**).

### 2.6.1.3 Step 3: Protection of two hydroxyl groups

#### 2.6.1.3.1 Using methoxymethyl chloride (MOM-Cl) as the protecting group

This reaction was only carried out on ( $\pm$ )-2-methylbutanoyl-phloroglucinol in a small scale as the last deprotection step was unsuccessful (**section 2.6.1.4.1**). To a suspended solution of ( $\pm$ )-2-methylbutanoyl-phloroglucinol (4.65 g, 22.2 mmol) in dry DCM (40 ml) at 0 °C, *N,N*-diisopropylethylamine (8.1 ml, 46.62 mmol, 2.1 eq) was added and the mixture was stirred for 15 min. Methoxymethyl chloride (MOM-Cl; 3.5 ml, 46.62 mmol, 2.1 eq) was added drop-wise at 0 °C and then stirred for another 15 min, after which time the temperature was increased to room temperature with stirring for 45 min. **WS-S-03** was purified from the reaction mixture.

### 2.6.1.3.2 Using *tert*-butyldimethylsilyl chloride (TBDMS-Cl) as the protecting group

Because the deprotection of MOM was unsuccessful with the simultaneous removal of the geranyl side-chain in step 4, the more labile *tert*-butyldimethylsilyl chloride (TBDMS-Cl) was used as the alternative protecting group. (*S*)-2-methylbutanoyl phloroglucinol (9.71 g, 46.19 mmol) was dissolved in 150 ml dry acetone. Imidazole (3.43 g, 138.57 mmol, 3 eq) was added to the solution and stirred for 5 minutes before the addition of TBDMS-Cl (14.61 g, 97.0 mmol, 2.1 eq). The reaction mixture was stirred for 2 hours at room temperature. It was then purified to give **WS-S-04**.

### 2.6.1.4 Step 4: Alkylation and deprotection

#### 2.6.1.4.1 MOM-protected phloroglucinol

MOM-protected phloroglucinol (627.8 mg, 2.11 mmol) was dissolved in dry dimethylformamide (DMF) (5 ml). Anhydrous potassium carbonate (1.5 eq) was added and stirred for approximately 5 minutes before adding geranyl bromide (1.2 eq). The mixture was stirred at 80 °C for 3 hours.

Purification of the reaction mixture afforded **WS-S-05**. **WS-S-05** (185.4 mg, 0.43 mmol) was dissolved in dry dichloromethane (20 ml) and then 2 M HCl (3 ml) was added. The solution was heated at 55 °C under reflux for 1 hour. However, the TLC profile of the mixture suggested that the geranyl side-chain was cleaved as well as the MOM protecting group, resulting in the production of 2-methylbutanoyl phloroglucinol. A weaker acid (trifluoroacetic acid) was also

used as an alternative to remove the MOM group under room temperature. Upon monitoring by TLC, the geranyl side-chain was also removed together with the MOM group after 15 minutes. It was apparent that the geranyl group could easily be removed by the addition of acid, a more labile leaving group would be more desirable, e.g. TBDMS-Cl.

#### **2.6.1.4.2 TBDMS-protected phloroglucinol**

TBDMS-protected phloroglucinol (6.6 g, 15.0 mmol) was dissolved in 100 ml dry DMF, to which anhydrous potassium carbonate was added (3.1 g, 22.5 mmol, 1.5 eq). The mixture was stirred for approximately 5 minutes before the addition of geranyl bromide (3.43 mL, 18 mmol, 1.2 eq). The mixture was heated at 80 °C for 3 hours with stirring. Purification of the reaction gave **WS-S-07**.

#### **2.6.2 Synthesis of 2-methylbutanoyl phloroglucinol derivatives**

The method described above was used to synthesize four other derivatives with different side-chains at an *ortho*- position to the acyl group, resulting in the prenyl (**WS-S-06**), farnesyl (**WS-S-09**), 3-methylbutyl (**WS-S-10**) and 3,7-dimethyloctyl derivatives (**WS-S-11**). The amount of reagents used in step 4 is summarized in Table 7.

Table 7. Amount of reagents used in the synthesis (step 4) of 2-methylbutanoyl phloroglucinol derivatives

Compound	TBDMS protected phloroglucinol	Anhydrous K <sub>2</sub> CO <sub>3</sub> (1.5 eq)	R-Br (1.2 eq)
WS-S-06	114.2 mg, 0.259 mmol	53.7 mg, 0.389 mmol	Prenyl Br 35.88 $\mu$ l, 0.311 mmol
WS-S-09	96.0 mg, 0.218 mmol	45.2 mg, 0.327 mmol	Farnesyl Br 70.9 $\mu$ l, 0.262 mol
WS-S-10	255.0 mg, 0.579 mmol	120.0 mg, 0.869 mmol	3-Methylbutyl Br 86.9 $\mu$ l, 0.695 mmol
WS-S-11	228.0 mg, 0.518 mmol	107.4 mg, 0.777 mmol	3,7-Dimethyloctyl Br 114.0 $\mu$ l, 0.622 mmol

### 2.6.3 Synthesis of acetylphloroglucinol derivatives

In an attempt to synthesize phloroglucinol derivatives in one step without using protecting group chemistry, the commercially available 2,4,6-trihydroxyacetophenone was dissolved in dry acetone, to which 1.5 eq anhydrous K<sub>2</sub>CO<sub>3</sub> was added. The mixture was stirred for 5 minutes before 1.2 eq alkyl bromide was added. The reaction mixture was stirred overnight at room temperature. The amount of reagents used is summarized in Table 8.

There are several advantages of using this method over synthesis using a protecting group. Because the aim of synthesizing these derivatives was to study the structure-activity relationship of the compounds, only a small amount (approximately 5 mg) product is required for structural elucidation and MIC assay. Synthesis without using a protecting group in this reaction resulted in the production of two products (Section 3.3.7), thus generating more derivatives in

one step compared with synthesis using protecting group chemistry. In addition, the reaction method and purification procedure were simpler and quicker than that using a protecting group. However, there were also some downsides in this method. Since the three hydroxyl groups in acetylphloroglucinol were not protected, the position at which alkylation occurred was difficult to predict due to non-selectivity. Another major disadvantage was that the yield was very poor since the reaction was often incomplete, leaving a large quantity of unreacted material in the reaction mixture. If the reaction had to be scaled up, a method using protecting group as discussed earlier would be more appropriate.

Table 8. Amount of reagents used in the synthesis of acetylphloroglucinol derivatives.

Compound	2,4,6-trihydroxy-acetophenone	Anhydrous K <sub>2</sub> CO <sub>3</sub> (1.5 eq)	R-Br (1.2 eq)
<b>WS-S-12, 13</b>	224.0 mg, 1.204 mmol	199.7 mg, 1.806 mmol	Prenyl Br 166.6 µl, 1.445 mmol
<b>WS-S-14, 15</b>	203.9 mg, 1.095 mmol	227.0 mg, 1.643 mmol	Geranyl Br 260.8 µl, 1.314 mmol
<b>WS-S-16, 17</b>	261.2 mg, 1.404 mmol	232.9 mg, 2.106 mmol	Farnesyl Br 456.9 µl, 1.685 mmol
<b>WS-S-18, 19</b>	249.3 mg, 1.338 mmol	221.9 mg, 2.007 mmol	3-Methylbutyl Br 200.8 µl, 1.606 mmol
<b>WS-S-20, 21</b>	258.0 mg, 1.386 mmol	230.1 mg, 2.079 mmol	3,7-Dimethyloctyl Br 345.0 µl, 1.663 mmol
<b>WS-S-22, 23</b>	220.0 mg, 1.182 mmol	196.0 mg, 1.773 mmol	Bromopentane 175.9 µl, 1.418 mmol
<b>WS-S-24, 25</b>	198.0 mg, 1.064 mmol	176.4 mg, 1.596 mmol	Bromodecane 264.0 µl, 1.277 mmol

## CHAPTER THREE

### 3 RESULTS AND DISCUSSION

#### 3.1 Isolation of natural products

##### 3.1.1 *H. forrestii*

The hexane and DCM extracts of *H. forrestii* were active against SA-1199B with MIC values of 512 and 256 µg/ml respectively. The methanol extract did not show any activity at 512 µg/ml. Fractionation of the hexane extract (2.6 g) using a combination of chromatographic techniques did not yield any pure natural products. This was due to the small quantity of a complex extract which contained a large amount of fats. Sephadex chromatography was carried out on the DCM extract (2.2 g), giving eight fractions eluted with chloroform:methanol 1:1 after combining fractions showing similar TLC profiles, and one fraction eluted with 100 % methanol. RP SPE was carried out on fraction 7 (189.4 mg) using an isocratic solvent system of methanol:water 7:3, giving ten fractions. SPE fractions 7 to 10 were combined together (20.7 mg) and purified by p-TLC (C<sub>18</sub>; acetonitrile:water 8:2 and 2 drops of acetic acid) to yield **WS-01** (4.6 mg; R<sub>f</sub> = 0.74). **WS-01** gave a yellow colour reaction with vanillin-sulphuric acid spray. The isolation procedure of **WS-01** is summarized in Fig. 17.

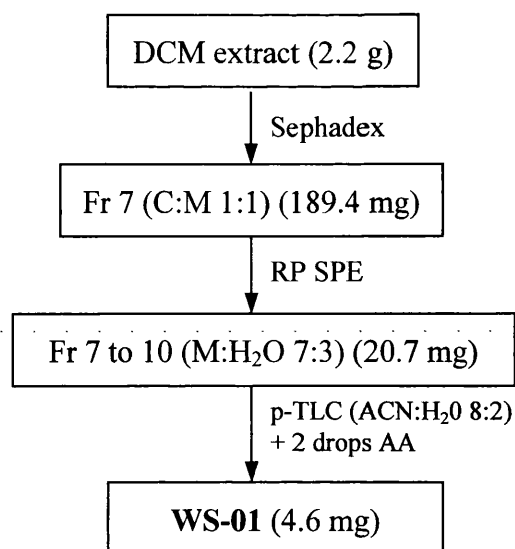


Fig. 17. Isolation of **WS-01** from *H. forrestii* DCM extract.  
Abbreviations: Fr: fraction; C: chloroform; M: methanol;  
ACN: acetonitrile; H<sub>2</sub>O: water; AA: acetic acid

### 3.1.2 *H. moserianum*

Both the hexane and DCM extracts showed anti-staphylococcal activity at a concentration of 256 µg/ml, whereas the methanol extract was not active at 512 µg/ml. Fractionation of the hexane extract (2.1 g) did not yield any pure compound as the majority of this extract consisted of fats and chlorophylls. The DCM extract (2.5 g) was fractionated by VLC using a step-gradient solvent system from 100 % hexane to 100 % ethyl acetate in 10 % increments, with a final methanol wash. Only fractions 6 to 9 showed antibacterial activity (MIC values ranged from 128 to 256 µg/ml). Due to the small quantity of each fraction and the similarity of their TLC profiles, they were combined together to give a fraction of 321.4 mg. Chlorophylls were removed by Sephadex chromatography which gave seven fractions eluted with chloroform and one fraction eluted with methanol. The fraction eluted with methanol (46.3 mg) was purified by p-TLC (silica; TEA 80:18:2), yielding **WS-02** (3.5 mg;  $R_f = 0.75$ ). **WS-02** gave a

yellow colour reaction with vanillin-sulphuric acid spray. The isolation procedure of **WS-02** is summarized in Fig. 18.

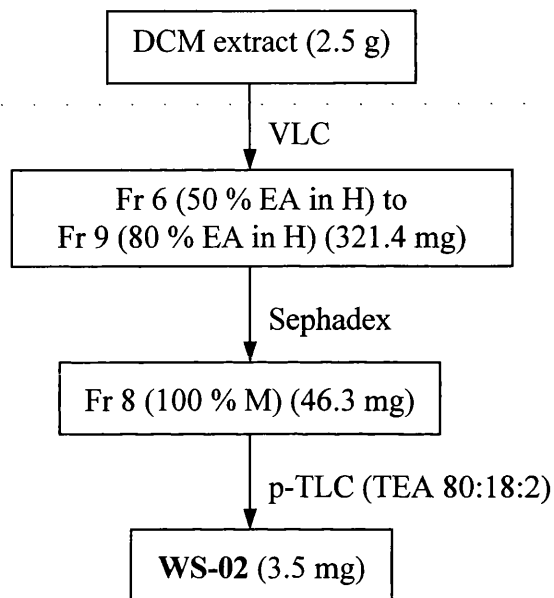


Fig. 18. Isolation of **WS-02** from *H. moserianum* DCM extract. Abbreviations: EA: ethyl acetate; H: hexane

### 3.1.3 *H. beanii*

The hexane, DCM and methanol extracts exhibited MIC values of 16, 64 and 512  $\mu\text{g/ml}$  against SA-1199B respectively. 10.5 g of the hexane extract was fractionated by VLC using a step-gradient solvent system from 100 % hexane to 100 % ethyl acetate in 10 % increments and a final wash with 100 % methanol, yielding 12 fractions. The TLC profile of the original extract and the 12 VLC fractions after spraying with vanillin-sulphuric acid is shown in Fig. 19. Fractions 4 and 5 were the most active with an activity against SA-1199B at 4 - 8  $\mu\text{g/ml}$ . All other fractions were active at 256 - 512  $\mu\text{g/ml}$ .

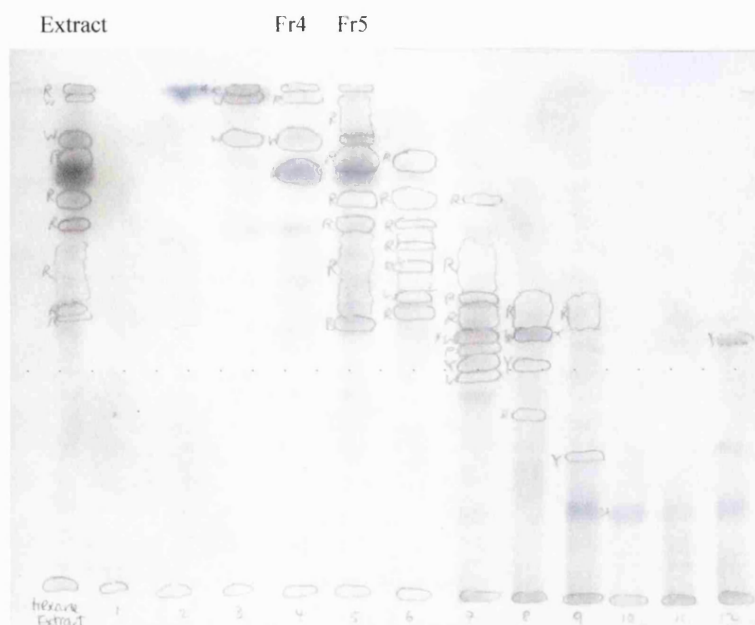


Fig. 19. *H. beanii* hexane extract - TLC profile of the extract and VLC fractions (silica; TEA 80:18:2).

VLC fractions 4 and 5 were combined together to give approximately 2 g of material for further fractionation. However, no pure compounds were isolated from these active fractions after using a combination of separation techniques. This may be due to the instability of compounds present in these fractions. Examples of methods used in an attempt to isolate compounds from the combined fraction are described below.

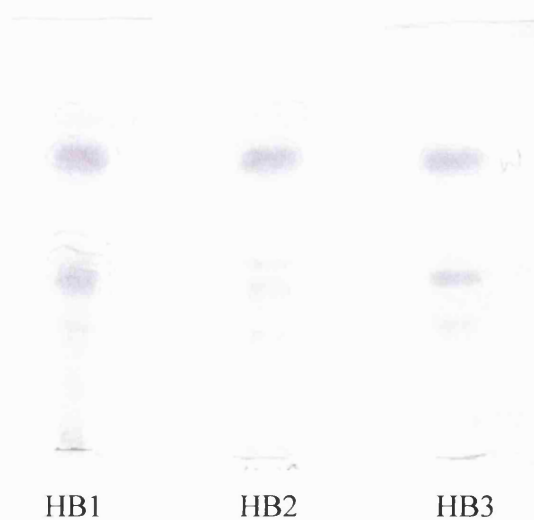


Fig. 20. *H. beanii* hexane extract - TLC profile of active fraction HB1 (silica; TEA 80:18:2). HB2 was purified from HB1 by p-TLC; HB3 was purified from HB1 by p-HPLC.

Fig. 20 shows the TLC profile of an active fraction, HB1, (MIC = 4  $\mu\text{g/ml}$ ) after separation of VLC fractions 4 and 5 by Sephadex chromatography eluted with DCM and then by RP SPE using a step-gradient system from 5 % methanol in water to 100 % methanol. P-TLC on HB1 using silica plates with TEA 80:18:2 as a solvent system was carried out to isolate the main burgundy band on the TLC plate. The isolated components (HB2) were monitored by TLC (TEA 80:18:2) as shown in Fig. 20. HB1 was also analyzed using analytical HPLC and the main peak was isolated by p-HPLC using a step-gradient system from 5 % methanol in water to 100 % methanol with 0.1 % acetic acid over 20 minutes. The main peak (HB3) was collected at 16.2 minutes. The TLC profile of HB3 is shown in Fig. 20. Both HB2 and HB3 were active against SA-1199B at 4  $\mu\text{g/ml}$ . However, further purification of these fractions using p-TLC (both normal-phase and reverse-phase) and isocratic p-HPLC gave the main burgundy band, with several minor bands at a lower  $R_f$  value. The isolation of the minor compounds was also unsuccessful. This may be due to the instability of these compounds, which may readily break down into multiple compounds. This challenge is commonly seen in natural product isolation. Although it would be very interesting to investigate this fraction from a phytochemical point of view, due to the time limitation and the instability of the compound, which is not desirable in a potential antibiotic lead, no further work was carried out on this fraction.

VLC fractions 9 - 11 of the hexane extract were combined together due to the similarity of their TLC profiles. White precipitates were formed upon the addition of methanol. The fraction was washed with methanol three times and then dried, yielding **WS-03** (3.2 mg). It appeared as a purple band after being

sprayed with vanillin-sulphuric acid with an  $R_f$  value of 0.64 (silica; TEA 60:38:2).

Sephadex chromatography of the DCM extract (5.7 g) eluted with DCM yielded five fractions after combining fractions showing similar TLC profiles, and one fraction with a final methanol wash. The fraction eluted with methanol (321.4 mg) was subjected to RP SPE using a step-gradient system with 10 % increments from 100 % water to 100 % methanol, yielding 11 fractions. The fraction eluted with 100 % methanol (46.3 mg), which was active at 64  $\mu\text{g/ml}$ , was further separated by p-TLC using TEA 80:18:2 (silica), yielding **WS-02** (1.7 mg;  $R_f = 0.75$ ) and **WS-04** (1.6 mg;  $R_f = 0.70$ ). The isolation of these natural products from the DCM extract is summarized in Fig. 21.

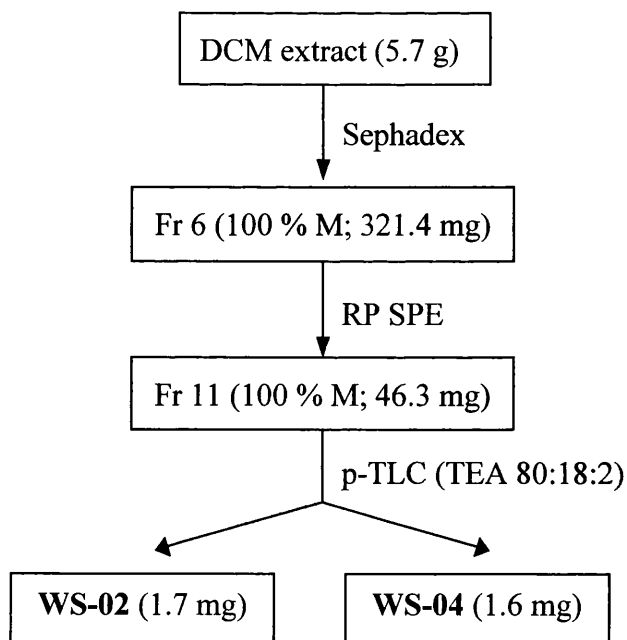


Fig. 21. Isolation of **WS-02** and **WS-04** from *H. beanii* DCM extract.

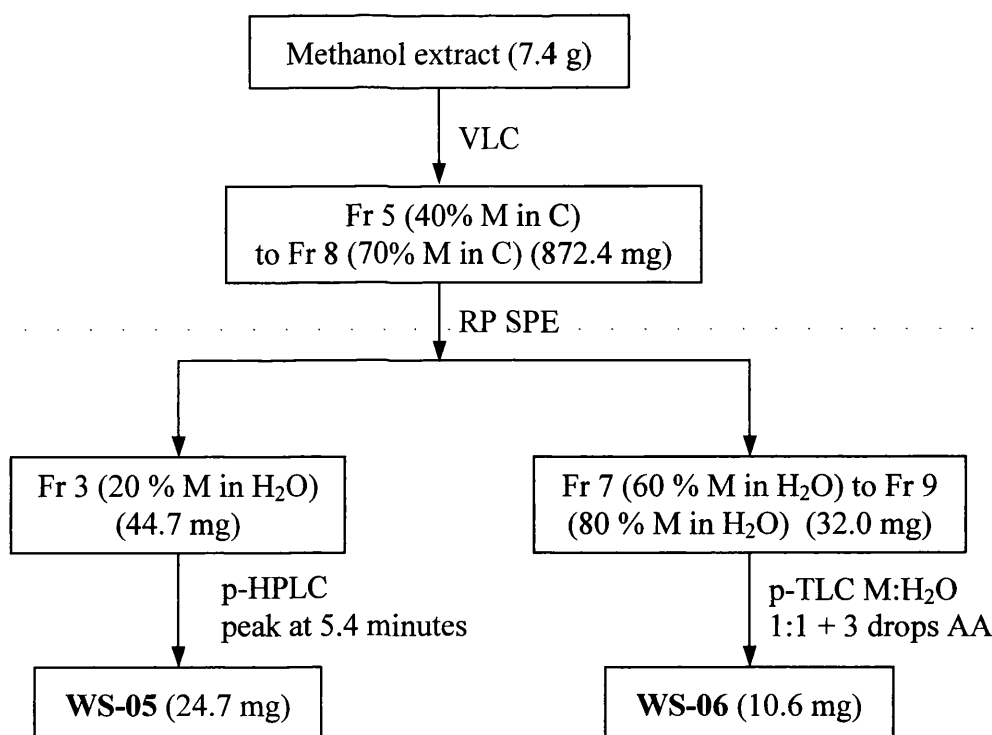


Fig. 22. Isolation of **WS-05** and **WS-06** from *H. beanii* methanol extract.

The methanol extract (7.4 g) was subjected to VLC fractionation over silica gel using a step-gradient solvent system from 100 % chloroform to 100 % methanol, yielding 11 fractions. VLC fractions 5 to 8 were combined together (872.4 mg) and separated using reverse-phase SPE eluted with a step-gradient system from 100 % water to 100 % methanol, yielding 11 fractions. SPE fraction 3 (44.7 mg) was further purified by p-HPLC using a gradient system from 5 % acetonitrile in water to 100 % acetonitrile over 20 minutes. **WS-05** (24.7 mg) was eluted at a retention time of 5.4 minutes. It did not give any colour reaction with vanillin-sulphuric acid spray on TLC plate. SPE fractions 7 to 9 were combined together (32.0 mg) and purified by reverse-phase p-TLC ( $C_{18}$ ; methanol:water 1:1, 3 drops acetic acid), yielding **WS-06** (10.6 mg,  $R_f = 0.83$ ). **WS-06** showed an orange colour reaction with vanillin-sulphuric acid spray on TLC. The methods used to isolate **WS-05** and **WS-06** are summarized in Fig. 22.

### 3.1.4 *H. revolutum ssp. revolutum*

Both the hexane and DCM extracts were active with an MIC value of 256 µg/ml, whereas the methanol extract was not active at a concentration of 512 µg/ml. Fractionation of the hexane extract (3.0 g) did not yield any pure compound. Sephadex chromatography was carried out on the DCM extract (1.8 g) and was eluted with chloroform and methanol in the ratio of 1:1, yielding five fractions and one fraction eluted with 100 % methanol. Fig. 23 shows a TLC profile of the Sephadex fractions together with commercial standards of stigmasterol and β-sitosterol. The TLC plate was viewed under short- and long-wave UV before being sprayed with vanillin-sulphuric acid. Since the phytosterols stigmasterol and β-sitosterol are ubiquitous in plants, running standards alongside with fractions was often useful to determine whether the fractions contained such compounds. The TLC profiles of fractions 4 and 5 showed a burgundy band which had the same  $R_f$  value as the phytosterols, implying that they might be present in these fractions.

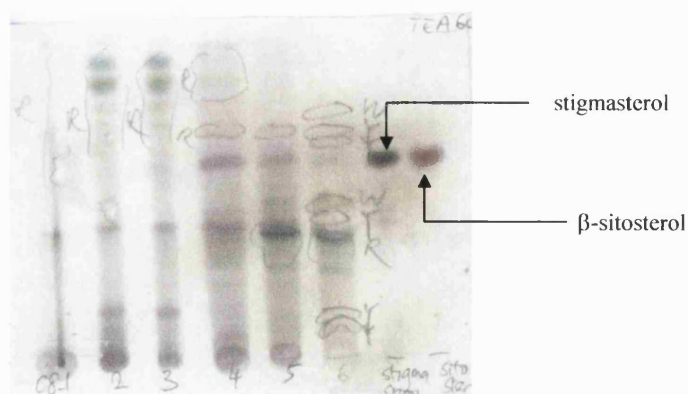


Fig. 23. *H. revolutum ssp. revolutum* DCM extract - TLC profile of Sephadex fractions (silica; TEA 60:38:2).

Fractions 1 to 4 showed no activity at an MIC of 512  $\mu\text{g/ml}$ . From the TLC profile of the Sephadex fractions, it could be seen that fractions 1 to 3 were mainly chlorophylls. Fractions 5 and 6 were weakly active at 256  $\mu\text{g/ml}$ . Fraction 4 (230.8 mg) was fractionated for phytochemical studies. It was subjected to SPE on a silica gel column with a step-gradient system from 100 % hexane to 100 % ethyl acetate with a final methanol wash, giving 12 fractions. SPE fractions 6 to 8 were combined together (27.0 mg) and purified by p-TLC (silica; TEA 60:38:2), giving **WS-07** (2.9 mg;  $R_f = 0.62$ ). **WS-07** turned burgundy after being sprayed with vanillin-sulphuric acid on TLC plate. Sephadex fractions 5 and 6 were combined (147.1 mg) and further fractionated on a Sephadex column, giving eight fractions eluted with chloroform:methanol 1:1 and one fraction eluted in the methanol wash. The fraction eluted with methanol (16.0 mg) was purified by p-TLC (silica) using TEA 60:38:2, yielding **WS-08** (4.5 mg;  $R_f = 0.58$ ). **WS-08** showed a yellow colour-reaction with vanillin-sulphuric acid spray on TLC plate. The isolation of **WS-07** and **WS-08** is summarized in Fig. 24.

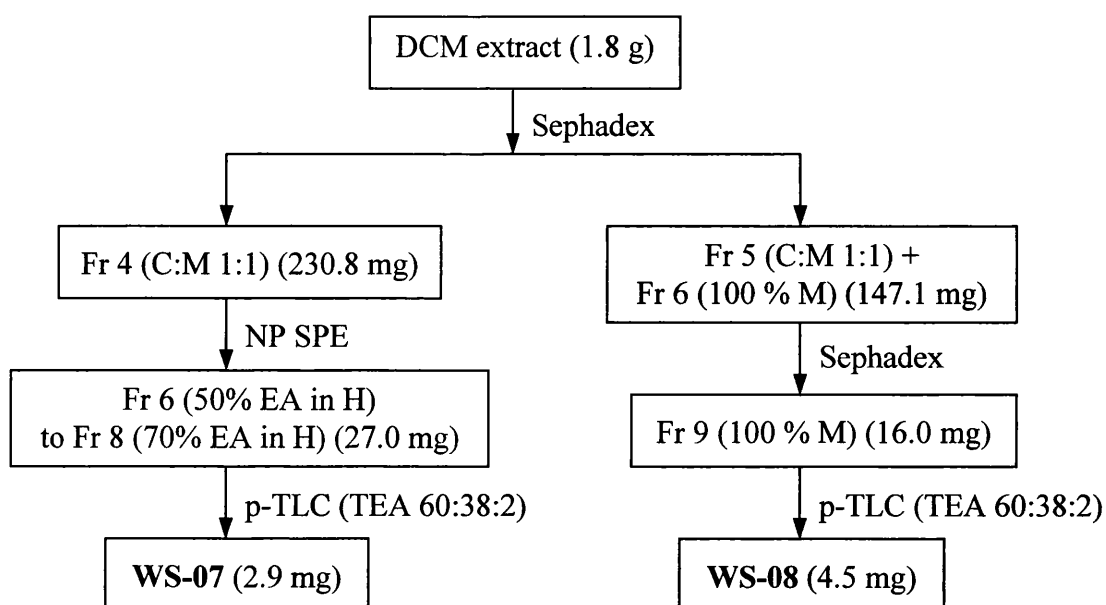


Fig. 24. Isolation of **WS-07** and **WS-08** from *H. revolutum ssp. revolutum* DCM extract.

### 3.1.5 *H. olympicum L. cf. uniflorum*

The hexane and DCM extracts were active at a concentration of 32 and 16  $\mu\text{g/ml}$  respectively, whereas the methanol extract was active at 512  $\mu\text{g/ml}$ . The hexane extract (15.2 g) was fractionated by VLC using a step-gradient solvent system from 100 % hexane to 100 % ethyl acetate with a 10 % increment and a final methanol wash.

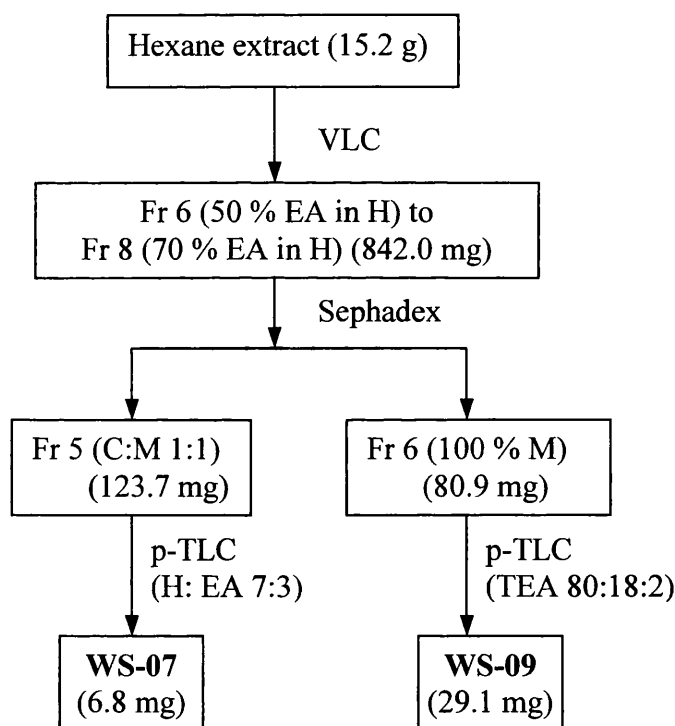


Fig. 25. Isolation of **WS-07** and **WS-09** from *H. olympicum L. cf. uniflorum* hexane extract.

VLC fractions 6 to 8 were active against SA-1199B with an MIC value of 64  $\mu\text{g/ml}$ . They displayed similar TLC profiles and were combined together (842.0 mg). Sephadex was used to separate the combined fraction, giving five fractions eluted with chloroform:methanol 1:1 and one fraction eluted with methanol. Fraction 5 (123.7 mg) was purified by p-TLC (silica) using hexane:ethyl acetate 7:3, yielding **WS-07** (6.8 mg). Sephadex fraction 6 (80.9 mg) was active at an

MIC of 1  $\mu\text{g/ml}$ . **WS-09** (29.1 mg) was isolated from this fraction using p-TLC (silica; TEA 80:18:2,  $R_f = 0.62$ ). **WS-09** gave an orange colour reaction with vanillin-sulphuric acid spray on TLC. The isolation procedure of **WS-07** and **WS-09** from the hexane extract is summarized in Fig. 25.

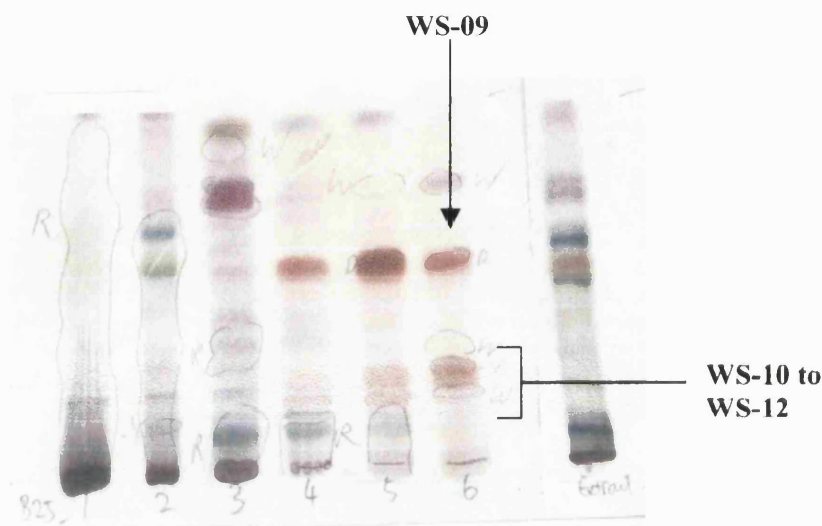


Fig. 26. *H. olympicum L. cf. uniflorum* DCM extract - TLC profile of Sephadex fractions and the original extract (silica; TEA 75:23:2).

2.5 g of DCM extract was applied to a Sephadex column, giving five fractions eluted with chloroform:methanol 1:1 and one fraction eluted with methanol. The TLC profile (silica; TEA 75:23:2) of the six Sephadex fractions and the DCM extract is shown in Fig. 26. Fractions 1 and 2 were not active at 512  $\mu\text{g/ml}$ . Sephadex fractions 4 to 6 exhibited excellent antibacterial activity at 0.5  $\mu\text{g/ml}$ . These fractions were combined (62.0 mg) and were directly purified by p-TLC (silica; TEA 75:23:2), yielding **WS-09** (15.5 mg,  $R_f = 0.71$ ), **WS-10** (4.2 mg,  $R_f = 0.48$ ), **WS-11** (3.8 mg,  $R_f = 0.44$ ) and **WS-12** (1.8 mg,  $R_f = 0.34$ ). Sephadex fraction 3 was active at 512  $\mu\text{g/ml}$ . It was further separated by SPE on a silica gel column using a step-gradient system from 100 % hexane to 100 % ethyl acetate. SPE Fraction 8 (17.8 mg), which was eluted with 70 % ethyl acetate in

hexane was purified by p-TLC (silica; TEA 75:23:2), yielding **WS-13** (1.3 mg,  $R_f = 0.57$ ). **WS-09** to **WS-13** appeared as orange spots on TLC plate after being sprayed with vanillin-sulphuric acid. The isolation procedure of compounds from the DCM extract is summarized in Fig. 27.

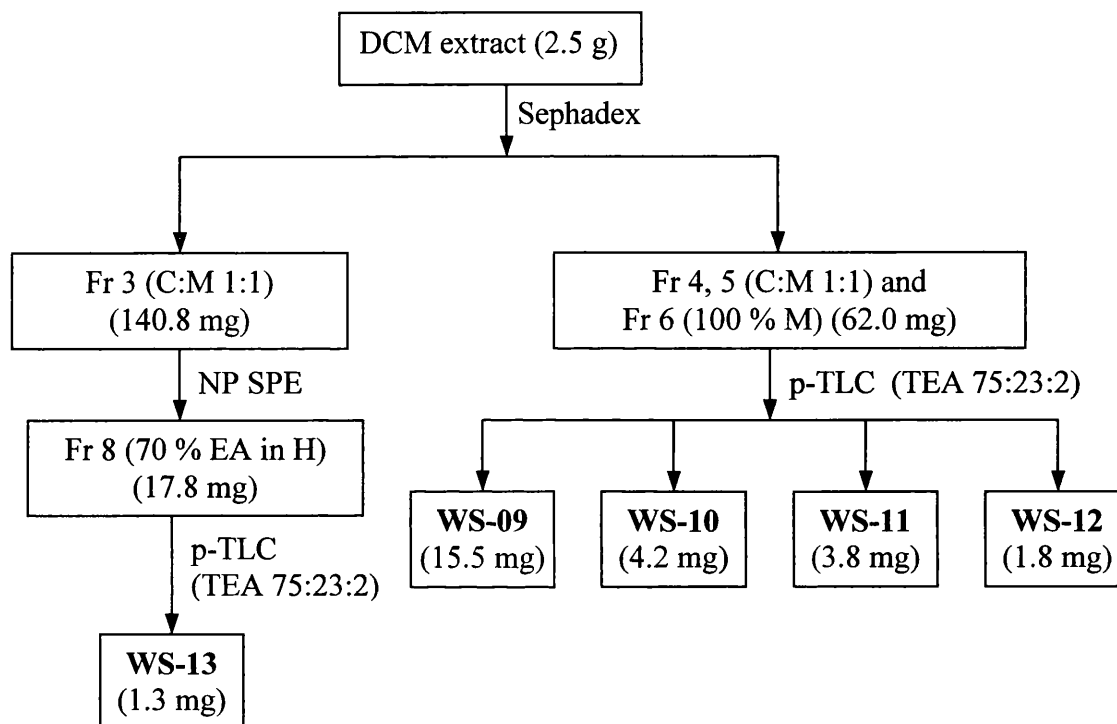


Fig. 27. Isolation of **WS-09** to **WS-13** from *H. olympicum L. cf. uniflorum* DCM extract.

### 3.1.6 *H. choisianum*

The hexane and DCM extract was active against SA-1199B with MIC values of 32 and 128  $\mu\text{g/ml}$  respectively. The methanol extract was, however, not active at a concentration of 512  $\mu\text{g/ml}$ . The hexane extract (9.9 g) was subjected to VLC using a step-gradient solvent system from 100 % hexane to 100 % ethyl acetate with a 10 % increment and a final methanol wash. Fraction 4 (315.1 mg), which was eluted with 30 % ethyl acetate in hexane, was active at 256  $\mu\text{g/ml}$ . This

fraction was further separated using SPE on a C<sub>18</sub> column, giving three fractions eluted with methanol and 1 fraction eluted with acetone. This is an example of the use of SPE cartridges in sample clean-up, as mentioned in **section 2.3.3**.

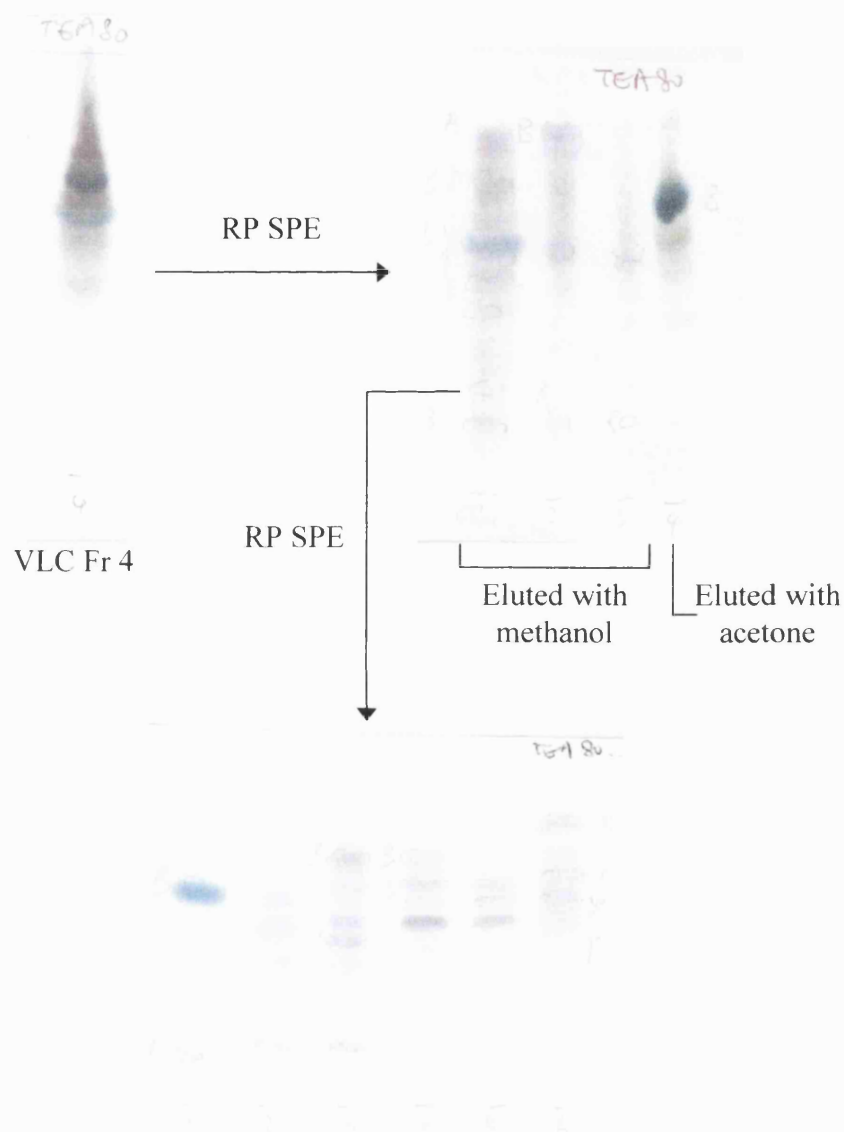


Fig. 28. *H. choisianum* hexane extract - TLC profile of VLC fraction 4 and fractions from further RP SPE separations (silica; TEA 80:18:2).

Fig. 28 shows the TLC profile of VLC fraction 4 and the fractions resulting from RP SPE separation. The compounds of interest were eluted in the first fraction, whereas the more non-polar compounds such as chlorophylls were eluted in the acetone fraction. The first fraction (99.5 mg) was further fractionated using RP SPE in an isocratic mode, giving five fractions eluted with 80 % acetonitrile in

water and one fraction eluted with 100 % acetone as a final wash. It can be seen from Fig. 28 that fraction 1 (19.9 mg) was almost pure. It was purified using p-TLC (silica; TEA 80:18:2), yielding **WS-14** (7.2 mg,  $R_f = 0.59$ ). This compound gave a blue colouration on TLC plate when sprayed with vanillin-sulphuric acid.

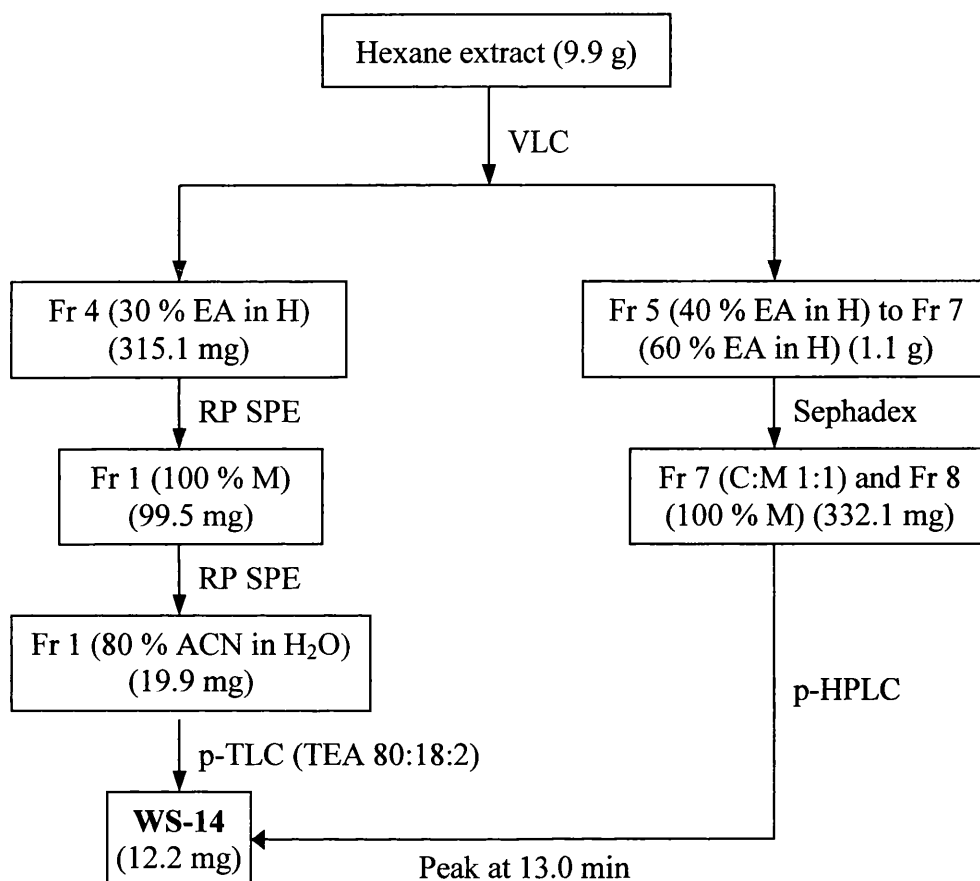


Fig. 29. Isolation of **WS-14** from *H. choisianum* hexane extract.

VLC fractions 5 to 7 from the hexane extract (1.1 g) were applied to a Sephadex column, giving seven fractions eluted with chloroform:methanol 1:1 and one fraction eluted with 100 % methanol. Fractions 7 and 8 were combined together (332.1 mg) and were separated by p-HPLC using a gradient mode from 5 % acetonitrile in water to 100 % acetonitrile over 30 minutes. A peak collected at 13.0 minutes was confirmed by NMR experiments to be **WS-14** (5.0 mg, giving

a total of 12.2 mg). The isolation procedure of **WS-14** from the hexane extract is summarized in Fig. 29.

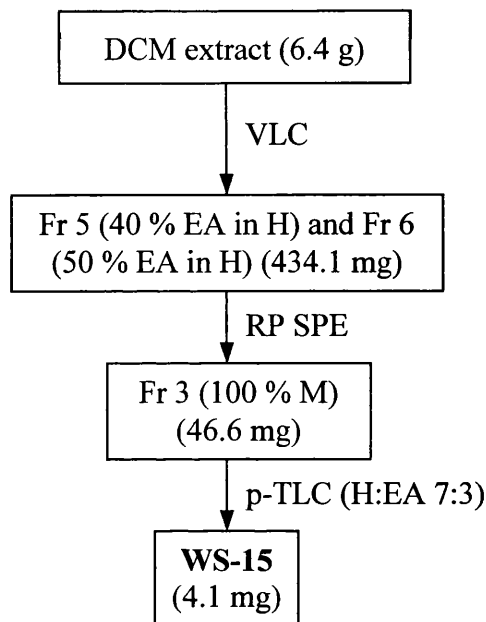


Fig. 30. Isolation of **WS-15** from *H. choisianum* DCM extract.

6.4 g of DCM extract was fractionated by VLC using a step-gradient system from 100 % hexane to 100 % ethyl acetate with a final methanol wash. Fractions 5 and 6 were active at 256 µg/ml. They were combined together (434.1 mg) and fractionated by RP SPE on a C<sub>18</sub> column. Three fractions were eluted with methanol and one fraction was eluted with acetone as a final wash. Fraction 3 (46.6 mg) was further separated by p-TLC (silica; hexane:ethyl acetate 7:3), yielding **WS-15** (4.1 mg, R<sub>f</sub> = 0.48). This compound appeared burgundy on TLC plate after being sprayed with vanillin-sulphuric acid. The isolation procedure of **WS-15** from the DCM extract is shown in Fig. 30.

## 3.2 Characterization of natural products

### 3.2.1 Characterization of WS-01 as 2,5-dihydroxy-1-methoxy-xanthone

**WS-01** was isolated as a yellow oil from the DCM extract of *H. forrestii*. The HR ESI-MS gave an  $[M+H]^+$  ion at  $m/z$  259 in accordance with a molecular formula of  $C_{14}H_{10}O_5$ . The  $^{13}C$  NMR (Table 9) and DEPT data showed the presence of one methoxyl group ( $\delta_C$  62.2), one carbonyl carbon ( $\delta_C$  178.6) and twelve aromatic carbons, including five deshielded carbons with resonances between  $\delta_C$  146.5 to 151.9, five methine carbons with resonances between  $\delta_C$  115.3 to 125.3 and two quaternary carbons ( $\delta_C$  117.2 and 124.0). These signals together with the mass spectrometry data are indicative of a methoxy-substituted xanthone (Minami *et al.*, 1996).

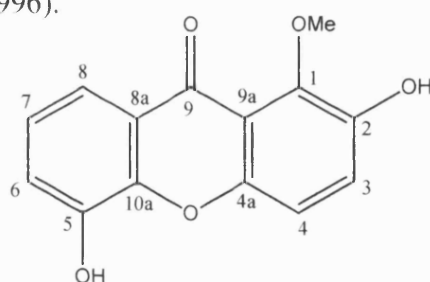


Fig. 31. Structure of **WS-01**.

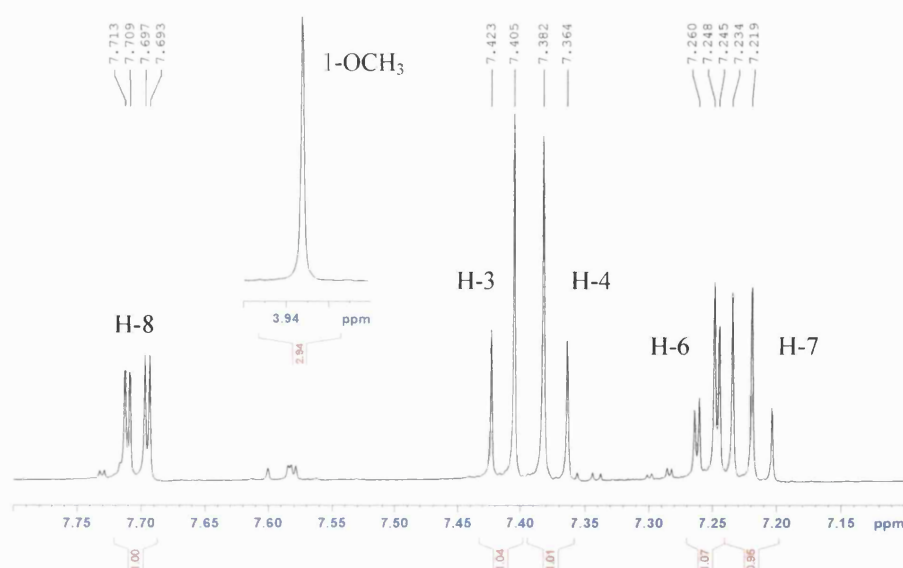


Fig. 32.  $^1H$  NMR spectrum of **WS-01** in methanol- $d_4$  recorded at 500 MHz.

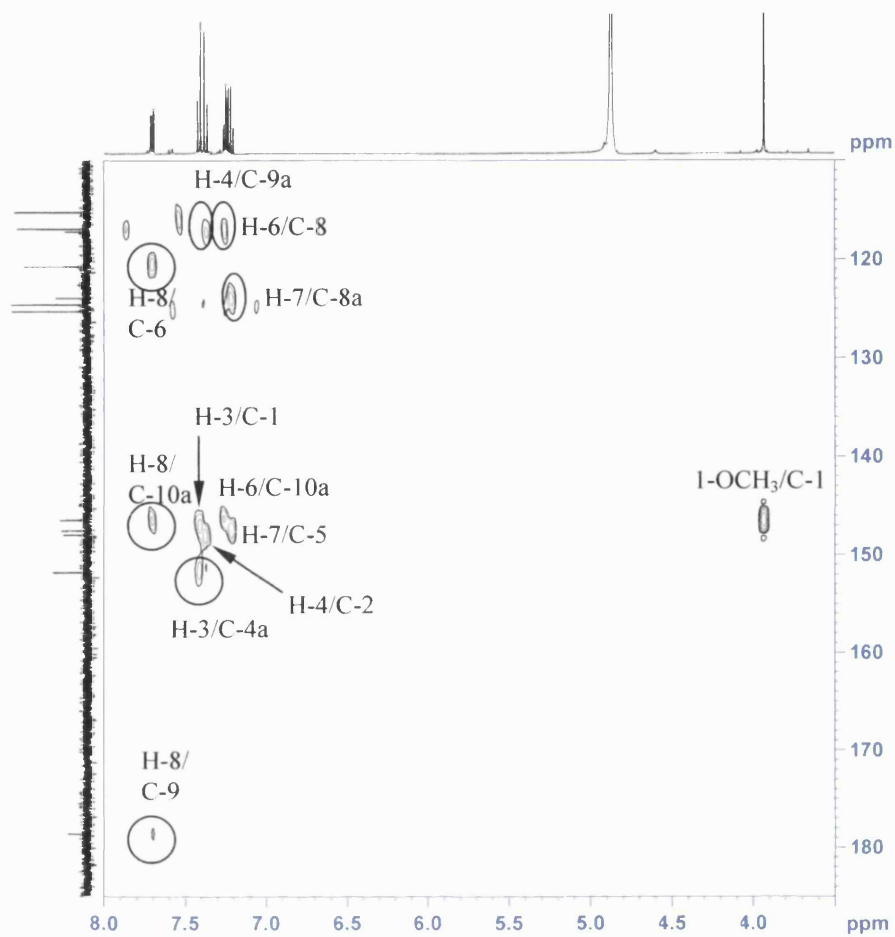


Fig. 33. HMBC spectrum of **WS-01**.

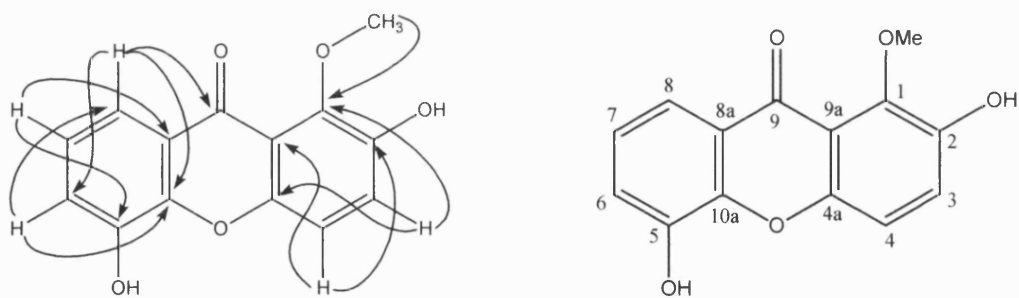


Fig. 34. HMBC correlations for **WS-01**.

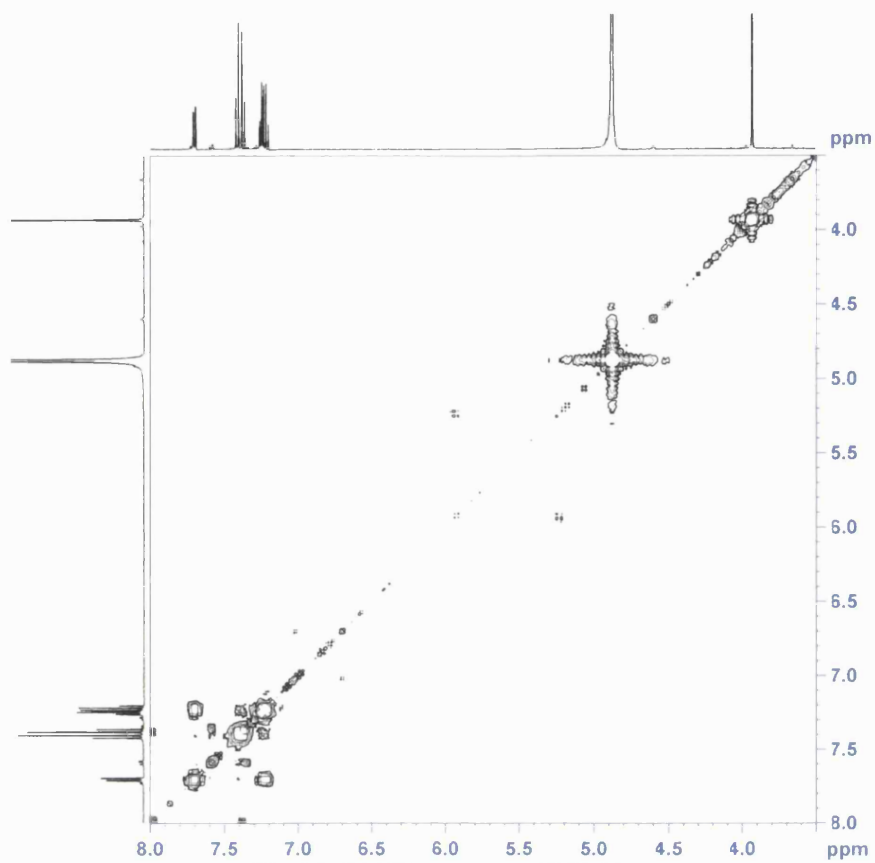


Fig. 35. COSY spectrum of **WS-01**.

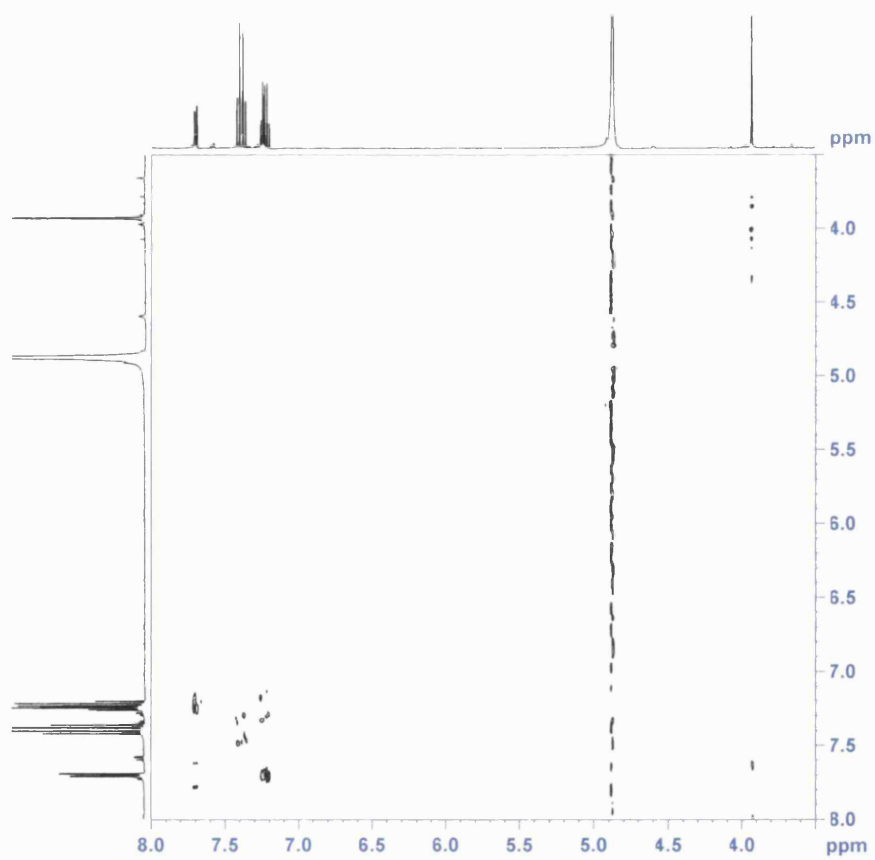


Fig. 36. NOESY spectrum of **WS-01**.

The  $^1\text{H}$  NMR spectrum (Fig. 32) revealed three aromatic protons in an ABC system with resonances at  $\delta_{\text{H}}$  7.25 (dd,  $J = 2, 8$  Hz, H-6),  $\delta_{\text{H}}$  7.22 (t,  $J = 7.5$  Hz, H-7) and  $\delta_{\text{H}}$  7.70 (dd,  $J = 2, 8$  Hz, H-8) and two *ortho*-coupled aromatic protons with resonances at  $\delta_{\text{H}}$  7.41 (d,  $J = 9$  Hz, H-3) and  $\delta_{\text{H}}$  7.37 (d,  $J = 9$  Hz, H-4). These proton-proton correlations were also confirmed on the COSY and NOESY spectra (Fig. 35, 36). Assuming a xanthone nucleus, the proton at  $\delta_{\text{H}}$  7.70 (H-8) in the ABC system displayed a  $^3J$  HMBC correlation with the carbonyl carbon, an oxygenated carbon ( $\delta_{\text{C}}$  146.5, C-10a) and a methine carbon ( $\delta_{\text{C}}$  120.8, C-6), thus placing it at C-8 (Fig. 33, 34). The other protons in the ABC system (H-6 and H-7) were therefore placed at C-6 and C-7. This was further confirmed by  $^3J$  HMBC correlations between H-6 and C-10a and C-8, and between H-7 and C-5 and C-8a (Fig. 33, 34). The methoxyl singlet showed a long-range  $^1\text{H}$ - $^{13}\text{C}$  correlation to a carbon at  $\delta_{\text{C}}$  146.5 to which it was directly attached. Finally, the *ortho*-coupled protons at  $\delta_{\text{H}}$  7.41 (H-3) and  $\delta_{\text{H}}$  7.37 (H-4) were placed at C-3 and C-4. This was confirmed by  $^3J$  HMBC correlations between H-3 and the oxygenated carbons at C-1 ( $\delta_{\text{C}}$  146.5) and C-4a ( $\delta_{\text{C}}$  151.9), and between H-4 and C-2 ( $\delta_{\text{C}}$  148.1) and C-9a ( $\delta_{\text{C}}$  117.2) (Fig. 33, 34). The substituents at C-2 and C-5 were found to be hydroxyl groups according to the mass spectrometry data. **WS-01** was identified as 2,5-dihydroxy-1-methoxyxanthone, which has been isolated from *Garcinia subelliptica* previously (Minami *et al.*, 1996). The NMR data were in close agreement with the published data.

Table 9.  $^1\text{H}$  (500MHz) and  $^{13}\text{C}$  NMR (125 MHz) spectral data and  $^1\text{H}$ - $^{13}\text{C}$  long-range correlations of **WS-01** recorded in methanol- $d_4$ .

WS-01 (methanol- $d_4$ )					Minami <i>et al.</i> , 1996 (DMSO- $d_6$ )	
Position	$^1\text{H}$ (J, Hz)	$^{13}\text{C}$	$^2J$	$^3J$	$^1\text{H}$ (J, Hz)	$^{13}\text{C}$
1	-	146.5	-	-	-	145.1
2	-	148.1	-	-	-	146.6
3	7.41 d (9)	125.3		C-1, C-4a	7.38 d (9.3)	124.0
4	7.37 d (9)	115.3		C-2, C-9a	7.29 d (9.3)	113.7
4a	-	151.9	-	-	-	149.5
5	-	147.6	-	-	-	146.2
6	7.25 dd (2, 8)	120.8	-	C-8, C-10a	7.24 dd (1.5, 7.8)	119.3
7	7.22 t (7.5)	124.6	-	C-5, C-8a	7.19 t (7.8)	123.4
8	7.70 dd (2, 8)	117.0	-	C-6, C-9, C-10a	7.53 dd (1.5, 7.8)	115.2
8a	-	124.0	-	-	-	122.6
9	-	178.6	-	-	-	175.4
9a	-	117.2	-	-	-	116.1
10a	-	146.5	-	-	-	144.4
1-OCH <sub>3</sub>	3.93 s	62.2	-	C-1	3.80 s	61.0

### 3.2.2 Characterization of WS-02 as 1,7-dihydroxyxanthone (euxanthone)

WS-02 was isolated as a yellow oil from the DCM extracts of *H. beanii* and *H. moserianum*. The ESI-MS gave the  $[M+H]^+$  ion at  $m/z$  229 in accordance with a molecular formula of  $C_{13}H_8O_4$ . The  $^{13}C$  NMR spectrum displayed twelve signals in the aromatic region and a carbonyl signal ( $\delta_C$  183.5, C-9) (Table 10). The DEPT-135 spectrum showed six positive signals, indicating that seven quaternary carbons were present and that methylene groups were absent. Of the seven quaternary carbons, one carbonyl carbon ( $\delta_C$  183.5) and four deshielded carbons ( $\delta_C$  151.5, 155.6, 157.9 and 163.0) were observed. These signals were characteristic for a xanthone nucleus (Li *et al.*, 1998).

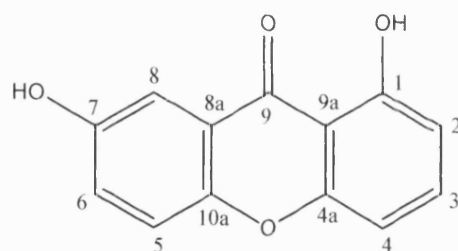


Fig. 37. Structure of WS-02.

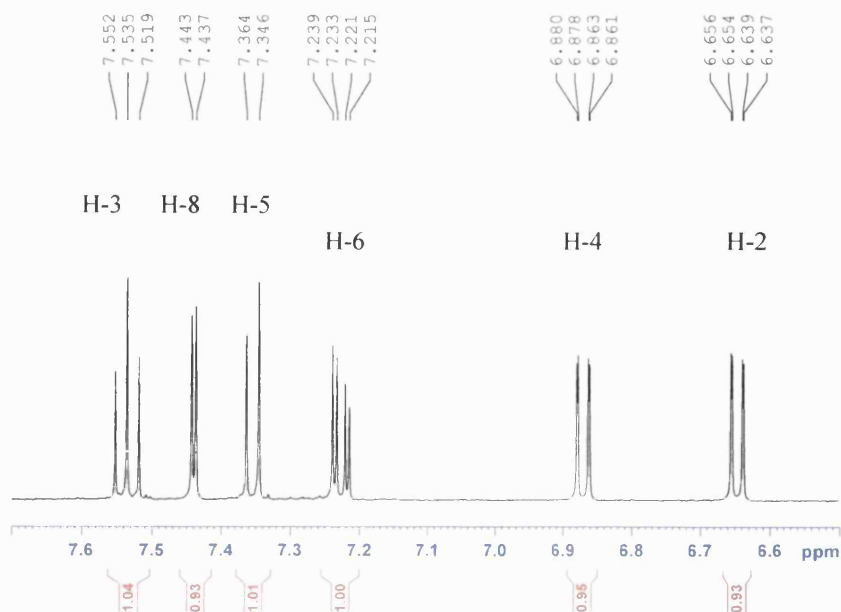


Fig. 38.  $^1H$  NMR spectrum of WS-02 in methanol- $d_4$  recorded at 500 MHz.

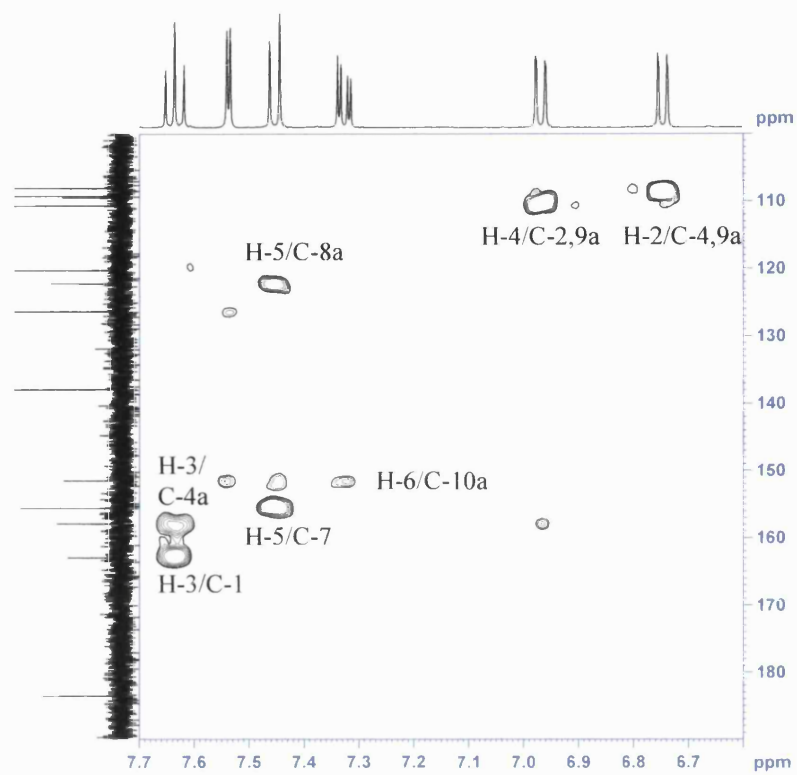


Figure 39. HMBC spectrum of **WS-02**.

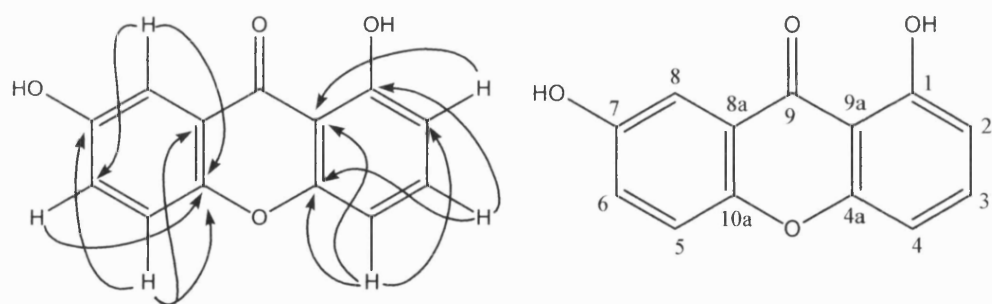


Fig. 40. HMBC correlations for **WS-02**.

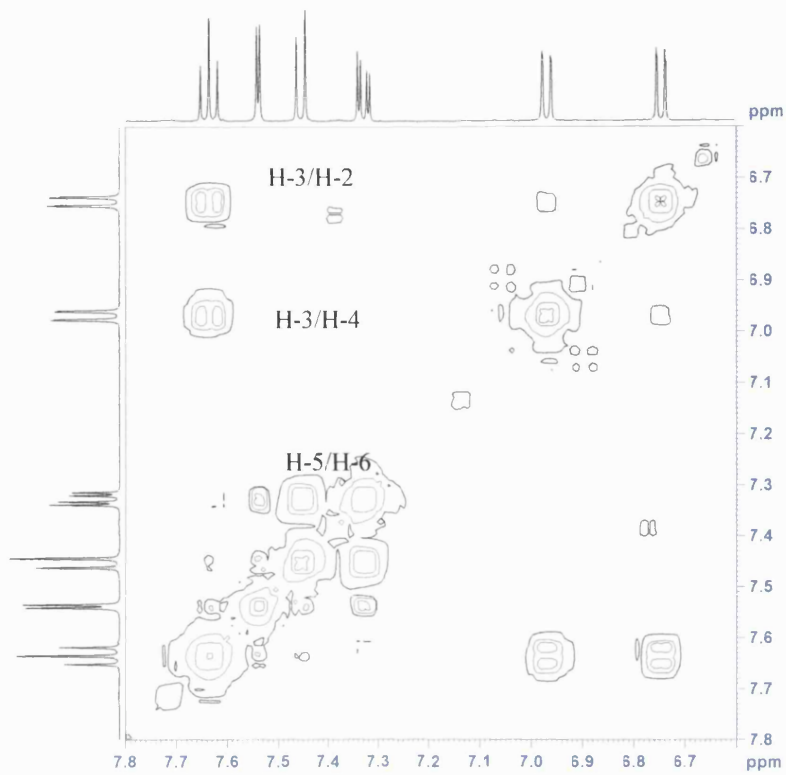


Figure 41. COSY spectrum of **WS-02**.

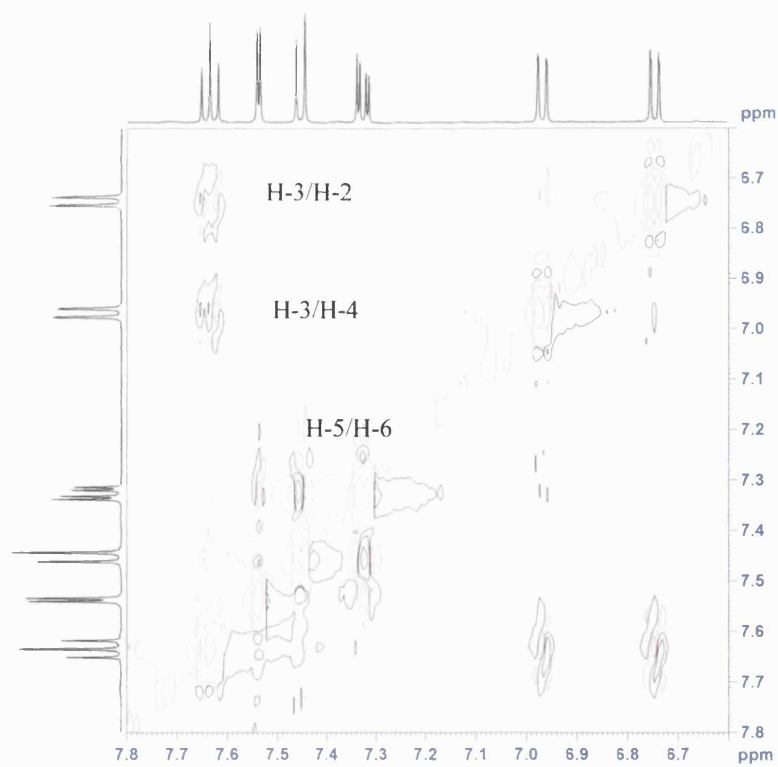


Figure 42. NOESY spectrum of **WS-02**.

The  $^1\text{H}$  NMR spectrum (Fig. 38) revealed three aromatic hydrogens in an ABD system with resonances at  $\delta_{\text{H}}$  7.45 (d,  $J = 9$  Hz, H-5),  $\delta_{\text{H}}$  7.33 (dd,  $J = 3, 9$  Hz, H-6) and  $\delta_{\text{H}}$  7.54 (d,  $J = 3$  Hz, H-8) and three aromatic protons in an ABC system with resonances at  $\delta_{\text{H}}$  6.75 (dd,  $J = 1, 8$  Hz, H-2),  $\delta_{\text{H}}$  7.64 (t,  $J = 8$  Hz, H-3) and  $\delta_{\text{H}}$  6.97 (dd,  $J = 1, 8.5$  Hz, H-4). The NOESY spectrum (Fig. 42) showed significant cross-peaks between H-2 and H-3, and between H-3 and H-4, indicating that these protons are in close proximity in space. These correlations were also seen in the COSY spectrum (Fig. 41). In addition, the COSY spectrum showed a correlation between the two *ortho*- protons (H-5 and H-6) in the ABD system. Since H-3 and H-6 showed correlations with C-4a and C-10a respectively in the HMBC spectrum (Fig. 39, 40), they were placed at position C-3 and C-6 rather than at C-2 and C-7, thus placing the hydroxyl groups at C-1 and C-7. **WS-02** was identified as 1,7-dihydroxyxanthone. The NMR data for this compound were in close agreement with the published data (Li *et al.*, 1998).

Table 10.  $^1\text{H}$  (500MHz) and  $^{13}\text{C}$  NMR (125 MHz) spectral data and  $^1\text{H}$ - $^{13}\text{C}$  long-range correlations of **WS-02** recorded in methanol- $d_4$ .

WS-02 (methanol- $d_4$ )					1,7-dihydroxyxanthone (DMSO- $d_6$ ) (Li <i>et al.</i> , 1998)	
Position	$^1\text{H}$ ( $J$ , Hz)	$^{13}\text{C}$	$^2J$	$^3J$	$^1\text{H}$ ( $J$ , Hz)	$^{13}\text{C}$
1	-	163.0	-	-	-	161.0
2	6.75 dd (1, 8)	110.7	-	C-4, C-9a	6.63 d (8.4)	109.4
3	7.64 t (8)	137.9	-	C-1, C-4a	7.54 t (8.4)	136.8
4	6.97 dd (1, 8.5)	108.1	C-4a	C-2, C-9a	6.83 d (8.4)	106.9
4a	-	157.9	-	-	-	155.8
5	7.45 d (9)	120.3	C-10a	C-7, C-8a	7.34 d (8.9)	119.5
6	7.33 dd (3, 9)	126.4	-	C-10a	7.24 dd (2.9, 8.9)	125.4
7	-	155.6	-	-	-	154.4
8	7.54 d (3)	109.3	-	C-6, C-10a	7.32 d (2.9)	107.9
8a	-	122.2	-	-	-	120.4
9	-	183.5	-	-	-	181.4
9a	-	109.5	-	-	-	107.8
10a	-	151.5	-	-	-	149.3

### 3.2.3 Characterization of WS-03 as a mixture of stigmasterol and $\beta$ -sitosterol

WS-03 was isolated as an amorphous solid from the hexane extract of *H. beanii*. The  $^1\text{H}$  NMR spectrum of WS-03 showed signals corresponding to that of stigmasterol (Fig. 44) and  $\beta$ -sitosterol (section 3.2.7), which are phytosterols in plants.

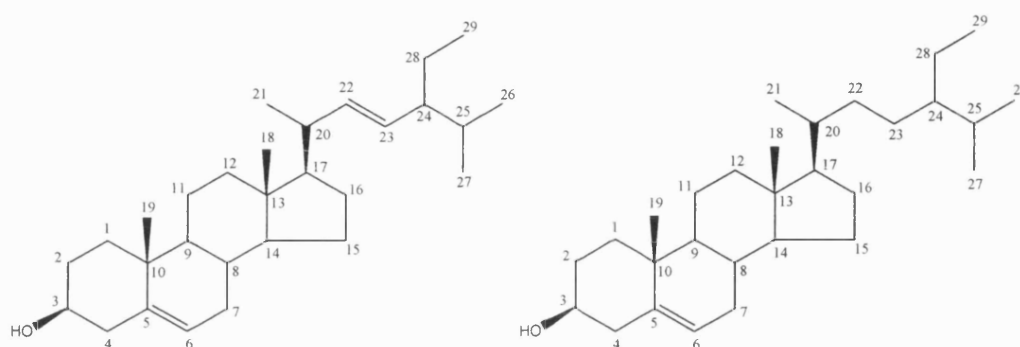


Fig. 43. Structures of stigmasterol (left) and  $\beta$ -sitosterol (right).

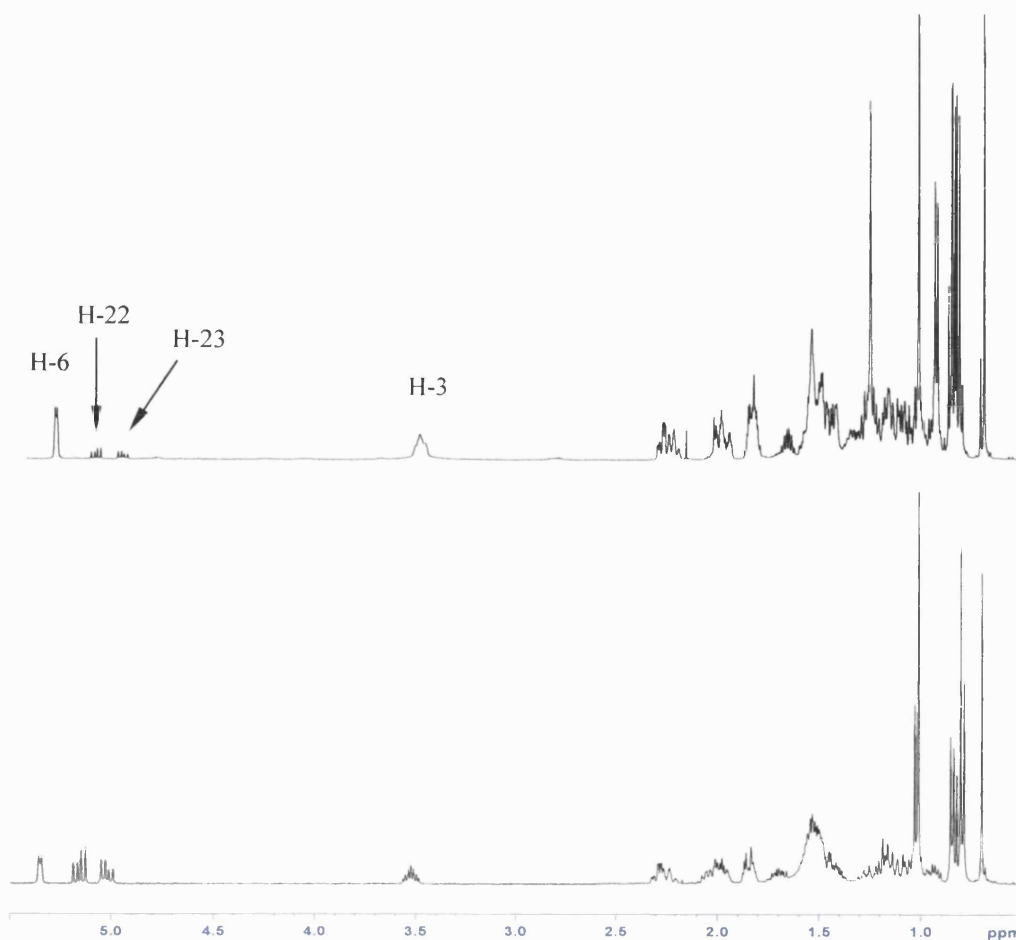


Fig. 44.  $^1\text{H}$  NMR spectrum of WS-03 (top) and stigmasterol standard (bottom) in chloroform-*d* recorded at 500 MHz.

The main features of the  $^1\text{H}$  NMR spectrum of stigmasterol included three olefinic protons in the  $\delta_{\text{H}}$  5.0 - 5.5 domain (H-6, H-22, H-23), an oxymethine multiplet at  $\delta_{\text{H}}$  3.54 (H-3), a series of methylene multiplets in the  $\delta_{\text{H}}$  1.0 - 2.4 region, two methyl singlets ( $\delta_{\text{H}}$  0.69, H-18;  $\delta_{\text{H}}$  1.02, H-19), three methyl doublets ( $\delta_{\text{H}}$  0.93, H-21;  $\delta_{\text{H}}$  0.85, H-26;  $\delta_{\text{H}}$  0.83, H-27) and a methyl triplet ( $\delta_{\text{H}}$  0.82, H-29). Two of the olefinic protons appeared as double doublets at  $\delta_{\text{H}}$  5.16 ( $J = 9, 15.5$  Hz; H-22) and  $\delta_{\text{H}}$  5.03 ( $J = 8.5, 15$  Hz; H-23). A large coupling constant of 15 Hz indicated that these two protons were coupled through a *trans*- double bond. Confirmation of the presence of stigmasterol was achieved by the comparison of the  $^1\text{H}$  NMR spectrum of **WS-03** with that of a stigmasterol commercial standard (Fig. 44). The  $^1\text{H}$  and  $^{13}\text{C}$  NMR data were in close agreement with the published literature (Forgo and Kövér, 2004) (Table 11). The main features of the  $^1\text{H}$  NMR spectrum of  $\beta$ -sitosterol will be discussed in section 3.2.7.

Table 11.  $^1\text{H}$  (500MHz) and  $^{13}\text{C}$  NMR (125 MHz) spectral data of **WS-03** recorded in chloroform-*d*.

Position	WS-03		Forgo and Kövér, 2004 Chloroform- <i>d</i>	
	$^1\text{H}$ ( <i>J</i> , Hz)	$^{13}\text{C}$	$^1\text{H}$ ( <i>J</i> , Hz)	$^{13}\text{C}$
1	1.10 m, 1.85 m	37.3	1.08 m, 1.84 m	37.6
2	1.52 m, 1.83 m	31.7	1.51 m, 1.83 m	31.9
3	3.54 m	71.8	3.51 m	72.0
4	2.25 m, 2.30 m	42.3	2.23 m, 2.30 m	42.5
5	-	140.8	-	140.8
6	5.36 m	121.7	5.34 m	121.8
7	1.52 m, 1.97 m	31.9	1.50 m, 1.97 m	32.1
8	1.48 m	31.9	1.46 m	32.2
9	0.95 m	50.2	0.94 m	50.5
10	-	36.5	-	36.5
11	1.51 m	21.1	1.50 m	21.1
12	1.19 m, 2.01 m	39.8	1.18 m, 2.00 m	40.4
13	-	42.3	-	42.2
14	1.04 m	56.8	1.01 m	57.1
15	1.07 m, 1.56 m	24.3	1.06 m, 1.56 m	24.5
16	1.27 m, 1.69 m	28.2	1.28 m, 1.71 m	28.9
17	1.17 m	56.1	1.15 q	56.3
18	0.69 s	11.9	0.70 s	12.2
19	1.02 s	19.0	1.01 s	19.5
20	2.04 m	40.4	2.06 m	40.4
21	0.93 d (6.5)	19.8	1.03 d	21.4
22	5.16 dd (9, 15.5)	138.3	5.17 dd	138.3
23	5.03 dd (8.5, 15)	129.3	5.04 dd	129.7
24	1.53 m	51.3	1.54 m	51.5
25	1.56 m	31.9	1.55 m	32.2
26	0.85 d (8.5)	19.4	0.85 d	21.2
27	0.83 d (8.5)	18.8	0.80 d	19.2
28	1.17 m, 1.45 m	26.2	1.18 m, 1.43 m	25.4
29	0.82 t (8.5)	12.0	0.81 t	12.2

**3.2.4 Characterization of WS-04 as a mixture of 2,4-dihydroxy-6-methoxy-3-methyl-1-(2'-methylpropionyl)-benzene (WS-04a) and 2,4-dihydroxy-6-methoxy-3-methyl-1-(2'-methylbutanoyl)-benzene (WS-04b)**

WS-04a and WS-04b were isolated as a pale yellow oil from the DCM extract of *H. beanii* in a ratio of 5:2. HR ESI-MS of the mixture gave the  $[M+H]^+$  ions at  $m/z$  225 and 239, suggesting the molecular formulae of  $C_{12}H_{16}O_4$  (WS-04a) and  $C_{13}H_{18}O_4$  (WS-04b) respectively. Due to the similarity in polarity and size of these compounds, it was not possible to further purify WS-04a and WS-04b.

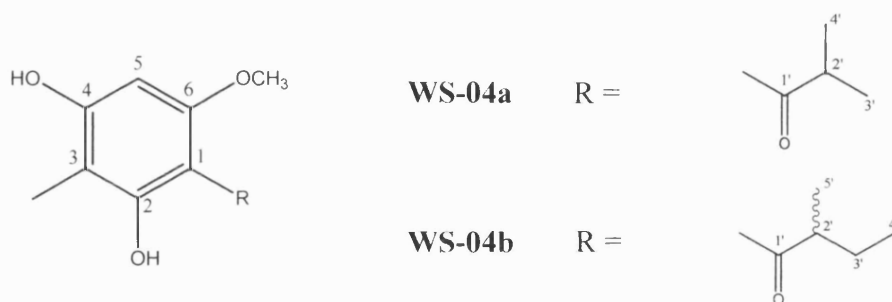


Fig. 45. Structures of WS-04a and WS-04b.

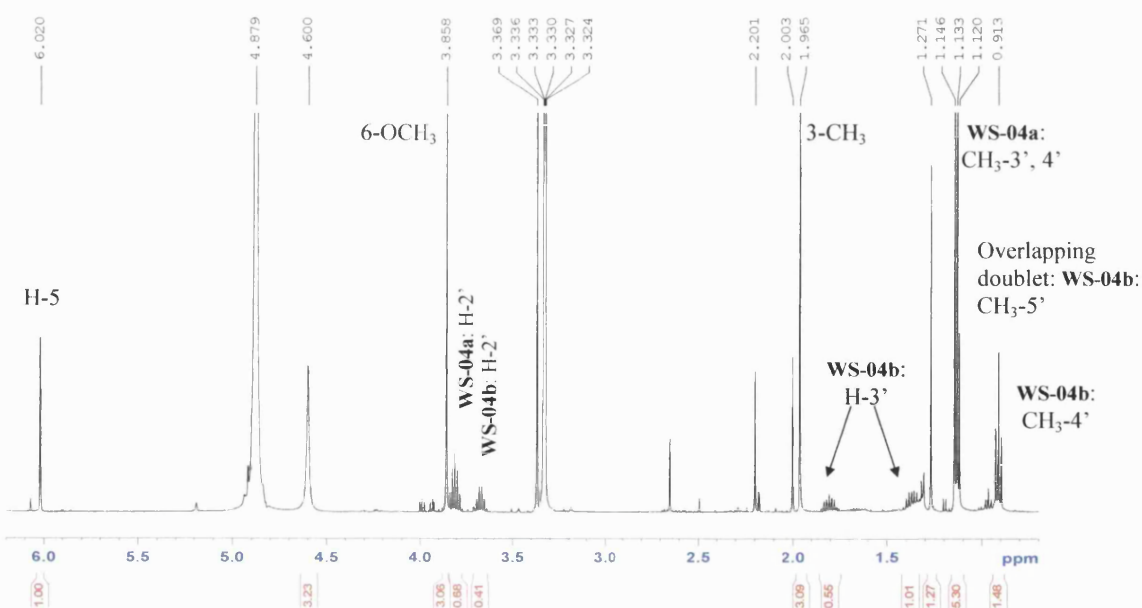


Fig. 46.  $^1H$  NMR spectrum of WS-04 in methanol- $d_4$  recorded at 500 MHz.



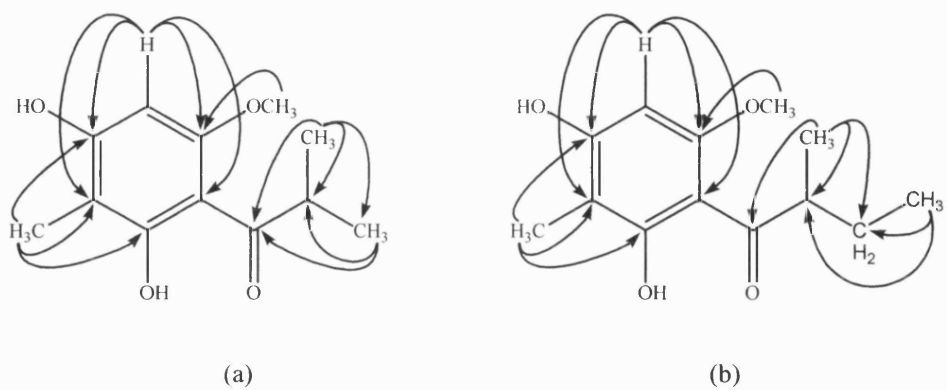


Fig. 49. HMBC correlations for **WS-04a** and **WS-04b**.

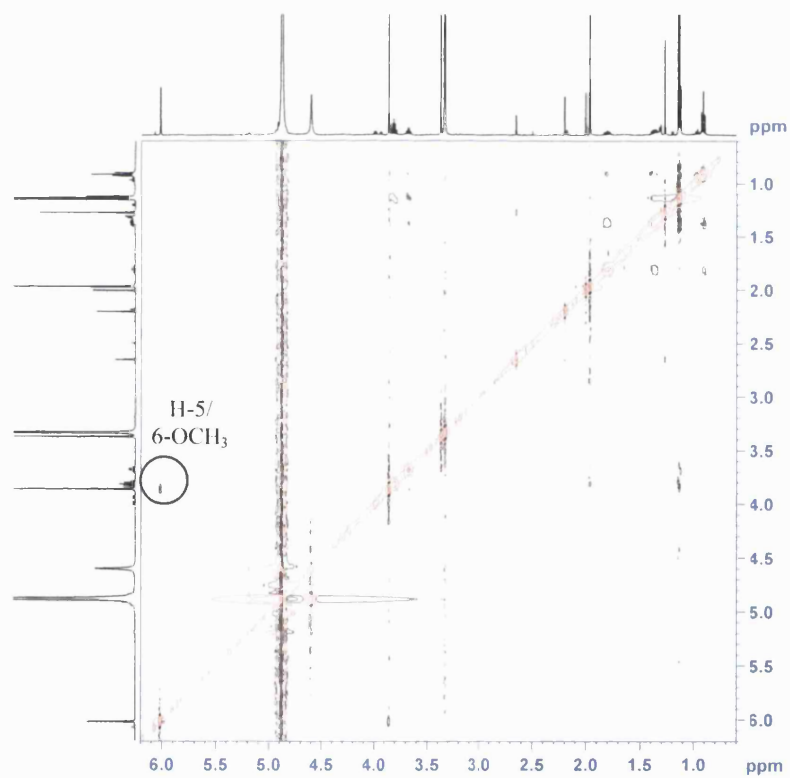


Fig. 50. NOESY spectrum of **WS-04**.

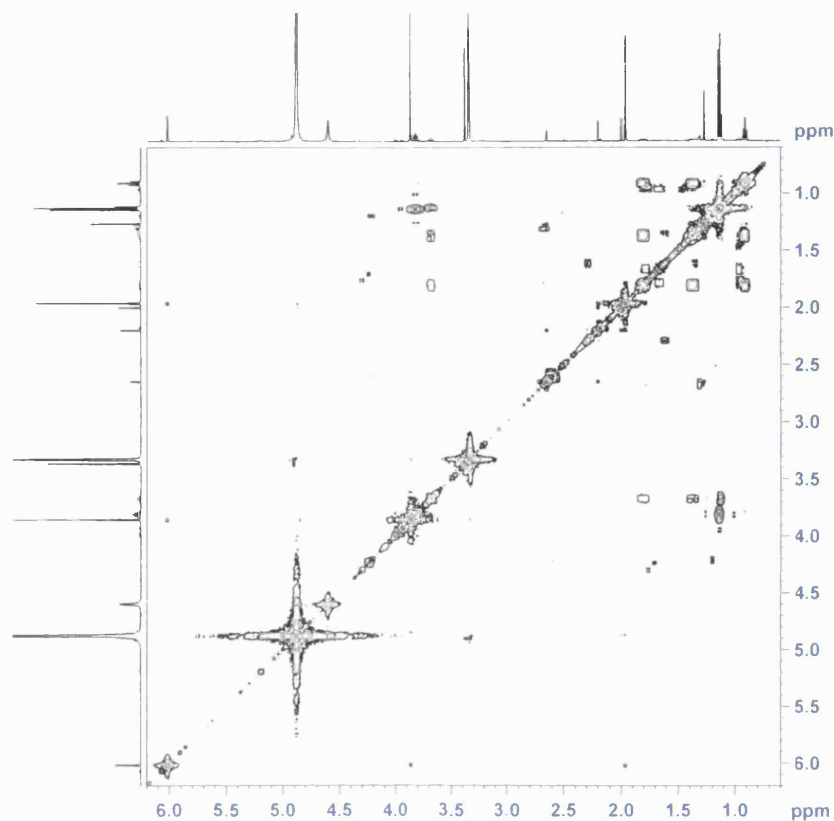


Fig. 51. COSY spectrum of **WS-04**.

The  $^1\text{H}$  NMR spectrum (Fig. 46, Table 12) showed the presence of one aromatic proton ( $\delta_{\text{H}}$  6.02, 1H), one methoxyl group ( $\delta_{\text{H}}$  3.86, 3H), one septet ( $\delta_{\text{H}}$  3.79, 1H), one deshielded methyl singlet ( $\delta_{\text{H}}$  1.97) and two overlapping methyl doublets ( $\delta_{\text{H}}$  1.14, 6H,  $J = 7$  Hz). Six aromatic carbon signals were observed in the  $^{13}\text{C}$  spectrum (Fig. 47), indicating the presence of an aromatic ring. The three signals with chemical shifts of approximately 160 ppm implied that they were attached to an electron-withdrawing group, for example an hydroxyl group or a methoxyl group as they were deshielded. These carbon resonances were typical for a phloroglucinol (1,3,5-trihydroxylated benzene) (Gibbons *et al.*, 2005). Assuming a phloroglucinol structure in the HMBC spectrum (Fig. 48), the aromatic proton (H-5) coupled to four aromatic quaternary carbons (C-1, C-

3, C-4 and C-6), two of which were oxygen-bearing. This hydrogen was placed between the two oxygen-bearing carbons (C-4 and C-6). The methoxyl group was then placed next to the aromatic hydrogen at C-6. This was confirmed by HMBC correlations (Fig. 48, 49) between H-5 and the carbon to which the methoxyl group was attached ( $\delta_C$  162.1, C-6). A correlation between H-5 and the methoxyl in the NOESY spectrum also provided evidence that these groups were *ortho*- to each other. The deshielded methyl group showed  $^1\text{H}$ - $^{13}\text{C}$  correlations in the HMBC spectrum with three aromatic carbons, one to which it was directly attached (C-3,  $\delta_C$  105.0) and two oxygen-bearing quaternary carbons (C-2,  $\delta_C$  166.1 and C-4,  $\delta_C$  162.2). This group was therefore placed at position C-3 in the phloroglucinol.

The final substituent at position C-1 included a methine septet which was coupled to the six-hydrogen methyl doublet in the COSY spectrum (Fig. 51), indicating the presence of an isopropyl side chain. In the HMBC spectrum, correlations were observed between the two methyl doublets. In addition, HMBC correlations were also observed between the methyl doublets and the methine ( $^2J$ ), methyl ( $^3J$ ) and the carbonyl carbon ( $^3J$ ,  $\delta_C$  211.4). This indicated that the isopropyl group was part of a 2-methylpropionyl group. In the NOESY spectrum (Fig. 50), cross-peaks were observed between the methoxyl group and the methyl groups of the isopropyl group. This correlation implied that the methoxyl group must be attached to a carbon next to the 2-methylpropionyl-bearing carbon in the aromatic ring. **WS-04a** was therefore identified as 2,4-dihydroxy-6-methoxy-3-methyl-1-(2'-methylpropionyl)-benzene.

Table 12.  $^1\text{H}$  (500MHz) and  $^{13}\text{C}$  NMR (125 MHz) spectral data and  $^1\text{H}$ - $^{13}\text{C}$  long-range correlations of **WS-04a** recorded in methanol- $d_4$ .

Position	$^1\text{H}$ (J, Hz)	$^{13}\text{C}$	$^2J$	$^3J$
1	-	105.0	-	-
2	-	166.1	-	-
3	-	105.0	-	-
4	-	162.2	-	-
5	6.02 s	91.2	C-4, C-6	C-1, C-3
6	-	162.1	-	-
1'	-	211.4	-	-
2'	3.79 m	40.5	C-3', C-4'	-
3'	1.14 d (7)	19.8	C-2'	C-1', C-4'
4'	1.14 d (7)	19.8	C-2'	C-1', C-3'
3-CH <sub>3</sub>	1.97 s	7.41	C-3	C-2, C-4
6-OCH <sub>3</sub>	3.86 s	55.9	-	C-6

A minor compound **WS-04b** was isolated with compound **WS-04a**. The  $^1\text{H}$  and  $^{13}\text{C}$  data (Table 13) were almost identical to those of **WS-04a** with the exception of the side-chain at C-1 (Table 13). In the same  $^1\text{H}$  spectrum, a methyl doublet ( $\delta_{\text{H}}$  1.16), a methine multiplet ( $\delta_{\text{H}}$  3.68, 0.4H), a methylene multiplet ( $\delta_{\text{H}}$  1.38 and  $\delta_{\text{H}}$  1.81) and a methyl triplet ( $\delta_{\text{H}}$  0.92, 1.5H) were observed. In the COSY spectrum, the methyl triplet was coupled to the methylene which was coupled to the methine. The methine was also coupled to the methyl doublet. In the HMBC spectrum, this methyl doublet showed correlations to the methine ( $^2J$ ), methylene ( $^3J$ ) and to a carbonyl carbon ( $^3J$ ) (Fig. 48, 49). The methyl triplet exhibited  $^1\text{H}$ - $^{13}\text{C}$  correlations to the methylene ( $^2J$ ) and methine ( $^3J$ ). This confirmed the presence of a 2-methylbutanoyl side-chain in compound **WS-04b**. This side-chain was also found in the acylphloroglucinol isolated from *Hypericum foliosum* by our group (Gibbons *et al.*, 2005). The NMR data for this side-chain showed a close agreement with those obtained by Gibbons *et al.* (2005). The molecular formula of **WS-04b** differed to that of **WS-04a** by an addition of a CH<sub>2</sub> as suggested by mass spectrometry. **WS-04b** was therefore

identified as 2,4-dihydroxy-6-methoxy-3-methyl-1-(2'-methylbutanoyl)-benzene. The measured specific rotation of **WS-04** was  $+3.3^\circ$  ( $c$  0.09, MeOH). This was compared with the specific rotation of the commercially available (*S*)-(+)-2-methylbutanoic acid, which was  $+19.0^\circ$  (neat) (Sigma-Aldrich product information). The same direction of rotation implies that **WS-04b** has the (*S*)-configuration at the chiral centre (C-2'). The isolation and characterization of **WS-04a** and **WS-04b** was first reported in Shiu and Gibbons, 2006.

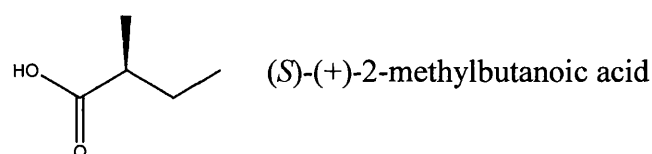


Table 13.  $^1\text{H}$  (500MHz) and  $^{13}\text{C}$  NMR (125 MHz) spectral data and  $^1\text{H}$ - $^{13}\text{C}$  long-range correlations of **WS-04b** recorded in methanol- $d_4$ .

Position	$^1\text{H}$ (J, Hz)	$^{13}\text{C}$	$^2J$	$^3J$
1	-	105.0	-	-
2	-	166.1	-	-
3	-	105.0	-	-
4	-	162.2	-	-
5	6.02 s	91.2	C-4, C-6	C-1, C-3
6	-	162.1	-	-
1'	-	211.2	-	-
2'	3.68 m	47.3	-	-
3'	1.38 m, 1.81 m	28.3	-	-
4'	0.92 t (7.5)	12.4	C-3'	C-2'
5'	1.17 d (6)	17.2	C-2'	C-1', C-3'
3-CH <sub>3</sub>	1.97 s	7.41	C-3	C-2, C-4
6-OCH <sub>3</sub>	3.86 s	55.9	-	C-6

### 3.2.5 Characterization of WS-05 as (-)-shikimic acid ((-)-(3*R*, 4*S*, 5*R*)-3,4,5-trihydroxy-1-cyclohexenecarboxylic acid)

**WS-05** was isolated from the methanol extract of *H. beanii* as white needles. The HR ESI-MS gave an  $[M-H]^-$  ion at  $m/z$  173, indicating a molecular formula of  $C_7H_{10}O_5$ . The  $^1H$  NMR spectrum of **WS-05** is shown to be identical to that of the commercially available (-)-shikimic acid (Fig. 53).

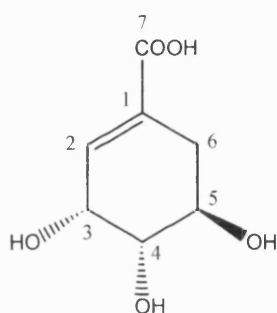


Fig. 52. Structure of **WS-05**.

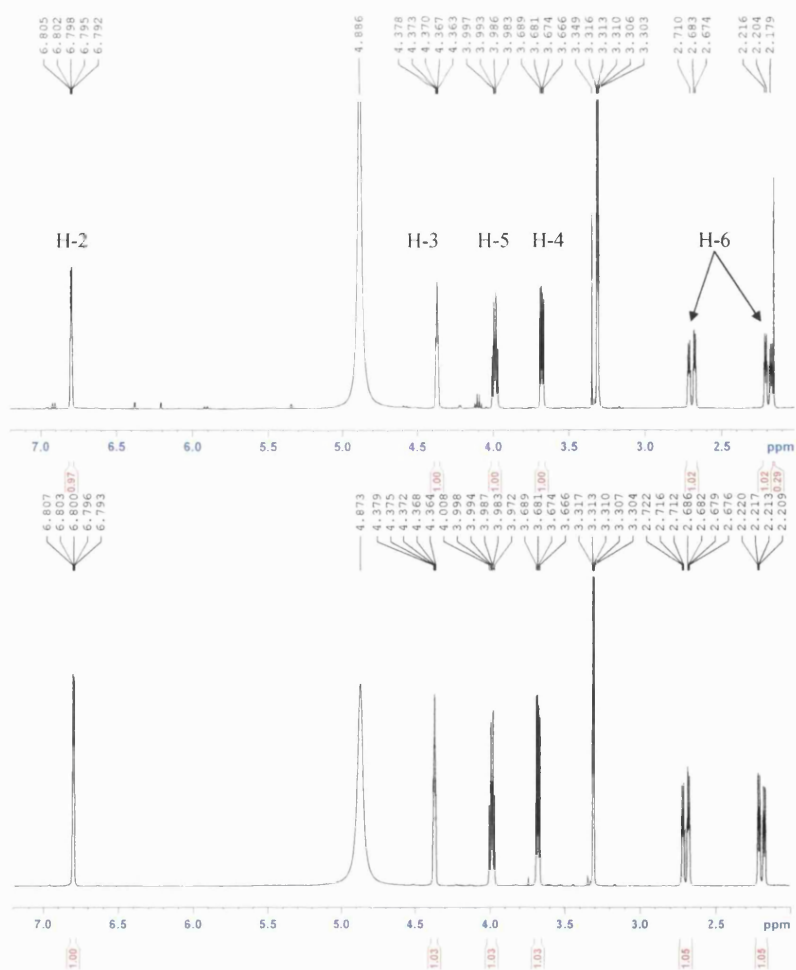


Fig. 53.  $^1H$  NMR spectrum of **WS-05** (top) and (-)-shikimic acid standard (bottom) in methanol- $d_4$  recorded at 500 MHz.

The seven signals in the  $^{13}\text{C}$  spectrum revealed the presence of a carbonyl (C-7), a quaternary olefine (C-1), an olefinic methine (C-2), three additional deshielded methines (C-3 to C-5) attached to an electron-withdrawing group (in this case hydroxyl) and finally a methylene (C-6) (Table 14). The resonance for the carbonyl group ( $\delta_{\text{C}}$  170.1) was typical for a carboxylic acid group, indicating the presence of this functionality in **WS-05**. The  $^1\text{H}$  NMR spectrum (Fig. 53, Table 14) also provided evidence for an olefinic hydrogen ( $\delta_{\text{H}}$  6.80 m, H-2), three oxymethines ( $\delta_{\text{H}}$  4.37 m, H-3;  $\delta_{\text{H}}$  3.68 m, H-4;  $\delta_{\text{H}}$  3.99 m, H-5) and a methylene group ( $\delta_{\text{H}}$  2.19 m, 2.70 m, H-6).

In the HMBC spectrum (Fig. 54), the olefinic hydrogen (H-2) and the methylene group (H-6) showed a  $^3J$  correlation to the carbonyl carbon (C-7), thus placing the carboxylic group at C-1 between these two groups. The oxymethine at  $\delta_{\text{H}}$  4.37 (H-3) showed correlations to both the olefinic carbons (C-1, C-2) and was placed next to the olefinic hydrogen at C-3. The oxymethine at  $\delta_{\text{H}}$  3.99 (H-5) showed  $^2J$  correlations to an oxymethine carbon (C-4) and the methylene carbon (C-6) and  $^3J$  correlations to the oxymethine carbon (C-3) and the quaternary olefinic carbon (C-1) and was therefore placed at C-5. The remaining oxymethine proton at  $\delta_{\text{H}}$  3.68 (H-4) which was correlated to the olefinic methine carbon (C-2) and the methylene carbon (C-6) was placed at C-4, thus completing the NMR assignment of **WS-05**. The COSY spectrum (Fig. 55) also revealed that H-2 was coupled to H-3, which was in turn coupled to H-4. H-4 was coupled to the neighbouring H-5, which was further coupled to H-6.

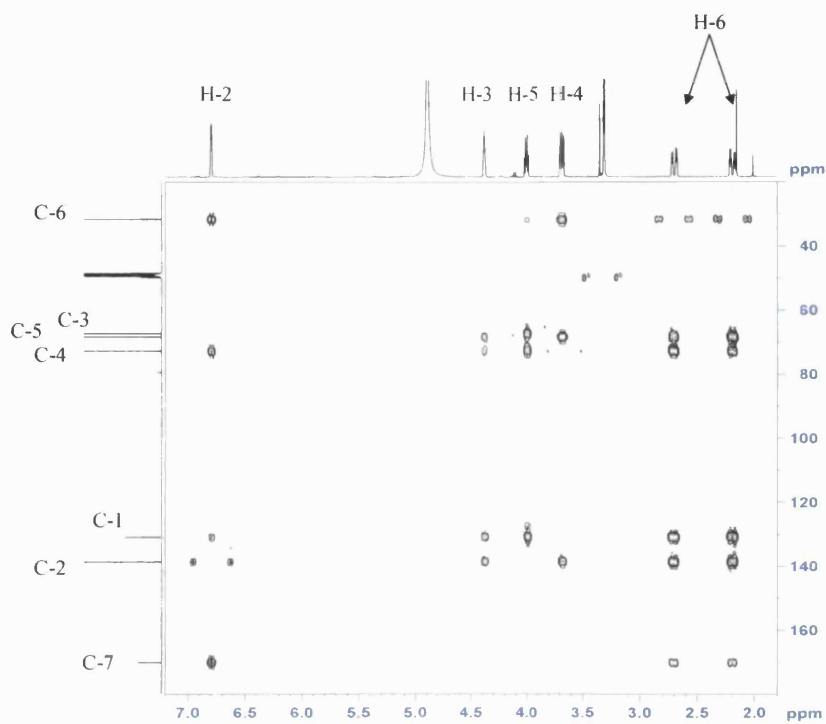


Figure 54. HMBC spectrum of **WS-05**.

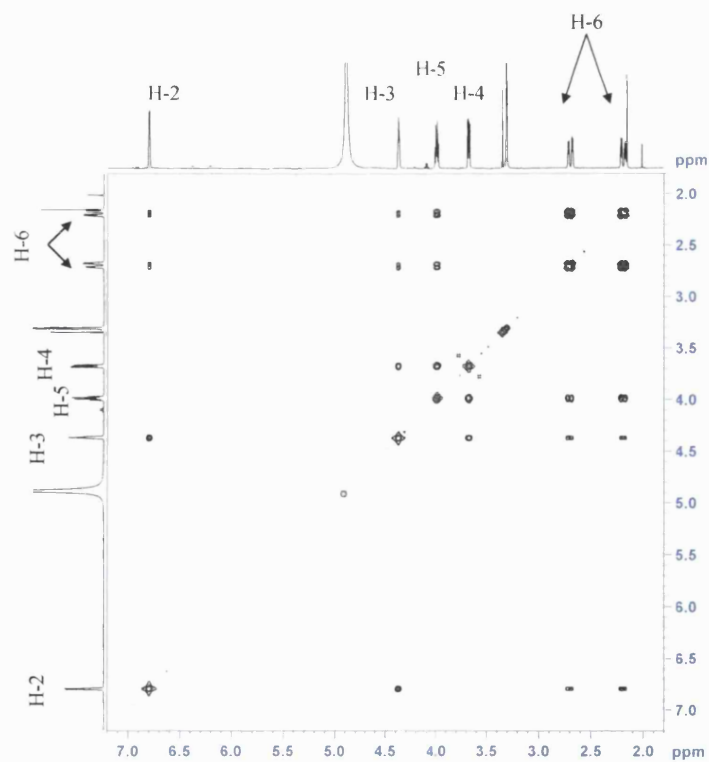


Figure 55. COSY spectrum of **WS-05**.

The relative stereochemistry of the isolated shikimic acid was determined by through space NOE interactions in the NOESY spectrum (Fig. 56, 57). The axial oxymethine, H-4, showed an NOE to the neighbouring equatorial oxymethine, H-3, and the axial proton, H-6 ( $\delta_{\text{H}}$  2.19 m) in the methylene group, suggesting that these protons were orientated in the beta position. The specific rotation of **WS-05** was found to be  $-166.5^{\circ}$  ( $c$  2.9, MeOH) and had a negative sign, which corresponded to the commercially available (-)-shikimic acid ( $[\alpha]_{\text{D}}^{22}$   $-181^{\circ}$  to  $-185^{\circ}$ ;  $c$  4.0, water; Sigma-Aldrich product information). **WS-05** was therefore identified as (-)-(3*R*, 4*S*, 5*R*)-3,4,5-trihydroxy-1-cyclohexenecarboxylic acid.

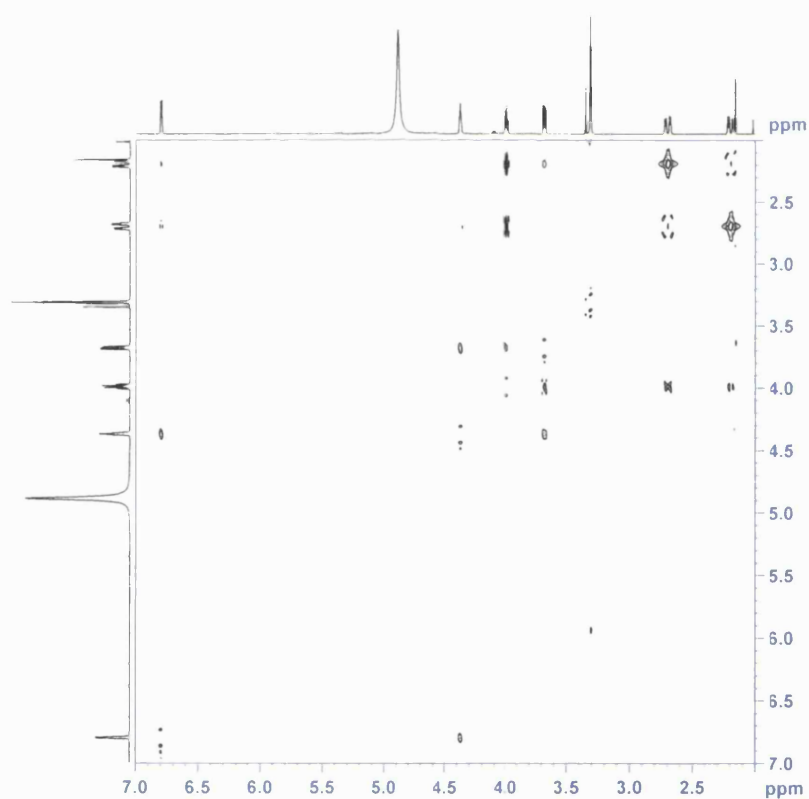


Fig. 56. NOESY spectrum of **WS-05**.

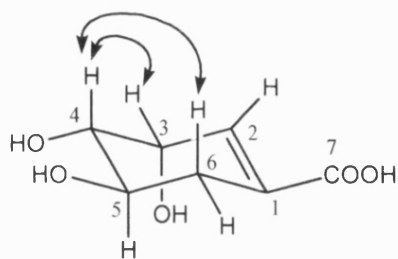


Fig. 57. Key NOE correlations for **WS-05**.

Table 14.  $^1\text{H}$  (500MHz) and  $^{13}\text{C}$  NMR (125 MHz) spectral data and  $^1\text{H}$ - $^{13}\text{C}$  long-range correlations of **WS-05** recorded in methanol- $d_4$ .

Position	$^1\text{H}$ ( $J$ , Hz)	$^{13}\text{C}$	$^2J$	$^3J$
1	-	130.8	-	-
2	6.80 m	138.7	C-1	C-4, C-6, C-7
3	4.37 m	67.4	C-2, C-4	C-1, C-5
4	3.68 m	72.8	C-3	C-2, C-6
5	3.99 m	68.4	C-4, C-6	C-1, C-3
6	2.70 m, 2.19 m	31.7	C-1, C-5	C-2, C-4, C-7
7	-	170.1	-	-

### 3.2.6 Characterization of WS-06 as (+)-3,3',4',5,7-flavanpentol ((+)-catechin)

WS-06 was isolated from the methanol extract of *H. beanii* as a brown solid. The HR ESI-MS showed an  $[M+H]^+$  ion at  $m/z$  291, indicating a molecular formula of  $C_{15}H_{14}O_6$ . The  $^1H$  and  $^{13}C$  NMR data (Table 15) were indicative of a flavonoid, in particular, a flavan-3-ol (Foo *et al.*, 1997).

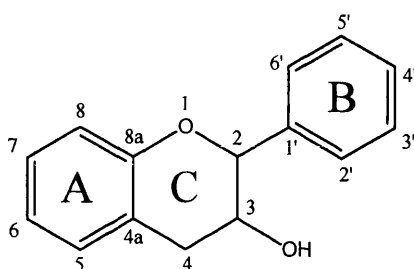


Fig. 58. Flavan-3-ol skeleton

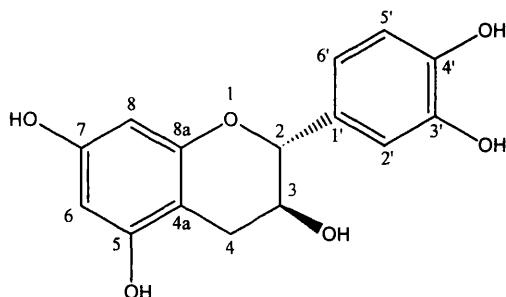


Fig. 59. Structure of WS-06.

The  $^1H$  NMR spectrum (Fig. 60) displayed evidence for two aromatic rings, one with a pair of *meta*-coupled doublets at  $\delta_H$  5.91 ( $J = 2.5$  Hz, H-6) and  $\delta_H$  5.94 ( $J = 2.5$  Hz, H-8) and one with a set of protons in an ABD system ( $\delta_H$  6.77 d,  $J = 8$  Hz, H-5';  $\delta_H$  6.80 dd,  $J = 2, 8$  Hz, H-6';  $\delta_H$  6.97 d,  $J = 2$  Hz, H-2'). Two non-equivalent double doublets of a methylene ( $\delta_H$  2.74 m, 2.86 m, H-4) and two oxymethines ( $\delta_H$  4.82 bs, H-2; 4.18 m, H-3) completed the  $^1H$  NMR signals. The  $^{13}C$  NMR spectrum showed twelve signals in the aromatic region, two oxymethines ( $\delta_C$  67.5 and  $\delta_C$  79.9) and a methylene ( $\delta_C$  29.3).

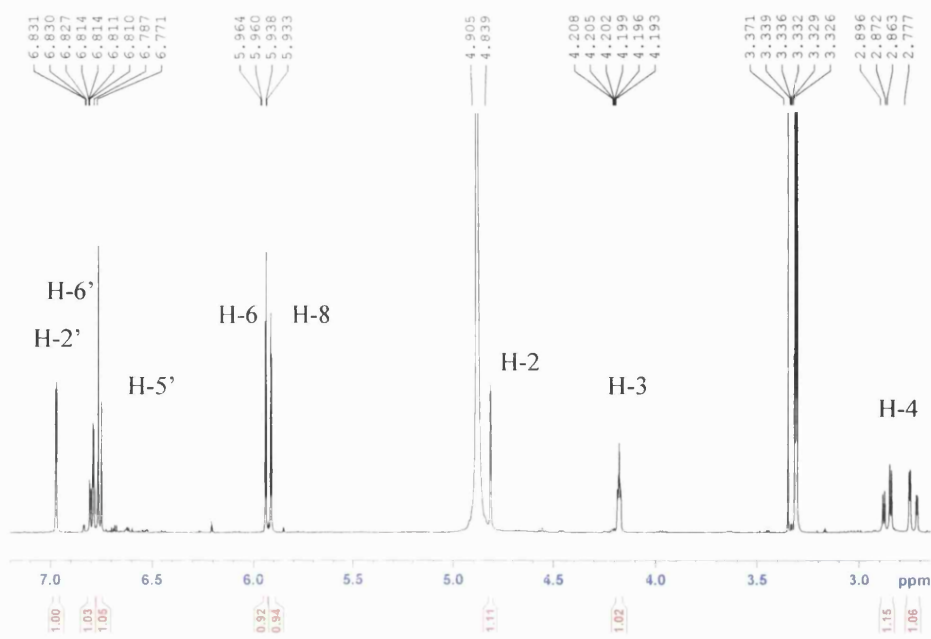


Fig. 60.  $^1\text{H}$  NMR spectrum of **WS-06** in methanol- $d_4$  recorded at 500 MHz.

The HMBC (Fig. 61) and COSY spectra (Fig. 63) were examined to identify  $^1\text{H}$ - $^{13}\text{C}$  and  $^1\text{H}$ - $^1\text{H}$  connectivities respectively. The oxymethine at  $\delta_{\text{H}}$  4.18 (H-3) showed a COSY correlation to the oxymethine at  $\delta_{\text{H}}$  4.82 (H-2) and the methylene protons (H-4), placing it between these two groups in the C ring. In the HMBC spectrum, the methylene protons showed  $^2J$  correlations to a quaternary aromatic carbon at  $\delta_{\text{C}}$  100.1 (C-4a) and an oxygenated carbon at  $\delta_{\text{C}}$  67.5 (C-3) and  $^3J$  correlations to two deshielded aromatic carbons at  $\delta_{\text{C}}$  158.0 (C-5) and  $\delta_{\text{C}}$  157.4 (C-8a) and an oxygenated carbon at  $\delta_{\text{C}}$  79.9 (C-2) (Fig. 62). The aromatic doublets at  $\delta_{\text{H}}$  5.91 (H-8) and  $\delta_{\text{H}}$  5.94 (H-6) were shown to be connected to the deshielded aromatic carbons *via* two bonds at  $\delta_{\text{C}}$  157.7 (H-7) and 158.0 (H-5) respectively. Both of these two hydrogens were also connected to C-4a *via* three bonds thus completing the connection of rings A and C.

Both the *meta*-coupled proton at  $\delta_{\text{H}}$  6.97 (H-2') and the *meta*-, *ortho*-coupled proton at  $\delta_{\text{H}}$  6.80 (H-6') in the B ring showed  $^3J$  correlations to the oxygenated carbon at C-2 and a oxygenated aromatic carbon at C-4'. The remaining *ortho*-coupled proton at  $\delta_{\text{H}}$  6.77 (H-5') was linked to a quaternary aromatic carbon at  $\delta_{\text{C}}$  132.3 (C-1') and a deshielded aromatic carbon at  $\delta_{\text{C}}$  145.8 (C-3') *via* three bonds. This completes the NMR assignment of ring B.

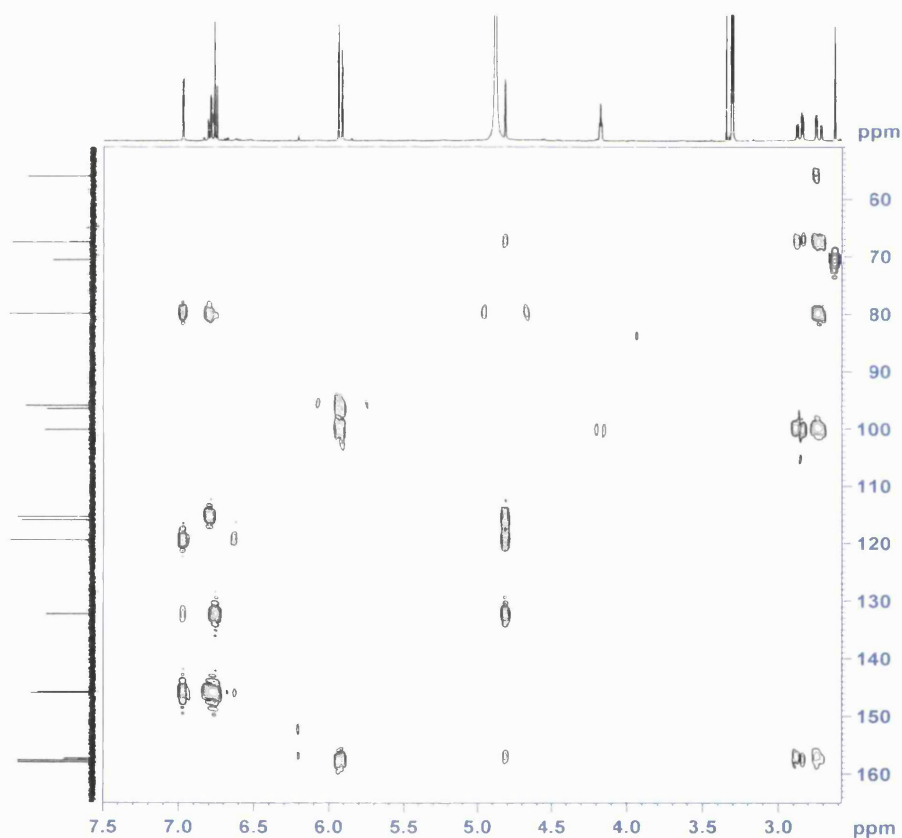


Fig. 61. HMBC spectrum of **WS-06**.

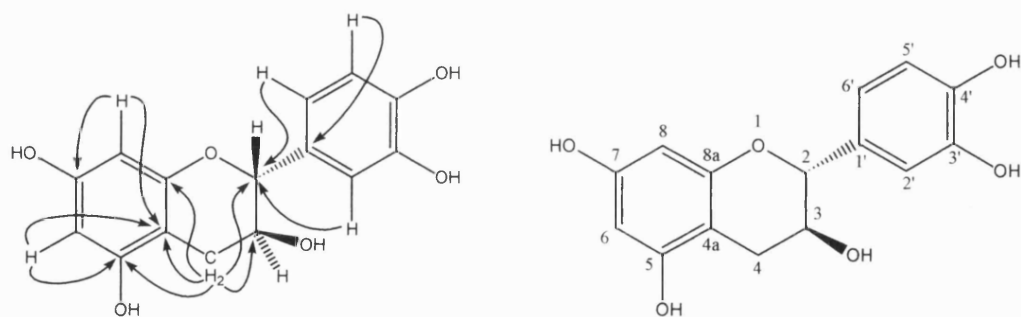


Fig. 62. Key HMBC correlations for **WS-06**.

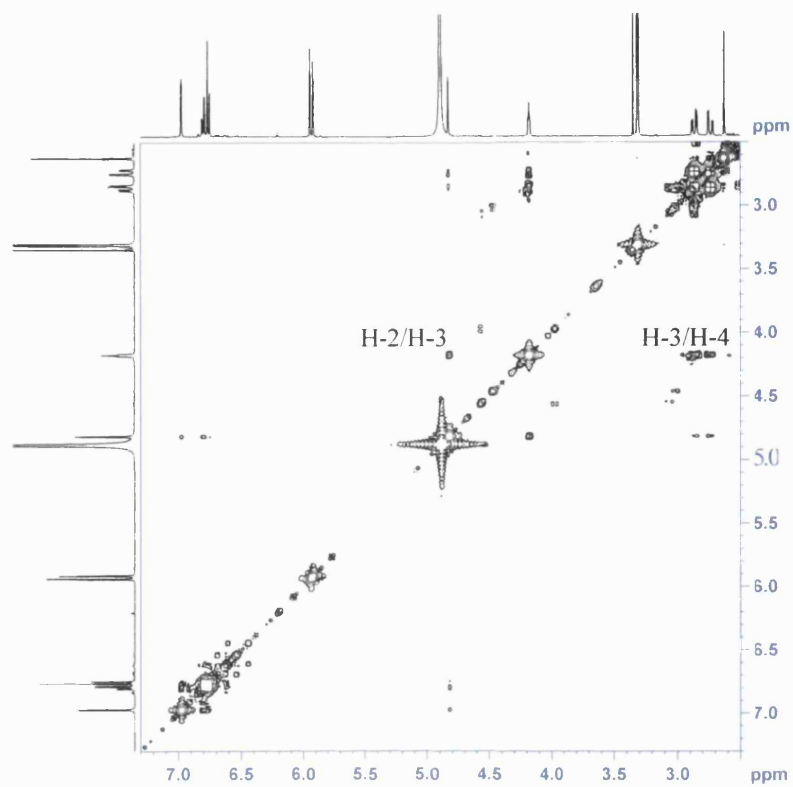


Fig. 63. COSY spectrum of **WS-06**.

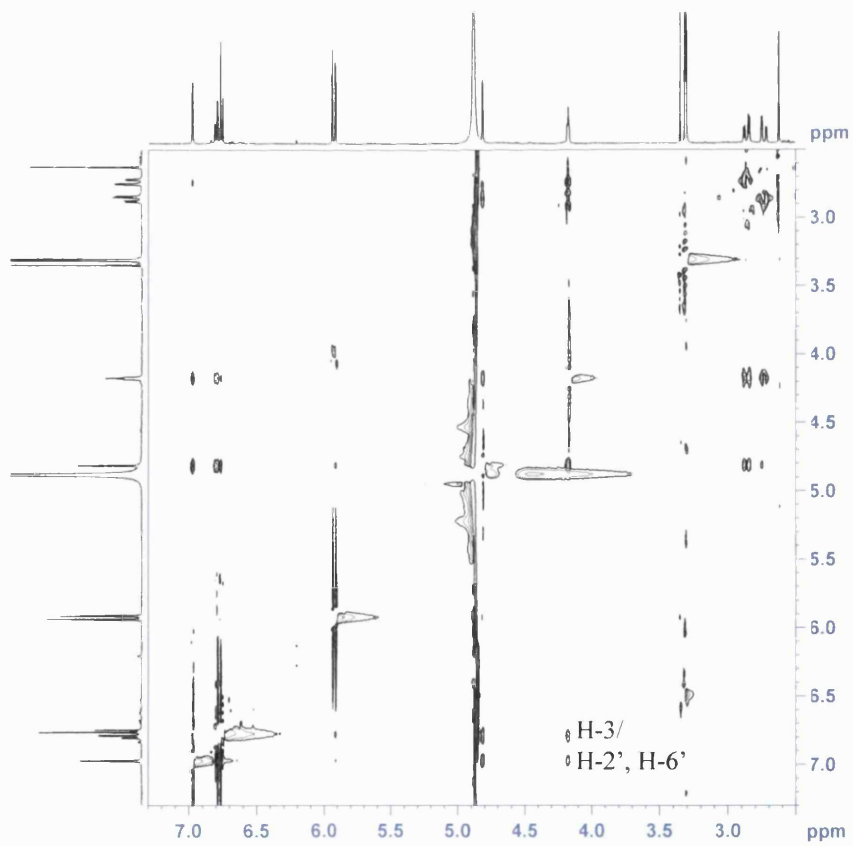


Fig. 64. NOESY spectrum of **WS-06**.

The relative stereochemistry of **WS-06** was assigned by inspecting the NOESY spectrum (Fig. 64). H-3 showed a significant NOE correlation to both H-2' and H-6' in the B ring which can freely rotate, suggesting that this proton and the phenyl group were in the same orientation in space, i.e., both  $\alpha$  orientation in ring C. Therefore, H-2 and the 3-hydroxyl group were assigned as the  $\beta$  orientation. The coupling constant between H-2 and H-3 was very small and H-3 appeared as a broad singlet. This suggested that H-2 and H-3 were in the axial-equatorial position. The specific optical rotation of **WS-06** was found to be  $+30.1^\circ$  ( $c = 0.82$ , methanol). **WS-06** was therefore identified as (+)-3,3',4',5,7-flavanpentol (+)-catechin. The  $^1\text{H}$  and  $^{13}\text{C}$  NMR data of **WS-06** were in good agreement with the published data (Foo *et al.*, 1997, Table 15).

Table 15.  $^1\text{H}$  (500MHz) and  $^{13}\text{C}$  NMR (125 MHz) spectral data and  $^1\text{H}$ - $^{13}\text{C}$  long-range correlations of **WS-06** recorded in methanol- $d_4$ .

Position	<b>WS-06</b> (Methanol- $d_4$ )				<b>(+)-catechin</b> (Acetone- $d_6$ ) (Foo <i>et al.</i> , 1997)	
	$^1\text{H}$ (J, Hz)	$^{13}\text{C}$	$^2J$	$^3J$	$^1\text{H}$ (J, Hz)	$^{13}\text{C}$
2	4.82 bs	79.9	C-3, C-1'	C-4, C-8a, C-2', C-6'	4.55 m	81.3
3	4.18 m	67.5	-	C-4a	4.0 m	68.2
4	2.74 dd (2.5, 17) 2.86 dd (4.5, 17)	29.3	C-3, C-4a	C-2, C-5, C-8a	2.43 - 2.95 m	28.8
4a	-	100.1	-	-	-	100.5
5	-	158.0	-	-	-	157.7
6	5.94 d (2.5)	96.5	C-5	C-4a, C-8	5.88 bs	96.2
7	-	157.7	-	-	-	157.2
8	5.91 d (2.5)	96.0	C-7	C-4a, C-6	6.04 bs	95.2
8a	-	157.4	-	-	-	157.6
1'	-	132.3	-	-	-	131.9
2'	6.97 d (2)	115.4	C-1'	C-2, C-6', C-4'	6.91 m	115.4
3'	-	145.8	-	-	-	145.6
4'	-	146.0	-	-	-	145.7
5'	6.77 d (8)	115.9	-	C-1', C-3'	6.80 m	115.8
6'	6.80 dd (2, 8)	119.4	-	C-2, C-2', C-4'	6.80 m	119.9

### 3.2.7 Characterization of WS-07 as $\beta$ -sitosterol

WS-07 was isolated as a white amorphous solid from the hexane extracts of *H. revolutum ssp. revolutum* and *H. olympicum L. cf. uniflorum*. The  $^1\text{H}$  NMR spectrum of WS-07 (Fig. 66) was identical to that of  $\beta$ -sitosterol, which is another phytosterol ubiquitous in plants.

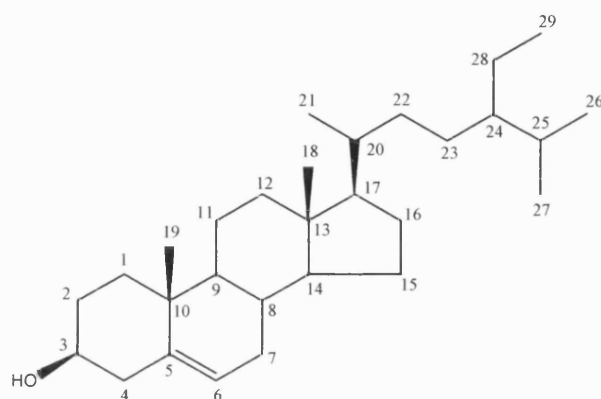


Fig. 65. Structure of WS-07

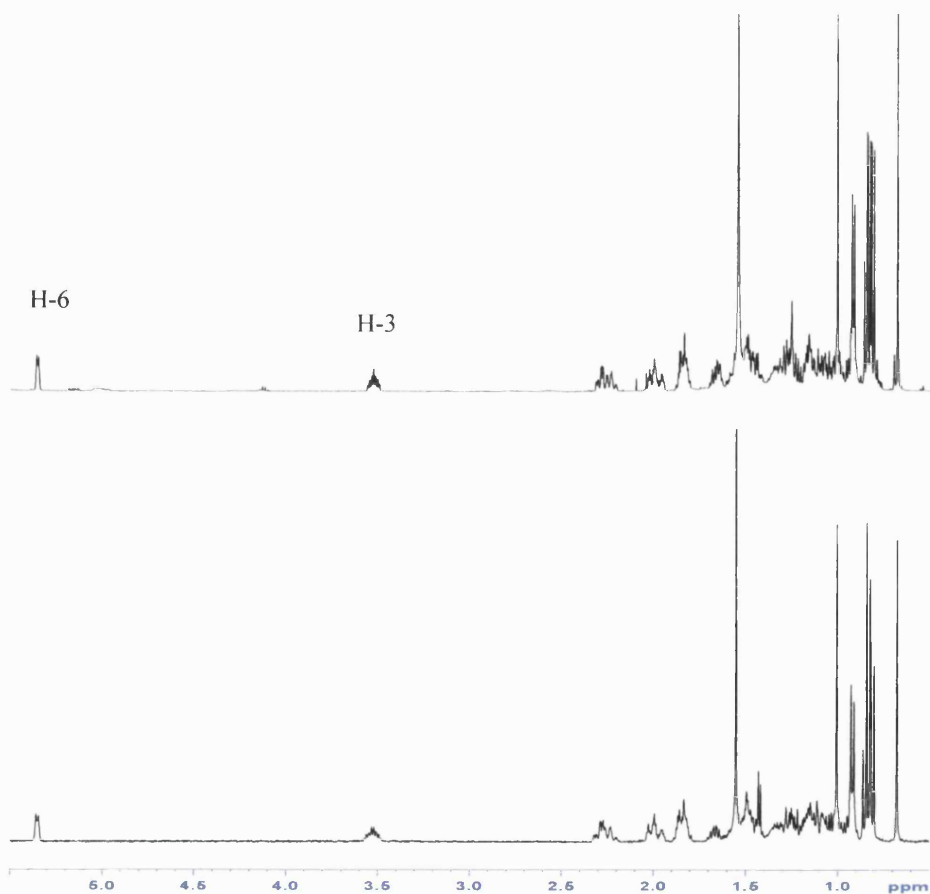


Fig. 66.  $^1\text{H}$  NMR spectrum of WS-07 (top) and  $\beta$ -sitosterol standard (bottom) in chloroform-*d* recorded at 500 MHz.

The  $^1\text{H}$  NMR spectrum of **WS-07** was almost identical to that of **WS-03**, differing in the absence of the two olefinic protons which appeared as double doublets at  $\delta_{\text{H}}$  5.16 and 5.03 in **WS-03**. This corresponded to the absence of a double bond between C-22 ( $\delta_{\text{C}}$  34.0) and C-23 ( $\delta_{\text{C}}$  26.1) in **WS-07**. The structure of **WS-07** was confirmed by comparing the  $^1\text{H}$  NMR spectrum with that of a commercial standard of  $\beta$ -sitosterol (Fig. 71). The  $^{13}\text{C}$  data of **WS-05** also showed an agreement with the literature (Rauter *et al.*, 2005) (Table 16).

Table 16.  $^{13}\text{C}$  NMR (125 MHz) spectral data of **WS-07** recorded in chloroform-*d*.

Position	<b>WS-07</b> (Chloroform- <i>d</i> )	Rauter <i>et al.</i> , 2005 (Chloroform- <i>d</i> )
1	37.3	37.2
2	31.7	31.7
3	71.8	71.8
4	42.3	42.3
5	140.8	140.7
6	121.7	121.8
7	31.9	31.9
8	31.9	31.8
9	50.2	51.2
10	36.5	36.5
11	21.1	21.1
12	39.8	39.8
13	42.3	42.4
14	56.8	56.8
15	24.3	24.3
16	28.3	28.2
17	56.1	55.9
18	11.9	11.9
19	19.4	19.4
20	36.2	36.1
21	18.8	18.8
22	34.0	33.9
23	26.1	26.4
24	45.9	45.8
25	19.2	19.1
26	19.8	19.8
27	19.0	19.2
28	23.1	23.0
29	12.0	12.1

### 3.2.8 Characterization of WS-08 as 3-hydroxy-1,4,7-trimethoxydibenzofuran

**WS-08** was isolated as a pale yellow oil from the DCM extract of *H. revolutum ssp. revolutum*. The HR ESI-MS gave an  $[M-H]^-$  ion at  $m/z$  273, suggesting a molecular formula of  $C_{15}H_{14}O_5$ . In the  $^{13}C$  NMR spectrum (Table 17), twelve signals in the aromatic region and three methoxyl signals were observed. The pattern of the aromatic carbon signals showed similarity to that of a xanthone nucleus, differing in the absence of a carbonyl signal in this compound. These data suggested that **WS-08** was a dibenzofuran substituted with three methoxyl groups (Kokubun *et al.*, 1995, 1995a).

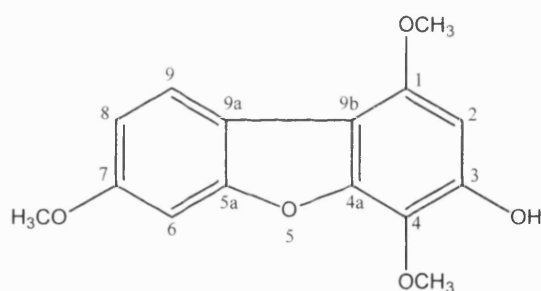


Fig. 67. Structure of **WS-08**.

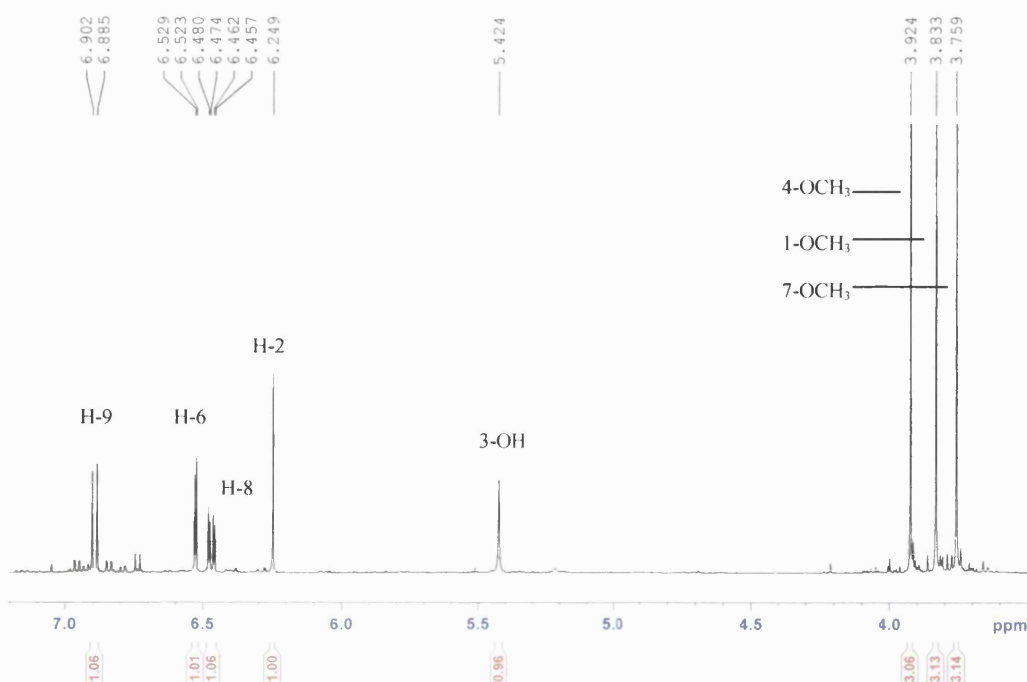


Fig. 68.  $^1H$  NMR spectrum of **WS-08** in chloroform-*d* recorded at 500 MHz.

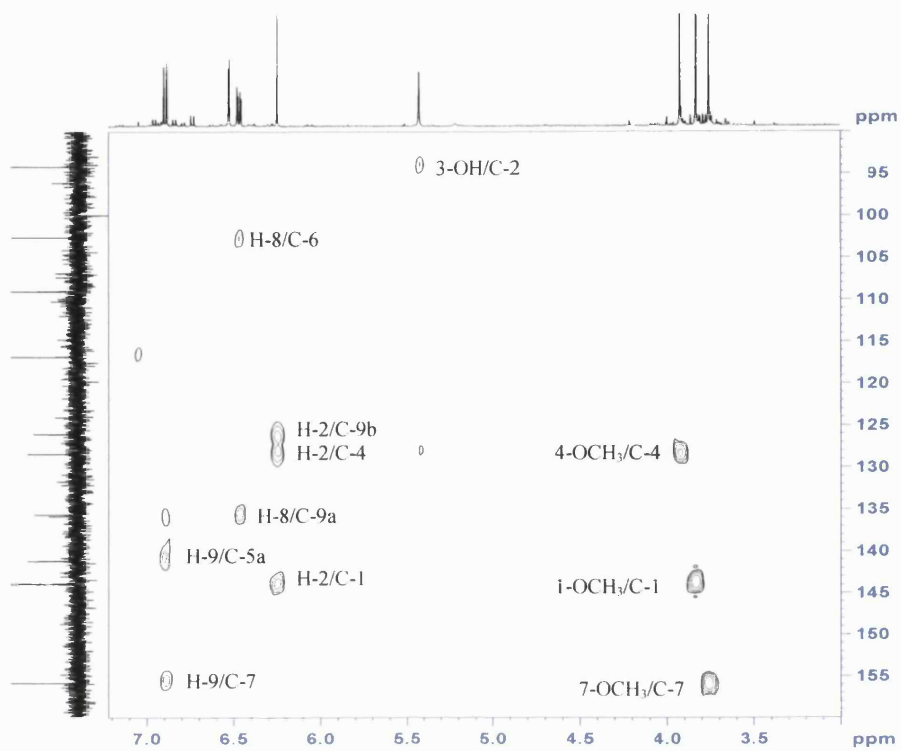


Fig. 69. HMBC spectrum of WS-08.

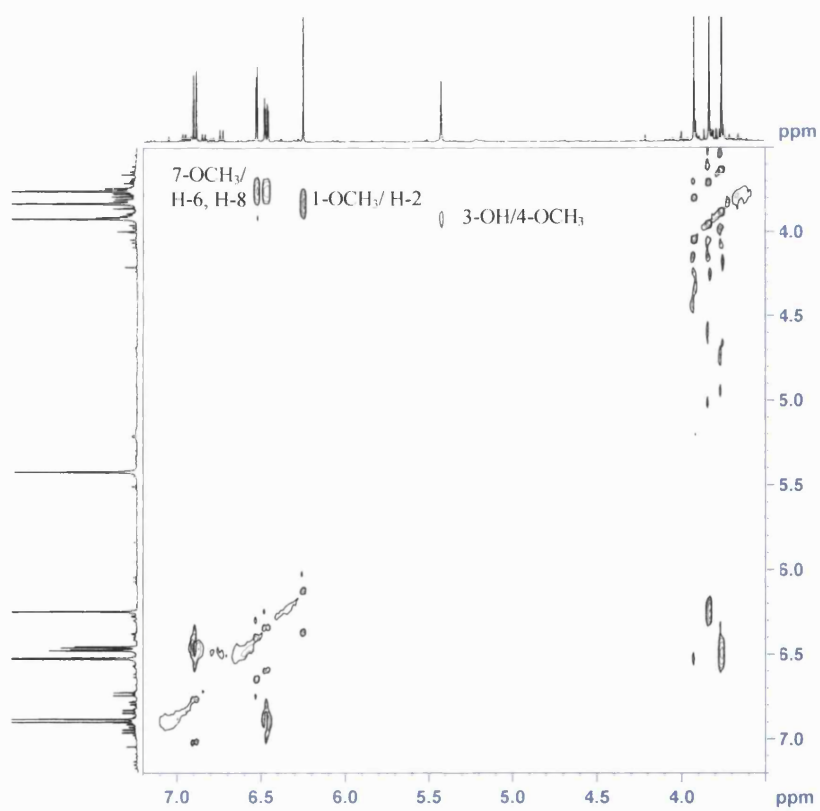


Fig. 70. NOESY spectrum of WS-08.

The  $^1\text{H}$  NMR spectrum (Fig. 68, Table 17) showed signals for three aromatic protons in an ABD system with resonances at  $\delta_{\text{H}}$  6.89 (d,  $J = 8.5$  Hz, H-9),  $\delta_{\text{H}}$  6.47 (dd,  $J = 3, 8.5$  Hz, H-8) and  $\delta_{\text{H}}$  6.53 (d,  $J = 3$  Hz, H-6), an aromatic proton singlet ( $\delta_{\text{H}}$  6.25 s, H-2), a broad signal at  $\delta_{\text{H}}$  5.42 corresponding to an hydroxyl group and three methoxyl singlets ( $\delta_{\text{H}}$  3.92 s, 3.83 s, 3.76 s).

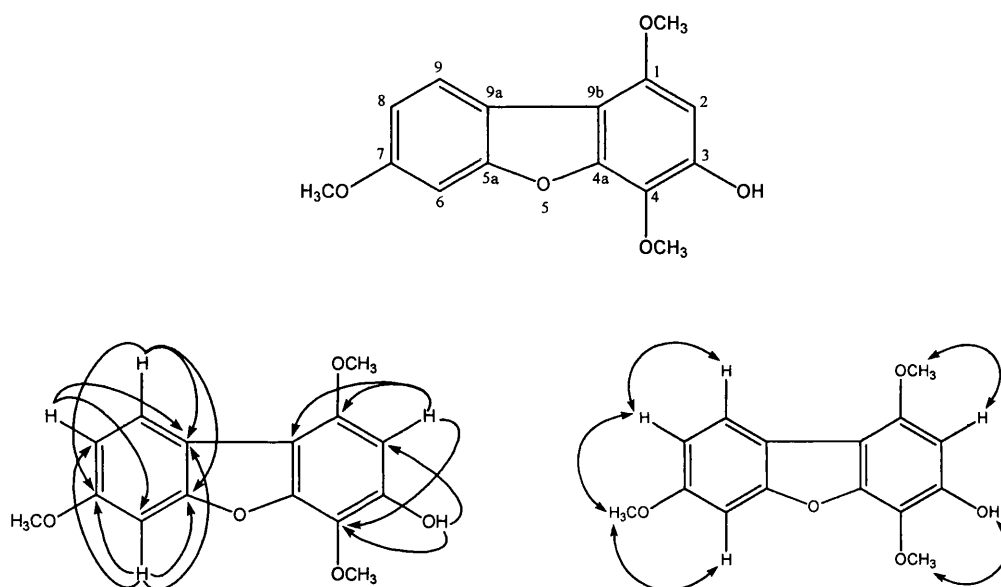


Fig. 71. HMBC (single-headed arrows) and NOESY (double-headed arrows) correlations for WS-08.

In the HMBC spectrum (Fig. 69), correlations were seen between the methoxyl groups with resonances at  $\delta_{\text{H}}$  3.76 (H-7), 3.83 (H-1) and 3.92 (H-4) and  $\delta_{\text{C}}$  155.9 (C-7), 143.9 (C-1) and 128.5 (C-4) respectively, confirming the chemical shifts of the carbons to which the methoxyl groups were attached (Fig. 71). By inspection of the NOESY spectrum (Fig. 70), a cross-peak was observed between the methoxyl group at C-1 and the aromatic proton singlet (H-2), and the methoxyl group at C-4 and the hydroxyl group, thus placing them next to each other (Fig. 71). The proton of the hydroxyl group showed a  $^3J$  correlation with

the carbon to which the aromatic proton singlet was attached ( $\delta_C$  94.2, C-2) and the carbon to which a methoxyl group was attached ( $\delta_C$  128.5, C-4). The hydroxyl group was placed between these groups in the same aromatic ring. The aromatic proton (H-2) also displayed a  $^3J$  HMBC correlation with C-9b ( $\delta_C$  126.2) but not the oxygen-bearing carbon at  $\delta_C$  144.0 (C-4a), thus placing it at C-2 and not C-3.

For the other aromatic ring, a cross-peak could be seen between the methoxyl singlet at  $\delta_H$  3.76 (7-OCH<sub>3</sub>) and H-6 and H-8 in the NOESY spectrum. This methoxyl group was therefore placed between the aromatic hydrogens in the ABD system. Since the *meta*- and *ortho*-coupled aromatic proton at  $\delta_H$  6.47 (H-8) showed a strong  $^3J$  HMBC correlation with carbons at  $\delta_C$  135.9 (C-9a) but not  $\delta_C$  141.2 (C-10a), it could be implied that the methoxyl group was placed at C-7 and not C-8, which would also yield an ABD system. This completed the NMR assignment of **WS-08**. **WS-08** was characterized as the new natural product 3-hydroxy-1,4,7-trimethoxy-dibenzofuran. This compound was structurally related to a series of dibenzofurans which are phytoalexins isolated from *Mespilus* species (Kokubun *et al.*, 1995, 1995a). However, no dibenzofuran has been isolated from *Hypericum* genus previously. These results were first presented in a poster in the GA meeting in Graz, Austria, 2007.

Table 17.  $^1\text{H}$  (500MHz) and  $^{13}\text{C}$  NMR (125 MHz) spectral data and  $^1\text{H}$ - $^{13}\text{C}$  long-range correlations of **WS-08** recorded in chloroform-*d*.

Position	$^1\text{H}$ ( <i>J</i> , Hz)	$^{13}\text{C}$	$^2J$	$^3J$
1	-	143.9	-	-
2	6.25 s	94.2	C-1	C-4, C-9b
3	-	135.7	-	-
4	-	128.5	-	-
4a	-	144.0	-	-
5a	-	141.2	-	-
6	6.53 d (3)	102.6	C-5a, C-7	C-8, C-9a
7	-	155.9	-	-
8	6.47 dd (3, 8.5)	109.1	-	C-6, C-9a
9	6.89 d (8.5)	116.9	C-9a	C-5a, C-7
9a	-	135.9	-	-
9b	-	126.2	-	-
1-OCH <sub>3</sub>	3.83 s	56.5	-	C-1
4-OCH <sub>3</sub>	3.92 s	61.9	-	C-4
7-OCH <sub>3</sub>	3.76 s	55.8	-	C-7
3-OH	5.42 bs	-	-	C-2, C-4

**3.2.9 Acylphloroglucinols isolated from *H. olympicum* L. cf. *uniflorum*.**

A series of 2-methylbutanoyl phloroglucinols were isolated from *H. olympicum* L. cf. *uniflorum* (Fig. 72). Due to the similarities in the compounds, the structural elucidation of the 2-methylbutanoyl phloroglucinol core structure will only be discussed in **WS-09**. The  $^1\text{H}$  and  $^{13}\text{C}$  NMR chemical shifts assignment of the side-chain will be discussed individually.

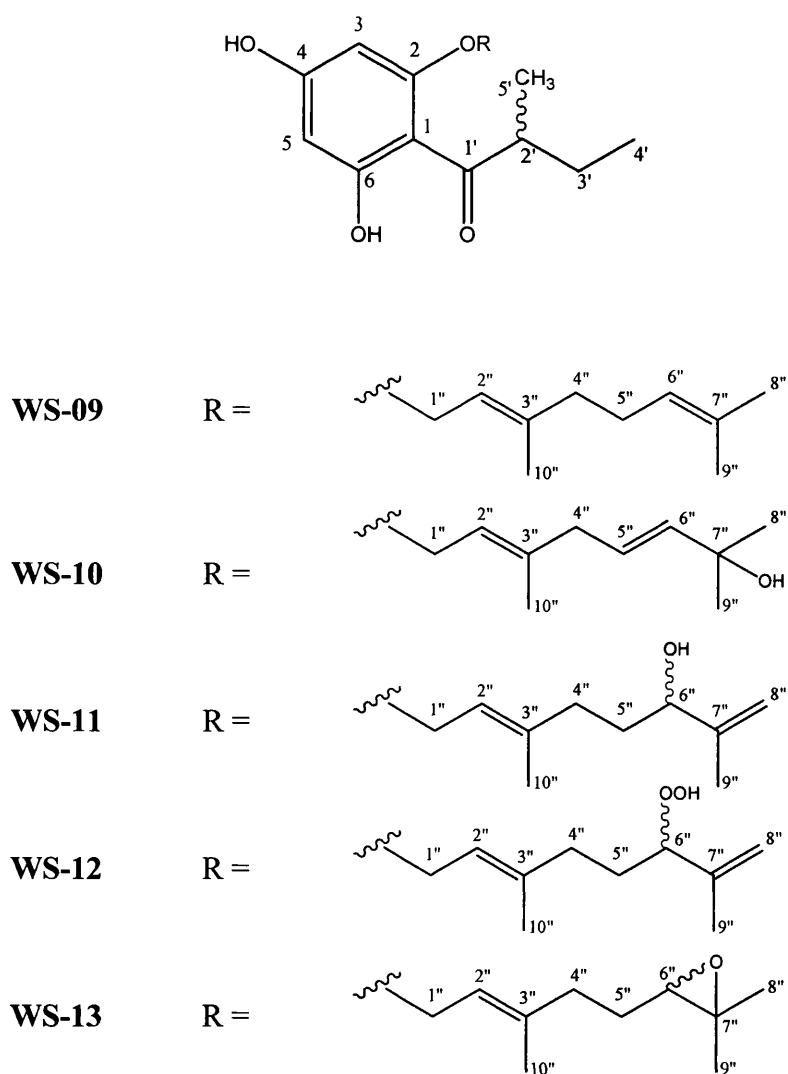


Fig. 72. Acylphloroglucinols isolated from *H. olympicum* L. cf. *uniflorum*.

### 3.2.9.1 Characterization of WS-09 as 4,6-dihydroxy-2-*O*-(3'',7''-dimethyl-2'',6''-octadienyl)-1-(2'-methylbutanoyl)-benzene

WS-09 was isolated from the hexane and DCM extract of *H. olympicum L. cf. uniflorum* as a pale yellow oil. HR ESI-MS gave an  $[M-H]^-$  ion at  $m/z$  345 suggesting a molecular formula of  $C_{21}H_{30}O_4$ . The  $^1H$  NMR and  $^{13}C$  NMR data were reminiscent of an acylphloroglucinol with a terpene substituent.

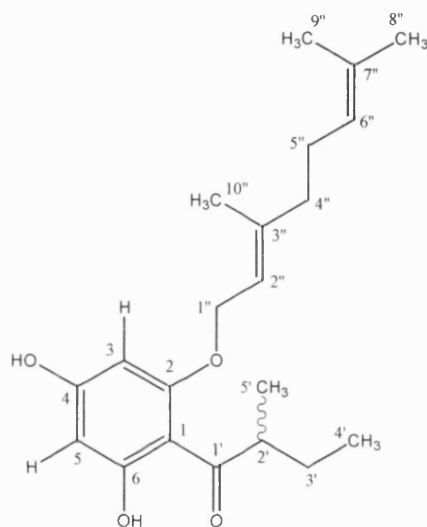


Fig. 73. Structure of WS-09.

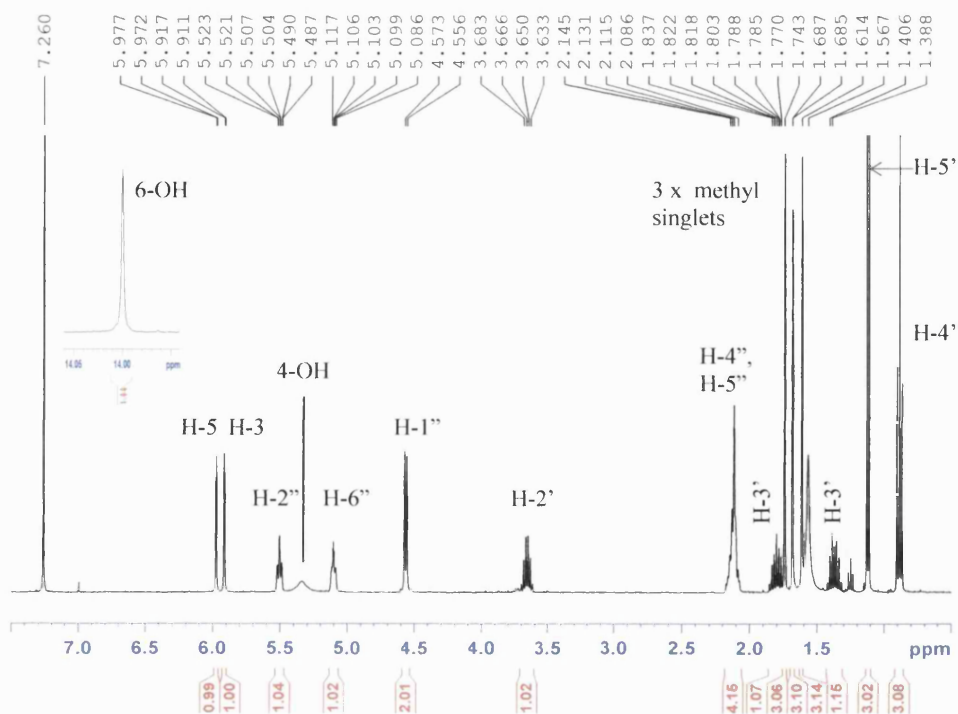


Fig. 74.  $^1H$  NMR spectrum of WS-09 in chloroform-*d* recorded at 500 MHz.

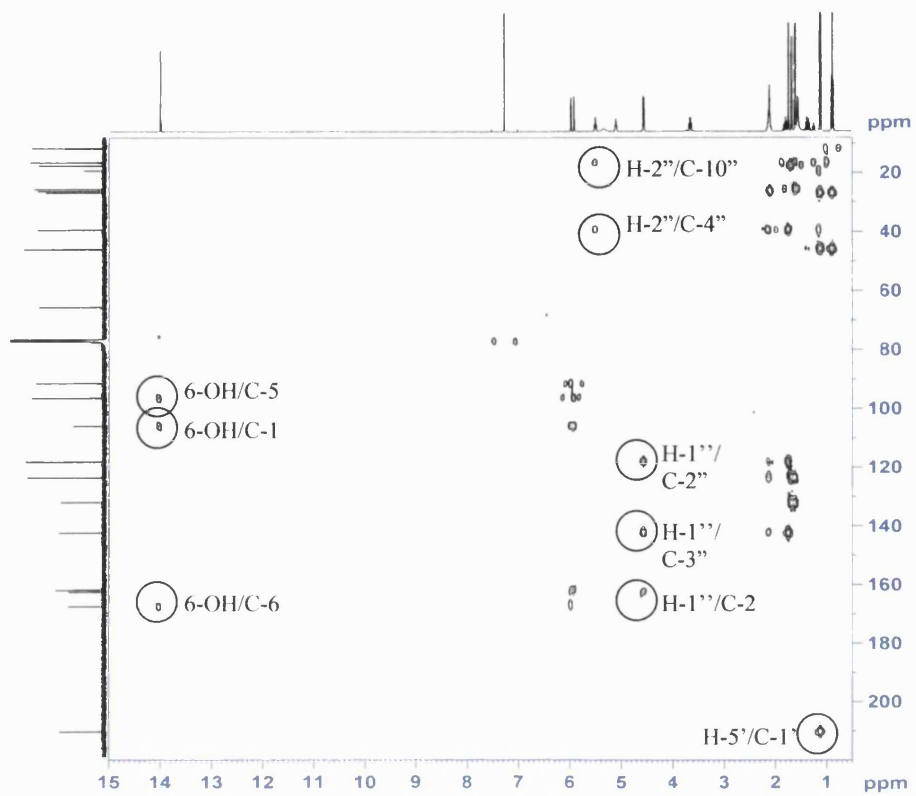


Fig. 75. HMBC spectrum of **WS-09**.

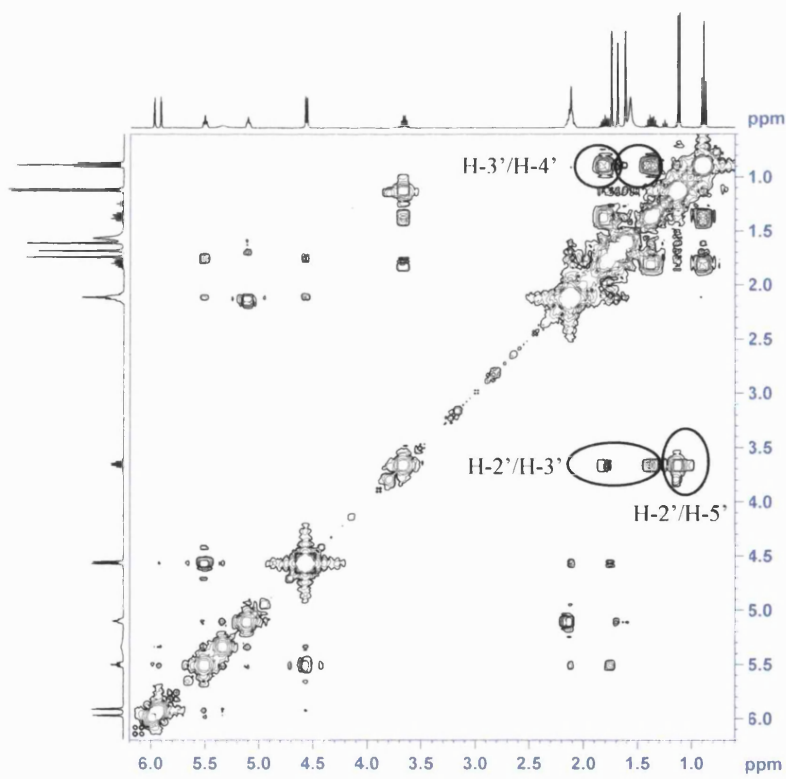


Fig. 76. COSY spectrum of **WS-09**.

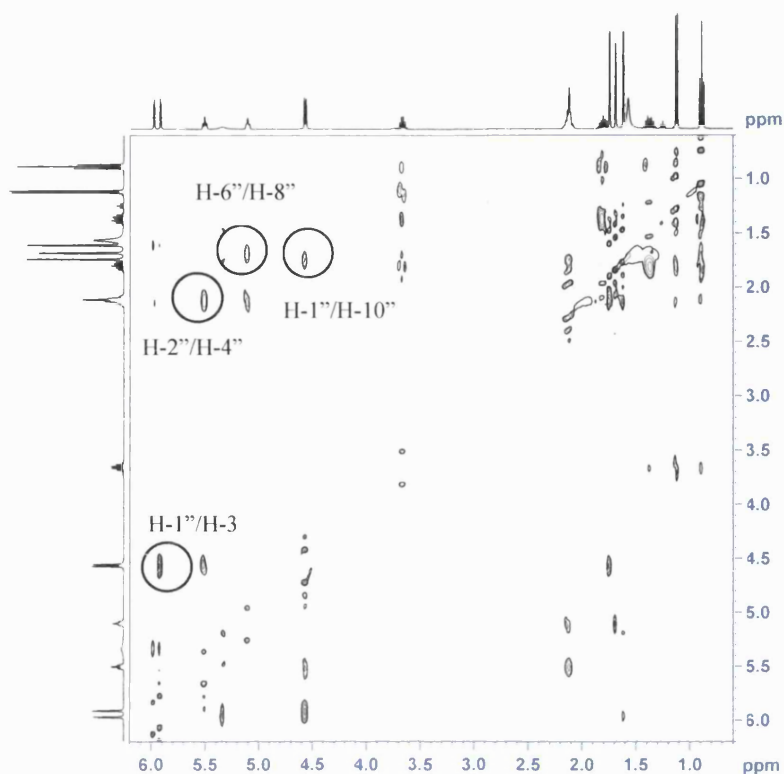


Fig. 77. NOESY spectrum of **WS-09**.

The  $^1\text{H}$  NMR spectrum (Fig. 74, Table 18) showed two signals for hydroxyl groups, one of which was highly deshielded hydrogen-bonded ( $\delta_{\text{H}}$  14.02) and the other appeared as a broad singlet at  $\delta_{\text{H}}$  5.32. Other signals observed in the  $^1\text{H}$  NMR spectrum included two *meta*-coupled aromatic protons ( $\delta_{\text{H}}$  5.98 d,  $J = 2.5$  Hz; 5.92 d,  $J = 2.5$  Hz), two olefinic protons ( $\delta_{\text{H}}$  5.51 m; 5.10 m), one methine ( $\delta_{\text{H}}$  3.66, 1H), four methylene groups, three methyl singlets ( $\delta_{\text{H}}$  1.74, 1.69, 1.62), one methyl doublet ( $\delta_{\text{H}}$  1.12,  $J = 6.5$  Hz) and one methyl triplet ( $\delta_{\text{H}}$  0.89,  $J = 7.5$  Hz). The  $^{13}\text{C}$  spectrum displayed signals for six aromatic carbons, three of which were highly deshielded, implying that these carbons were attached to electron-withdrawing groups. The pattern of these signals suggested a 1,3,5-trihydroxybenzene (phloroglucinol) structure. In the HMBC spectrum (Fig. 75) the hydrogen-bonded proton showed  $^2J$  correlation with the carbon to which it

was directly attached ( $\delta_C$  167.5, C-6), and  $^3J$  correlations with an aromatic methine carbon ( $\delta_C$  96.5, C-5) and a quaternary aromatic carbon ( $\delta_C$  105.0, C-1), confirming the position of this hydroxyl group. The other aromatic hydrogen at  $\delta_H$  5.92 was then placed at C-3 as it was *meta*-coupled to H-5. This was further confirmed by HMBC correlations (Fig. 78) between this proton and C-1, C-5 and a deshielded carbon ( $\delta_C$  161.9, C-4). The second hydroxyl group was therefore placed between the aromatic protons at C-4.

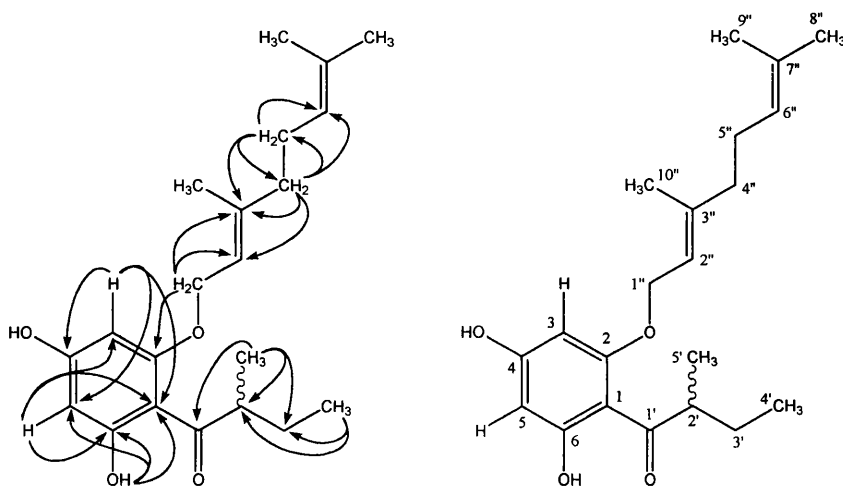


Fig. 78. HMBC correlations for **WS-09**.

The substituent at position C-1 included a methine multiplet ( $\delta_H$  3.66, H-2'), a methylene multiplet ( $\delta_H$  1.37, 1.80, H-3'), a methyl triplet ( $\delta_H$  0.89, H-4') and a methyl doublet ( $\delta_H$  1.12, H-5'). In the COSY spectrum (Fig. 76), the methylene (H-3') was coupled to the methyl triplet (H-4') and the methine multiplet (H-2') which was coupled to the methyl doublet (H-5'). The HMBC spectrum showed crosspeaks between the methyl doublet and C-2', C-3' and a carbonyl carbon ( $\delta_C$  210.4, C-1') which could interact with the hydroxyl group at C-6 *via* the hydrogen bond. This confirmed the 2-methylbutanoyl side-chain at position C-1.

The final substituent at C-2 included an oxymethylene group ( $\delta_{\text{H}}$  4.57 d,  $J = 6.5$  Hz), which showed  $^1\text{H}$ - $^{13}\text{C}$  correlations with a deshielded aromatic carbon ( $\delta_{\text{C}}$  162.6, C-2) and two carbons associated with an olefin group ( $\delta_{\text{C}}$  118.2, C-2'';  $\delta_{\text{C}}$  142.3, C-3''). In the HMBC spectrum, the olefinic proton ( $\delta_{\text{H}}$  5.51 m) at C-2'' was coupled to a methyl group ( $\delta_{\text{C}}$  16.7, C-10'') and a methylene group ( $\delta_{\text{C}}$  39.5, C-4'') *via* three bonds. This methylene group ( $\delta_{\text{H}}$  2.13 m, H-4'') showed  $^2J$  correlations with C-3'' and C-5'' ( $\delta_{\text{C}}$  26.3), and  $^3J$  correlations with C-2'' and C-6'' ( $\delta_{\text{C}}$  123.6). The two methyl singlets ( $\delta_{\text{H}}$  1.62, 1.69) which coupled to C-6'' and a quaternary carbon associated with this olefin ( $\delta_{\text{C}}$  132.0, C-7'') completed the substituent at C-2. This side-chain consisted of ten carbons, including two olefin groups and three methyl groups, and is characteristic of a geranyl group. The COSY and NOESY spectra also provided evidence for the geranyl side-chain. Both olefinic hydrogens and olefinic methyls were assigned as the *trans* configuration based on the nature of the biosynthesis of a geranyl side-chain from two isoprene units. This was also supported by an NOE correlation between H-6'' and H-8''. The  $^1\text{H}$  and  $^{13}\text{C}$  NMR data on the geranyloxy side-chain (Table 18) showed a good agreement with that in the literature (Hu *et al.*, 2000).

The position of the geranyl side-chain was assigned as *ortho*- to the 2-methylbutanoyl group based on the HMBC correlations as described and also the observation that the *meta*-coupled aromatic protons were non-equivalent. A geranyl substitution at the hydroxyl group *para*- to the acyl side-chain would mean that the two *meta*-coupled protons were equivalent due to a plane of symmetry in the molecule, thus showing a singlet integrating to two protons

instead of two doublets in the  $^1\text{H}$  NMR spectrum. The stereochemistry at the chiral centre C-2' can be identified by comparing the specific rotation of this compound with that of the synthetic compound **WS-S-07**, which was synthesized from (+)-*S*-2-methylbutanoic acid. The specific rotation of **WS-09** and **WS-S-07** was found to be  $+6.0^\circ$  ( $c = 0.25$ , chloroform) and  $+6.0^\circ$  ( $c = 0.30$ , chloroform) respectively. The data implied that the chiral centre in the natural product **WS-09** was in the *S*-configuration. **WS-09** was therefore identified as the new natural product 4,6-dihydroxy-2-*O*-(3'',7''-dimethyl-2'',6''-octadienyl)-1-(2'-methylbutanoyl)-benzene. A patent has been filed for this compound in 2007 for its application as a potential antibacterial agent. The method of synthesizing this compound was also described in the same patent.

Table 18.  $^1\text{H}$  (500MHz) and  $^{13}\text{C}$  NMR (125 MHz) spectral data and  $^1\text{H}$ - $^{13}\text{C}$  long-range correlations for **WS-09** recorded in chloroform-*d*.

Position	$^1\text{H}$ ( <i>J</i> , Hz)	$^{13}\text{C}$	$^2J$	$^3J$
1	-	105.0	-	-
2	-	162.6	-	-
3	5.92 d (2.5)	91.5	C-4	C-1, C-5
4	-	161.9	-	-
5	5.98 d (2.5)	96.5	C-6	C-1, C-3
6	-	167.5	-	-
1'	-	210.4	-	-
2'	3.66 m	46.1	-	-
3'	1.37 m, 1.80 m	26.8	-	-
4'	0.89 t (7.5)	11.8	C-3'	C-2'
5'	1.12 d (6.5)	16.6	C-2'	C-1', C-3'
1''	4.57 d (6.5)	65.7	C-2''	C-2, C-3''
2''	5.51 m	118.2	-	C-4'', C-10''
3''	-	142.3	-	-
4''	2.13 m	39.5	C-3'', C-5''	C-2'', C-6''
5''	2.10 m	26.3	C-4'', C-6''	C-3''
6''	5.10 m	123.6	-	-
7''	-	132.0	-	-
8''	1.69 s	25.7	C-7''	C-6'', C-9''
9''	1.62 s	17.7	C-7''	C-6'', C-8''
10''	1.74 s	16.7	C-3''	C-2'', C-4''
4-OH	5.32 bs	-	-	-
6-OH	14.02 s	-	C-6	C-1, C-5

### 3.2.9.2 Characterization of WS-10 as 4,6-dihydroxy-2-*O*-(7''-hydroxy-3'',7''-dimethyl-2'',5''-octadienyl)-1-(2'-methylbutanoyl)-benzene

WS-10 was isolated as a pale yellow oil from the DCM extract of *H. olympicum* *L. cf. uniflorum*. HR ESI-MS gave an  $[M+H]^+$  ion at  $m/z$  363, indicating a molecular formula of  $C_{21}H_{30}O_5$ .

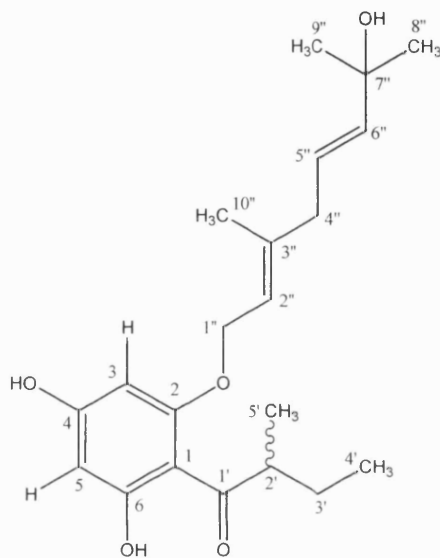


Fig. 79. Structure of WS-10.

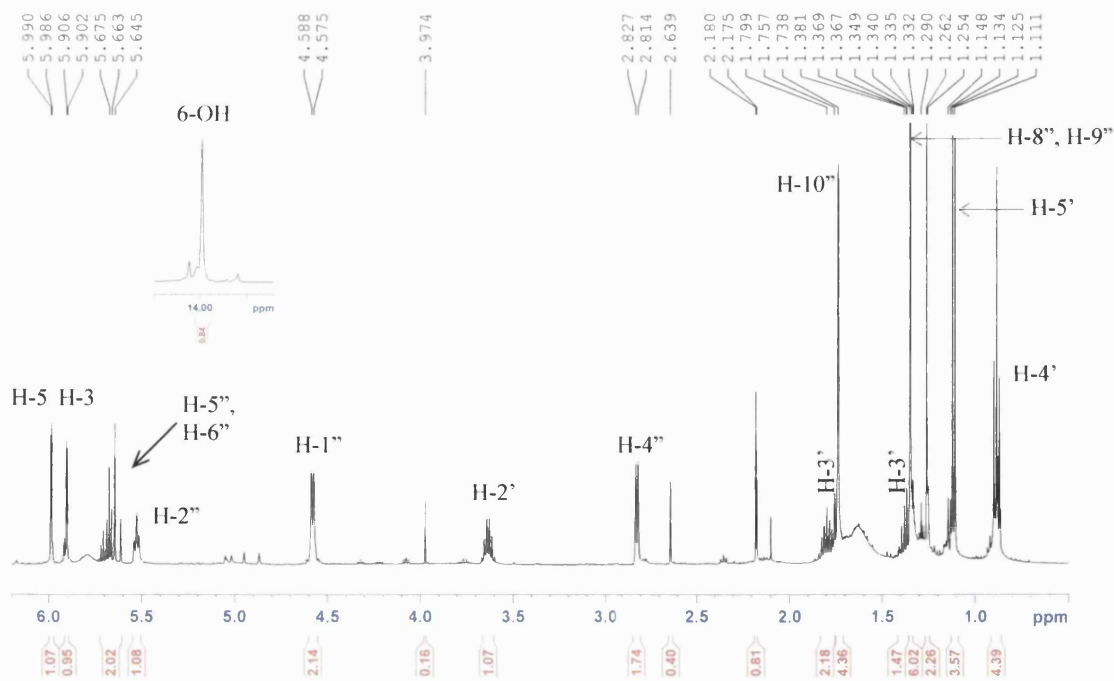


Fig. 80.  $^1H$  NMR spectrum of WS-10 in chloroform-*d* recorded at 500 MHz.

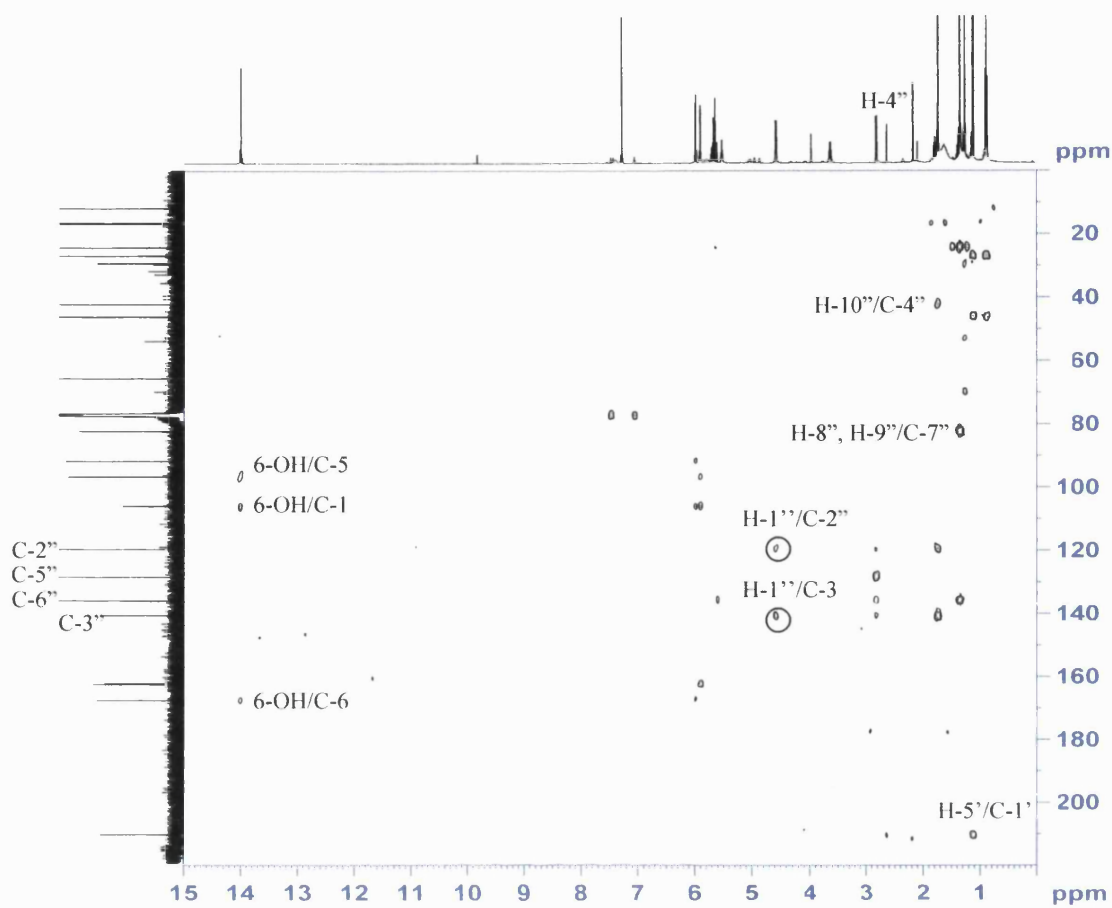


Fig. 81. HMBC spectrum of WS-10.

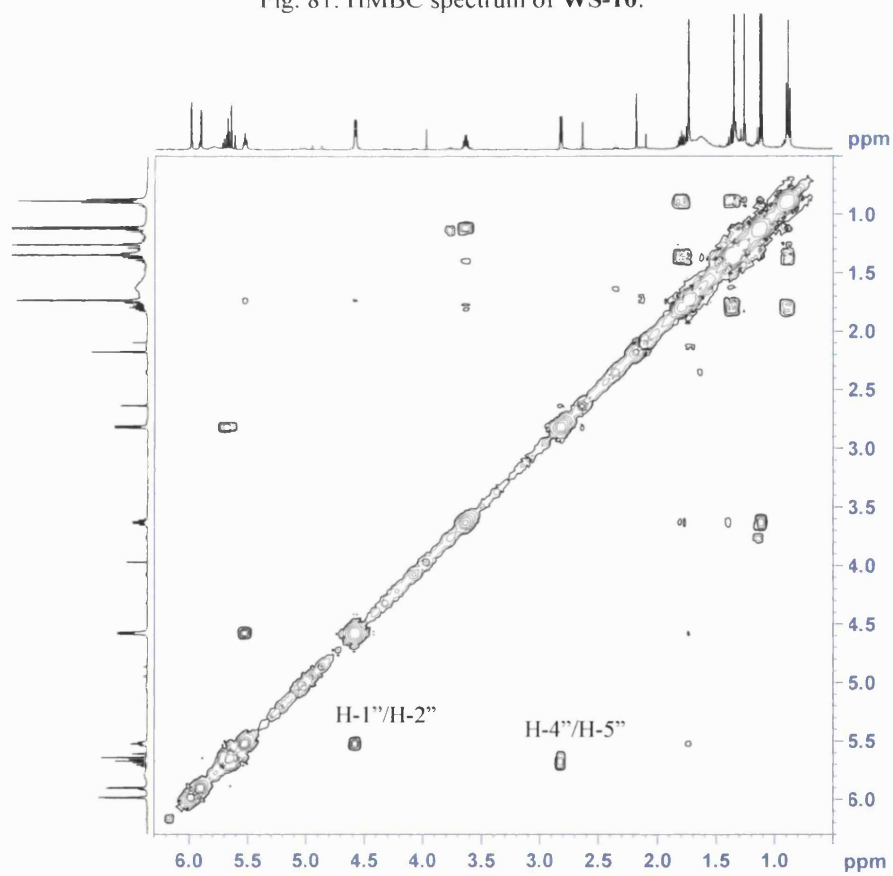


Fig. 82. COSY spectrum of WS-10.

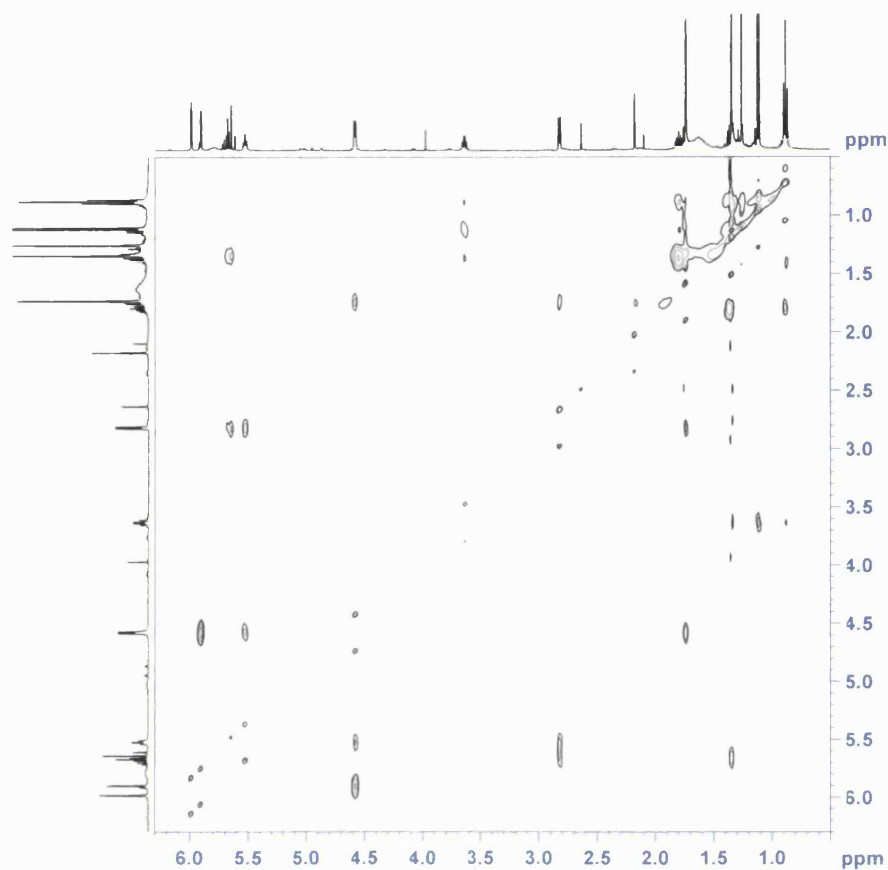


Fig. 83. NOESY spectrum of **WS-10**.

The  $^1\text{H}$  and  $^{13}\text{C}$  NMR spectral data (Table 19) were very similar to that of **WS-09**. The  $^1\text{H}$  NMR signals (Fig. 80) indicated the presence of a 2-methylbutanoyl phloroglucinol nucleus with one highly-desielded hydrogen-bonded hydroxyl group ( $\delta_{\text{H}}$  14.00), two *meta*-coupled aromatic protons ( $\delta_{\text{H}}$  5.90 d,  $J = 2$  Hz, H-3; 5.99 d,  $J = 2$  Hz, H-5), one methine multiplet ( $\delta_{\text{H}}$  3.63, 1 H, H-2'), one methylene ( $\delta_{\text{H}}$  1.37 m, 1.80 m, H-3'), one methyl triplet ( $\delta_{\text{H}}$  0.88,  $J = 7.5$  Hz, H-4') and one methyl doublet ( $\delta_{\text{H}}$  1.12,  $J = 7$  Hz, H-5'). The  $^{13}\text{C}$  signals of **WS-10** (Table 19) were indicative of a phloroglucinol with six aromatic carbons, comprising three deshielded quaternary carbons ( $\delta_{\text{C}}$  167.5, C-6; 162.4, C-2; 162.1, C-4), one quaternary carbon at  $\delta_{\text{C}}$  105.9 (C-1) and two methines at  $\delta_{\text{C}}$  96.6 (C-5) and 91.7 (C-3). The presence of a carbonyl carbon ( $\delta_{\text{C}}$  210.3, C-1'), one methine ( $\delta_{\text{C}}$  46.1, C-2'), one methylene ( $\delta_{\text{C}}$  26.9, C-3') and two methyl carbon signals ( $\delta_{\text{C}}$  11.9, C-

4'; 16.7, C-5') suggested a 2-methylbutanoyl side-chain as seen in **WS-09**. The structure of the 2-methylbutanoyl phloroglucinol nucleus was further confirmed by HMBC correlations (Fig. 81 and 84), which was described earlier in the structural elucidation of **WS-09**.

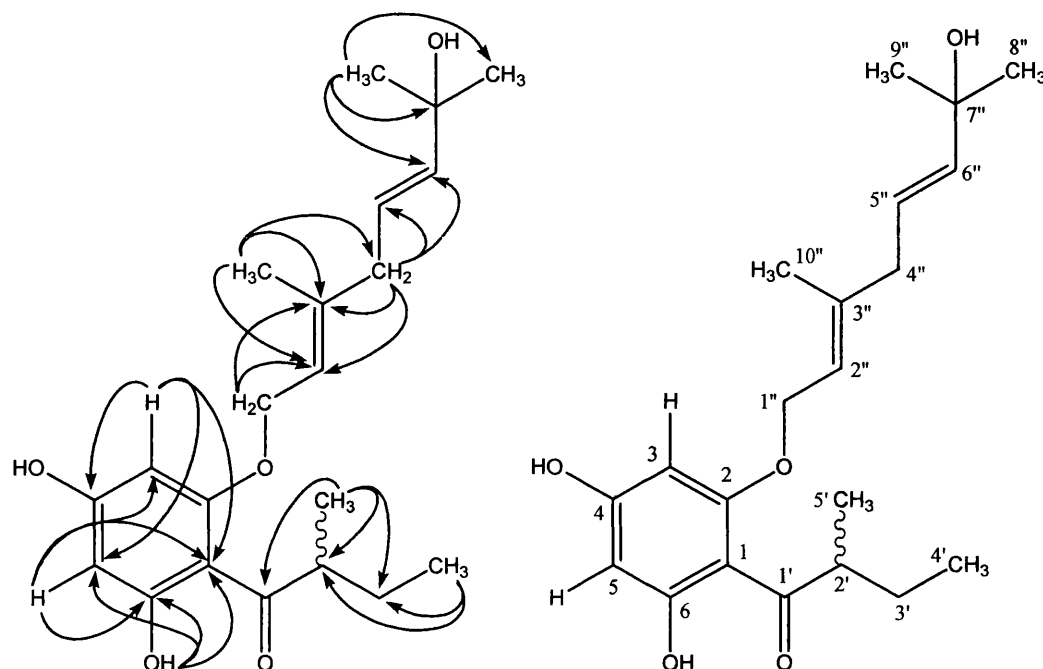


Fig. 84. HMBC correlations for **WS-10**.

The remaining signals in the  $^1\text{H}$  NMR spectrum included three olefinic protons ( $\delta_{\text{H}}$  5.30 m, H-2'', 5.68 m, H-5''; 5.66 d,  $J = 15$  Hz, H-6''), two methylene doublets including one shifted downfield at  $\delta_{\text{H}}$  4.58 ( $J = 6.5$  Hz, H-1'') and one at  $\delta_{\text{H}}$  2.81 ( $J = 6.5$  Hz, H-4''), two equivalent methyl groups integrating to six protons ( $\delta_{\text{H}}$  1.35, s, H-8'', H-9'') and an additional methyl singlet ( $\delta_{\text{H}}$  1.74, H-10''). The remaining signals in the  $^{13}\text{C}$  NMR spectra included one quaternary olefinic carbon ( $\delta_{\text{C}}$  140.5, C-3''), three olefinic methines ( $\delta_{\text{C}}$  119.6, C-2''; 128.4, C-5''; 135.9, C-6''), an oxygenated quaternary carbon ( $\delta_{\text{C}}$  82.2, C-7''), two methylenes

( $\delta_C$  65.6, C-1''; 42.2, C-4''), two equivalent methyl carbons at  $\delta_C$  24.3 (C-8'', C-9'') and a further methyl carbon at  $\delta_C$  16.8 (C-10'').

An oxymethylene ( $\delta_H$  4.58 d, H-1'') was correlated to the olefinic proton at  $\delta_H$  5.30 (H-2'') in the COSY spectrum (Fig. 82). It also displayed  $^1H$ - $^{13}C$   $^2J$  correlation to the olefinic carbon at  $\delta_C$  119.6 (C-2'') and  $^3J$  correlation to a quaternary olefinic carbon ( $\delta_C$  140.5, C-3'') to which a methyl group ( $\delta_H$  1.74, s, H-10'') was directly attached (Fig. 84). The olefinic hydrogen (H-2'') and the methyl group (H-10'') were assigned as the *trans* configuration because of the nature of the biosynthesis pathway. This methyl group was correlated to a methylene carbon at  $\delta_C$  42.2 (C-4'') in the HMBC spectrum, thus placing the methylene group ( $\delta_H$  2.81 d, H-4'') next to C-3''. This methylene doublet in turn displayed  $^1H$ - $^{13}C$  correlations to the four olefinic carbons, therefore further confirming its position between the two olefinic groups. The olefinic multiplet at  $\delta_H$  5.68 (H-5'') was then placed between the methylene group (H-4'') and the olefinic doublet ( $\delta_H$  5.66, H-6'') as they showed correlations in the COSY spectrum. The splitting of the olefinic multiplet ( $\delta_H$  5.68, H-5'') was due to the fact that the signal was split by the neighbouring methylene and olefinic proton at C-6''. On the other hand, the olefinic proton at  $\delta_H$  5.66 (H-6'') appeared as a doublet because the signal was only split by the neighbouring H-5''. The large coupling constant between H-5'' and H-6'' ( $J = 15$  Hz) indicated that these two protons were in a *trans* configuration. The equivalent methyl singlets ( $\delta_C$  1.35 s, 6 H, H-8'', H-9'') at the terminus of the side-chain were directly attached to a quaternary carbon shifted downfield by an electron-withdrawing group (hydroxyl

group in this case) at  $\delta_C$  82.2 (C-7''). This connection was supported by the HMBC correlations between the methyl singlet and C-7'' and the olefinic carbon at C-6''. This completed the structural elucidation of **WS-10**. The specific rotation of **WS-10** was found to be  $+5.8^\circ$  ( $c = 0.12$ , chloroform), which might again imply that the chiral centre at C-2' was in an *S*-configuration (synthetic compound **WS-S-07**,  $+6.0^\circ$  ( $c = 0.30$ , chloroform)). **WS-10** was identified as 4,6-dihydroxy-2-*O*-(7''-hydroxy-3'',7''-dimethyl-2'',5''-octadienyl)-1-(2'-methylbutanoyl)-benzene. It is a new natural product and is described here for the first time.

Table 19.  $^1\text{H}$  (500MHz) and  $^{13}\text{C}$  NMR (125 MHz) spectral data and  $^1\text{H}$ - $^{13}\text{C}$  long-range correlations of **WS-10** recorded in chloroform-*d*.

Position	$^1\text{H}$ ( <i>J</i> , Hz)	$^{13}\text{C}$	$^2J$	$^3J$
1	-	105.9	-	-
2	-	162.4	-	-
3	5.90 d (2)	91.7	C-4	C-1, C-5
4	-	162.1	-	-
5	5.99 d (2)	96.6	C-6	C-1, C-3
6	-	167.5	-	-
1'	-	210.3	-	-
2'	3.63 m	46.1	-	-
3'	1.37 m, 1.80 m	26.9	-	-
4'	0.88 t (7.5)	11.9	C-3'	C-2'
5'	1.12 d (7)	16.7	C-2'	C-1', C-3'
1''	4.58 d (6.5)	65.6	C-2''	C-3''
2''	5.30 m	119.6	-	-
3''	-	140.5	-	-
4''	2.81 d (6.5)	42.2	C-3'', C-5''	C-2'', C-6''
5''	5.68 m	128.4	-	-
6''	5.66 d (15)	135.9	-	-
7''	-	82.2	-	-
8''/9''	1.35 s	24.3	C-7''	C-6'', C-9''/8''
10''	1.74 s	16.8	C-3''	C-2'', C-4''
6-OH	14.00 s	-	C-6	C-1, C-5

3.2.9.3 Characterization of WS-11 as 4,6-dihydroxy-2-*O*-(6''-hydroxy-3'',7''-dimethyl-2'',7''-octadienyl)-1-(2'-methylbutanoyl)-benzene

WS-11 was isolated as a pale yellow oil from the DCM extract of *H. olympicum L. cf. uniflorum*. HR ESI-MS gave an  $[M+H]^+$  ion at  $m/z$  363, giving a molecular formula of  $C_{21}H_{30}O_5$ .

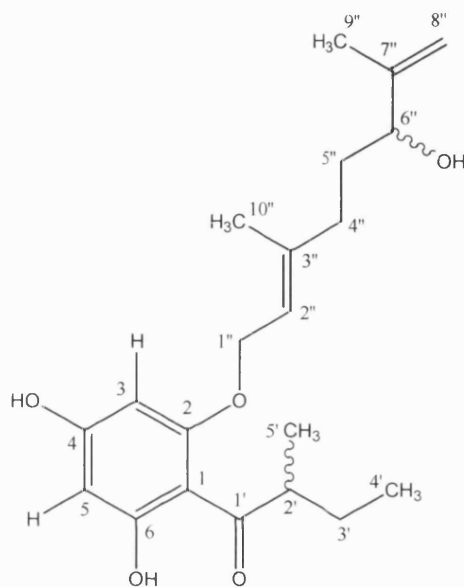


Fig. 85. Structure of WS-11.

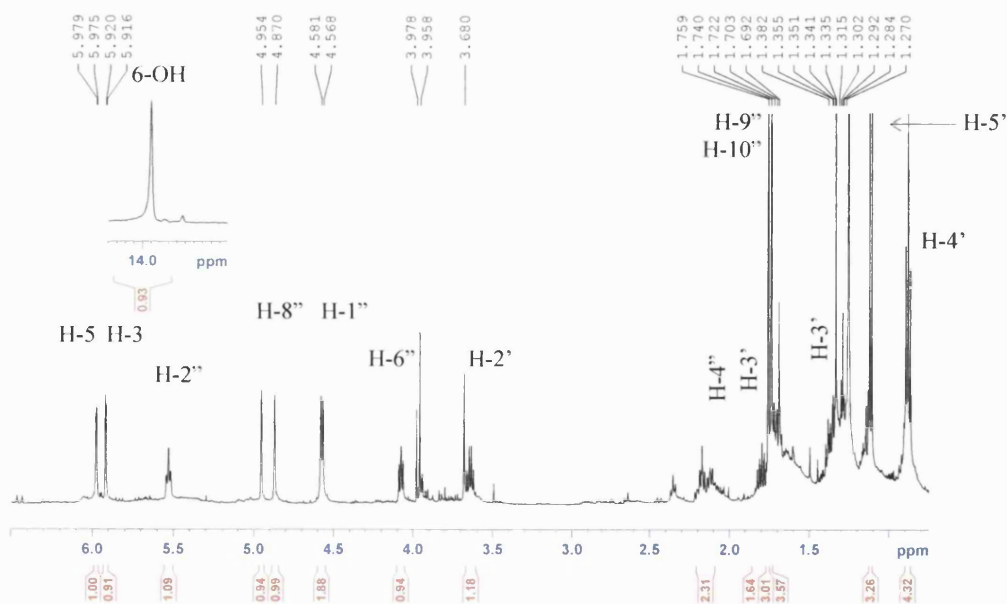


Fig. 86.  $^1H$  NMR spectrum of WS-11 in chloroform-*d* recorded at 500 MHz.

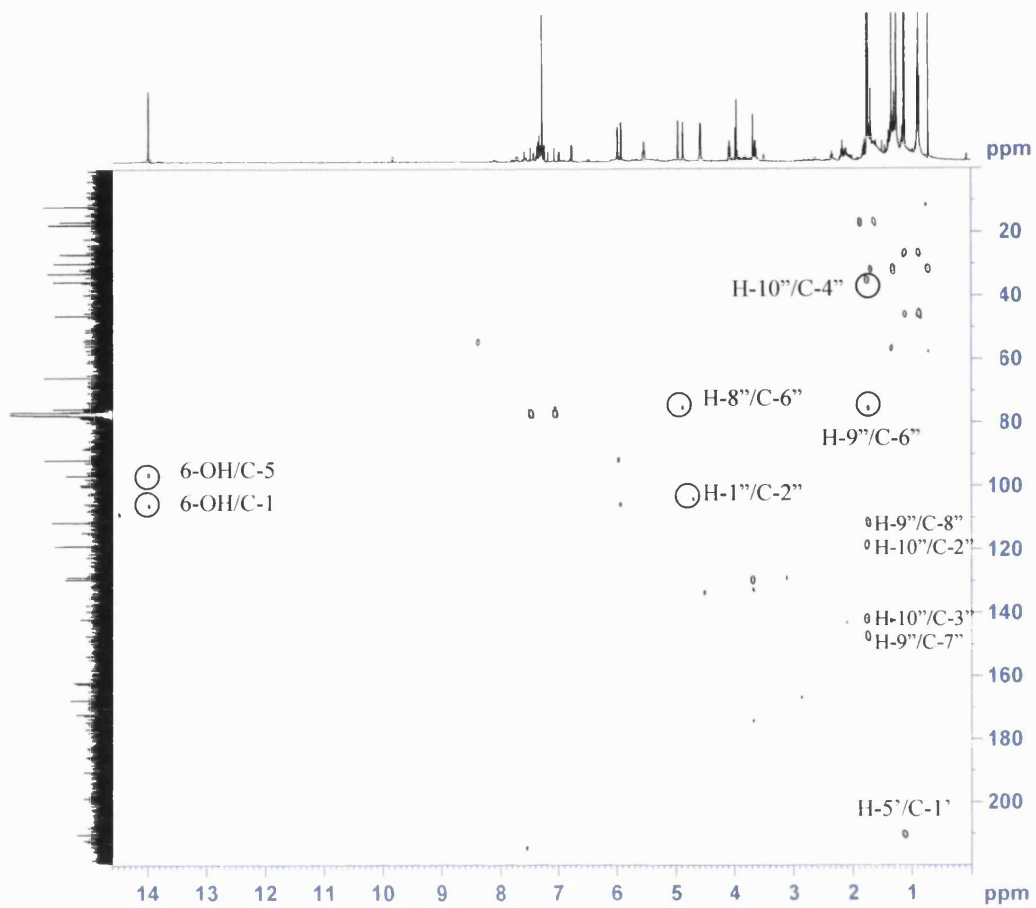


Fig. 87. HMBC spectrum of WS-11.

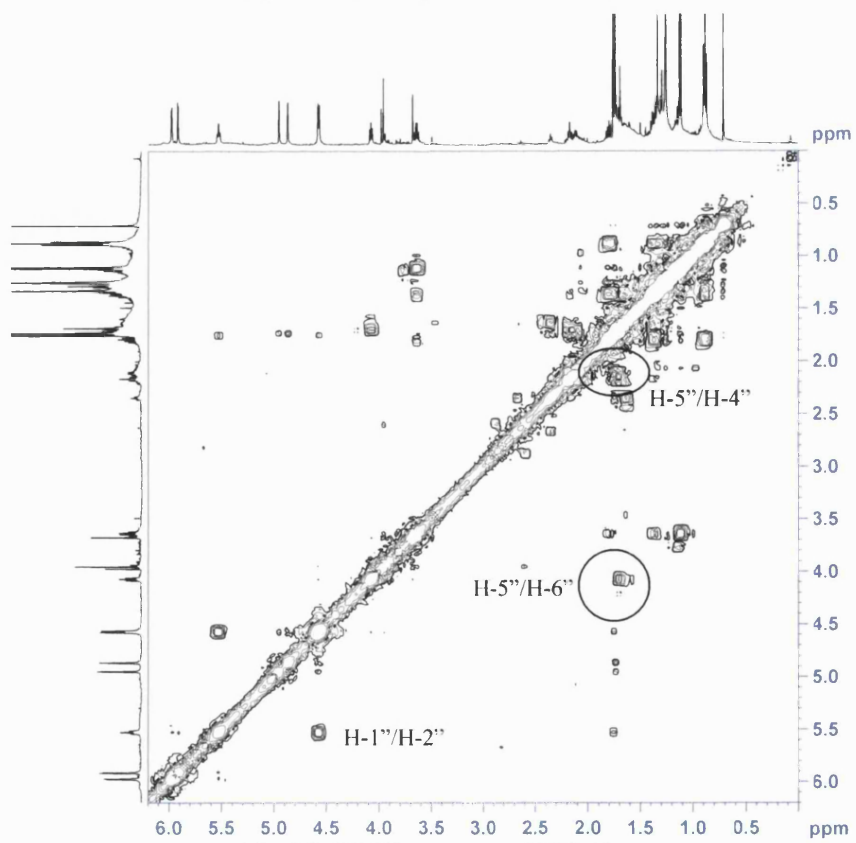


Fig. 88. COSY spectrum of WS-11.

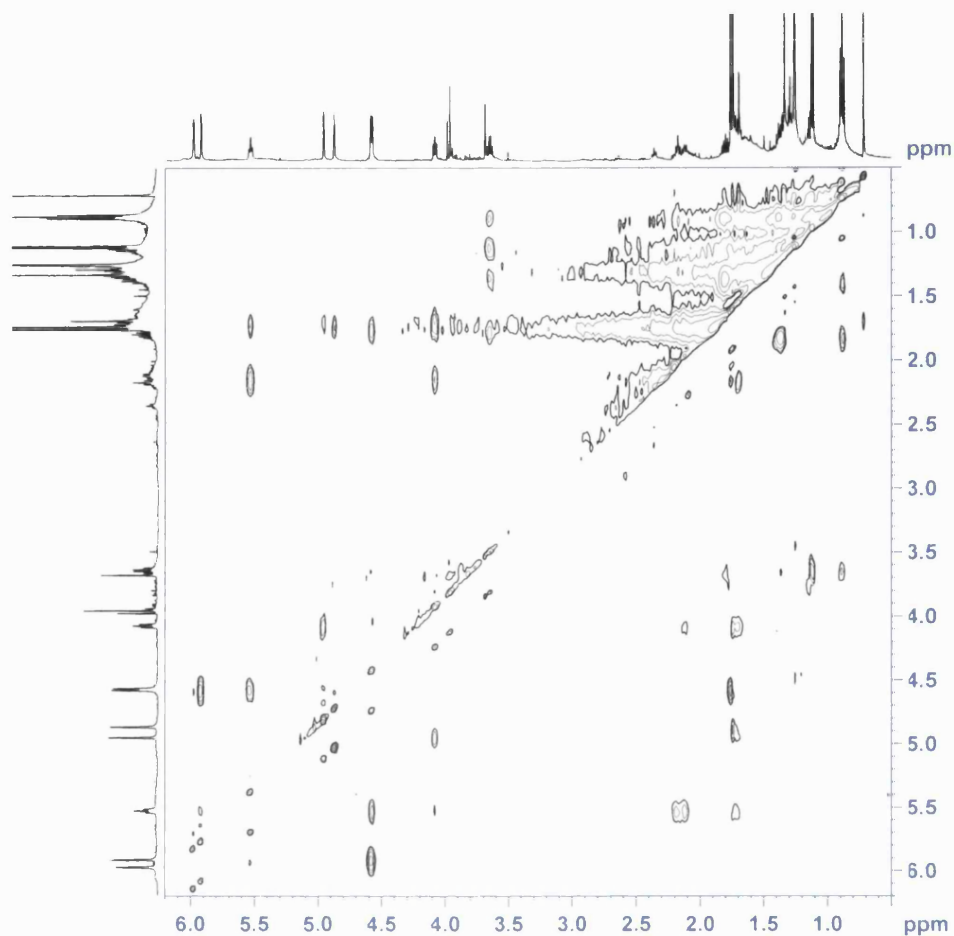


Fig. 89. NOESY spectrum of **WS-11**.

The  $^1\text{H}$  and  $^{13}\text{C}$  NMR spectral data (Table 20) were again very similar to that of **WS-09**. The common signals in the  $^1\text{H}$  NMR spectrum (Fig. 86) included one highly-deshielded hydrogen-bonded hydroxyl group ( $\delta_{\text{H}}$  13.99, 6-OH), two *meta*-coupled aromatic protons ( $\delta_{\text{H}}$  5.92 d,  $J = 2$  Hz, H-3; 5.98 d,  $J = 2$  Hz, H-5), one methine ( $\delta_{\text{H}}$  3.64 m, H-2'), one methylene ( $\delta_{\text{H}}$  1.37 m, 1.80 m, H-3'), one methyl triplet ( $\delta_{\text{H}}$  0.88 t,  $J = 7.5$  Hz, H-4') and one methyl doublet ( $\delta_{\text{H}}$  1.12 d,  $J = 6.5$  Hz, H-5'). In the  $^{13}\text{C}$  spectrum, signals suggesting a 2-methylbutanoyl phloroglucinol nucleus were again seen, including three deshielded quaternary aromatic carbons ( $\delta_{\text{C}}$  167.6, C-6; 162.4, C-2; 161.9, C-4) one quaternary aromatic carbon ( $\delta_{\text{C}}$  105.9, C-1), two methine aromatic carbons ( $\delta_{\text{C}}$  91.6 C-3;

96.6, C-5), one carbonyl carbon ( $\delta_C$  210.3, C-1'), one methine ( $\delta_C$  46.1, C-2'), one methylene ( $\delta_C$  26.8, C-3') and two methyl carbons ( $\delta_C$  11.9, C-4'; 16.7, C-6'). HMBC correlations (Fig. 90, Table 20) further confirmed the structure of the 2-methylbutanoyl phloroglucinol nucleus and were very similar to those described in the structural elucidation of **WS-09**.

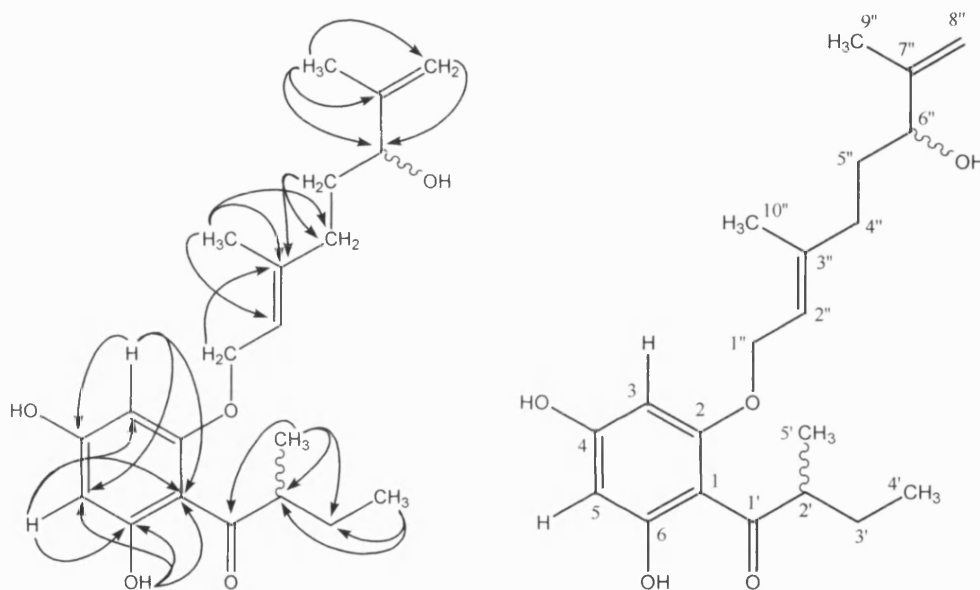


Fig. 90. HMBC correlations for **WS-11**.

The  $^1\text{H}$  NMR signals for the side-chain at the 2-*O* position consisted of four methylenes, including one shifted downfield ( $\delta_H$  4.57 d,  $J = 6.5$  Hz, H-1'') and an *exo*-methylene ( $\delta_H$  4.87 bs, 4.95 s, H-8''), one olefinic proton ( $\delta_H$  5.53 t, H-2''), one deshielded methine triplet ( $\delta_H$  4.08,  $J = 6.5$  Hz, H-6'') and two methyl singlets ( $\delta_H$  1.76, H-9''; 1.74, H-10''). Ten carbons were accountable for this side-chain, including two methines ( $\delta_C$  118.7, C-2''; 75.5, C-6''), four methylenes ( $\delta_C$  65.6, C-1''; 35.5, C-4''; 26.8, C-5''; 111.4, C-8''), two quaternary olefinic carbons ( $\delta_C$  141.9, C-3'', 147.2, C-7'') and two methyl carbons ( $\delta_C$  16.7, C-9'', 17.6, C-10'').

The oxymethylene group showed HMBC correlations (Fig. 90) with an olefinic carbon at  $\delta_C$  118.7 (C-2'') and COSY correlation (Fig. 88) to the olefinic proton ( $\delta_H$  5.53) at C-2''. The methyl singlet at  $\delta_H$  1.74 (H-10'') showed HMBC correlations with C-2'', an olefinic carbon to which it was directly attached ( $\delta_C$  141.9, C-3''), and a methylene carbon at  $\delta_C$  35.5 (C-4''). The methylene protons at C-4'' were coupled to another methylene group ( $\delta_H$  1.75 m) which was coupled to a methine triplet ( $\delta_H$  4.08, H-6'') as shown in the COSY spectrum. This triplet was shifted downfield and was attached to a carbon at  $\delta_C$  75.5 (C-6''), indicating that an electron-withdrawing group (in this case an hydroxyl group as suggested by the mass spectrometry results) was present at this carbon. The remaining methyl ( $\delta_H$  1.76) was placed at C-7'' as the methyl singlet showed  $^2J$  HMBC correlation to a quaternary carbon at  $\delta_C$  143.3 (C-7'') and  $^3J$  correlations to the oxygenated methine carbon (C-6'') and an olefinic carbon at  $\delta_C$  111.4 (C-8''), bearing two *exo*-methylene hydrogens. The specific rotation of **WS-11** was  $+2.5^\circ$  (c 0.41, chloroform). Although it showed the same direction of rotation as **WS-S-07**, the synthetic (*S*)-isomer of **WS-09** ( $[\alpha]_D^{22} +2.5^\circ$ ), the stereochemistry of **WS-11** could not be determined as two chiral centres were present in this compound. **WS-11** was identified as the new natural product, 4,6-dihydroxy-2-*O*-(6''-hydroxy-3'',7''-dimethyl-2'',7''-octadienyl)-1-(2'-methylbutanoyl)-benzene, and is reported here for the first time.

Table 20.  $^1\text{H}$  (500MHz) and  $^{13}\text{C}$  NMR (125 MHz) spectral data and  $^1\text{H}$ - $^{13}\text{C}$  long-range correlations of **WS-11** recorded in chloroform-*d*.

Position	$^1\text{H}$ ( <i>J</i> , Hz)	$^{13}\text{C}$	$^2J$	$^3J$
1	-	105.9	-	-
2	-	162.4	-	-
3	5.92 d (2)	91.6	-	C-1
4	-	161.9	-	-
5	5.98 d (2)	96.6	-	C-3
6	-	167.6	-	-
1'	-	210.3	-	-
2'	3.64 m	46.1	-	-
3'	1.37 m, 1.80 m	26.8	-	-
4'	0.88 t (7.5)	11.9	C-3'	C-2'
5'	1.12 d (6.5)	16.7	C-2'	C-1', C-3'
1''	4.57 d (6.5)	65.6	-	C-3''
2''	5.53 t	118.7	-	-
3''	-	141.9	-	-
4''	2.15 m	35.5	-	-
5''	1.75 m	26.8	C-4''	C-3''
6''	4.08 t (6.5)	75.5	-	-
7''	-	147.2	-	-
8''	4.95 s, 4.87 bs	111.4	-	C-6''
9''	1.76 s	16.7	C-7''	C-6'', C-8''
10''	1.74 s	17.6	C-3''	C-2'', C-4''
6-OH	13.99 s	-	-	C-1, C-5

**3.2.9.4 Characterization of WS-12 as 4,6-dihydroxy-2-*O*-(6''-hydroperoxy-3'',7''-dimethyl-2'',7''-octadienyl)-1-(2'-methylbutanoyl)-benzene**

WS-12 was isolated as a pale yellow oil from the DCM extract of *H. olympicum* *L. cf. uniflorum*. HR ESI-MS gave an  $[M+H]^+$  ion at  $m/z$  379, indicating a molecular formula of  $C_{21}H_{30}O_6$ .

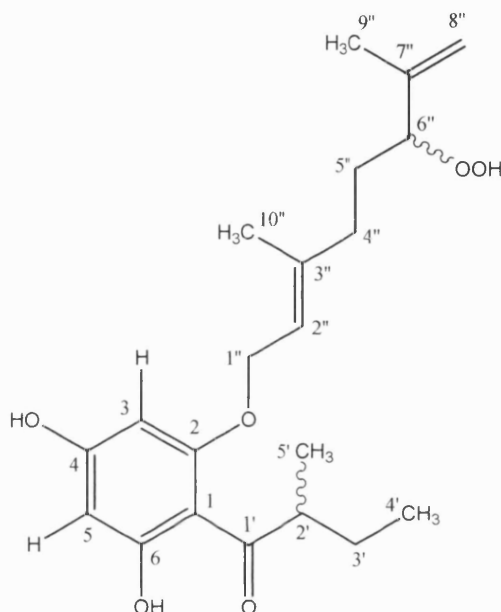


Fig. 91. Structure of WS-12.

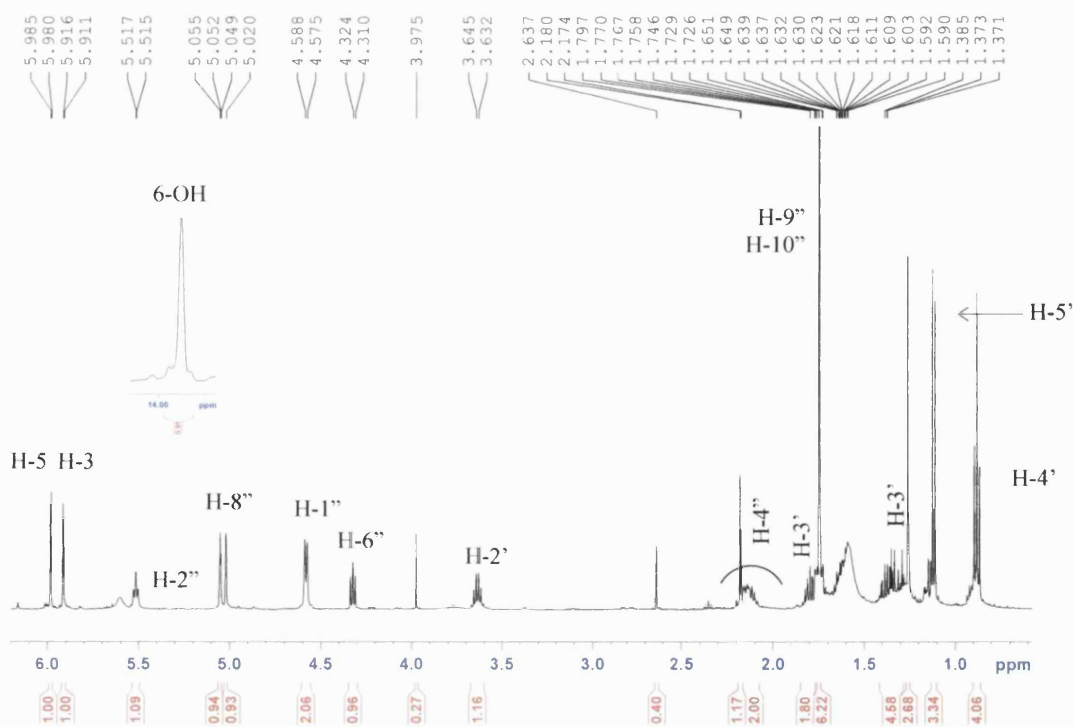


Fig. 92.  $^1H$  NMR spectrum of WS-12 in chloroform-*d* recorded at 500 MHz.

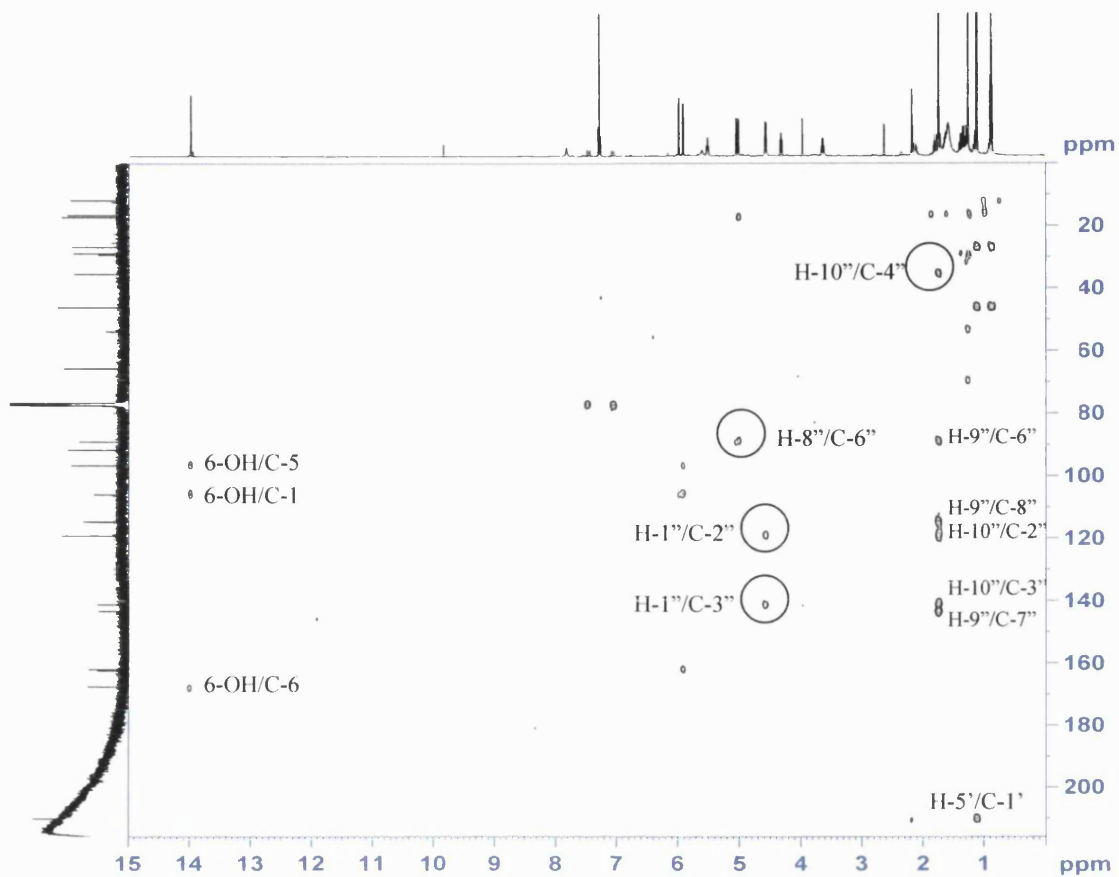


Fig. 93. HMBC spectrum of WS-12.

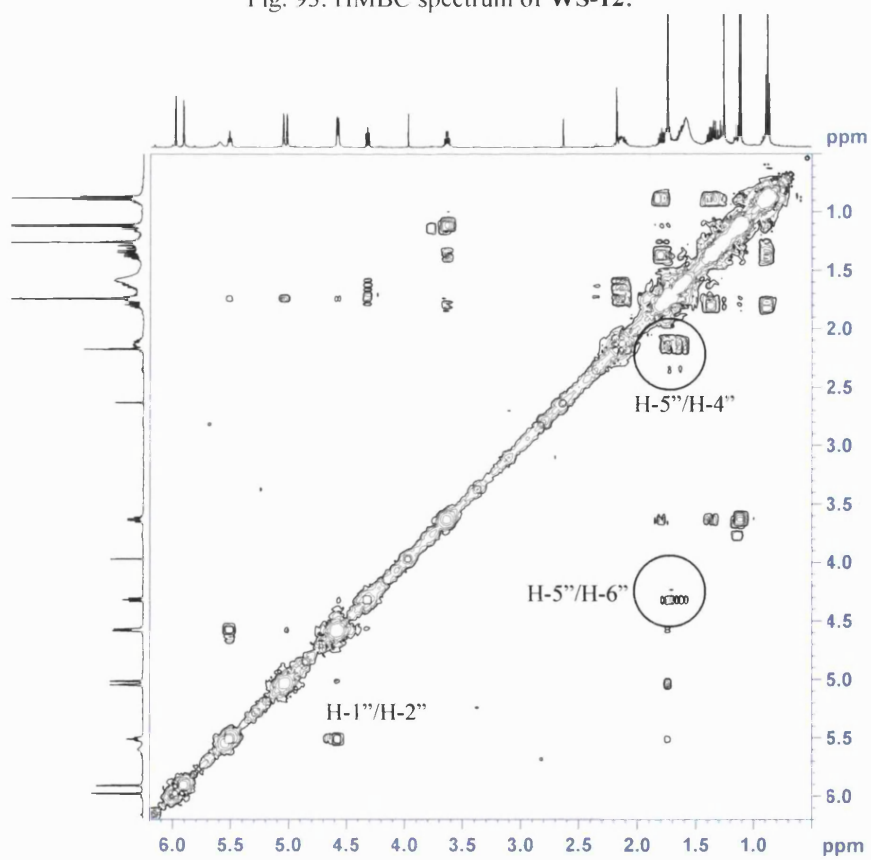


Fig. 94. COSY spectrum of WS-12.

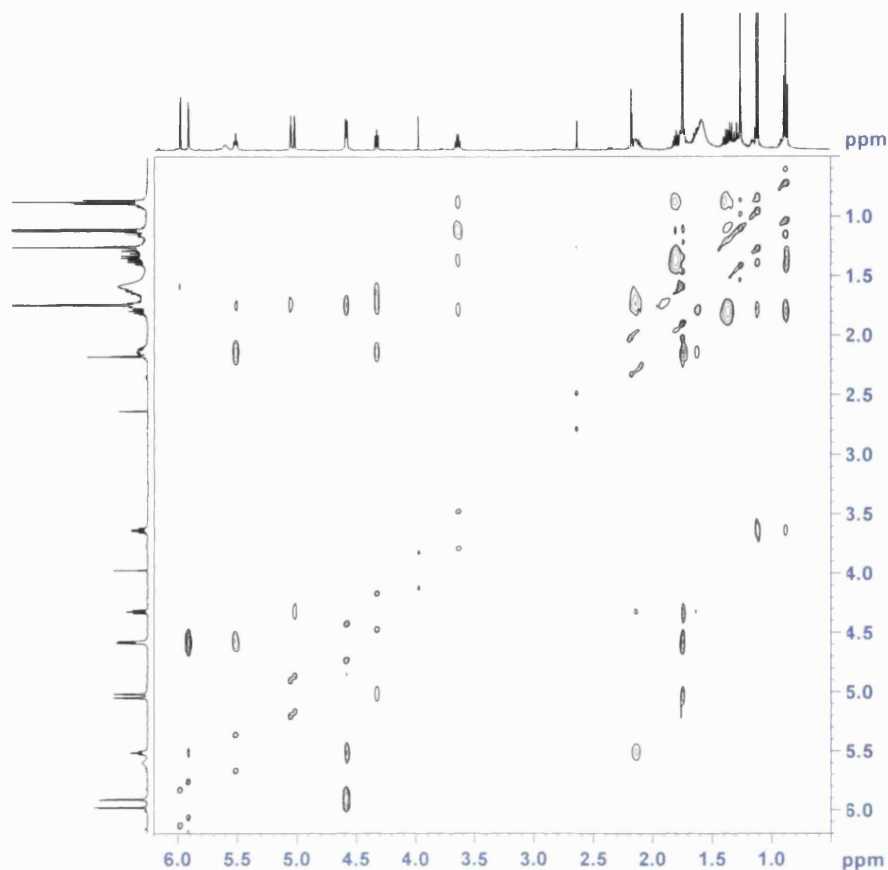


Fig. 95. NOESY spectrum of **WS-12**.

The  $^1\text{H}$  and  $^{13}\text{C}$  NMR data (Table 21) of **WS-12** were almost identical to those of **WS-11**. The characteristic  $^1\text{H}$  NMR features of a 2-methylbutanoyl phloroglucinol were again seen in this compound, including one highly-deshielded hydrogen-bonded hydroxyl group ( $\delta_{\text{H}}$  13.99, 6-OH), two *meta*-coupled aromatic protons ( $\delta_{\text{H}}$  5.91 d,  $J = 2.5$  Hz, H-3; 5.98 d,  $J = 2.5$  Hz, H-5), one methine ( $\delta_{\text{H}}$  3.63 m, H-2'), one methylene ( $\delta_{\text{H}}$  1.35 m, 1.80 m, H-3'), one methyl triplet ( $\delta_{\text{H}}$  0.88,  $J = 7.5$  Hz, H-4') and one methyl doublet ( $\delta_{\text{H}}$  1.11,  $J = 6$  Hz, H-5'). Signals in the  $^{13}\text{C}$  NMR spectrum accounting for a 2-methylbutanoyl phloroglucinol nucleus consisted of three deshielded quaternary aromatic carbons ( $\delta_{\text{C}}$  167.5, C-6; 162.4, C-3; 162.0, C-4), one quaternary aromatic carbon ( $\delta_{\text{C}}$

105.9, C-1), two aromatic methine carbons ( $\delta_C$  91.7, C-3; 96.6, C-5), one carbonyl carbon ( $\delta_C$  210.3, C-1'), one methine ( $\delta_C$  46.1, C-2'), one methylene ( $\delta_C$  26.8, C-3') and two methyl carbons ( $\delta_C$  11.9, C-4'; 16.6, C-5'). The connection of these protons and carbons was made through HMBC studies (Fig. 96, Table 21) and was described in the structural elucidation of **WS-09**.

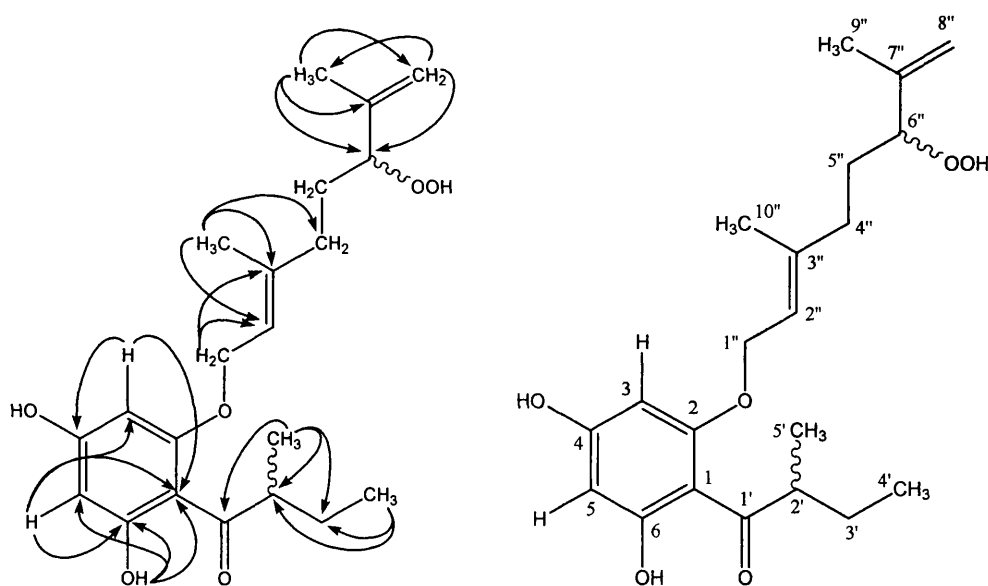


Fig. 96. HMBC correlations for **WS-12**.

The  $^1\text{H}$  NMR signals for the side-chain at the 2-*O* position consisted of four methylenes, including an oxymethylene ( $\delta_H$  4.58 d,  $J = 6.5$  Hz, H-1'') and an exo-methylene ( $\delta_H$  5.02 s, 5.05 bs, H-8''), one olefinic proton ( $\delta_H$  5.52 t,  $J = 6$  Hz, H-2''), one deshielded methine triplet ( $\delta_H$  4.32,  $J = 6.5$  Hz, H-6'') and two overlapping methyl singlets ( $\delta_H$  1.75, 6H, H-9'', H-10''). Ten carbon signals were observed in the  $^{13}\text{C}$  NMR spectrum for this side-chain, including two methines ( $\delta_C$  89.0, C-6''; 119.2, C-2''), four methylenes ( $\delta_C$  65.6, C-1''; 35.2, C-4''; 26.8, C-5'', 114.6, C-8''), two quaternary olefinic carbons ( $\delta_C$  141.2, C-3'';

143.3, C-7'') and two methyl carbons ( $\delta_C$  17.2, C-9''; 16.6, C-10''). These signals were indicative of a geranyl derivative and were again very similar to **WS-11**.

The oxymethylene group ( $\delta_H$  4.58, H-1'') showed HMBC correlations with two carbons at  $\delta_C$  119.2 (C-2'') and  $\delta_C$  141.2 (C-3''), and COSY correlation (Fig. 94) with the olefinic hydrogen at C-2''. The methyl singlet at  $\delta_H$  1.74 (H-10'') showed  $^2J$  HMBC correlation to the olefinic carbon to which it was directly attached (C-3''), and  $^3J$  HMBC correlations to C-2'' and a methylene carbon at  $\delta_C$  35.2 (C-4''). The methylene group at C-4'' (2.21 m) were coupled to another methylene group ( $\delta_H$  1.75 m; H-5'') which was coupled to a methine triplet ( $\delta_H$  4.32; H-6'') as shown in the COSY spectrum (Fig. 94). This was again very similar to **WS-11**. This triplet was shifted downfield and was attached to a carbon at  $\delta_C$  89.0 (C-6''), indicating that an electron-withdrawing group with a stronger deshielding effect than a hydroxyl group was present at this carbon ( $\delta_C$  75.5 for hydroxy-bearing C-6'' in **WS-11**). This chemical shift is characteristic of a hydroperoxy-bearing methine (Kuo *et al.*, 2000). The molecular formula for this compound (C<sub>21</sub>H<sub>30</sub>O<sub>6</sub>) indicated that it had an extra oxygen when compared to that of **WS-11** (C<sub>21</sub>H<sub>30</sub>O<sub>5</sub>). The remaining methyl group ( $\delta_H$  1.75; H-9'') was placed at C-7'' ( $\delta_C$  143.3) as the methyl singlet showed HMBC correlations to this carbon, the hydroperoxy-bearing carbon (C-6'') and the *exo*-methylene carbon at  $\delta_C$  114.6 (C-8''). This was further confirmed by HMBC correlations between the exomethylene group and C-6'' and C-9''. This completed the structural elucidation of **WS-12**. Like **WS-S-07** (synthetic *S*-isomer of **WS-09**) and other acylphloroglucinols isolated from *H. olympicum* L. *cf. uniflorum*, the

specific rotation of **WS-12** showed a positive value ( $[\alpha]_D^{22} +2.7^\circ$ ,  $c = 0.32$ , chloroform). However, two chiral centres (C-2' and C-6'') are present in **WS-12**. The stereochemistry at each chiral centre could not be determined by direct comparison with the specific rotation of **WS-S-07**. **WS-12** was identified as the new natural product, 4,6-dihydroxy-2-*O*-(6''-hydroperoxy-3'',7''-dimethyl-2'',7''-octadienyl)-1-(2'-methylbutanoyl)-benzene, and is reported here for the first time.

A further experiment using a starch-iodide test strip (Fisher) was conducted to confirm the presence of the hydroperoxide group in this compound. A starch-iodide test strip was dipped into a chloroform solution of **WS-12** (approximately 2 mg/ml) and showed a positive colour reaction (light brown). Chloroform was used as a negative control and did not result in any colour change. A chloroform solution of 3-chloroperoxybenzoic acid (Sigma; approximately 20 mg/ml) was used as a positive control, and it turned the test strip dark blue. When a lower concentration of 3-chloroperoxybenzoic acid was used (approximately 2 mg/ml), the test strip was turned light brown, implying that the colour change was dependent on the concentration of the hydroperoxide present.

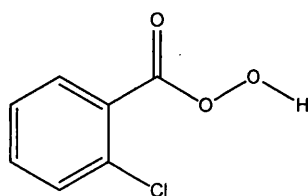


Fig. 97. Structure of 3-chloroperoxybenzoic acid.

Table 21.  $^1\text{H}$  (500MHz) and  $^{13}\text{C}$  NMR (125 MHz) spectral data and  $^1\text{H}$ - $^{13}\text{C}$  long-range correlations of **WS-12** recorded in chloroform-*d*.

Position	$^1\text{H}$ ( <i>J</i> , Hz)	$^{13}\text{C}$	$^2J$	$^3J$
1	-	105.9	-	-
2	-	162.4	-	-
3	5.91 d (2.5)	91.7	-	C-1, C-5
4	-	162.0	-	-
5	5.98 d (2.5)	96.6	C-6	C-1, C-3
6	-	167.5	-	-
1'	-	210.3	-	-
2'	3.63 m	46.1	-	-
3'	1.35 m, 1.80 m	26.8	-	-
4'	0.88 t (7.5)	11.9	C-3'	C-2'
5'	1.11 d (6)	16.6	C-2'	C-1', C-3'
1''	4.58 d (6.5)	65.6	C-2''	C-3''
2''	5.52 m	119.2	-	-
3''	-	141.2	-	-
4''	2.21 m	35.2	-	-
5''	1.75 m	26.8	-	-
6''	4.32 t (6)	89.0	-	-
7''	-	143.3	-	-
8''	5.02 s, 5.05 bs	114.6	-	C-6'', C-9''
9''	1.75 s	17.2	C-7''	C-6'', C-8''
10''	1.75 s	16.6	C-3''	C-2'', C-4''
4-OH	5.32 bs	-	-	-
6-OH	13.99 s	-	C-6	C-1, C-5

**3.2.9.5 Characterization of WS-13 as 4,6-dihydroxy-2-*O*-(6'',7''-epoxy-3'',7''-dimethyl-oct-2''-enyl)-1-(2'-methylbutanoyl)-benzene**

WS-13 was isolated as a pale yellow oil from the DCM extract of *H. olympicum* *L. cf. uniflorum*. The molecular formula of WS-13 was C<sub>21</sub>H<sub>30</sub>O<sub>5</sub>, indicated by an [M+H]<sup>+</sup> ion at m/z 363 in HR ESI-MS.

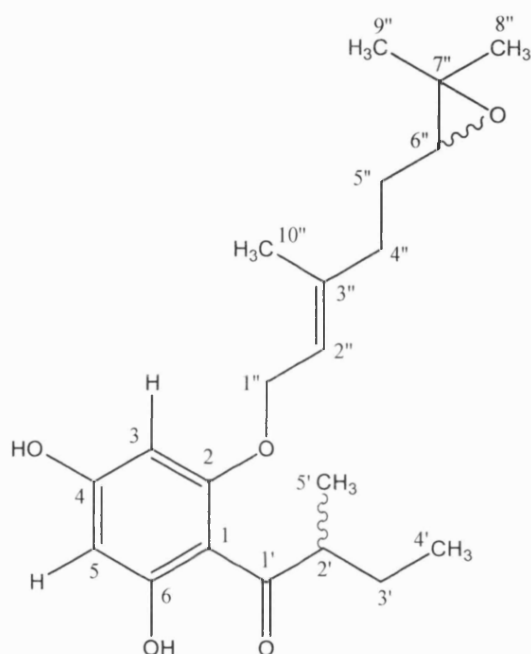


Fig. 98. Structure of WS-13.

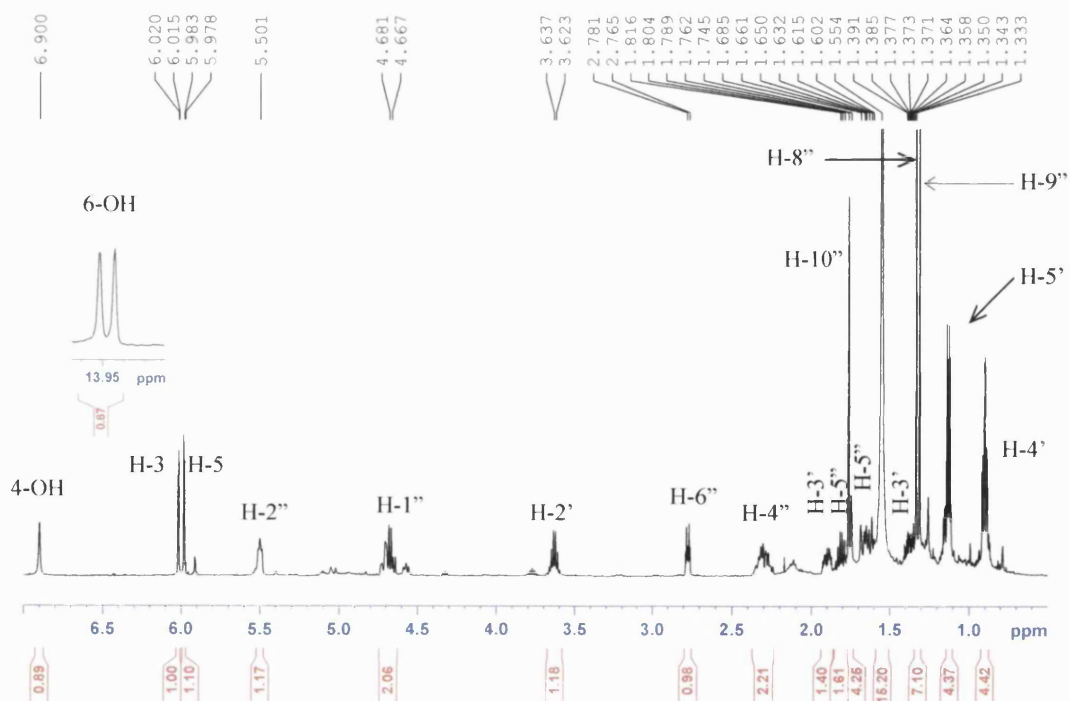


Fig. 99. <sup>1</sup>H NMR spectrum of WS-13 in chloroform-*d* recorded at 500 MHz.

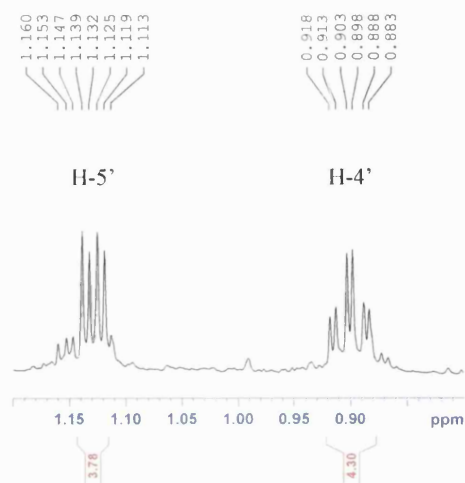


Fig. 100. Expansion of <sup>1</sup>H NMR spectrum of **WS-13**.

The <sup>1</sup>H NMR spectrum (Fig. 99) revealed signals typical of a 2-methylbutanoyl phloroglucinol, including a broad signal accounting for an hydroxyl group ( $\delta_{\text{H}}$  6.90, 4-OH), two *meta*-coupled aromatic protons ( $\delta_{\text{H}}$  6.02 d,  $J = 2.5$  Hz, H-3; 5.98 d,  $J = 2.5$  Hz, H-5), a methine multiplet ( $\delta_{\text{H}}$  3.63, 1H, H-2') and a methylene group ( $\delta_{\text{H}}$  1.38 m, 1.81 m, H-3'). More interestingly, duplication of the following signals was observed (Fig. 99, 100): a highly-deshielded hydrogen-bonded singlet ( $\delta_{\text{H}}$  13.95, 6-OH), a methyl triplet ( $\delta_{\text{H}}$  0.90,  $J = 7.5$  Hz, H-4') and a methyl doublet ( $\delta_{\text{H}}$  1.13,  $J = 7$  Hz, H-5'). The carbon signals corresponding to the phloroglucinol nucleus included three deshielded aromatic carbons ( $\delta_{\text{C}}$  167.6, C-6; 162.3, C-2; 162.8, C-4), a quaternary aromatic carbon ( $\delta_{\text{C}}$  105.5, C-1) and two aromatic methines ( $\delta_{\text{H}}$  92.7, C-3; 96.8, C-5) (Table 22). Duplication of the signals in the <sup>13</sup>C NMR spectrum was also observed for the 2-methylbutanoyl side-chain: a carbonyl carbon ( $\delta_{\text{C}}$  210.1, 210.0, C-1'), a methine ( $\delta_{\text{C}}$  46.09, 46.12, C-2'), a methylene ( $\delta_{\text{C}}$  26.93, 26.96, C-3') and two methyl carbons ( $\delta_{\text{C}}$  11.96, 12.00, C-4'; 16.52, 16.55, C-5'). The HMBC correlations (Fig. 101, Fig. 104) observed for the acylphloroglucinol nucleus of this compound were identical to those of **WS-09** and were described previously. The duplication of

NMR signals might suggest the presence of two rotamers. This phenomenon was observed in some natural products (Vazquez *et al.*, 2001), including acylphloroglucinols (Appendino *et al.*, 2002). In the case of acylphloroglucinols, two isomers in rotameric forms were possible: one with the acyl chain above the plane of the phloroglucinol, and the other below the plane. Molecular modelling calculation could be carried out to determine whether two rotamers were present. This is because two relatively stable conformations are possible for this **WS-13** and therefore two different energy minima would be expected.

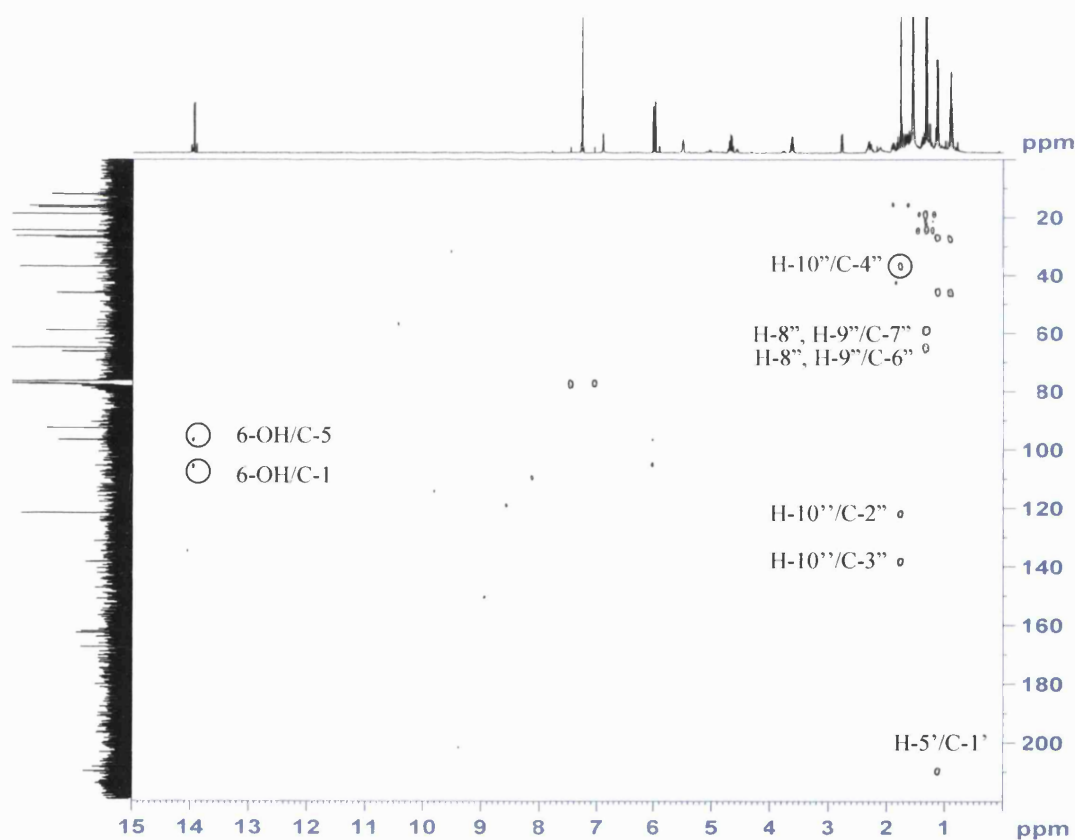


Fig. 101. HMBC spectrum of **WS-13**.

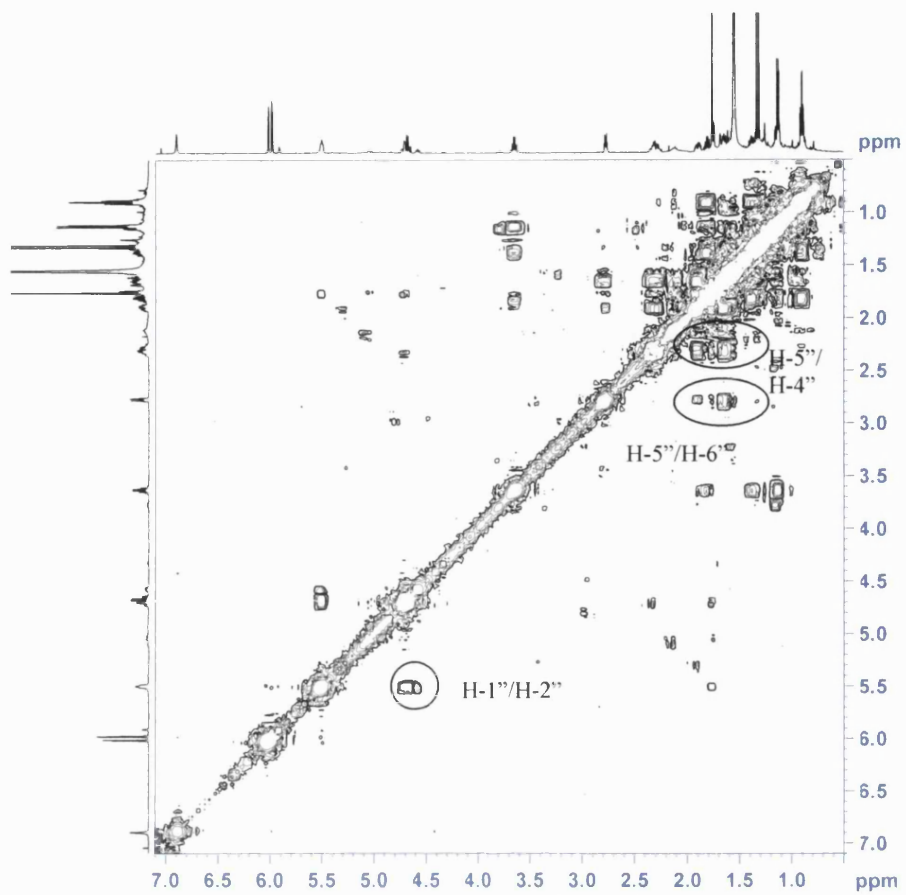


Fig. 102. COSY spectrum of WS-13.

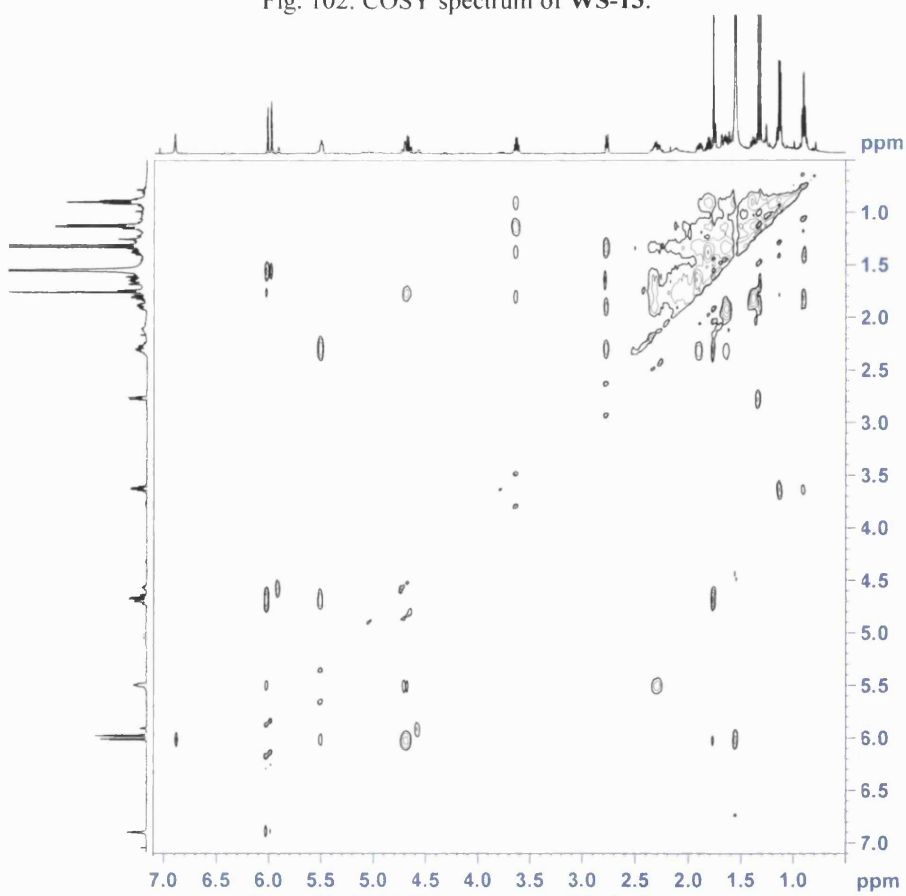


Fig. 103. NOESY spectrum of WS-13.

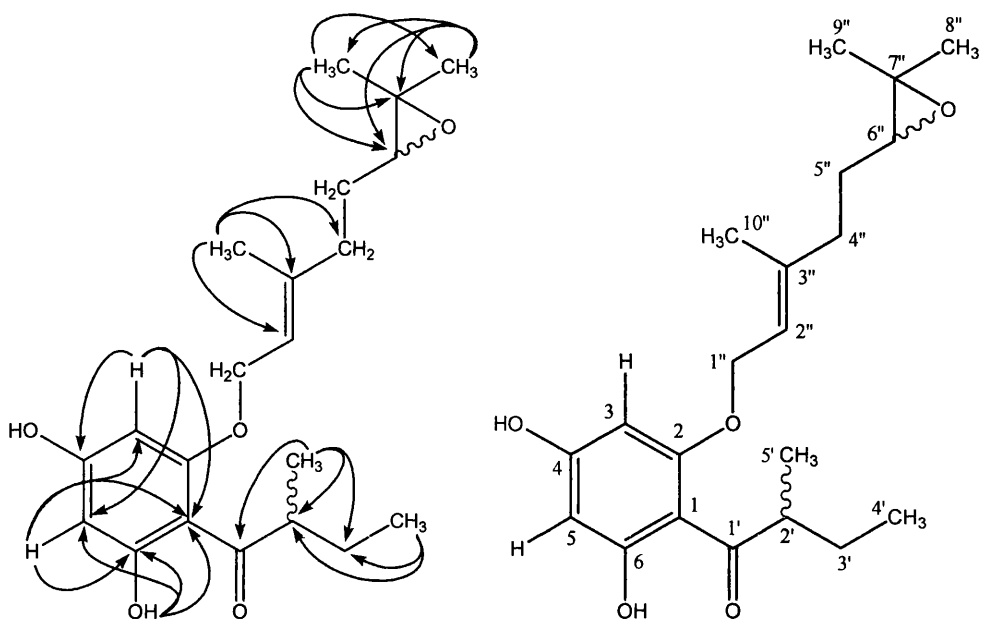


Fig. 104. HMBC correlations for **WS-13**.

The  $^1\text{H}$  NMR signals for the side-chain at the 2-*O* position included three methylenes ( $\delta_{\text{H}}$  4.67 m, H-1''; 2.30 m, H-4''; 1.65 m, 1.90 m; H-5''), one olefinic proton ( $\delta_{\text{H}}$  5.50 m, H-2''), one deshielded oxymethine ( $\delta_{\text{H}}$  2.77 m, H-6'') and three methyl singlets ( $\delta_{\text{H}}$  1.34 s, H-8''; 1.31 s, H-9''; 1.76 s, H-10''). Ten carbon signals were observed in the  $^{13}\text{C}$  NMR spectrum for this side-chain, including three methylenes ( $\delta_{\text{C}}$  66.4, C-1''; 37.0, C-4''; 26.5, C-5''), two olefinic carbons ( $\delta_{\text{C}}$  121.9, C-2''; 138.5, C-3''), one oxymethine ( $\delta_{\text{C}}$  65.1, C-6''), one quaternary carbon at  $\delta_{\text{C}}$  59.1 (C-7'') and three methyl carbons ( $\delta_{\text{C}}$  18.9, C-8''; 24.6, C-9''; 16.0, C-10'').

Due to the small quantity of the compound, signals in the HMBC spectrum (Fig. 101) were very weak. The COSY spectrum (Fig. 102) and the structures of other related derivatives isolated from this plant played an important role in the

structural elucidation of this compound. As with the other acylphloroglucinols isolated from *H. olympicum L. cf. uniflorum*, the oxymethylene group ( $\delta_{\text{H}}$  4.67 m, H-1'') was placed at the C-2 position of the acylphloroglucinol. The oxymethylene protons showed a COSY correlation (Fig. 102) with the olefinic proton ( $\delta_{\text{H}}$  5.50 m, H-2''), thus placing the olefinic proton at C-2''. The methyl group shifted downfield at  $\delta_{\text{H}}$  1.76 (H-10'') showed a  $^2J$  HMBC correlation to a quaternary olefinic carbon at  $\delta_{\text{C}}$  138.5 (C-3'') and  $^3J$  HMBC correlations to C-2'' and a methylene carbon at  $\delta_{\text{C}}$  37.0 (C-4''). The methylene protons at C-4'' ( $\delta_{\text{H}}$  2.30 m) showed a COSY correlation to another methylene group ( $\delta_{\text{H}}$  1.65 m, 1.90 m, C-5''), which was coupled to an oxymethine as shown in the COSY spectrum ( $\delta_{\text{H}}$  2.77 m, H-6''). The remaining methyl groups at  $\delta_{\text{H}}$  1.34 (H-8'') and 1.31 (H-9'') showed HMBC correlations to  $\delta_{\text{C}}$  18.9 (C-8'') and 24.6 (C-9'') respectively, indicating that the methyl groups were in a geminal position. They were also correlated to a quaternary carbon at  $\delta_{\text{H}}$  59.1 (C-7'') and the oxymethine at C-6''. The  $^{13}\text{C}$  NMR chemical shifts of C-6'' and C-7'' were indicative of an epoxide (Row *et al.*, 2006). The  $^1\text{H}$  and  $^{13}\text{C}$  NMR data of this side-chain showed a close agreement with the corresponding substituent of 6',7'-epoxygeranyloxypsoralen in the literature (Row *et al.*, 2006). Again, **WS-13** showed a positive specific rotation ( $[\alpha]_{\text{D}}^{22} +2.6^\circ$ ,  $c = 0.19$ , chloroform). However, due to the presence of two chiral centres (C-2' and C-6'') in the molecule, the stereochemistry at each chiral centre could not be determined by direct comparison with that of **WS-S-07**. **WS-13** is identified as the new 4,6-dihydroxy-2-*O*-(6'',7''-epoxy-3'',7''-dimethyl-oct-2''-enyl)-1-(2'-methylbutanoyl)-benzene and is described here for the first time.

Table 22.  $^1\text{H}$  (500MHz) and  $^{13}\text{C}$  NMR (125 MHz) spectral data and  $^1\text{H}$ - $^{13}\text{C}$  long-range correlations of **WS-13** recorded in chloroform-*d*.

Position	$^1\text{H}$ ( <i>J</i> , Hz)	$^{13}\text{C}$	$^2J$	$^3J$
1	-	105.5	-	-
2	-	162.3	-	-
3	6.02 d (2.5)	92.7	-	C-1, C-5
4	-	162.8	-	-
5	5.98 d (2.5)	96.8	-	C-3
6	-	167.6	-	-
1'	-	210.0	-	-
2'	3.63 m	46.1	-	-
3'	1.38 m, 1.81m	26.5	-	-
4'	0.90 t (7.5)	12.0	C-3'	C-2'
5'	1.1 d (7)	16.6	C-2'	C-1', C-3'
1''	4.67 m	66.4	-	-
2''	5.50 m	121.9	-	-
3''	-	138.5	-	-
4''	2.30 m	37.0	-	-
5''	1.65 m, 1.90 m	26.5	-	-
6''	2.77 m	65.1	-	-
7''	-	59.1	-	-
8''	1.31 s	18.9	C-7''	C-6'', C-9''
9''	1.34 s	24.6	C-7''	C-6'', C-8''
10''	1.76 s	16.0	C-3''	C-2'', C-4''
4-OH	6.90 bs	-	-	-
6-OH	13.95 s	-	-	C-1, C-5

### 3.2.10 Characterization of WS-14 as 4-(3-*O*-3'')-3''-methylbutenyl-6-phenyl-pyran-2-one

WS-14 was isolated as a yellow oil from the hexane extract of *H. choisianum*. The HR ESI-MS of WS-14 showed an  $[M+H]^+$  ion at  $m/z$  255, indicating a molecular formula of  $C_{16}H_{14}O_3$ .

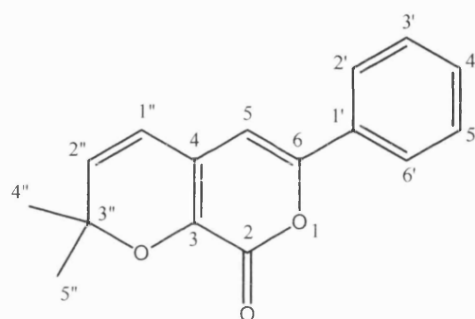


Fig. 105. Structure of WS-14.

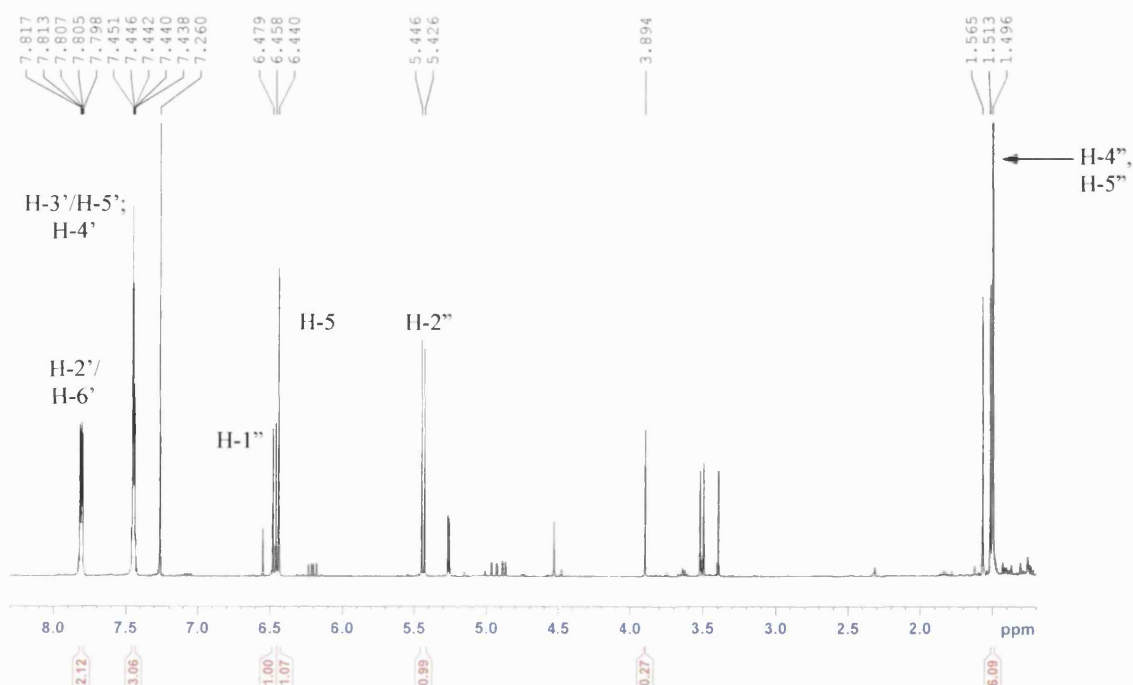


Fig. 106.  $^1H$  NMR spectrum of WS-14 in chloroform-*d* recorded at 500 MHz.

The  $^1\text{H}$  NMR spectrum (Fig. 106, Table 23) revealed signals for five aromatic protons in a mono-substituted benzene ring with resonances at  $\delta_{\text{H}}$  7.78 (m, 2H, H-2', H-6'),  $\delta_{\text{H}}$  7.43 (m, 2H, H-3', H-5') and  $\delta_{\text{H}}$  7.42 (m, 1H, H-4'), an aromatic singlet ( $\delta_{\text{H}}$  6.42, H-5), two olefinic protons with resonances at  $\delta_{\text{H}}$  6.45 (d,  $J = 10$  Hz, H-1'') and  $\delta_{\text{H}}$  5.42 (d,  $J = 10$  Hz, H-2''), and a methyl singlet integrating for six protons ( $\delta_{\text{H}}$  1.48 s, H-4'', H-5''). The  $^{13}\text{C}$  NMR spectrum (Table 23) displayed signals for three highly deshielded aromatic carbons ( $\delta_{\text{C}}$  161.7, C-2; 163.9, C-3; 160.1, C-6), two quaternary aromatic carbons at  $\delta_{\text{C}}$  131.3 (C-1') and 99.3 (C-4), three aromatic methines belonging to the mono-substituted benzene ring ( $\delta_{\text{C}}$  125.6, C-2', C-6'; 128.9, C-3', C-5'; 130.9, C-4'), two olefinic methines ( $\delta_{\text{C}}$  116.4, C-1''; 125.5, C-2''), a further aromatic methine at  $\delta_{\text{C}}$  97.8 (C-5), a deshielded quaternary aliphatic carbon at  $\delta_{\text{C}}$  80.2 and two methyl carbons at  $\delta_{\text{C}}$  28.6 (C-4'', C-5''). The molecular formula ( $\text{C}_{16}\text{H}_{14}\text{O}_3$ ) determined by mass spectrometry suggested that the deshielded carbons were oxygen-bearing.

In the HMBC spectrum (Fig. 107), a cross-peak was seen between the methyl singlet ( $\delta_{\text{H}}$  1.48, 6H, H-4'', H-5'') and a methyl carbon at  $\delta_{\text{C}}$  28.6 (H-4'', H-5''), indicating the presence of two methyl groups in a geminal position. The methyl groups also correlated to an oxygen-bearing quaternary carbon at  $\delta_{\text{C}}$  80.2 (C-3'') and an olefinic methine carbon at  $\delta_{\text{C}}$  125.5 (C-2''). The olefinic proton at C-2'' ( $\delta_{\text{H}}$  5.42) was correlated to the neighbouring olefinic proton ( $\delta_{\text{H}}$  6.45, H-1'') as shown in the COSY spectrum (Fig. 109). The coupling constant between the olefinic protons was 10 Hz, implying that they were in the *cis*- configuration. H-1'' exhibited HMBC correlation to a highly-deshielded oxygen-bearing carbon at

$\delta_C$  163.9 (C-3), whereas H-2'' showed HMBC correlations to a quaternary aromatic carbon at  $\delta_C$  99.3 (C-4). These  $^1\text{H}$  and  $^{13}\text{C}$  NMR data were suggestive of the presence of a dimethylpyran ring (Seo *et al.*, 1999).

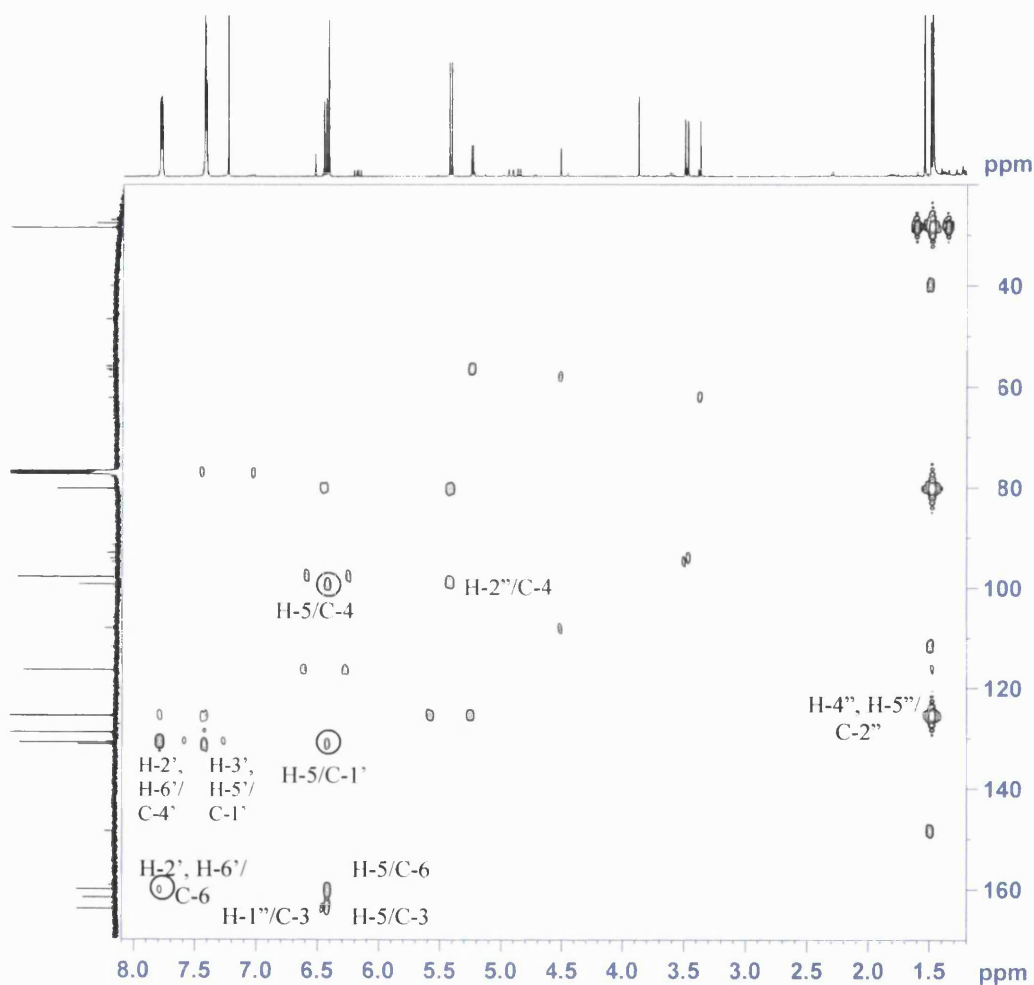


Fig. 107. HMBC spectrum of **WS-14**.

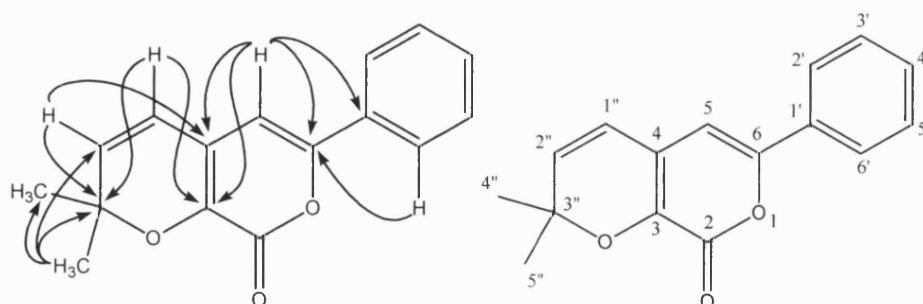


Fig. 108. Key HMBC correlations for **WS-14**.

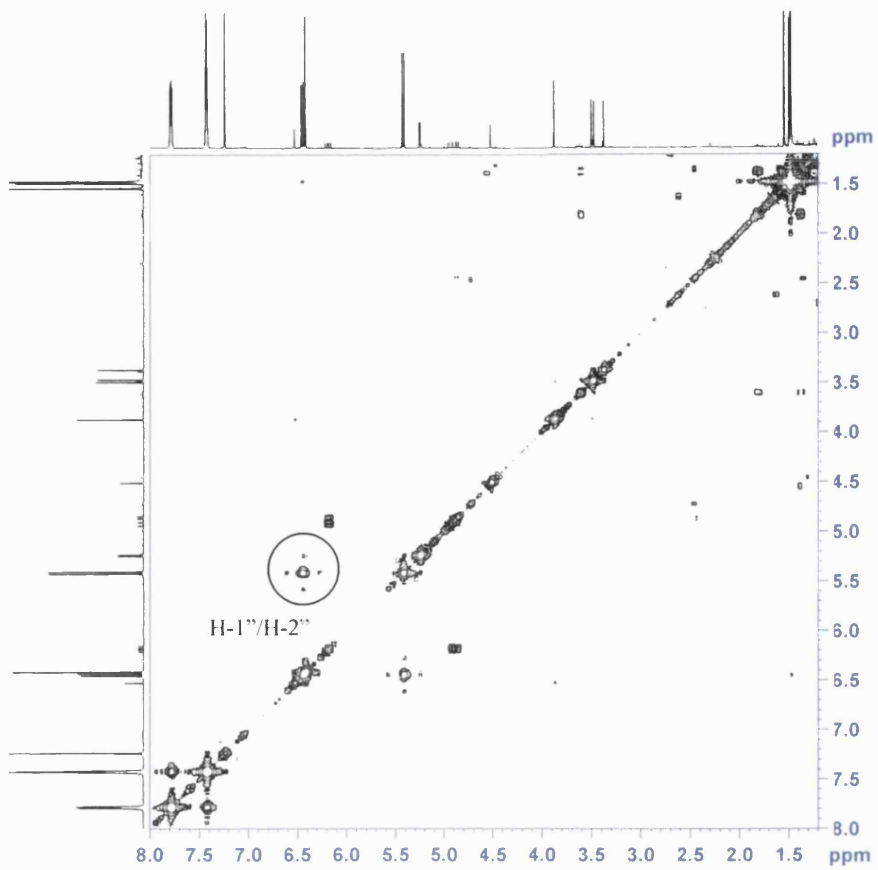


Fig. 109. COSY spectrum of **WS-14**.

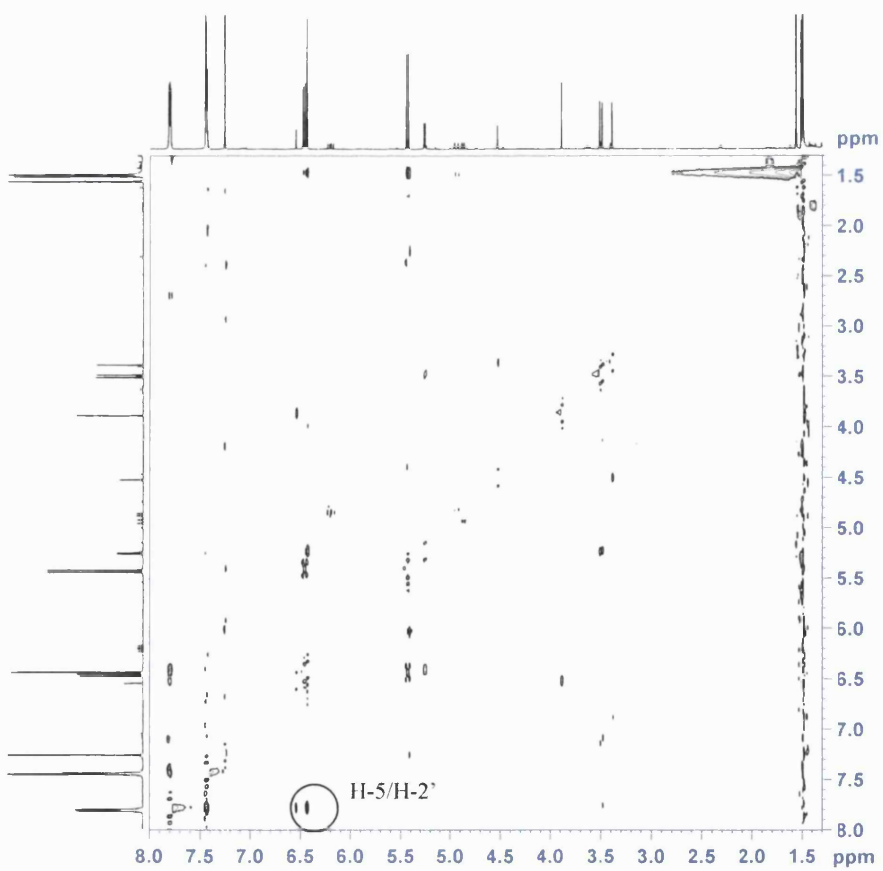


Fig. 110. NOESY spectrum of **WS-14**.

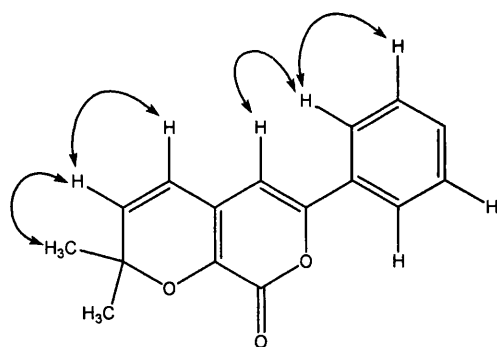


Fig. 111. NOESY correlations for **WS-14**.

Further inspection of the HMBC spectrum revealed correlations between the aromatic proton singlet at  $\delta_{\text{H}}$  6.42 (H-5) and C-3, C-4, and two quaternary carbons at  $\delta_{\text{C}}$  160.1 (C-6) and 131.1 (C-1'), thus placing it at C-5. The presence of a mono-substituted phenyl group at C-6 was confirmed by investigating the HMBC spectrum. The proton at  $\delta_{\text{H}}$  7.42 (H-4') was correlated to the equivalent carbons, C-2' and C-6', at  $\delta_{\text{C}}$  125.6 *via* three bonds. The two equivalent aromatic protons at  $\delta_{\text{H}}$  7.43 (2H, H-3', H-5') showed a  $^2J$  correlation to C-4', and  $^3J$  correlations to the corresponding equivalent carbon (C-5', C-3') and the substituent-bearing quaternary aromatic carbon ( $\delta_{\text{C}}$  131.3, C-1'). The remaining equivalent protons in the phenyl moiety ( $\delta_{\text{H}}$  7.78, 2H, H-2', H-6') showed  $^3J$  correlations to the corresponding equivalent carbon ( $\delta_{\text{C}}$  125.6, C-6', C-2'), C-4', and an oxygen-bearing carbon at  $\delta_{\text{C}}$  160.1 (C-6). Finally, the position of the phenyl substituent at C-6 was also confirmed by an NOE correlation between H-5 and H-2' (Fig. 110, 111).

The remaining carbon ( $\delta_{\text{C}}$  160.1), which was not correlated to any proton in the HMBC spectrum, was placed at C-2 to complete the structure of this compound, giving a pyran-2-one nucleus. The chemical shift of C-2 was typical of the

carbonyl group in a pyran-2-one ring (Dharmarantne *et al.*, 2002). **WS-14** was therefore identified as the new 4-(3-*O*-3'')-3''-methylbutenyl-6-phenyl-pyran-2-one, and is reported here for the first time.

Table 23. <sup>1</sup>H (500MHz) and <sup>13</sup>C NMR (125 MHz) spectral data and <sup>1</sup>H-<sup>13</sup>C long-range correlations of **WS-14** recorded in chloroform-*d*.

Position	<sup>1</sup> H (J, Hz)	<sup>13</sup> C	<sup>2</sup> J	<sup>3</sup> J
1	-	-	-	-
2	-	161.7	-	-
3	-	163.9	-	-
4	-	99.3	-	-
5	6.42 s	97.8	C-4, C-6	C-3, C-1'
6	-	160.1	-	-
1'	-	131.3	-	-
2'/6'	7.78 m	125.6	-	C-6, C-4', C-6'/2'
3'/5'	7.43 m	128.9	C-4'	C-1', C-5'/3'
4'	7.42 m	130.9	-	C-2'/6'
1''	6.45 d (10)	116.4	-	C-3, C-3''
2''	5.42 d (10)	125.5	C-3''	C-4
3''	-	80.2	-	-
4''	1.48 s	28.6	C-3''	C-2'', C-5''
5''	1.48 s	28.6	C-3''	C-2'', C-4''

### 3.2.12 Characterization of WS-15 as lupeol

WS-15 was isolated as a white amorphous solid from the hexane extract of *H. choisianum*. The  $^1\text{H}$  and  $^{13}\text{C}$  NMR data were identical to that of the triterpene lupeol (Aratanechemuge *et al.*, 2004) (Table 24).

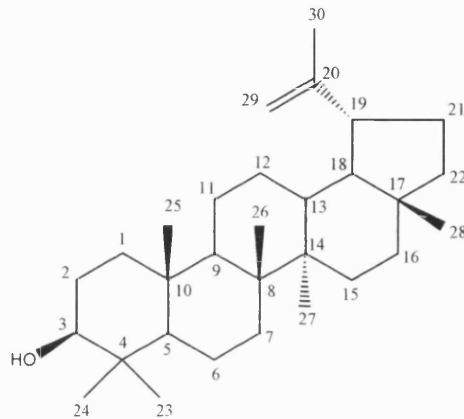


Fig. 112. Structure of WS-15.

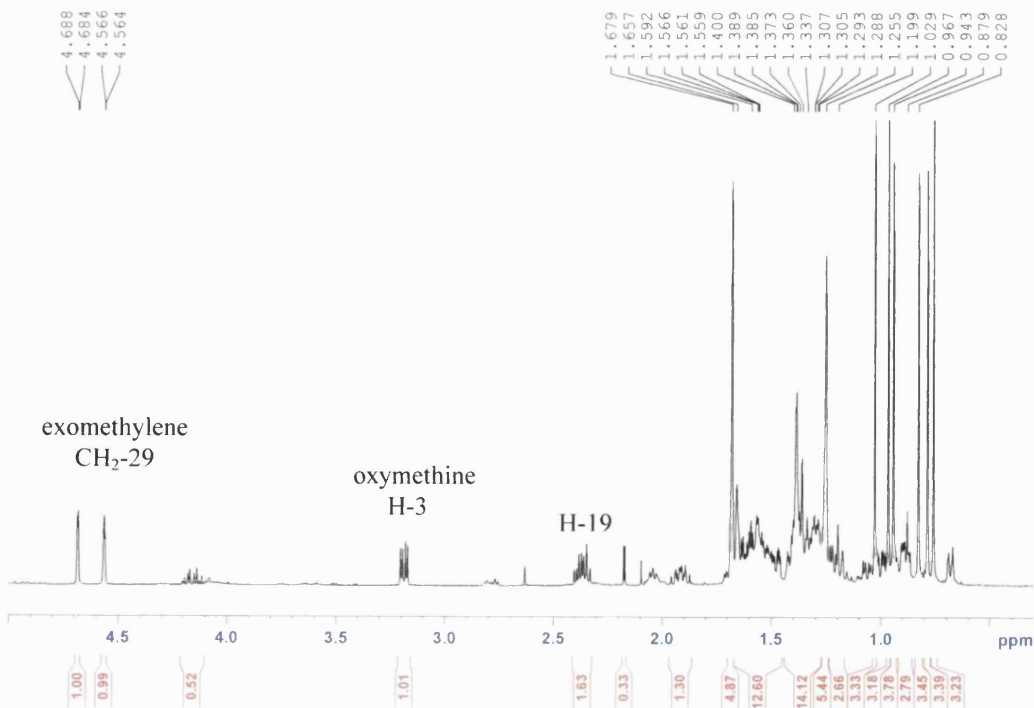


Fig. 113.  $^1\text{H}$  NMR spectrum of WS-15 in chloroform-*d* recorded at 500 MHz.

The presence of 30 carbon signals in the  $^{13}\text{C}$  NMR spectrum (Table 24) suggested that the compound was a triterpene. The signals for this compound in the  $^1\text{H}$  NMR spectrum included an *exo*-methylene ( $\delta_{\text{H}}$  4.56, 4.68; H-29), an oxymethine ( $\delta_{\text{H}}$  3.19, H-3), a deshielded methine ( $\delta_{\text{H}}$  2.37, H-19), a series of methylenes with resonances between  $\delta_{\text{H}}$  0.8 - 2.0 and seven methyl singlets ( $\delta_{\text{H}}$  0.76 - 1.68). The methyl singlet shifted downfield at  $\delta_{\text{H}}$  1.68 was correlated to a deshielded carbon at  $\delta_{\text{C}}$  48.0 (C-19) and olefinic carbons at  $\delta_{\text{C}}$  109.3 (C-29) and 151.0 (C-20), whereas the *exo*-methylene protons were correlated to C-19 and C-30 (Fig. 114). This indicated an isopropenyl group, which is characteristic of lupeol. The  $^1\text{H}$  and  $^{13}\text{C}$  NMR data of **WS-15** were in close agreement with those in the published literature (Aratanechemuge *et al.*, 2004; Table 24).

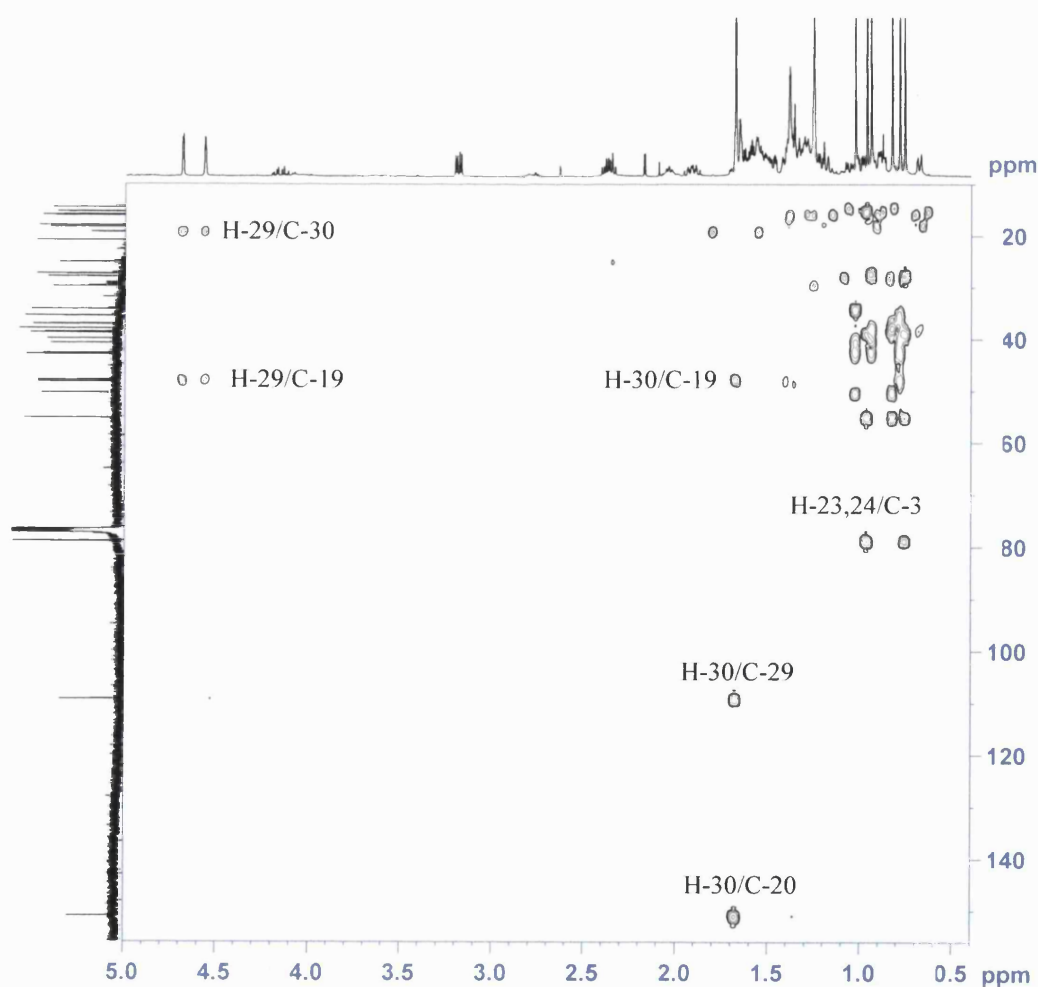


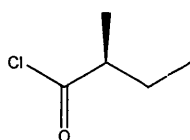
Fig. 114. HMBC spectrum of **WS-15**.

Table 24.  $^1\text{H}$  (500MHz) and  $^{13}\text{C}$  NMR (125 MHz) spectral data of **WS-15** recorded in chloroform-*d*.

Position	WS-15		Aratanechemuge <i>et al.</i> , 2004 Chloroform- <i>d</i>	
	$^1\text{H}$	$^{13}\text{C}$	$^1\text{H}$	$^{13}\text{C}$
1	1.65 m, 0.89 m	38.7	1.65 m, 0.90 m	38.7
2	1.59 m, 1.66 m	27.4	1.59 m, 1.67 m	27.4
3	3.19 dd (5.0, 11.5)	79.0	3.20 dd (5.0, 11.5)	79.0
4	-	38.9	-	38.8
5	0.68 m	55.3	0.68 m	55.3
6	1.39 m, 1.50 m	18.3	1.40 m, 1.50 m	18.3
7	1.34 - 1.40 m	34.3	1.32 m, 1.42 m	34.3
8	-	40.8	-	40.8
9	1.27 m	50.4	1.29 m	50.4
10	-	37.2	-	37.1
11	1.20 m, 1.38 m	20.9	1.20 m, 1.40 m	20.9
12	1.07 m, 1.67 m	25.1	1.07 m, 1.68 m	25.1
13	1.66 m	38.0	1.68 m	38.1
14	-	42.8	-	42.8
15	1.00 m, 1.68 m	27.4	1.00 m, 1.68 m	27.4
16	1.37 m, 1.47 m	35.6	1.37 m, 1.48 m	35.6
17	-	43.0	-	42.9
18	1.38 m	48.3	1.37 m	48.3
19	2.37 m	48.0	2.38 ddd (5.6, 11.0, 11.0)	47.9
20	-	151.0	-	150.9
21	1.34 m, 1.91 m	29.8	1.32 m, 1.92 m	29.8
22	1.38 m, 1.20 m	40.0	1.37 m, 1.19 m	39.9
23	0.97 s	28.0	0.97 s	27.9
24	0.76 s	15.4	0.76 s	15.4
25	0.83 s	16.1	0.83 s	16.1
26	1.03 s	16.0	1.03 s	15.9
27	0.94 s	14.5	0.94 s	14.5
28	0.79 s	18.0	0.79 s	17.9
29	4.56 d (2), 4.68 d (2)	109.3	4.54 bs, 4.67 bs	109.3
30	1.68 s	19.3	1.68 s	19.3

### 3.3 Purification and characterization of synthetic compounds

Twenty-five compounds were synthesized using the reactions described in section 2.6. The structures of these compounds are summarized in Table 25. NMR experiments performed on these compounds included  $^1\text{H}$ ,  $^{13}\text{C}$ , DEPT 135, HMQC, HMBC, COSY and NOESY. Because the  $^1\text{H}$  NMR spectrum and mass spectrometry data can provide enough evidence to confirm the chemical structure of the product in each reaction, only the  $^1\text{H}$  NMR spectra are shown. The  $^1\text{H}$  and  $^{13}\text{C}$  chemical shifts of these compounds will be reported in each section.



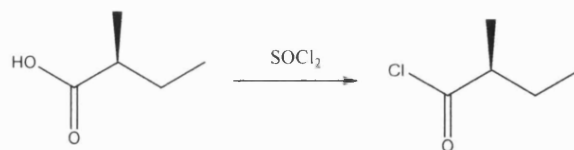
WS-S-01

Table 25. Chemical structures of synthetic compounds.

	$\text{R}_1$	$\text{R}_2$	$\text{R}_3$
	WS-S-03	H	MOM
	WS-S-05	Geranyl	MOM
	WS-S-08	Geranyl	H
	WS-S-02	H	H
	WS-S-04	H	TBDMS
	WS-S-06	Prenyl	H
	WS-S-07	Geranyl	H
	WS-S-09	Farnesyl	H
	WS-S-10	3-Methylbutyl	H
	WS-S-11	3,7-Dimethyl-octyl	H
	WS-S-12	Prenyl	H
	WS-S-13	H	Prenyl
	WS-S-14	Geranyl	H
	WS-S-15	H	Geranyl
	WS-S-16	Farnesyl	H
	WS-S-17	H	Farnesyl
	WS-S-18	3-Methylbutyl	H
	WS-S-19	H	3-Methylbutyl
	WS-S-20	3,7-Dimethyl-octyl	H
	WS-S-21	H	3,7-Dimethyl-octyl
	WS-S-22	Pentyl	H
	WS-S-23	H	Pentyl
	WS-S-24	Decyl	H
	WS-S-25	H	Decyl

### 3.3.1 Reaction product from Step 1: WS-S-01

Step 1:



**WS-S-01**

Distillation of the reaction mixture afforded (*S*)-2-methylbutyryl chloride (**WS-S-01**) (10.63 g, 88.21 mmol, 90.1 %). The boiling point of (*S*)-2-methylbutyryl chloride was 119-120 °C and showed an agreement with the literature (Begley *et al.*, 1987). The  $^1\text{H}$  NMR spectrum of **WS-S-01** is shown in Fig. 115. The  $^1\text{H}$  NMR spectrum of (*S*)-2-methylbutyric acid is shown in Fig. 116 for comparison.

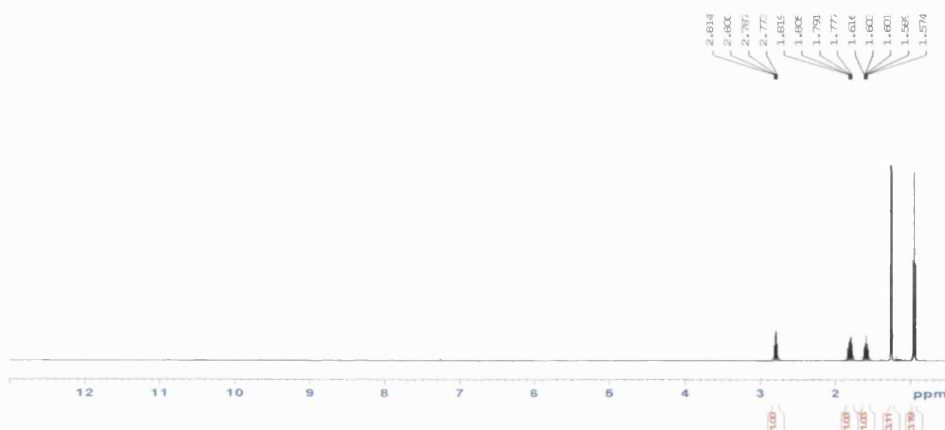


Fig. 115.  $^1\text{H}$  NMR spectrum of **WS-S-01** in chloroform-*d* recorded at 500 MHz.

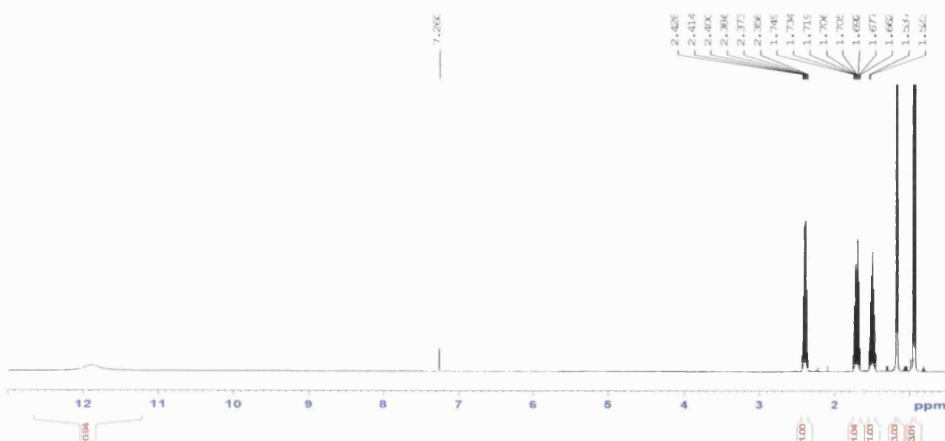


Fig. 116.  $^1\text{H}$  NMR spectrum of (*S*)-2-methylbutyric acid in chloroform-*d* recorded at 500 MHz.

It can be seen that the broad singlet at approximately 12 ppm disappeared in the  $^1\text{H}$  NMR spectrum of **WS-S-01**. The  $^1\text{H}$  and  $^{13}\text{C}$  NMR spectral data of **WS-S-01** are shown in Table 26.

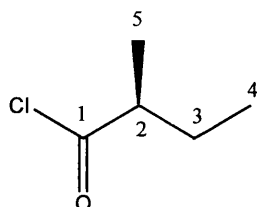


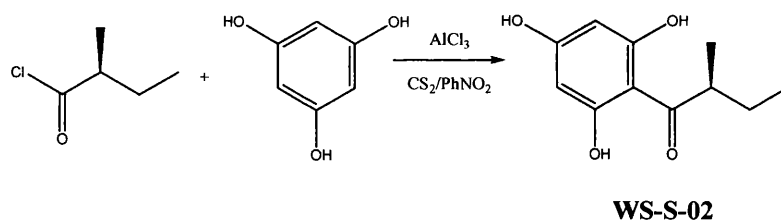
Fig. 117. Structure of **WS-S-01**.

Table 26.  $^1\text{H}$  (500MHz) and  $^{13}\text{C}$  NMR (125 MHz) spectral data of **WS-S-01** recorded in chloroform-*d*.

Position	$^1\text{H}$ (J, Hz)	$^{13}\text{C}$
1	-	177.5
2	2.79 m	52.8
3	1.60 m, 1.80 m	26.5
4	0.95 t (7.5)	11.0
5	1.26 d (7)	16.4

### 3.3.2 Reaction product from Step 2: **WS-S-02**

#### Step 2: *Friedel-Crafts acylation*



The reaction mixture from the Friedel-Crafts acylation was allowed to cool with stirring and then poured on to an ice-water bath (400 ml). 100 ml of hydrochloric acid (3 M) was added. The organic solvents were removed under reduced pressure and the oily residue containing the acylphloroglucinol was extracted into ether. After the removal of ether using a rotary evaporator, the crude product was purified by VLC using a gradient system starting from 100 %

hexane with 10 % increments of ethyl acetate. The fraction eluted with 6:4 hexane-ethyl acetate was identified to be 2-methylbutanoyl phloroglucinol (**WS-S-02**) (9.71 g, 46.19 mmol, 53.8 %).

HR ESI-MS of **WS-S-02** gave an  $[M-H]^-$  ion at  $m/z$  209, suggesting a molecular formula of  $C_{11}H_{14}O_4$ . The  $^1H$  NMR spectrum of **WS-S-02** is shown in Fig. 119. It shows signals for a typical 2-methylbutanoyl side-chain, comprising a methine multiplet ( $\delta_H$  3.84), a methylene group ( $\delta_H$  1.34 m, 1.78 m), a methyl doublet ( $\delta_H$  1.10) and a methyl triplet ( $\delta_H$  0.88). Due to a plane of symmetry in **WS-S-02**, the two *meta*-coupled aromatic protons were equivalent, thus appearing as a singlet integrating for two protons at  $\delta_H$  5.81 instead of two doublets as seen in the natural product (**WS-09**). The  $^1H$  and  $^{13}C$  NMR spectral data of **WS-S-02** are summarized in Table 27.

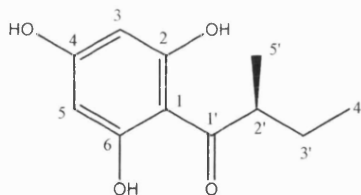


Fig. 118. Structure of **WS-S-02**.

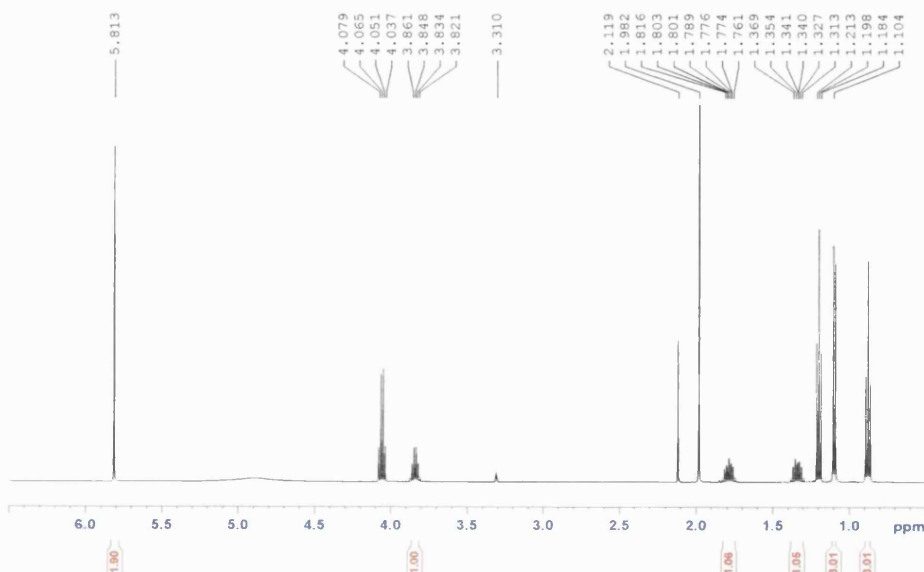


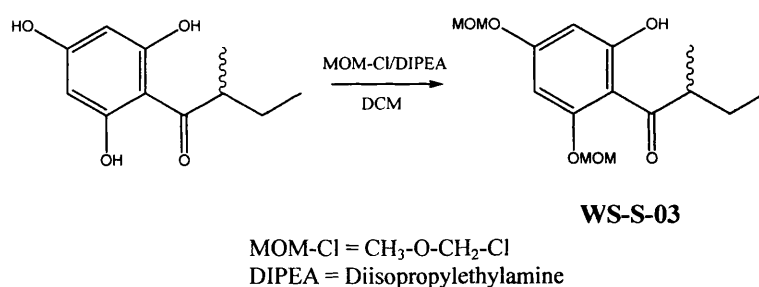
Fig. 119.  $^1H$  NMR spectrum of **WS-S-02** in methanol- $d_4$ , recorded at 500 MHz.

Table 27.  $^1\text{H}$  (500MHz) and  $^{13}\text{C}$  NMR (125 MHz) spectral data of **WS-S-02** recorded in methanol- $d_4$ .

Position	$^1\text{H}$ (J, Hz)	$^{13}\text{C}$
1	-	105.3
2	-	165.8
3	5.81 s	96.0
4	-	165.7
5	5.81 s	96.0
6	-	165.8
1'	-	211.5
2'	3.84 m	46.7
3'	1.34 m, 1.78 m	28.2
4'	0.88 t (7)	12.5
5'	1.10 d (6.5)	17.2

### 3.3.3 Reaction product from Step 3 (MOM): **WS-S-03**

*Step 3: Using MOM as the protecting group*



Water was added to the reaction mixture, which was then extracted with chloroform. The organic layer was dried over anhydrous magnesium sulphate and the solvent was removed under reduced pressure. The MOM-protected acylphloroglucinol (**WS-S-03**; 1.21 g, 4.06 mmol, 18.3 %) was purified from the mixture by VLC over silica eluted with 9:1 hexane-ethyl acetate.

HR ESI-MS indicated an  $[\text{M}+\text{H}]^+$  ion at  $m/z$  299, suggesting a molecular formula of  $\text{C}_{15}\text{H}_{22}\text{O}_6$ . The  $^1\text{H}$  NMR spectrum of **WS-S-03** is shown in Fig. 121. Apart from the presence of signals attributable to a 2-methylbutanoyl phloroglucinol nucleus as described above, two methoxyl singlets ( $\delta_{\text{H}}$  3.40, 3H;  $\delta_{\text{H}}$  3.47, 3H) and two oxymethylene singlets ( $\delta_{\text{H}}$  5.10, 2H;  $\delta_{\text{H}}$  5.20, 2H) were also observed. These

signals corresponded to the two MOM groups. Furthermore, the  $^1\text{H}$  NMR spectrum displayed a signal for a hydrogen-bonded hydroxyl group at  $\delta_{\text{H}}$  13.70 and two *meta*-coupled doublets at  $\delta_{\text{H}}$  6.21 and  $\delta_{\text{H}}$  6.23, indicating that the two aromatic protons were in different magnetic environments. These data suggested that two hydroxyl groups were protected by the MOM groups at the *ortho*- and *para*- positions. The  $^1\text{H}$  and  $^{13}\text{C}$  NMR spectral data of **WS-S-03** are shown in Table 28.

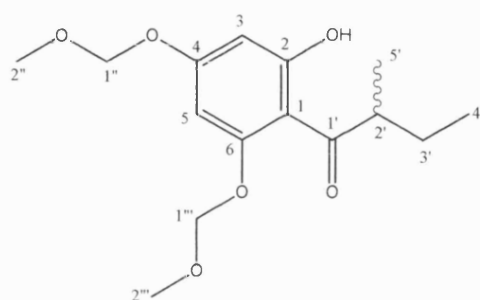


Fig. 120. Structure of **WS-S-03**.

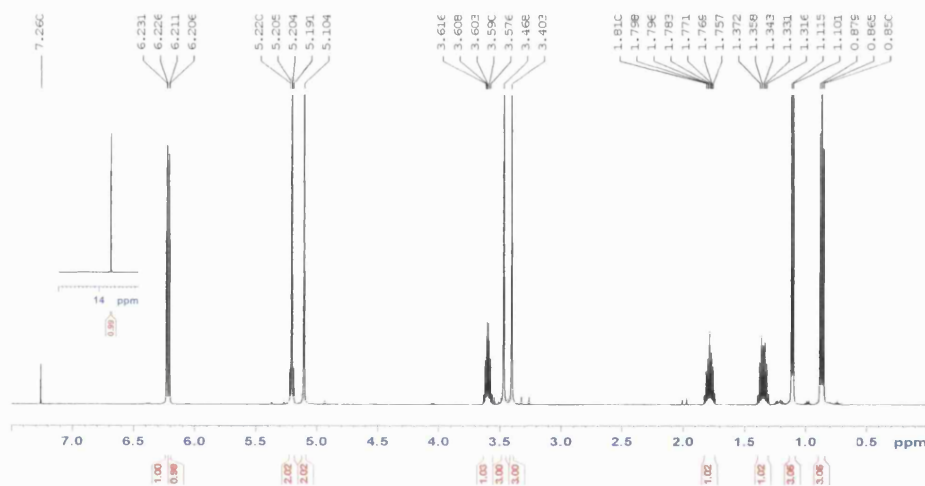


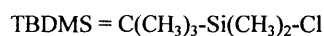
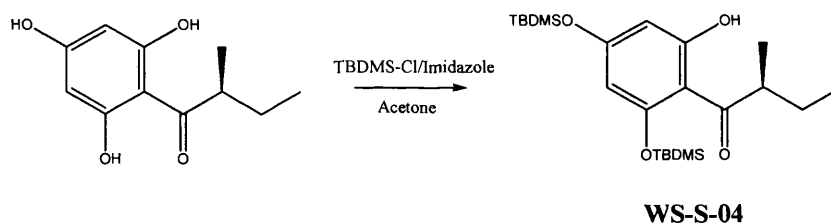
Fig. 121.  $^1\text{H}$  NMR spectrum of **WS-S-03** in chloroform-*d* recorded at 500 MHz.

Table 28.  $^1\text{H}$  (500MHz) and  $^{13}\text{C}$  NMR (125 MHz) spectral data of **WS-S-03** recorded in chloroform-*d*.

Position	$^1\text{H}$ (J, Hz)	$^{13}\text{C}$
1	-	106.2
2	-	163.1
3	6.23 d (2.5)	97.2
4	-	160.0
5	6.21 d (2.5)	93.8
6	-	167.0
1'	-	209.9
2'	3.60 m	46.2
3'	1.34 m, 1.78 m	26.8
4'	0.87 t (7)	11.7
5'	1.10 d (6.5)	16.4
1''	5.10 s	94.0
2''	3.40 s	56.2
1'''	5.20 s	94.6
2'''	3.47 s	56.5
2-OH	13.70 s	-

### 3.3.4 Reaction product from Step 3 (TBDMS): **WS-S-04**

*Step 3: Using TBDMS as the protecting group*



The reaction mixture was diluted in chloroform and washed with 1 M HCl (150 ml). The organic layer was dried using anhydrous magnesium sulphate. The solvent was filtered and removed under reduced pressure. The crude product was purified by VLC over silica to afford TBDMS-protected phloroglucinol (**WS-S-04**) (16.4 g, 37,26 mmol, 80.7 %) in the fraction eluted with 9:1 hexane-ethyl acetate.

The molecular formula of **WS-S-04** obtained by HR ESI-MS was  $\text{C}_{23}\text{H}_{42}\text{O}_4\text{Si}_2$ , as indicated by the presence of an  $[\text{M-H}]^-$  ion at  $m/z$  437. The  $^1\text{H}$  NMR spectrum

of **WS-S-04** is shown in Fig. 123. Apart from the presence of signals attributable to a 2-methylbutanoyl phloroglucinol nucleus as described above, two methyl singlets each integrating for nine protons ( $\delta_{\text{H}}$  0.96;  $\delta_{\text{H}}$  0.99) and two additional methyl signals shifted upfield, each integrating for six protons ( $\delta_{\text{H}}$  0.23;  $\delta_{\text{H}}$  0.32) were also observed. These signals corresponded to the two TBDMS groups. Furthermore, the  $^1\text{H}$  NMR spectrum displayed a signal for a hydrogen-bonded hydroxyl group at  $\delta_{\text{H}}$  13.43 and two *meta*-coupled doublets at  $\delta_{\text{H}}$  5.84 and  $\delta_{\text{H}}$  6.03, indicating that the two aromatic protons were in different magnetic environments. These data suggested that two hydroxyl groups were protected by the TBDMS groups at the *ortho*- and *para*- positions. The  $^1\text{H}$  and  $^{13}\text{C}$  spectral data of **WS-S-04** are shown in Table 29.

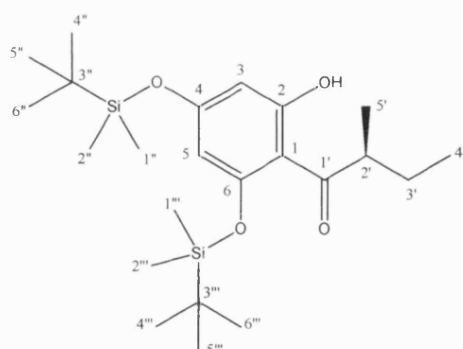


Fig. 122. Structure of **WS-S-04**.

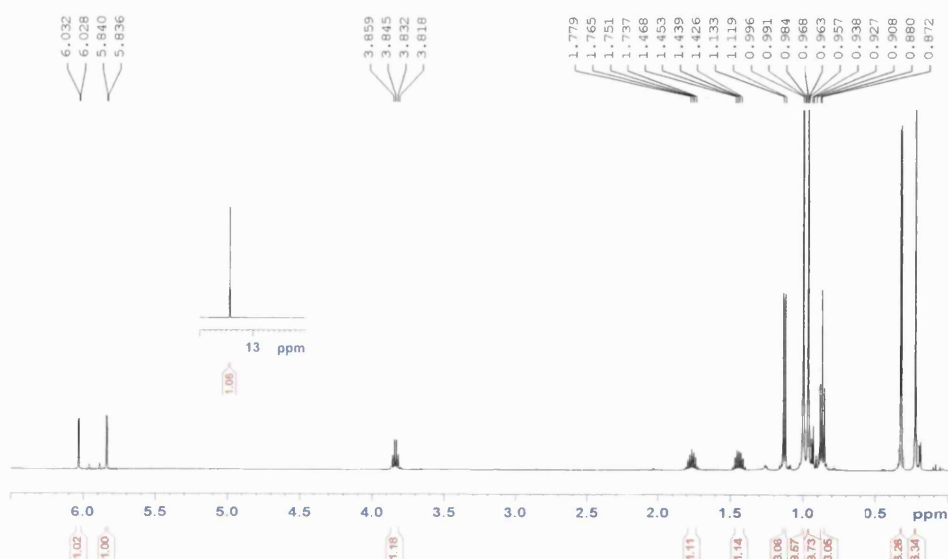


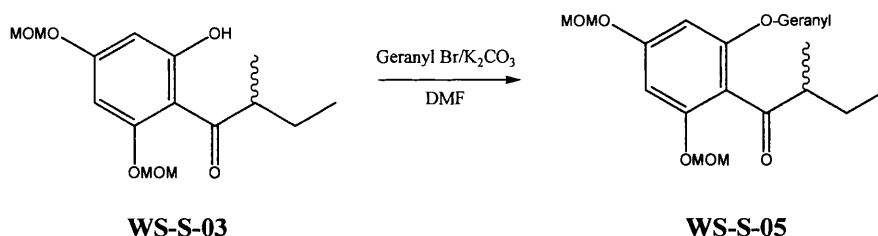
Fig. 123.  $^1\text{H}$  NMR spectrum of **WS-S-04** in chloroform-*d* recorded at 500 MHz.

Table 29.  $^1\text{H}$  (500MHz) and  $^{13}\text{C}$  NMR (125 MHz) spectral data of **WS-S-04** recorded in chloroform-*d*.

Position	$^1\text{H}$ (J, Hz)	$^{13}\text{C}$
1	-	108.4
2	-	161.7
3	5.84 d (2)	102.0
4	-	158.8
5	6.03 d (2)	103.1
6	-	166.5
1'	-	210.6
2'	3.83 m	45.0
3'	1.44 m, 1.76 m	26.5
4'	0.87 t (7.5)	11.5
5'	1.12 d (7)	17.0
1''/2''	0.23 s	-4.4
3''	-	18.1
4''/5''/6''	0.96 s	25.5
1'''/2'''	0.32 s	-3.7
3'''	-	18.9
4'''/5'''/6'''	0.99 s	26.1
2-OH	13.43 s	-

### 3.3.5 Reaction product from Step 4: **WS-S-05**

#### Step 4: Alkylation of **WS-S-03**



The reaction mixture was poured over water and extracted with chloroform. The organic layer was dried over anhydrous magnesium sulphate and the solvent was removed under reduced pressure. The crude product was chromatographed over silica and was eluted with 9:1 hexane-ethyl acetate to give **WS-S-05** (185.4 mg, 0.43 mmol, 20.2 %).

HR ESI-MS gave an  $[\text{M}+\text{H}]^+$  ion at  $m/z$  435, suggesting a molecular formula of  $\text{C}_{25}\text{H}_{38}\text{O}_6$ . Fig. 125 shows the  $^1\text{H}$  NMR spectrum of **WS-S-05**. It differs from

the  $^1\text{H}$  NMR spectrum of **WS-S-03** (Fig. 121) in the absence of the signal for a hydrogen-bonded hydroxyl group at approximately 14 ppm and the presence of signals corresponding to a geranyl side-chain substituted at an oxygen (an oxymethylene at  $\delta_{\text{H}}$  4.48, two olefinic protons at  $\delta_{\text{H}}$  5.06 and 5.38, two overlapping methylenes at  $\delta_{\text{H}}$  2.08 and three methyl singlets at  $\delta_{\text{H}}$  1.58, 1.65, 1.68). The *O*-alkylation reaction with geranyl bromide at the remaining hydroxyl group can account for the disappearance of the signal for the hydrogen-bonded hydroxyl group since no further hydroxyl group at the *ortho*- position was available. Table 30 shows the  $^1\text{H}$  and  $^{13}\text{C}$  spectral data of **WS-S-05**.

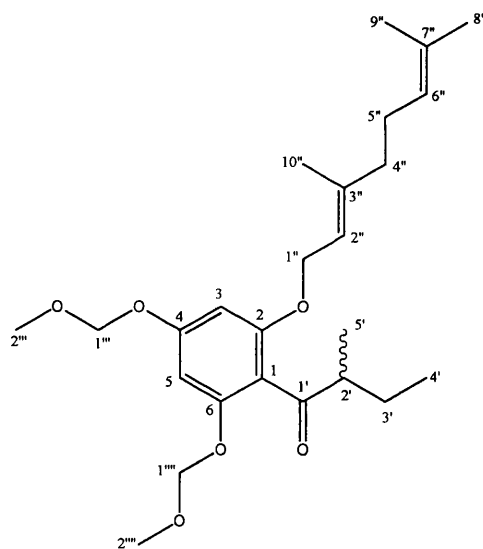


Fig. 124. Structure of **WS-S-05**.

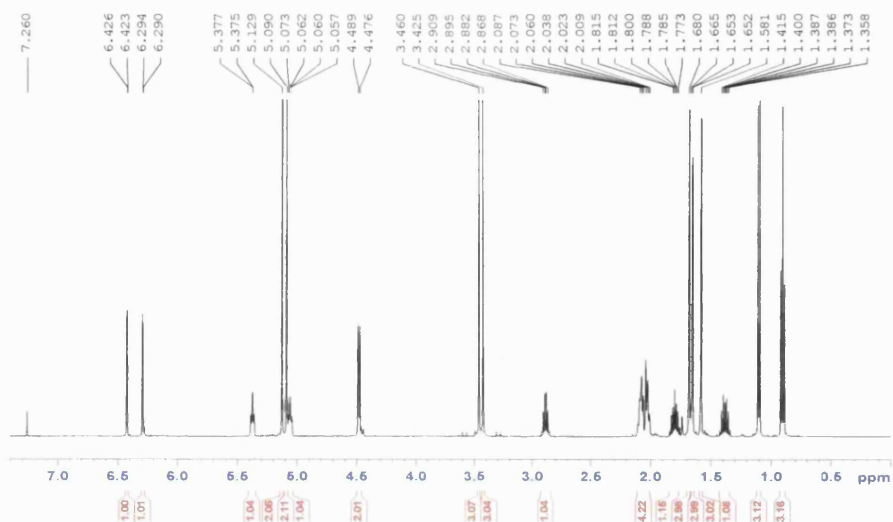


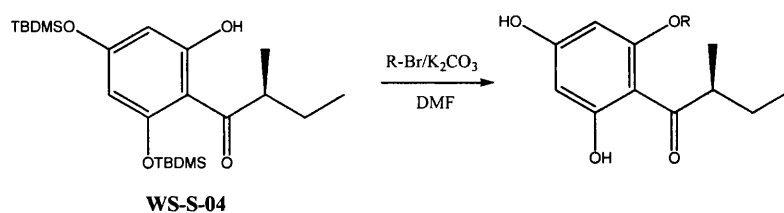
Fig. 125.  $^1\text{H}$  NMR spectrum of **WS-S-05** in chloroform-*d* recorded at 500 MHz.

Table 30.  $^1\text{H}$  (500MHz) and  $^{13}\text{C}$  NMR (125 MHz) spectral data of **WS-S-05** recorded in chloroform-*d*.

Position	$^1\text{H}$ ( <i>J</i> , Hz)	$^{13}\text{C}$
1	-	115.9
2	-	157.2
3	6.42 d (2.5)	95.7
4	-	155.2
5	6.29 d (2.5)	94.4
6	-	159.3
1'	-	207.8
2'	2.88 m	48.8
3'	1.38 m, 1.80 m	26.2
4'	0.91 t (7.5)	11.6
5'	1.11 d (7)	16.5
1''	4.48 d (6.5)	65.4
2''	5.38 m	119.1
3''	-	141.0
4''	2.08 m	39.4
5''	2.02 m	25.6
6''	5.06 m	123.7
7''	-	132.7
8''	1.65	25.2
9''	1.58	17.6
10''	1.68	15.1
1'''	5.09 s	94.6
2'''	3.43 s	56.0
1''''	5.13 s	94.8
2''''	3.46 s	56.2

### 3.3.6 2-Methylbutanoyl phloroglucinol derivatives

Five acylphloroglucinols (**WS-S-06**, **07**, **09**, **10**, **11**) with a (*S*)-2-methylbutanoyl side-chain were synthesized from **WS-S-04** using the following reaction:



An additional acylphloroglucinol with a ( $\pm$ )-2-methylbutanoyl side-chain (**WS-S-08**) was also synthesized in the initial small-scale reaction. Since the hydroxyl group at the *para*- position and one of the hydroxyl groups at the *ortho*- position were protected by TBDMS, the alkylation reaction took place at the remaining hydroxyl group at the *ortho*- position. Because TBDMS is a very labile leaving group (Greene, 1981), hydrogen bromide generated during the reaction was thought to have cleaved the TBDMS group, giving the final acylphloroglucinol derivative. The simultaneous cleavage of silyl ethers by hydrogen halide generated *in situ* had been reported previously (Grieco and Markworth, 1999). This is very useful in synthesizing **WS-S-07** as the alkylation of the acylphloroglucinol and deprotection of the protecting group took place in one single step.

The yields of the (*S*)-2-methylbutanoyl phloroglucinol derivatives ranged from 4.2 to 12.5 % (Table 31), and were significantly lower than that of **WS-S-08**, which was the racemic mixture (46.0 %). Due to time restriction, the reason for this had not been investigated further. Because the main aim of the synthesis work was to (1) successfully synthesize the natural product with potent

antibacterial activity (**WS-09**) and (2) synthesize various derivatives to obtain an idea on the structure-activity relationship, the conditions of this reaction were not yet optimized to achieve a good yield. Since the yields of the previous three reactions were good, optimization of this reaction must be carried out in order to facilitate the synthesis of derivatives in the future. More experiments need to be done to achieve this, including the variation of the solvent, temperature, base and the duration of the reaction.

Table 31. Yield of 2-methylbutanoyl phloroglucinol derivatives.

	R	Yield of reaction (Step 3)			Overall Yield (%)	Novelty
		(mg)	(mmol)	(%)		
<b>WS-S-06</b>	Prenyl	5.2	0.0187	7.2	2.8	New
<b>WS-S-07</b>	Geranyl	220.1	0.638	4.2	1.6	New
<b>WS-S-08</b> ( <i>S</i> )-isomer	Geranyl	10.5	0.0304	46.0	19.9	New
<b>WS-S-09</b> Racemic	Farnesyl	4.6	0.0111	5.1	2.0	New
<b>WS-S-10</b>	3-Methylbutyl	20.3	0.0725	12.5	4.9	New
<b>WS-S-11</b>	3,7-Dimethyloctyl	21.6	0.0617	11.9	4.7	New

To purify these derivatives, the reaction mixture was poured over water and extracted with chloroform. The organic layer was dried over anhydrous magnesium sulphate and the solvent was removed under reduced pressure. All crude products were chromatographed over silica. The C<sub>5</sub> derivatives, **WS-S-06** and **WS-S-10**, were eluted with 8:2 hexane-ethyl acetate. The C<sub>10</sub> derivatives, **WS-S-07**, **WS-S-08** and **WS-S-11**, were eluted with 9:1 hexane-ethyl acetate. The C<sub>15</sub> derivative, **WS-S-09**, was eluted with 9.5:0.5 hexane-ethyl acetate. **WS-S-06** to **WS-S-11** are new compounds, which have not been isolated as natural products nor synthesized previously.

### 3.3.6.1 Characterization of WS-S-06 as (*S*)-2-*O*-prenyl-2'-methylbutanoyl phloroglucinol

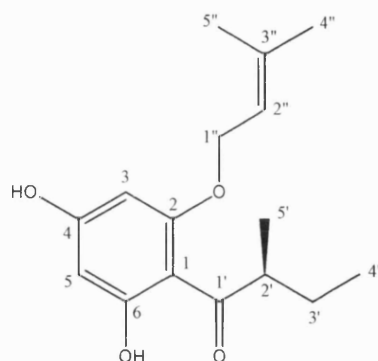


Fig. 126. Structure of **WS-S-06**.

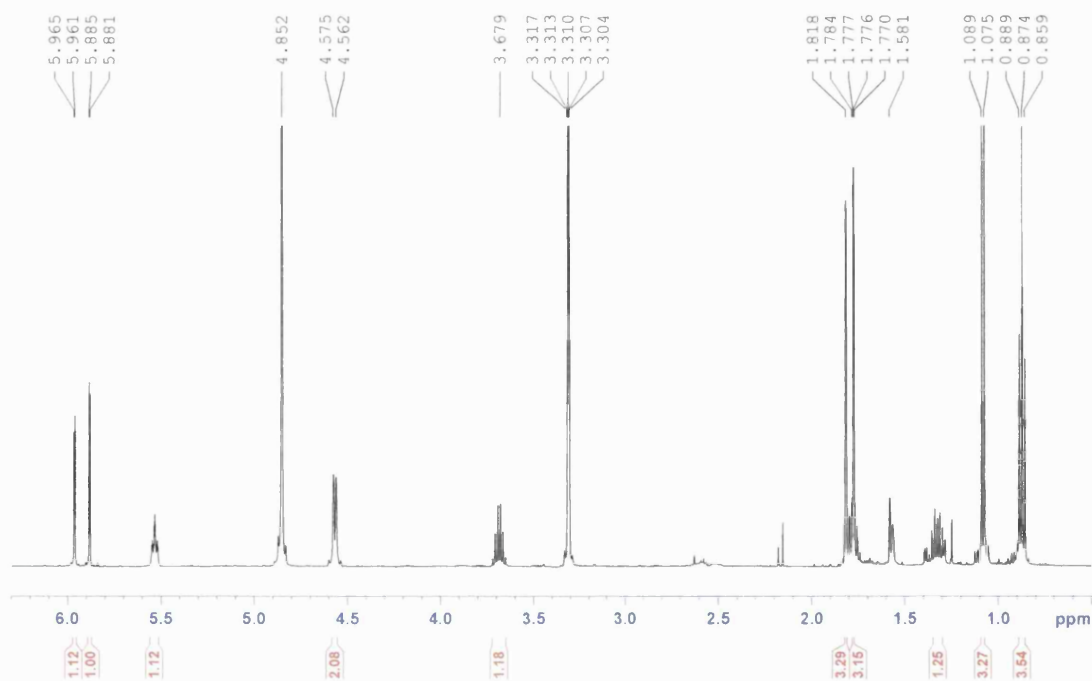


Fig. 127.  $^1\text{H}$  NMR spectrum of **WS-S-06** in methanol- $d_4$  recorded at 500 MHz.

The molecular formula of **WS-S-06** was shown to be  $\text{C}_{16}\text{H}_{22}\text{O}_4$  by HR ESI-MS, with an  $[\text{M}-\text{H}]^-$  ion at  $m/z$  277. The  $^1\text{H}$  NMR spectrum of **WS-S-06** is shown in Fig. 127. It shows signals characteristic for an *ortho*-substituted 2-methylbutanoyl phloroglucinol: two *meta*-coupled aromatic protons ( $\delta_{\text{H}}$  5.88 d,  $J = 2$  Hz; 5.96 d,  $J = 2$  Hz), one methine ( $\delta_{\text{H}}$  3.68 m), one methylene ( $\delta_{\text{H}}$  1.32 m,

1.78 m), one methyl doublet ( $\delta_{\text{H}}$  1.08,  $J = 7.5$  Hz) and one methyl triplet ( $\delta_{\text{H}}$  0.87 t,  $J = 7.5$  Hz). The remaining signals corresponded to the prenyl moiety at the 2-*O* position, including an oxymethylene ( $\delta_{\text{H}}$  4.57 d,  $J = 7.5$  Hz), an olefinic proton ( $\delta_{\text{H}}$  5.53 m) and two methyl singlets ( $\delta_{\text{H}}$  1.77; 1.82). **WS-S-06** was therefore identified as (*S*)-2-*O*-prenyl-2'-methylbutanoyl phloroglucinol. The  $^1\text{H}$  and  $^{13}\text{C}$  NMR spectral data are summarized in Table 32.

Table 32.  $^1\text{H}$  (500MHz) and  $^{13}\text{C}$  NMR (125 MHz) spectral data of **WS-S-06** recorded in methanol- $d_4$ .

Position	$^1\text{H}$ ( $J$ , Hz)	$^{13}\text{C}$
1	-	106.2
2	-	166.1
3	5.88 d (2)	93.9
4	-	163.8
5	5.96 d (2)	96.9
6	-	168.3
1'	-	211.2
2'	3.68 m	47.1
3'	1.32 m, 1.78 m	28.0
4'	0.87 t (7.5)	12.2
5'	1.08 d (7.5)	17.1
1''	4.57 d (7.5)	66.5
2''	5.53 m	112.0
3''	-	140.2
4''	1.82 s	25.8
5''	1.77 s	18.2

3.3.6.2

Characterization of WS-S-07 as (*S*)-2-*O*-geranyl-2'-methylbutanoyl phloroglucinol

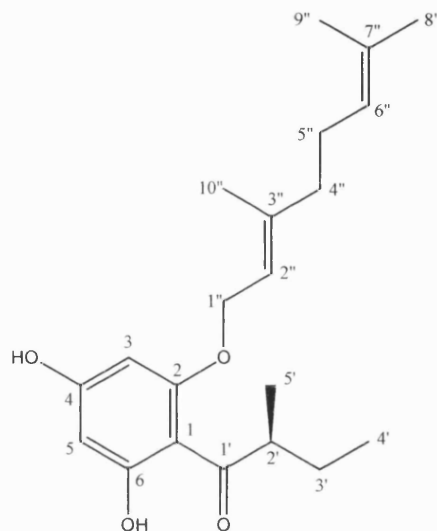


Fig. 128. Structure of WS-S-07.

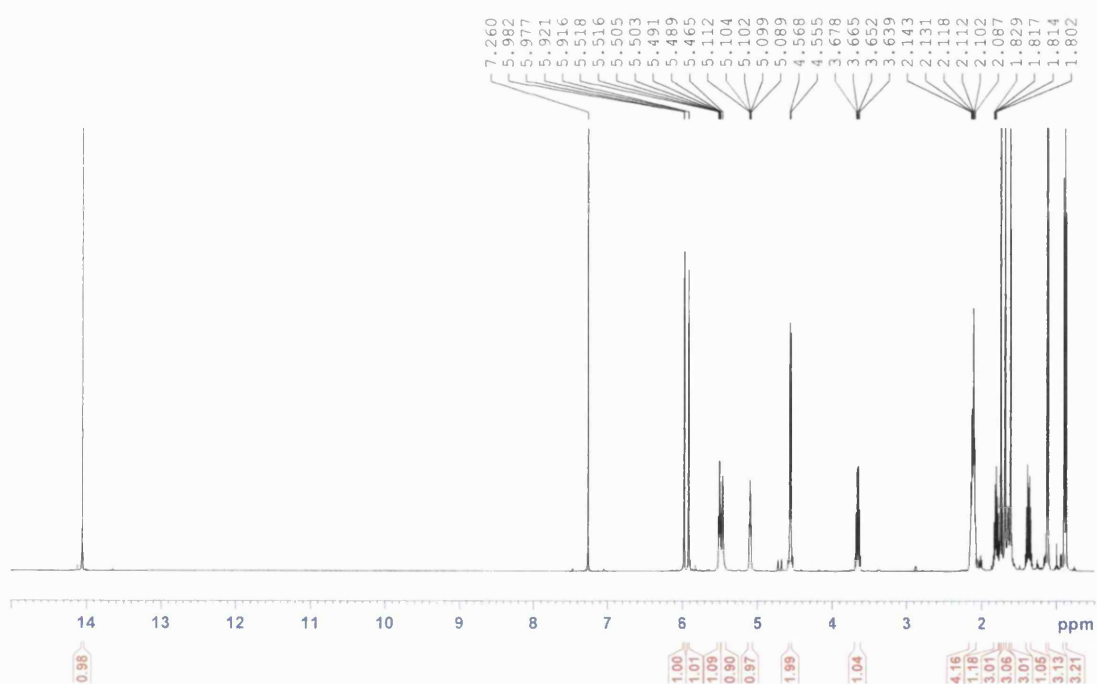


Fig. 129. <sup>1</sup>H NMR spectrum of WS-S-07 in chloroform-*d* recorded at 500 MHz.

HR ESI-MS revealed an  $[M-H]^-$  ion at  $m/z$  345, suggesting a molecular formula of  $C_{21}H_{30}O_4$ . The  $^1H$  NMR spectrum of **WS-S-07** is shown in Fig. 129. The characteristic signals for an *ortho*-substituted 2-methylbutanoyl phloroglucinol were observed, including: a highly-deshielded hydrogen-bonded hydroxyl group ( $\delta_H$  14.05), two *meta*-coupled aromatic protons ( $\delta_H$  5.92 d,  $J = 2.5$  Hz; 5.98 d,  $J = 2.5$  Hz), one methine ( $\delta_H$  3.66 m), one methylene ( $\delta_H$  1.37 m, 1.80 m), one methyl doublet ( $\delta_H$  1.12,  $J = 6.5$  Hz) and one methyl triplet ( $\delta_H$  0.89 t,  $J = 6.5$  Hz).  $^1H$  NMR signals corresponding to the geranyl moiety included an oxymethylene ( $\delta_H$  4.56 d,  $J = 6.5$ ), two further methylenes ( $\delta_H$  2.10 m, 2.13 m), two olefinic protons ( $\delta_H$  5.10 m, 5.50 m) and three methyl singlets ( $\delta_H$  1.61, 1.69, 1.74). **WS-S-07** was identified as (*S*)-2-*O*-geranyl-2'-methylbutanoyl phloroglucinol. The  $^1H$  and  $^{13}C$  NMR data of **WS-S-07** were in close agreement with that of the new natural product, **WS-09** (Table 18).

Table 33.  $^1H$  (500MHz) and  $^{13}C$  NMR (125 MHz) spectral data of **WS-S-07** recorded in chloroform-*d*.

Position	$^1H$ ( $J$ , Hz)	$^{13}C$
1	-	105.9
2	-	162.6
3	5.92 d (2.5)	91.5
4	-	162.0
5	5.98 d (2.5)	96.5
6	-	167.5
1'	-	210.4
2'	3.66 m	46.1
3'	1.37 m, 1.80 m	26.8
4'	0.89 t (6.5)	11.8
5'	1.12 d (6.5)	16.6
1''	4.56 d (6.5)	65.7
2''	5.50 m	118.2
3''	-	142.4
4''	2.13 m	39.5
5''	2.10 m	26.3
6''	5.10 m	123.6
7''	-	132.0
8''	1.69 s	25.7
9''	1.61 s	17.7
10''	1.74 s	16.6
4-OH	5.47 bs	-
6-OH	14.05 s	-

### 3.3.6.3

### Characterization of WS-S-08 as (±)-2-*O*-geranyl-2'-methylbutanoyl phloroglucinol

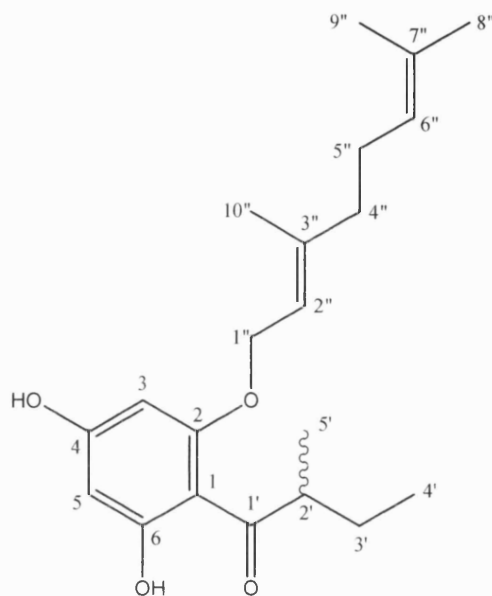


Fig. 130. Structure of **WS-S-08**.

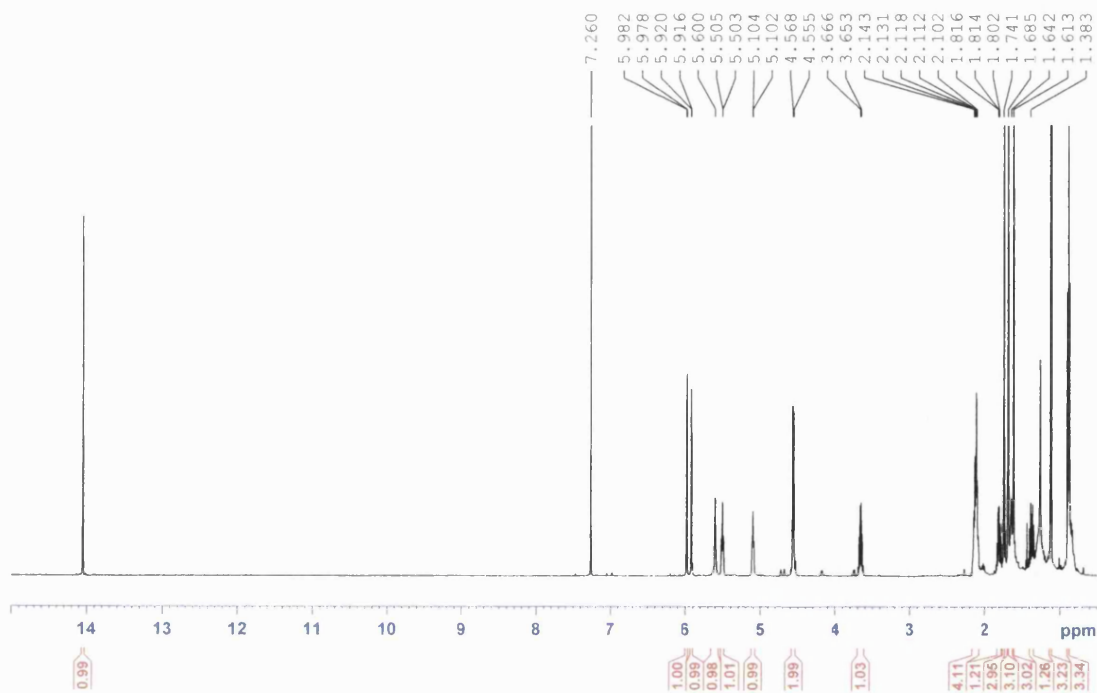


Fig. 131.  $^1\text{H}$  NMR spectrum of **WS-S-08** in chloroform-*d* recorded at 500 MHz.

HR ESI-MS indicated an  $[M-H]^-$  ion at  $m/z$  345, which corresponded to a molecular formula of  $C_{21}H_{30}O_4$ . The  $^1H$  NMR spectrum of **WS-S-08** is shown in Fig. 131. The  $^1H$  NMR and  $^{13}C$  NMR signals (Table 34) were identical to that of **WS-S-07**. The specific rotation of this compound was found to be  $0^\circ$ , implying that the (*R*)- and (*S*)- isomers were present in the same quantity. **WS-S-08** was therefore identified as ( $\pm$ )-2-*O*-geranyl-2'-methylbutanoyl phloroglucinol.

Table 34.  $^1H$  (500MHz) and  $^{13}C$  NMR (125 MHz) spectral data of **WS-S-08** recorded in chloroform-*d*.

Position	$^1H$ (J, Hz)	$^{13}C$
1	-	106.0
2	-	162.6
3	5.92 d (2.5)	91.5
4	-	162.0
5	5.98 d (2.5)	96.5
6	-	167.5
1'	-	210.4
2'	3.66 m	46.1
3'	1.37 m, 1.80 m	26.8
4'	0.89 t (6.5)	11.8
5'	1.12 d (6.5)	16.6
1''	4.56 d (6.5)	65.7
2''	5.50 m	118.2
3''	-	142.4
4''	2.13 m	39.5
5''	2.10 m	26.3
6''	5.10 m	123.6
7''	-	132.0
8''	1.69 s	25.7
9''	1.61 s	17.7
10''	1.74 s	16.6
4-OH	5.60 bs	-
6-OH	14.04 s	-

## 3.3.6.4

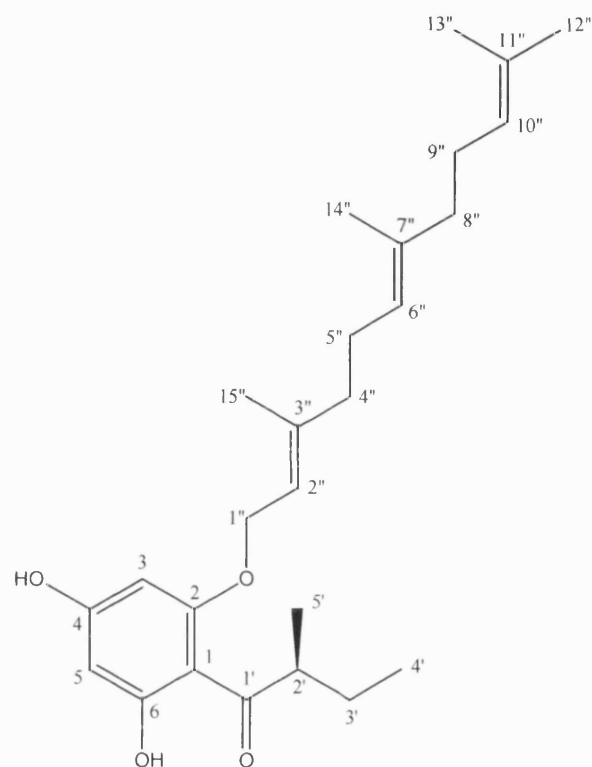
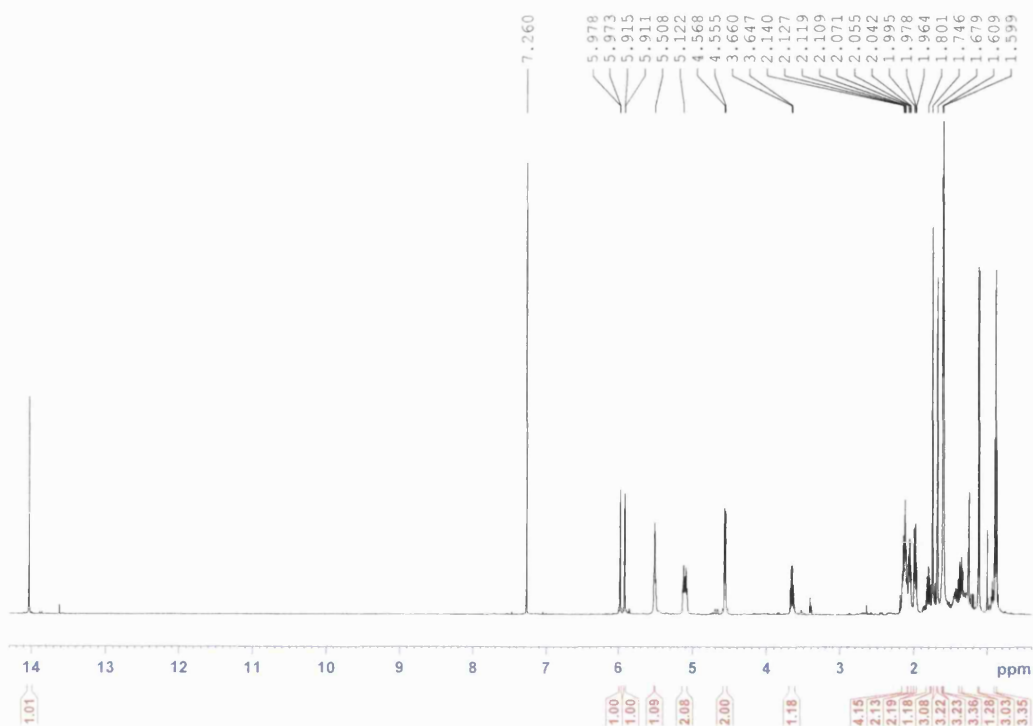
Characterization of WS-S-09 as (*S*)-2-*O*-farnesyl-2'-methylbutanoyl phloroglucinol

Fig. 132. Structure of WS-S-09.

Fig. 133. <sup>1</sup>H NMR spectrum of WS-S-09 in chloroform-*d* recorded at 500 MHz.

HR ESI-MS indicated an  $[M-H]^-$  ion at  $m/z$  413, in accordance with a molecular formula of  $C_{26}H_{38}O_4$ . The  $^1H$  NMR spectrum of **WS-S-09** is shown in Fig. 133. The signals for an *ortho*-substituted 2-methylbutanoyl phloroglucinol included a highly-deshielded hydrogen-bonded hydroxyl group ( $\delta_H$  14.03), two *meta*-coupled aromatic protons ( $\delta_H$  5.91 d,  $J = 2$  Hz; 5.98 d,  $J = 2.5$  Hz), one methine ( $\delta_H$  3.65 m), one methylene ( $\delta_H$  1.36 m, 1.80 m), one methyl doublet ( $\delta_H$  1.12,  $J = 7.5$  Hz) and one methyl triplet ( $\delta_H$  0.88 t,  $J = 7.5$  Hz). Signals accounting for a farnesyl side-chain included an oxymethylene ( $\delta_H$  4.56 d,  $J = 6.5$  Hz), four further methylenes appearing as multiplets between  $\delta_H$  1.98 and 2.14, three olefinic protons ( $\delta_H$  5.07 m; 5.12 m; 5.51 m) and four methyl singlets ( $\delta_H$  1.60; 1.61; 1.68; 1.75). **WS-S-09** was identified as (*S*)-2-*O*-farnesyl-2'-methylbutanoyl phloroglucinol.

Table 35.  $^1H$  (500MHz) and  $^{13}C$  NMR (125 MHz) spectral data of **WS-S-09** recorded in chloroform-*d*.

Position	$^1H$ ( $J$ , Hz)	$^{13}C$	Position	$^1H$ ( $J$ , Hz)	$^{13}C$
1	-	105.9	1''	4.56 d (6.5)	66.7
2	-	162.5	2''	5.51 m	118.2
3	5.91 d (2)	91.5	3''	-	142.5
4	-	162.0	4''	2.14 m	39.5
5	5.98 d (2.5)	96.5	5''	2.10 m	26.3
6	-	167.5	6''	5.12 m	123.5
1'	-	210.4	7''	-	135.7
2'	3.65 m	46.1	8''	1.98 m	39.7
3'	1.36 m, 1.80 m	26.8	9''	2.06 m	26.7
4'	0.88 t (7.5)	11.9	10''	5.07 m	124.3
5'	1.12 d (7.5)	16.6	11''	-	131.4
6-OH	14.03 s	-	12''	1.68 s	25.7
			13''	1.60 s	16.0
			14''	1.61 s	17.0
			15''	1.75 s	16.7

### 3.3.6.5

### Characterization of WS-S-10 as (*S*)-2-*O*-(3''-methylbutyl)-2'-methylbutanoyl phloroglucinol

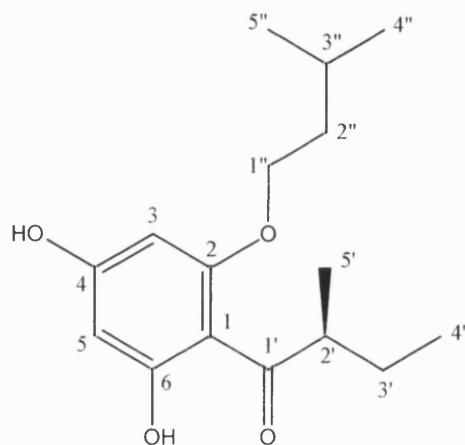


Fig. 134. Structure of **WS-S-10**.

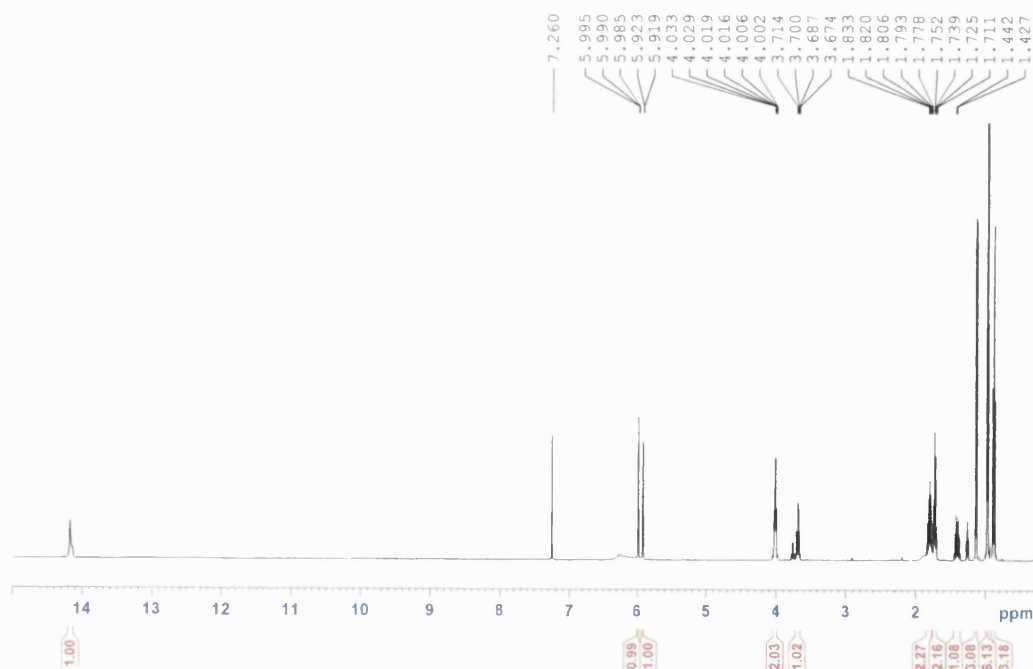


Fig. 135.  $^1\text{H}$  NMR spectrum of **WS-S-10** in chloroform-*d* recorded at 500 MHz.

HR ESI-MS gave an  $[M-H]^-$  ion at  $m/z$  279, suggesting a molecular formula of  $C_{16}H_{24}O_4$ . The  $^1H$  NMR spectrum of **WS-S-10** is shown in Fig. 135. The NMR signals corresponding to an *ortho*-substituted 2-methylbutanoyl phloroglucinol included a highly-deshielded hydrogen-bonded hydroxyl group ( $\delta_H$  14.17), two *meta*-coupled aromatic protons ( $\delta_H$  5.92 d,  $J = 2$  Hz; 5.99 d,  $J = 2.5$  Hz), one methine ( $\delta_H$  3.69 m), one methylene ( $\delta_H$  1.41 m, 1.81 m), one methyl doublet ( $\delta_H$  1.14,  $J = 7$  Hz) and one methyl triplet ( $\delta_H$  0.89 t,  $J = 7.5$  Hz). The signals accounting for the 3-methylbutyl substituent at the 2-*O* position included an oxymethylene ( $\delta_H$  4.02 t,  $J = 7.5$  Hz), a further methylene at  $\delta_H$  1.73, one methine at  $\delta_H$  1.80 and a methyl doublet integrating for six protons at ( $\delta_H$  0.98 d,  $J = 6.5$  Hz). **WS-S-10** was therefore identified as (*S*)-2-*O*-(3''-methylbutyl)-2'-methylbutanoyl phloroglucinol.

Table 36.  $^1H$  (500MHz) and  $^{13}C$  NMR (125 MHz) spectral data of **WS-S-10** recorded in chloroform-*d*.

Position	$^1H$ ( $J$ , Hz)	$^{13}C$
1	-	105.8
2	-	162.8
3	5.92 d (2)	91.5
4	-	162.4
5	5.99 d (2.5)	96.5
6	-	167.4
1'	-	210.4
2'	3.69 m	46.0
3'	1.41 m, 1.81 m	26.6
4'	0.89 t (7.5)	11.7
5'	1.14 d (7)	16.8
1''	4.02 t (7)	67.5
2''	1.73 m	37.7
3''	1.80 m	25.2
4''	0.98 d (6.5)	22.5
5''	0.98 d (6.5)	22.5
6-OH	14.17 s	-

## 3.3.6.6

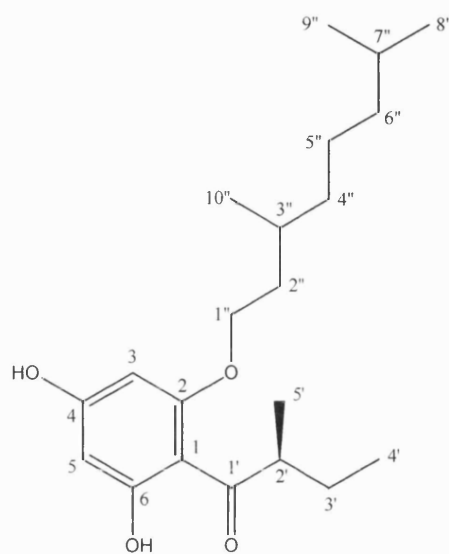
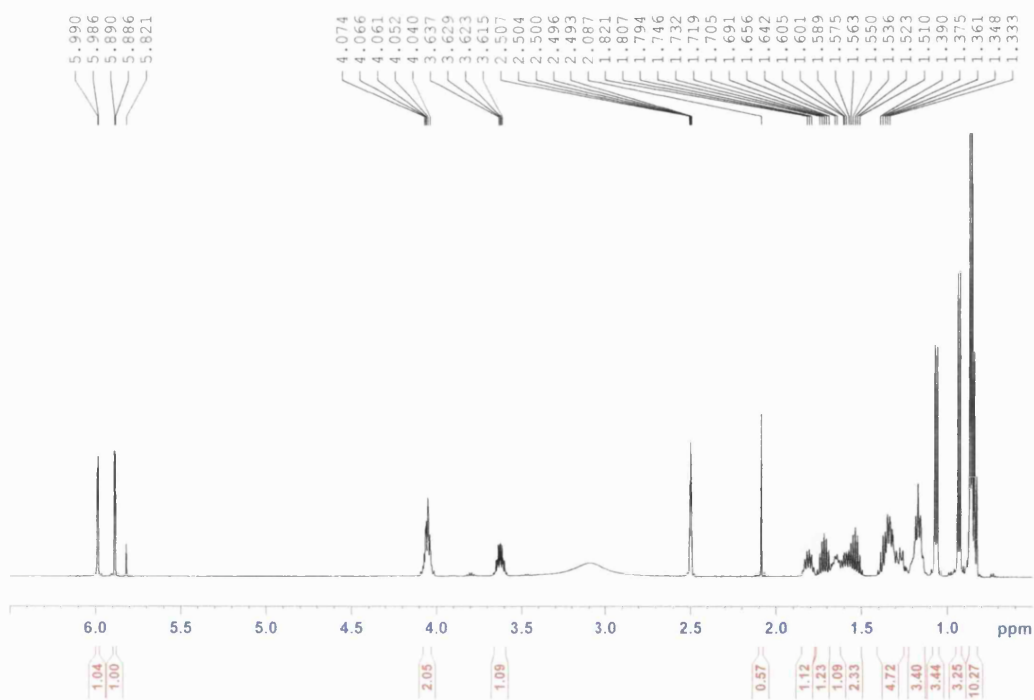
Characterization of WS-S-11 as (*S*)-2-*O*-(3'',7''-dimethyloctyl)-2'-methylbutanoyl phloroglucinol

Fig. 136. Structure of WS-S-11.

Fig. 137.  $^1\text{H}$  NMR spectrum of WS-S-11 in  $\text{DMSO}-d_6$  recorded at 500 MHz.

The molecular formula of **WS-S-11** was found to be C<sub>21</sub>H<sub>34</sub>O<sub>4</sub>, as indicated by an [M+H]<sup>+</sup> ion at m/z 351 in HR ESI-MS. The <sup>1</sup>H NMR spectrum of **WS-S-11** (Fig. 137) shows signals indicative of a 2-methylbutanoyl phloroglucinol nucleus, including two *meta*-coupled aromatic protons appearing as doublets ( $\delta_{\text{H}}$  5.89 d,  $J = 2$  Hz; 5.99 d,  $J = 2$  Hz), one methine ( $\delta_{\text{H}}$  3.63 m), one methylene ( $\delta_{\text{H}}$  1.33 m, 1.81 m), one methyl doublet ( $\delta_{\text{H}}$  1.11,  $J = 7$ ) and one methyl triplet ( $\delta_{\text{H}}$  0.87 t,  $J = 7.5$ ). The signals representing a 3,7-dimethyloctyl substituent at the 2-*O* position included an oxymethylene ( $\delta_{\text{H}}$  4.08 m), four further methylene groups between  $\delta_{\text{H}}$  1.18 and 1.83, two methine multiplets at  $\delta_{\text{H}}$  1.58 and 1.65, one methyl doublet at  $\delta_{\text{H}}$  0.93 ( $J = 6.5$  Hz) and a further methyl doublet integrating for six protons at  $\delta_{\text{H}}$  0.88 d ( $J = 6.5$  Hz). **WS-S-11** was therefore identified as (*S*)-2-*O*-(3'',7''-dimethyloctyl)-2'-methylbutanoyl phloroglucinol.

Table 37. <sup>1</sup>H (500MHz) and <sup>13</sup>C NMR (125 MHz) spectral data of **WS-S-11** recorded in DMSO-*d*<sub>6</sub>.

Position	<sup>1</sup> H ( $J$ , Hz)	<sup>13</sup> C
1	-	105.8
2	-	162.8
3	5.89 d (2)	91.5
4	-	162.4
5	5.99 d (2)	96.5
6	-	167.4
1'	-	210.4
2'	3.63 m	46.0
3'	1.33 m, 1.81 m	26.6
4'	0.87 t (7.5)	11.7
5'	1.11 d (7)	16.8
1''	4.08 m	66.7
2''	1.19 m, 1.33 m	37.3
3''	1.65 m	29.9
4''	1.59 m, 1.83 m	36.0
5''	1.35 m	24.6
6''	1.18 m	39.2
7''	1.58 m	28.0
8''	0.88 d (6.5)	22.6
9''	0.88 d (6.5)	22.6
10''	0.93 d (6.5)	19.6

### 3.3.7 Acetylphloroglucinol derivatives

Fourteen acetylphloroglucinol derivatives (Table 38) were synthesized from the commercially available acetylphloroglucinol (2,4,6-trihydroxyacetophenone) using the following reaction:

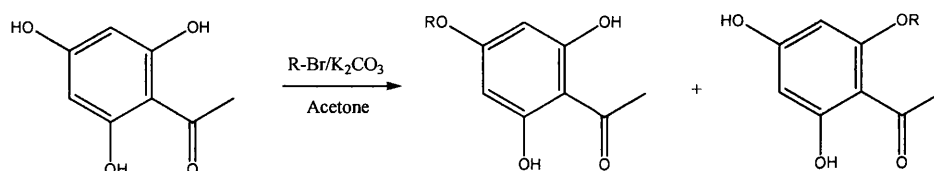


Table 38. Yield of acetylphloroglucinol derivatives

	R	Position	Yield			Novelty
			(mg)	(mmol)	(%)	
WS-S-12	Prenyl	<i>ortho</i> -	3.4	0.0144	1.2	New
WS-S-13		<i>para</i> -	3.5	0.0148	1.2	New
WS-S-14	Geranyl	<i>ortho</i> -	4.8	0.0158	1.4	Known
WS-S-15		<i>para</i> -	4.6	0.0151	1.4	Known
WS-S-16	Farnesyl	<i>ortho</i> -	8.9	0.0239	1.7	Known
WS-S-17		<i>para</i> -	9.7	0.0261	1.9	Known
WS-S-18	3-Methylbutyl	<i>ortho</i> -	4.6	0.0193	1.4	New
WS-S-19		<i>para</i> -	4.7	0.0197	1.5	Known
WS-S-20	3,7-Dimethyl-	<i>ortho</i> -	5.2	0.0169	1.2	New
WS-S-21	octyl	<i>para</i> -	5.4	0.0175	1.3	New
WS-S-22	Pentyl	<i>ortho</i> -	6.3	0.0265	2.2	New
WS-S-23		<i>para</i> -	6.8	0.0286	2.4	New
WS-S-24	Decyl	<i>ortho</i> -	8.3	0.0269	2.5	New
WS-S-25		<i>para</i> -	8.7	0.0282	2.6	New

To isolate these compounds, the reaction mixture was washed with water and extracted with chloroform. The organic layer was dried over anhydrous magnesium sulphate and then removed by a rotary evaporator. The crude products were purified by p-TLC using hexane-ethyl acetate (8:2 for C<sub>10</sub> and C<sub>15</sub> derivatives, and 7:3 for C<sub>5</sub> derivatives) as the solvent systems. Among these compounds, only **WS-14** to **17** and **WS-19** are known. The rest of the compounds are new and their NMR data are reported here for the first time.

Because no protecting group was used in the above reaction, alkylation took place in a non-specific manner, i.e. at the hydroxyl group either *para*- or *ortho*- to the acetyl group in the acylphloroglucinol. This resulted in the production of two acylphloroglucinols with approximately the same yield. The yield of the compounds ranged from 1.2 to 2.6 % and is summarized in Table 38. Obviously when a large amount of the derivatives is required, reactions using protecting group will be more appropriate.

The *para*- and *ortho*-substituted acylphloroglucinols were easily distinguished by observing the <sup>1</sup>H NMR spectra of the two derivatives. This will be illustrated using the <sup>1</sup>H NMR spectra of **WS-S-14** and **WS-S-15**.

3.3.7.1. Characterization of WS-S-14 and WS-S-15 as 2-*O*-geranyl-acetylphloroglucinol and 4-*O*-geranyl-acetylphloroglucinol

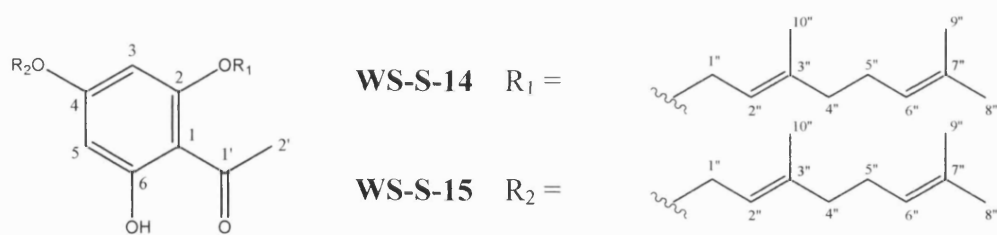


Fig. 138. Structures of WS-S-14 and WS-S-15.

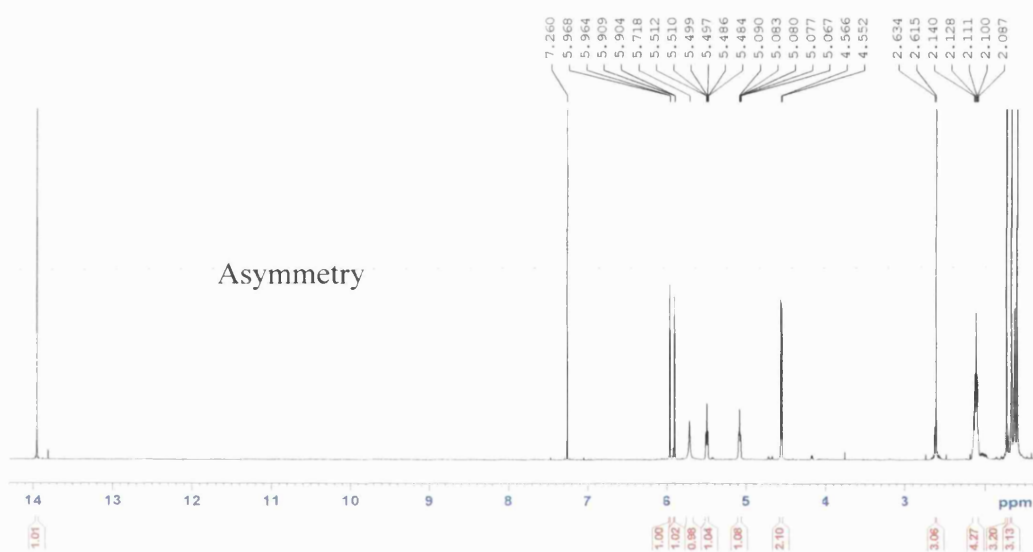


Fig. 139.  $^1\text{H}$  NMR spectrum of WS-S-14 in chloroform-*d* recorded at 500 MHz.

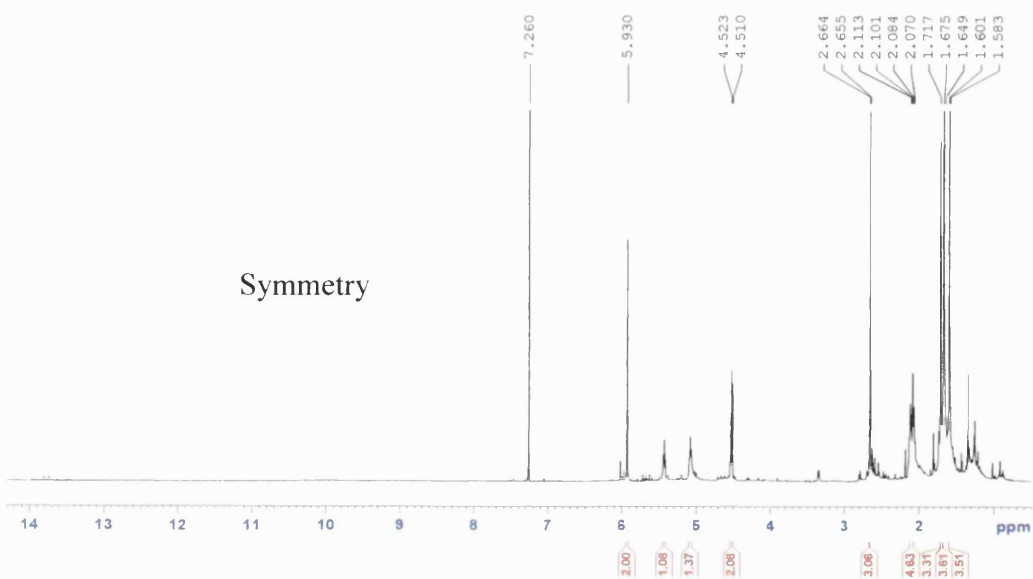


Fig. 140.  $^1\text{H}$  NMR spectrum of WS-S-15 in chloroform-*d* recorded at 500 MHz.

HR ESI-MS gave an  $[M-H]^-$  ion at  $m/z$  303, suggesting a molecular formula of  $C_{18}H_{24}O_4$  for both **WS-S-14** and **WS-S-15**. The  $^1H$  NMR spectrum of **WS-S-14** (Fig. 139) showed the characteristic signals for a highly-desielded hydrogen-bonded hydroxyl group ( $\delta_H$  13.95), two *meta*-coupled aromatic protons ( $\delta_H$  5.97 d,  $J = 2$  Hz; 5.91 d,  $J = 2$  Hz), an acetyl methyl singlet ( $\delta_H$  2.62 s) and a geranyloxy side-chain (one oxymethylene at  $\delta_H$  4.56,  $J = 7$  Hz, two olefinic protons at  $\delta_H$  5.08 and 5.50, two overlapping methylene multiplets at  $\delta_H$  2.11 (4H), and three methyl singlets at  $\delta_H$  1.61, 1.68, 1.74). The pattern of the signals was indicative of an *ortho*-substituted phloroglucinol as seen in the natural products and the synthetic derivatives discussed earlier. The only difference in the  $^1H$  NMR spectrum of **WS-S-15** (Fig. 140) included the absence of the signal for the hydrogen-bonded hydroxyl group at approximately 14 ppm and the appearance of an aromatic singlet at  $\delta_H$  5.93 integrating for two protons. This could be explained by the fact when the geranyl side-chain was attached at the hydroxyl group *para*- to the acetyl group, the molecule displayed a plane of symmetry. The two *meta*-coupled aromatic protons were equivalent, thus appearing as a singlet instead of two doublets. This confirmed that **WS-S-15** was different from **WS-S-14** in that the geranyl side-chain was *para*- to the acetyl group. These observations were seen in all other acetylphloroglucinol derivatives synthesized using this method.

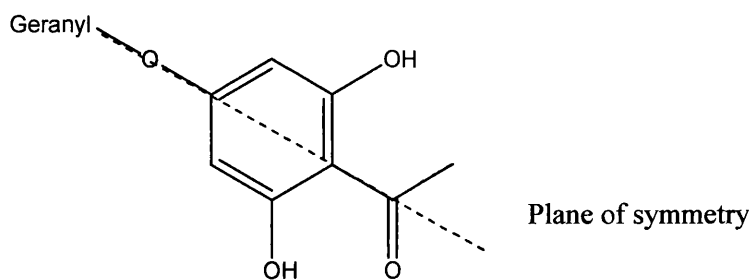


Fig. 141. Plane of symmetry in *para*-substituted acylphloroglucinol.

**WS-S-14** has been isolated from the fruits of *Evodia merrillii* as a natural product (Chou and Lin, 1992). The  $^1\text{H}$  and  $^{13}\text{C}$  NMR spectral data of **WS-S-14** (Table 39) are in close agreement with the published data (Chou and Lin, 1992).

**WS-S-15** has been synthesized previously by Huang *et al.* (1999). The  $^1\text{H}$  and  $^{13}\text{C}$  NMR data of **WS-S-15** reported in Table 39 are again very close to the data in the literature (Huang *et al.*, 1999).

Table 39.  $^1\text{H}$  (500MHz) and  $^{13}\text{C}$  NMR (125 MHz) spectral data of **WS-S-14** and **WS-S-15** recorded in chloroform-*d*.

Position	<b>WS-S-14</b>		<b>WS-S-15</b>	
	$^1\text{H}$ (J, Hz)	$^{13}\text{C}$	$^1\text{H}$ (J, Hz)	$^{13}\text{C}$
1	-	106.3	-	105.9
2	-	163.1	-	165.1
3	5.91 d (2)	91.5	5.93 s	94.8
4	-	162.6	-	165.1
5	5.97 d (2)	96.2	5.93 s	94.8
6	-	167.2	-	163.4
1'	-	203.4	-	203.2
2'	2.62 s	33.1	2.67 s	32.9
1''	4.56 d (7)	65.7	4.52 d (6.5)	65.2
2''	5.50 m	118.4	5.43 m	118.4
3''	-	142.2	-	142.2
4''	2.13 m	39.4	2.12 m	39.5
5''	2.11 m	26.2	2.09 m	26.3
6''	5.08 m	123.5	5.10 m	123.7
7''	-	132.0	-	132.0
8''	1.68 s	25.7	1.68 s	25.7
9''	1.61 s	17.7	1.60 s	17.7
10''	1.74 s	16.6	1.72 s	16.7
4-OH	5.72 bs	-	-	-
6-OH	13.95 s	-	-	-

3.3.7.2 Characterization of WS-S-12 and WS-S-13 as 2-*O*-prenyl-acetylphloroglucinol and 4-*O*-prenyl-acetylphloroglucinol

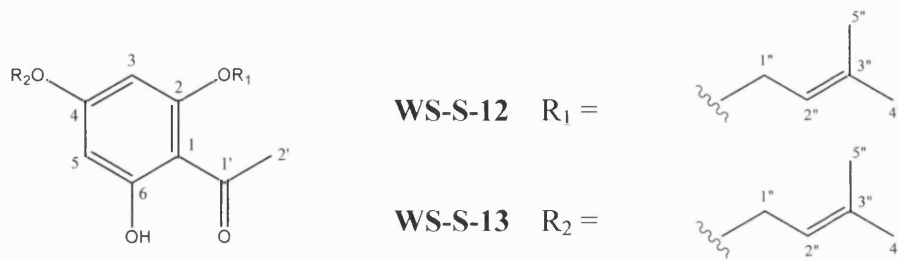


Fig. 142. Structures of WS-S-12 and WS-S-13.

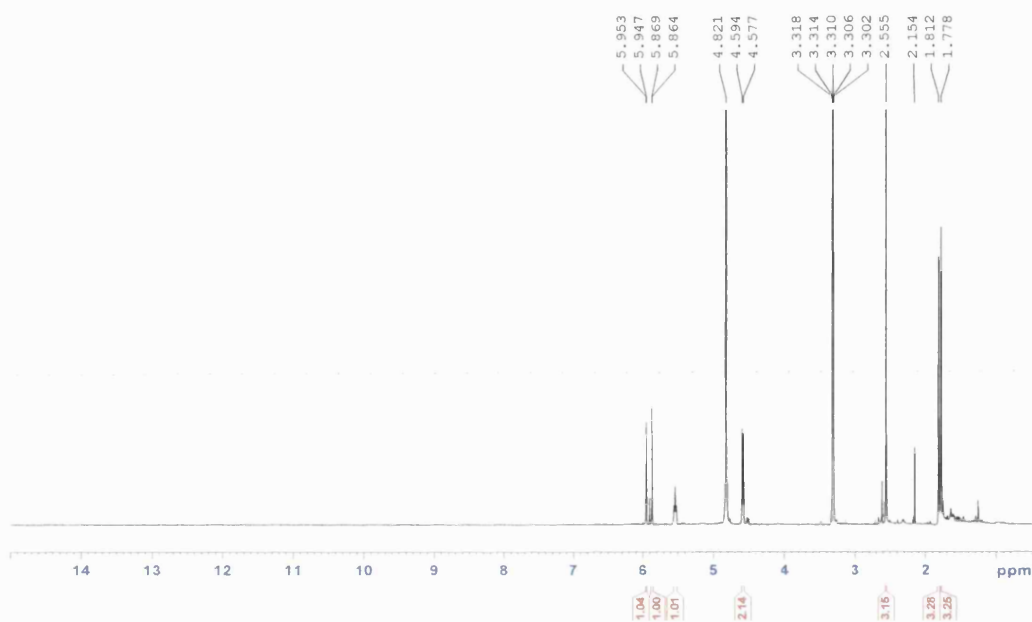


Fig. 143.  $^1\text{H}$  NMR spectrum of WS-S-12 in methanol- $d_4$  recorded at 400 MHz.

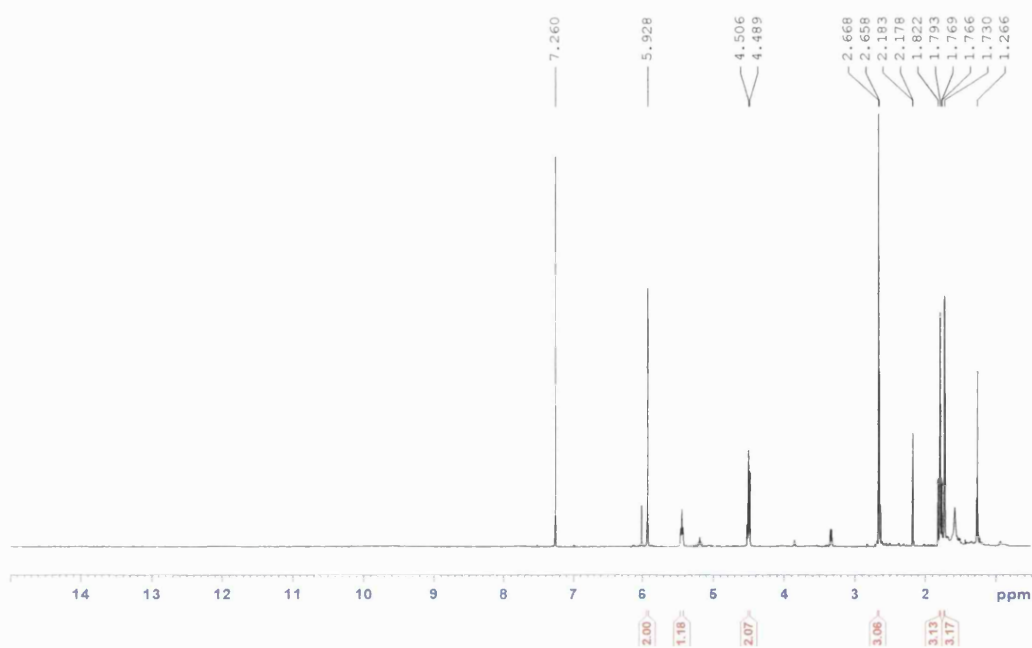


Fig. 144.  $^1\text{H}$  NMR spectrum of WS-S-13 in chloroform- $d$  recorded at 400.

HR ESI-MS gave an  $[M-H]^-$  ion at  $m/z$  235, suggesting a molecular formula of  $C_{13}H_{16}O_4$  for both **WS-S-12** and **WS-S-13**. The  $^1H$  and  $^{13}C$  spectral data of **WS-S-12** and **WS-S-13** are summarized in Table 40. The  $^1H$  NMR spectrum of **WS-S-12** (Fig. 143) revealed two *meta*-coupled aromatic protons at  $\delta_H$  5.86 (d,  $J = 2.4$  Hz) and 5.95 (d,  $J = 2$  Hz), an acetyl methyl singlet at  $\delta_H$  2.56, and signals corresponding to a prenyl moiety, including an oxymethylene  $\delta_H$  4.58 (d,  $J = 6.8$  Hz), an olefinic proton at  $\delta_H$  5.54 and two methyl singlets at  $\delta_H$  1.78 and 1.81. **WS-S-12** was identified as 2-*O*-prenyl-acetylphloroglucinol. The  $^1H$  NMR spectrum of **WS-S-13** (Fig. 144) showed signals for a prenyl group as described above, as well as an acetyl methyl singlet at  $\delta_H$  2.67 and an aromatic singlet integrating for two protons at  $\delta_H$  5.93. **WS-S-13** was identified as 4-*O*-prenyl-acetylphloroglucinol.

Table 40.  $^1H$  (400MHz) and  $^{13}C$  NMR (100 MHz) spectral data of **WS-S-12** and **WS-S-13** recorded in methanol- $d_4$  and chloroform- $d$ .

Position	WS-S-12		WS-S-13	
	$^1H$ ( $J$ , Hz)	$^{13}C$	$^1H$ ( $J$ , Hz)	$^{13}C$
1	-	106.7	-	106.2
2	-	165.6	-	163.3
3	5.86 d (2.4)	94.7	5.93 s	91.6
4	-	167.1	-	162.5
5	5.95 d (2)	94.7	5.93 s	96.2
6	-	165.7	-	167.3
1'	-	204.2	-	203.4
2'	2.56 s	33.7	2.67 s	33.2
1''	4.58 d (6.8)	66.5	4.50 d (6.8)	65.7
2''	5.54 m	112.1	5.44 m	118.2
3''	-	140.4	-	142.0
4''	1.81 s	25.7	1.79 s	25.6
5''	1.78 s	18.3	1.77 s	16.7

3.3.7.3

Characterization of WS-S-16 and WS-S-17 as 2-*O*-farnesyl-acetylphloroglucinol and 4-*O*-farnesyl-acetylphloroglucinol

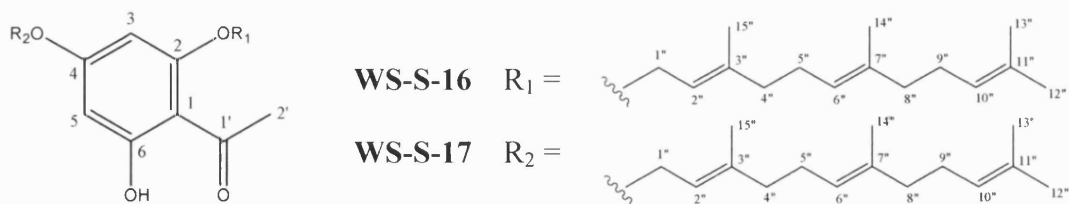


Fig. 145. Structures of WS-S-16 and WS-S-17.

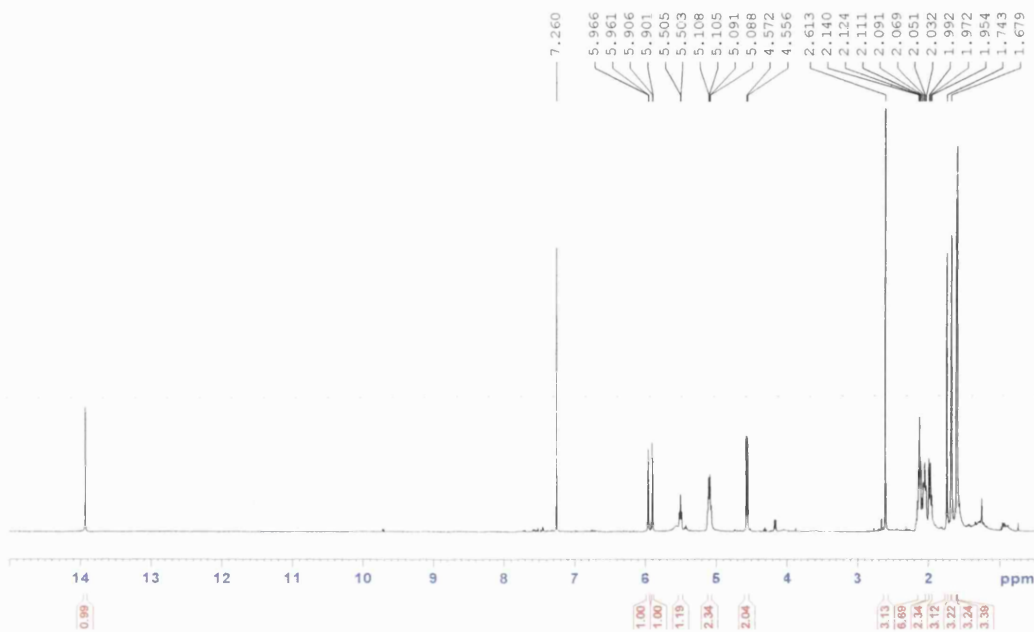


Fig. 146.  $^1\text{H}$  NMR spectrum of WS-S-16 in chloroform-*d* recorded at 400 MHz.

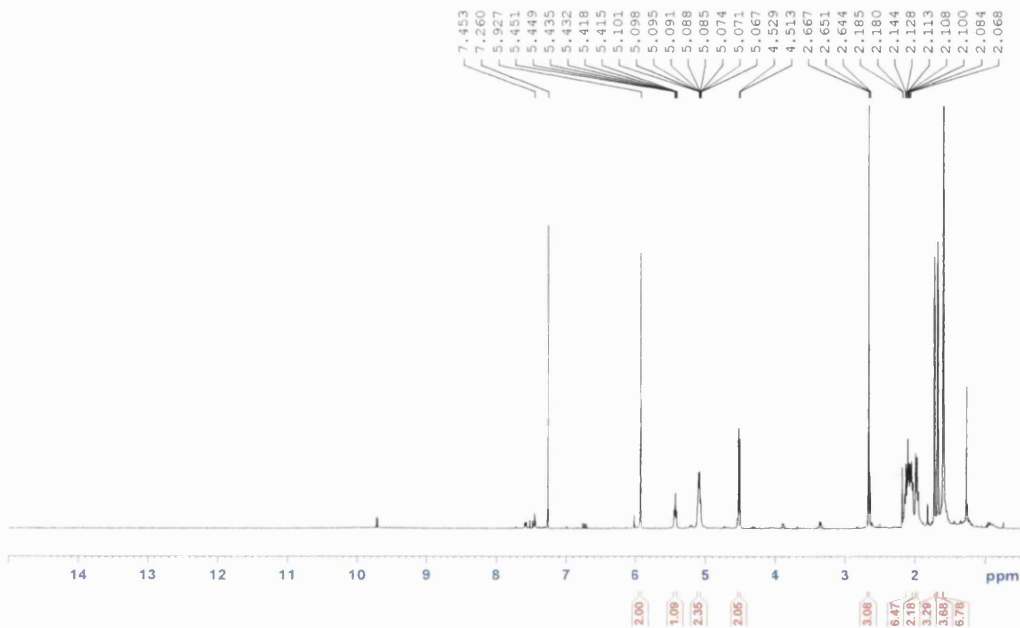


Fig. 147.  $^1\text{H}$  NMR spectrum of WS-S-17 in chloroform-*d* recorded at 400 MHz.

HR ESI-MS gave an  $[M-H]^-$  ion at  $m/z$  371, suggesting a molecular formula of  $C_{23}H_{32}O_4$  for both **WS-S-16** and **WS-S-17**. The  $^1H$  and  $^{13}C$  NMR spectral data of **WS-S-16** and **WS-S-17** are shown in Table 41. For **WS-S-16**, the  $^1H$  NMR spectrum (Fig. 146) displayed signals for a highly-deshielded hydrogen-bonded hydroxyl group ( $\delta_H$  13.93), two *meta*-coupled aromatic protons ( $\delta_H$  5.90 d,  $J = 2$  Hz; 5.96 d,  $J = 2$  Hz), an acetyl methyl singlet ( $\delta_H$  2.61 s) and a farnesyl side-chain (an oxymethylene doublet at  $\delta_H$  4.56, four additional methylene multiplets ranging from  $\delta_H$  1.98 to 2.14, three olefinic multiplets at  $\delta_H$  5.09, 5.11 and 5.50, and four methyl singlets at  $\delta_H$  1.60, 1.61, 1.68 and 1.74). **WS-S-16** was identified as 2-*O*-farnesyl-acetylphloroglucinol. For **WS-S-17**, the  $^1H$  NMR spectrum (Fig. 147) showed signals for a farnesyl side-chain as described above, an aromatic singlet at  $\delta_H$  5.93 integrating for two protons and an acetyl methyl singlet at  $\delta_H$  2.67. **WS-S-17** was identified as 4-*O*-farnesyl-acetylphloroglucinol.

The synthesis of **WS-S-16** has been reported in Huang *et al.* (1997). Unfortunately, the journal Gaodeng xuexiao Huaxue Xuebao was written in Chinese and was also inaccessible, the method of synthesis and the published data have not been reviewed. On the other hand, **WS-S-17** has been isolated from *Boronia ramosa* (Ashan *et al.*, 1994) and also synthesized (Huang *et al.*, 1999) previously. The NMR data of **WS-S-17** showed a good agreement with the data in both publications.

Table 41. <sup>1</sup>H (400MHz) and <sup>13</sup>C NMR (100 MHz) spectral data of **WS-S-16** and **WS-S-17** recorded in chloroform-*d*.

Position	WS-S-16		WS-S-17	
	<sup>1</sup> H (J, Hz)	<sup>13</sup> C	<sup>1</sup> H (J, Hz)	<sup>13</sup> C
1	-	106.4	-	105.0
2	-	163.1	-	165.1
3	5.90 d (2)	91.4	5.93 s	94.9
4	-	162.5	-	165.1
5	5.96 d (2)	96.3	5.93 s	94.9
6	-	167.2	-	163.2
1'	-	203.4	-	210.4
2'	2.61 s	33.1	2.67 s	32.7
1''	4.56 d (6.4)	65.7	4.52 d (6.4)	65.2
2''	5.50 m	118.4	5.44 m	118.5
3''	-	142.2	-	142.2
4''	2.14 m	39.5	2.12 m	39.5
5''	2.10 m	26.2	2.06 m	26.2
6''	5.11 m	123.5	5.10 m	123.5
7''	-	135.6	-	135.6
8''	1.98 m	39.7	1.97 m	39.7
9''	2.06 m	26.7	2.04 m	26.7
10''	5.09 m	124.3	5.08 m	124.3
11''	-	131.4	-	131.4
12''	1.68 s	25.7	1.68 s	25.7
13''	1.60 s	16.0	1.60 s	16.0
14''	1.61 s	17.7	1.61 s	17.7
15''	1.74 s	16.7	1.72 s	16.7
6-OH	13.93 s	-	-	-

### 3.3.7.4

### Characterization of WS-S-18 and WS-S-19 as 2-*O*-(3''-methylbutyl)-acetylphloroglucinol and 4-*O*-(3''-methylbutyl)-acetylphloroglucinol

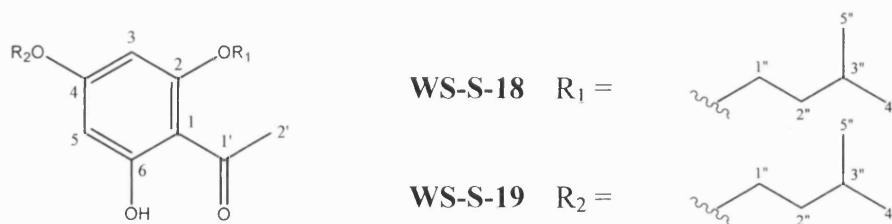


Fig. 148. Structures of WS-S-18 and WS-S-19.

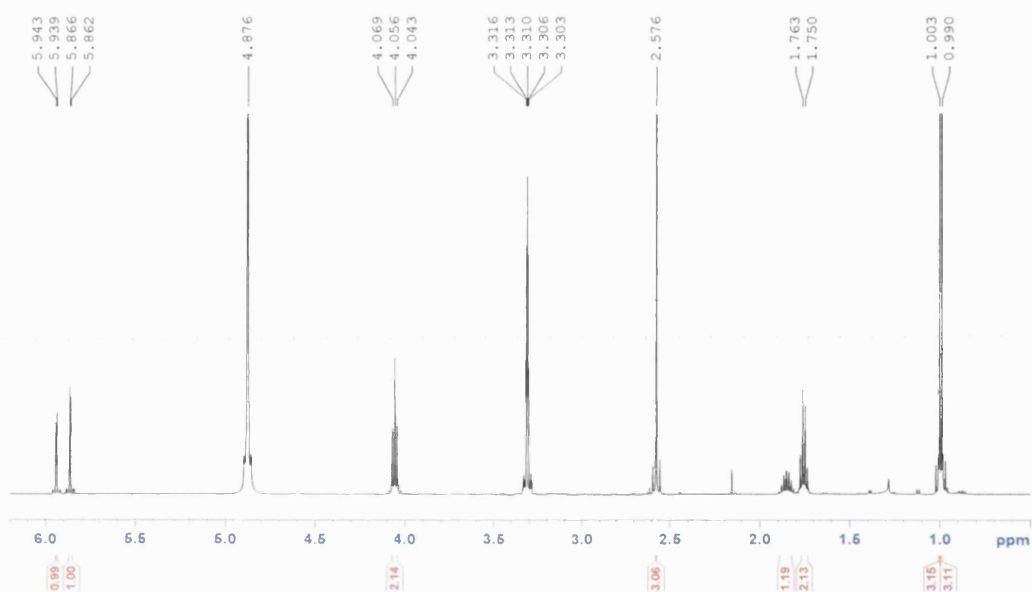


Fig. 149.  $^1\text{H}$  NMR spectrum of WS-S-18 in methanol- $d_4$  recorded at 500 MHz.

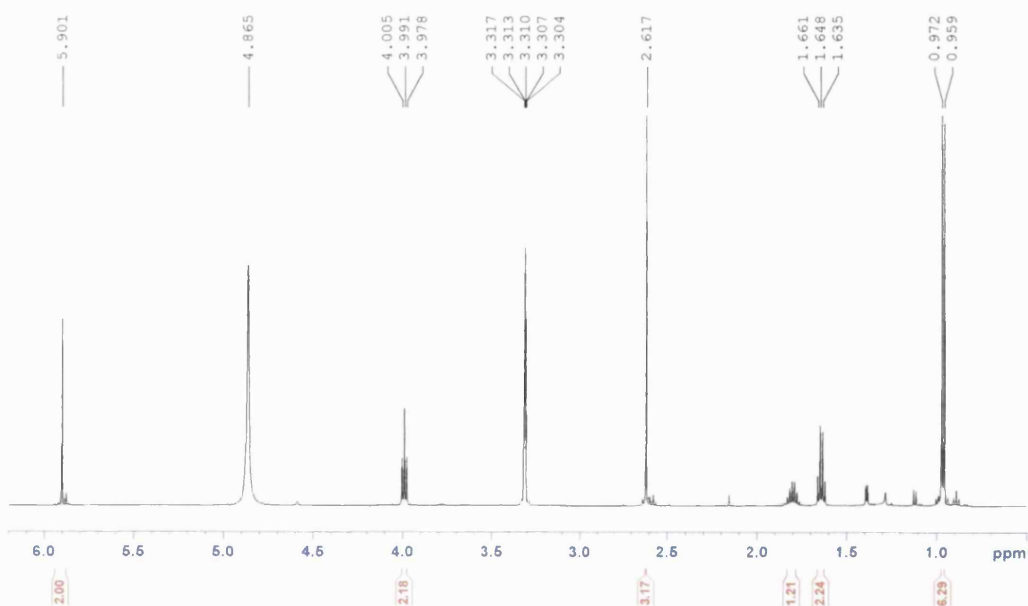


Fig. 150.  $^1\text{H}$  NMR spectrum of WS-S-19 in methanol- $d_4$  recorded at 500 MHz.

HR ESI-MS gave an  $[M-H]^-$  ion at  $m/z$  237, suggesting a molecular formula of  $C_{13}H_{18}O_4$  for both **WS-S-18** and **WS-S-19**. The  $^1H$  and  $^{13}C$  NMR spectral data are summarized in Table 42. The  $^1H$  NMR spectrum of **WS-S-18** displayed two *meta*-coupled aromatic protons at  $\delta_H$  5.86 ( $J = 2$  Hz) and 5.94 ( $J = 2$  Hz), an acetyl methyl singlet at  $\delta_H$  2.58, and signals corresponding to a 3-methylbutyl substituent (an oxymethylene triplet at  $\delta_H$  4.06 ( $J = 6.5$  Hz); a further methylene multiplet at  $\delta_H$  1.76; a methine multiplet at  $\delta_H$  1.83 and a methyl doublet integrating for six protons at  $\delta_H$  1.00 ( $J = 6.5$  Hz)). **WS-S-18** was identified as 2-*O*-(3''-methylbutyl)-acetylphloroglucinol. The  $^1H$  NMR spectrum of **WS-S-19** also displayed signals for a 3-methylbutyl substituent and an acetyl methyl singlet (Table 42). Additionally, it showed a singlet at  $\delta_H$  5.90 integrating for two protons. **WS-S-19** was identified as 4-*O*-(3''-methylbutyl)-acetylphloroglucinol. This compound has been synthesized previously (Bharate *et al.*, 2007). The  $^1H$  NMR data of **WS-S-19** shown in Table 42 are nearly identical to the published data. The  $^{13}C$  NMR data of this compound were not documented in the publication.

Table 42.  $^1H$  (500MHz) and  $^{13}C$  NMR (125 MHz) spectral data of **WS-S-18** and **WS-S-19** recorded in methanol- $d_4$ .

Position	<b>WS-S-18</b>		<b>WS-S-19</b>	
	$^1H$ ( $J$ , Hz)	$^{13}C$	$^1H$ ( $J$ , Hz)	$^{13}C$
1	-	106.8	-	106.2
2	-	166.7	-	165.7
3	5.86 d (2)	92.6	5.90 s	94.6
4	-	164.6	-	167.2
5	5.94 d (2)	96.7	5.90 s	94.6
6	-	168.3	-	165.7
1'	-	204.1	-	204.9
2'	2.58 s	33.3	2.62 s	32.8
1''	4.06 t (6.5)	68.5	3.99 t (7)	67.6
2''	1.76 m	39.0	1.65 m	38.9
3''	1.83 m	26.3	1.80 m	26.2
4''	1.00 d (6.5)	22.9	0.96 d (6.5)	22.9
5''	1.00 d (6.5)	22.9	0.96 d (6.5)	22.9

3.3.7.5 Characterization of WS-S-20 and WS-S-21 as 2-*O*-(3'',7''-dimethyloctyl)-acetylphloroglucinol and 4-*O*-(3'',7''-dimethyloctyl)-acetylphloroglucinol

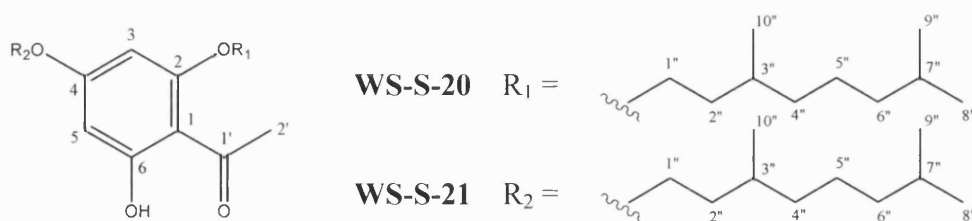


Fig. 151. Structures of WS-S-20 and WS-S-21.

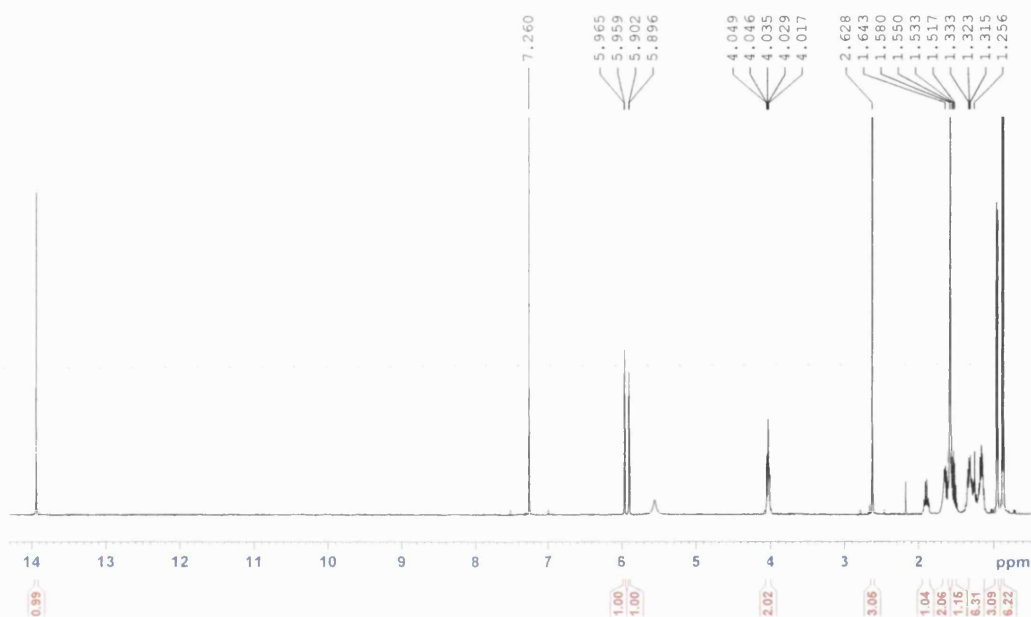


Fig. 152.  $^1\text{H NMR}$  spectrum of WS-S-20 in chloroform-*d* recorded at 500 MHz.

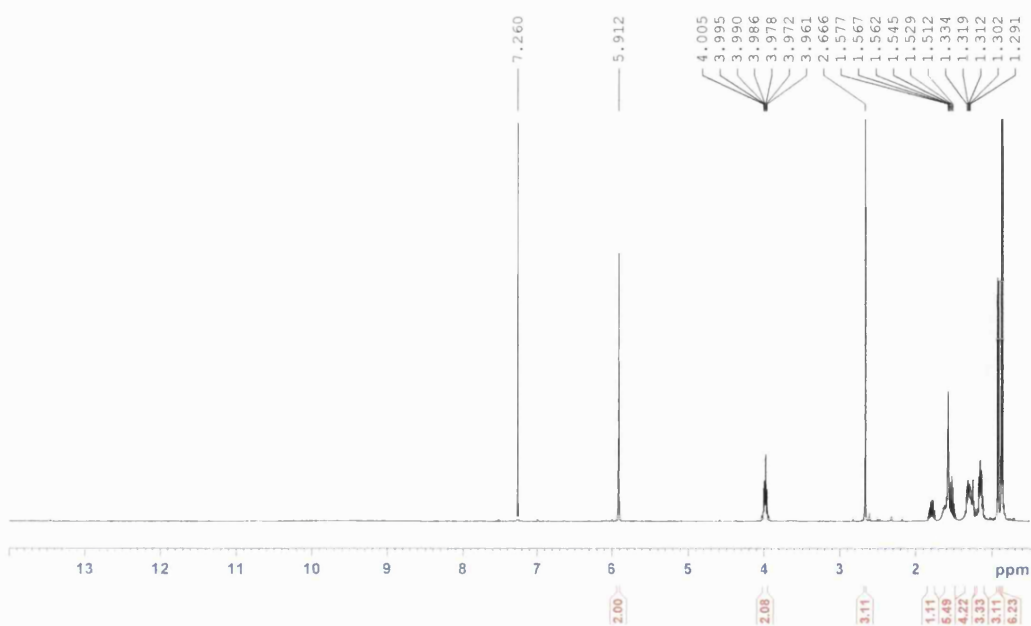


Fig. 153.  $^1\text{H NMR}$  spectrum of WS-S-21 in chloroform-*d* recorded at 500 MHz.

HR ESI-MS gave an  $[M-H]^-$  ion at  $m/z$  307, suggesting a molecular formula of  $C_{18}H_{28}O_4$  for both **WS-S-20** and **WS-S-21**. The  $^1H$  and  $^{13}C$  NMR spectral data are summarized in Table 43. The  $^1H$  NMR spectrum of **WS-S-20** (Fig. 152) showed two *meta*-coupled aromatic protons at  $\delta_H$  5.90 (d,  $J = 2.5$  Hz) and 5.96 (d,  $J = 2.5$  Hz), an acetyl methyl singlet at  $\delta_H$  2.63, and signals indicating a 3,7-dimethyloctyl side-chain (an oxymethylene multiplet at  $\delta_H$  4.03, four additional methylene multiplets between  $\delta_H$  1.18 and 1.90, two methine multiplets at  $\delta_H$  1.52 and 1.63, one methyl doublet at  $\delta_H$  0.95 (3H,  $J = 6.5$  Hz) and a further methyl doublet integrating for six protons at  $\delta_H$  0.87 ( $J = 6.5$  Hz). **WS-S-20** was identified as 2-*O*-(3'',7''-dimethyloctyl)-acetylphloroglucinol. The  $^1H$  NMR spectrum of **WS-S-21** displayed signals for a 3,7-dimethyloctyl moiety, an acetyl methyl singlet at  $\delta_H$  2.67 and an aromatic singlet at  $\delta_H$  5.91 integrating for two protons. This indicated that the two aromatic hydrogens were equivalent due to a plane of symmetry in **WS-S-21**. **WS-S-21** is therefore identified as 4-*O*-(3'',7''-dimethyloctyl)-acetyl-phloroglucinol.

Table 43.  $^1H$  (500MHz) and  $^{13}C$  NMR (125 MHz) spectral data of **WS-S-20** and **WS-S-21** recorded in chloroform-*d*.

Position	<b>WS-S-20</b>		<b>WS-S-21</b>	
	$^1H$ ( $J$ , Hz)	$^{13}C$	$^1H$ ( $J$ , Hz)	$^{13}C$
1	-	106.2	-	105.0
2	-	163.2	-	165.3
3	5.90 d (2.5)	91.2	5.91 s	94.8
4	-	162.5	-	163.1
5	5.96 d (2.5)	96.2	5.91 s	94.8
6	-	167.3	-	165.3
1'	-	203.2	-	203.1
2'	2.63 s	33.2	2.67 s	32.7
1''	4.03 m	67.4	3.96 m	66.8
2''	1.18 m, 1.32 m	37.3	1.17 m, 1.32 m	37.2
3''	1.63 m	30.0	1.62 m	29.8
4''	1.65 m, 1.90 m	36.0	1.57 m, 1.78 m	35.8
5''	1.31 m	24.7	1.32 m	24.6
6''	1.16 m	39.2	1.16 m	39.2
7''	1.52 m	28.0	1.55 m	28.0
8''	0.87 d (6.5)	22.6	0.87 d (6.5)	22.6
9''	0.87 d (6.5)	22.6	0.87 d (6.5)	22.6
10''	0.95 d (6.5)	19.6	0.92 d (6.5)	19.6
4-OH	5.53 bs	-	-	-
6-OH	13.96 s	-	-	-

3.3.7.6 Characterization of WS-S-22 and WS-S-23 as 2-*O*-pentyl-acetylphloroglucinol and 4-*O*-pentyl-acetylphloroglucinol

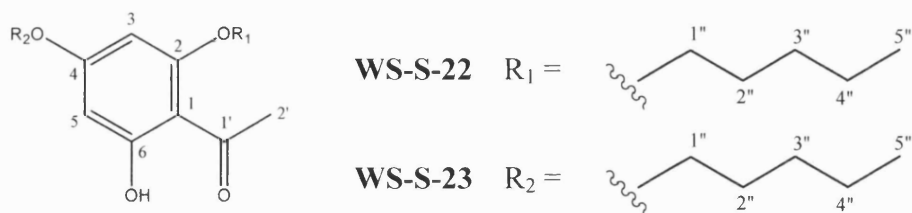


Fig. 154. Structures of WS-S-22 and WS-S-23.

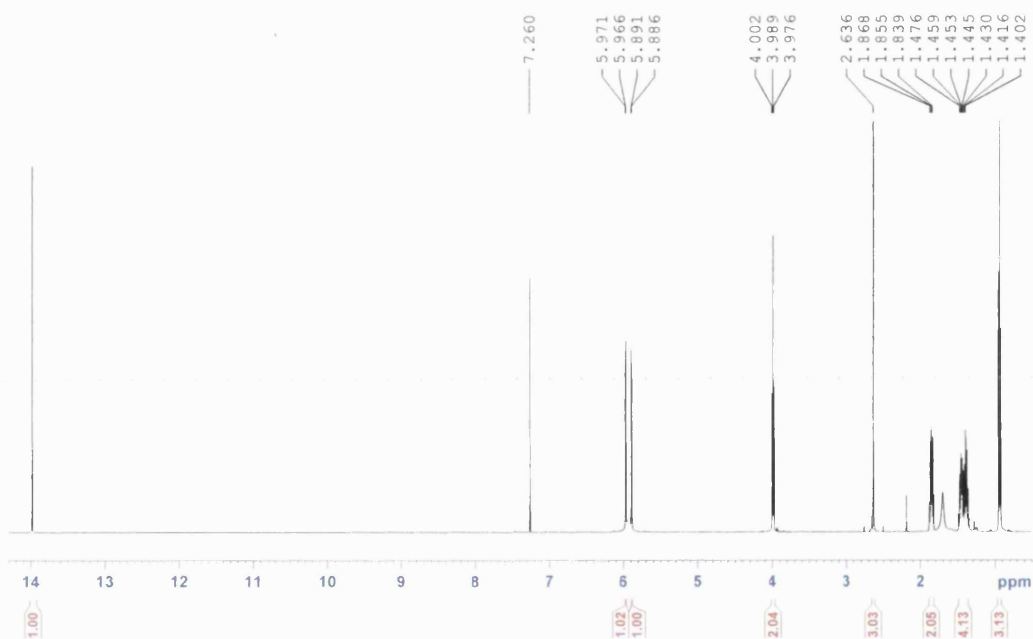


Fig. 155.  $^1\text{H}$  NMR spectrum of WS-S-22 in chloroform-*d* recorded at 500 MHz.

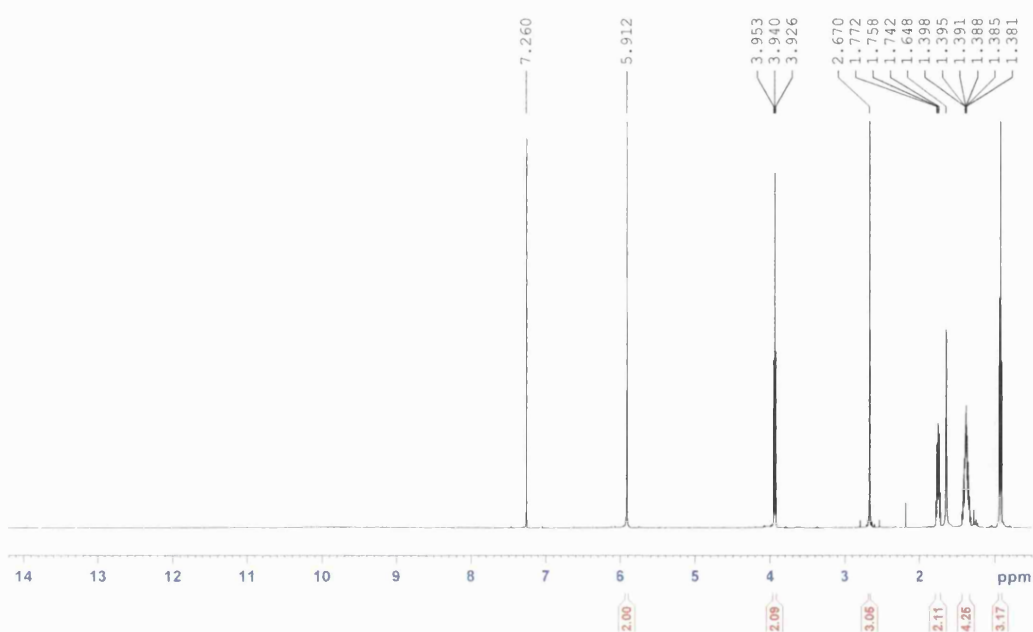


Fig. 156.  $^1\text{H}$  NMR spectrum of WS-S-23 in chloroform-*d* recorded at 500 MHz.

HR ESI-MS gave an  $[M-H]^+$  ion at  $m/z$  239, suggesting a molecular formula of  $C_{13}H_{18}O_4$  for both **WS-S-22** and **WS-S-23**. The  $^1H$  and  $^{13}C$  NMR spectral data are shown in Table 44. The  $^1H$  NMR spectrum of **WS-S-22** (Fig. 155) revealed a highly-deshielded hydrogen-bonded hydroxyl group at  $\delta_H$  14.01, two *meta*-coupled aromatic protons at  $\delta_H$  5.89 (d,  $J = 2.5$  Hz) and  $\delta_H$  5.97 (d,  $J = 2.5$  Hz), an acetyl methyl singlet at  $\delta_H$  2.64, and signals for a pentyl group, including an oxymethylene triplet at  $\delta_H$  3.99 ( $J = 6.5$  Hz), three additional methylenes ( $\delta_H$  1.44 to 1.86) and a methyl triplet at  $\delta_H$  0.94 ( $J = 7.5$  Hz). **WS-S-22** was identified as 2-*O*-pentyl-acetylphloroglucinol. The  $^1H$  NMR of **WS-S-23** showed almost identical signals, apart from the presence of a singlet at  $\delta_H$  5.91 integrating for two protons. **WS-S-23** was identified as 4-*O*-pentyl-acetylphloroglucinol.

Table 44.  $^1H$  (500MHz) and  $^{13}C$  NMR (125 MHz) spectral data of **WS-S-22** and **WS-S-23** recorded in chloroform-*d*.

Position	WS-S-22		WS-S-23	
	$^1H$ ( $J$ , Hz)	$^{13}C$	$^1H$ ( $J$ , Hz)	$^{13}C$
1	-	106.1	-	105.0
2	-	163.3	-	165.4
3	5.89 d (2.5)	91.2	5.91 s	94.7
4	-	162.8	-	163.8
5	5.97d (2.5)	96.2	5.91 s	94.7
6	-	167.2	-	165.4
1'	-	203.3	-	203.2
2'	2.64 s	33.2	2.67 s	32.7
1''	3.99 t (6.5)	69.5	3.94 t (6.5)	68.3
2''	1.86 m	28.7	1.76 m	28.6
3''	1.44 m	28.4	1.38 m	28.1
4''	1.44 m	22.4	1.38 m	22.4
5''	0.94 t (7.5)	14.0	0.94 t (7)	14.0
6-OH	14.01 s	-	-	-

### 3.3.7.7 Characterization of WS-S-24 and WS-S-25 as 2-*O*-decyl-acetylphloroglucinol and 4-*O*-decyl-acetylphloroglucinol

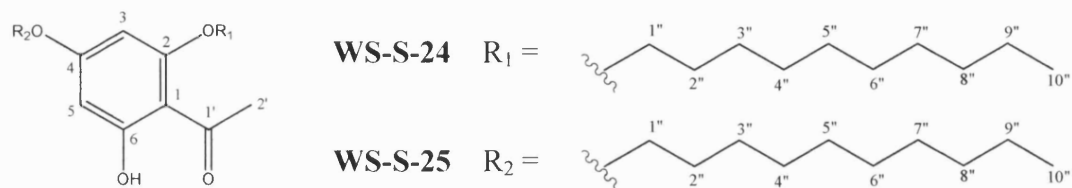


Fig. 157. Structures of WS-S-24 and WS-S-25.

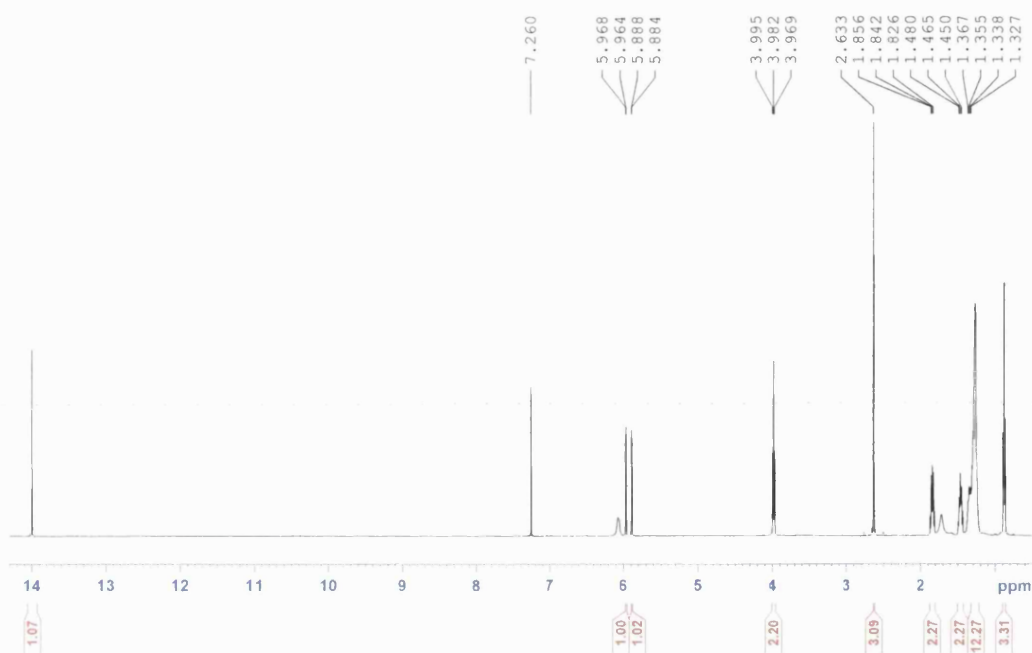


Fig. 158.  $^1\text{H}$  NMR spectrum of WS-S-24 in chloroform-*d* recorded at 500 MHz.

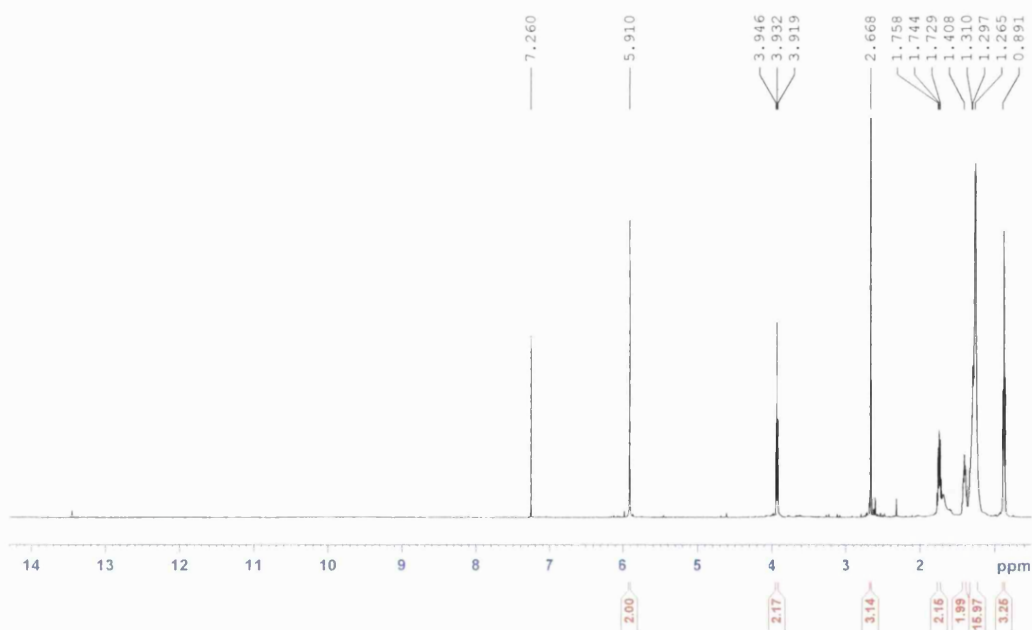


Fig. 159.  $^1\text{H}$  NMR spectrum of WS-S-25 in chloroform-*d* recorded at 500 MHz.

HR ESI-MS gave an  $[M+H]^+$  ion at  $m/z$  309, suggesting a molecular formula of  $C_{18}H_{28}O_4$  for both **WS-S-24** and **WS-S-25**. The  $^1H$  and  $^{13}C$  NMR spectral data of **WS-S-24** and **WS-S-25** are shown in Table 45. The  $^1H$  NMR spectrum of **WS-S-24** (Fig. 158) showed a highly-deshielded hydrogen-bonded hydroxyl group at  $\delta_H$  14.03, two *meta*-coupled aromatic protons at  $\delta_H$  5.88 ( $J = 2$  Hz) and 5.96 ( $J = 2$  Hz), an acetyl methyl singlet at  $\delta_H$  2.63 and signals for a decyl side-chain (an oxymethylene triplet at  $\delta_H$  3.98 ( $J = 6.5$  Hz); further methylene groups between  $\delta_H$  1.30 and 1.84; and a methyl triplet at  $\delta_H$  0.88 ( $J = 6.5$  Hz)). The number of methylene groups in the decyl side-chain was confirmed by data obtained from mass spectrometry. **WS-S-24** was identified as 2-*O*-decyl-acetylphloroglucinol. The  $^1H$  NMR spectrum of **WS-S-25** (Fig. 159) displayed signals for a decyl moiety, an acetyl methyl singlet at  $\delta_H$  2.67 as well as a singlet integrating for two protons at  $\delta_H$  5.91. **WS-S-25** was identified as 4-*O*-decyl-acetylphloroglucinol.

Table 45.  $^1H$  (500MHz) and  $^{13}C$  NMR (125 MHz) spectral data of **WS-S-24** and **WS-S-25** recorded in chloroform-*d*.

Position	WS-S-24		WS-S-25	
	$^1H$ ( $J$ , Hz)	$^{13}C$	$^1H$ ( $J$ , Hz)	$^{13}C$
1	-	106.2	-	105.0
2	-	163.2	-	165.4
3	5.88 d (2)	91.2	5.91 s	94.8
4	-	162.7	-	163.2
5	5.96 d (2)	96.3	5.91 s	94.8
6	-	167.3	-	165.4
1'	-	203.2	-	203.1
2'	2.63 s	33.0	2.67 s	32.6
1''	3.98 t (6.5)	69.1	3.93 t (7)	68.4
2''	1.84 m	29.0	1.74 m	28.9
3''	1.47 m	26.2	1.41 m	25.9
4''-9''	1.30 m	22.6	1.28 m	22.6
		29.3		29.3
		29.3		29.3
		29.5		29.5
		29.7		29.7
		31.9		31.9
10''	0.88 t (6.5)	14.0	0.88 t (6.5)	14.0
6-OH	14.03 s	-	-	-

### 3.6 Physical properties of compounds

#### Properties of **WS-01**

Yellow oil;  $[\alpha]_D^{22}$   $0^\circ$  ( $c$  0.28, MeOH); UV (MeOH)  $\lambda_{\max}$  ( $\log \epsilon$ ): 238 (4.00), 250 (4.22), 298 (3.98), 380 (4.19) nm; IR  $\nu_{\max}$  (thin film)  $\text{cm}^{-1}$ : 3250, 1635, 1587, 1498;  $^1\text{H}$  NMR and  $^{13}\text{C}$  NMR (MeOD): see Table 9; HR EI-MS ( $m/z$ ): 259.0605  $[\text{M}+\text{H}]^+$  (calc. for  $\text{C}_{14}\text{H}_{10}\text{O}_5$ , 259.0601).

#### Properties of **WS-02**

Yellow oil;  $[\alpha]_D^{22}$   $0^\circ$  ( $c$  0.07, MeOH); UV (MeOH)  $\lambda_{\max}$  ( $\log \epsilon$ ): 235 (3.89), 289 (4.00), 387 (3.80) nm; IR  $\nu_{\max}$  (thin film)  $\text{cm}^{-1}$ : 3330, 1647, 1600, 1575, 1489;  $^1\text{H}$  NMR and  $^{13}\text{C}$  NMR (MeOD): see Table 10; HR ES-MS ( $m/z$ ): 229.0506  $[\text{M}+\text{H}]^+$  (calc. for  $\text{C}_{13}\text{H}_8\text{O}_4$ , 229.0495).

#### Properties of **WS-03**

White solid;  $[\alpha]_D^{22}$   $-48.5^\circ$  ( $c$  0.24,  $\text{CHCl}_3$ ); UV ( $\text{CHCl}_3$ )  $\lambda_{\max}$  ( $\log \epsilon$ ): 208 (3.98) nm; IR  $\nu_{\max}$  (thin film)  $\text{cm}^{-1}$ : 3422, 1645, 1449, 1380, 1372;  $^1\text{H}$  NMR and  $^{13}\text{C}$  NMR ( $\text{CDCl}_3$ ): see Table 11.

#### Properties of **WS-04**

Pale yellow oil;  $[\alpha]_D^{22}$   $+3.3^\circ$  ( $c$  0.09, MeOH); UV (MeOH)  $\lambda_{\max}$  ( $\log \epsilon$ ): 206 (4.30), 293 (4.05) nm; IR  $\nu_{\max}$  (thin film)  $\text{cm}^{-1}$ : 3650, 3174, 1655, 1560, 1543, 1458, 1026; (a)  $^1\text{H}$  NMR and  $^{13}\text{C}$  NMR (MeOD): see Table 12; HR ES-MS ( $m/z$ ): 225.1122  $[\text{M}+\text{H}]^+$  (calc. for  $\text{C}_{12}\text{H}_{16}\text{O}_4$ , 225.1120); (b)  $^1\text{H}$  NMR and  $^{13}\text{C}$  NMR (MeOD): see Table 13; HR ES-MS ( $m/z$ ): 239.1275  $[\text{M}+\text{H}]^+$  (calc. for  $\text{C}_{13}\text{H}_{18}\text{O}_4$ , 239.1278).

#### Properties of **WS-05**

White solid;  $[\alpha]_D^{22}$   $-144.3^\circ$  (*c* 1.5, MeOH); UV (MeOH)  $\lambda_{\max}$  (log  $\epsilon$ ): 215 (3.97) nm; IR  $\nu_{\max}$  (thin film)  $\text{cm}^{-1}$ : 3381, 2927, 1700, 1651;  $^1\text{H}$  NMR and  $^{13}\text{C}$  NMR (MeOD): see Table 14; HR ESI-MS (*m/z*): 173.0455  $[\text{M-H}]^-$  (calc. for  $\text{C}_7\text{H}_{10}\text{O}_5$ , 173.0455).

#### Properties of **WS-06**

Brown solid;  $[\alpha]_D^{22}$   $+31.1^\circ$  (*c* 0.82, MeOH); UV (MeOH)  $\lambda_{\max}$  (log  $\epsilon$ ): 213 (4.10), 268 (4.21) nm; IR  $\nu_{\max}$  (thin film)  $\text{cm}^{-1}$ : 3396, 1679, 1517, 1478, 1373;  $^1\text{H}$  NMR and  $^{13}\text{C}$  NMR (MeOD): see Table 15; HR ESI-MS (*m/z*): 291.0865  $[\text{M+H}]^+$  (calc. for  $\text{C}_{15}\text{H}_{14}\text{O}_6$ , 291.0863).

#### Properties of **WS-07**

White solid;  $[\alpha]_D^{22}$   $-24.4^\circ$  (*c* 0.16,  $\text{CHCl}_3$ ); UV ( $\text{CHCl}_3$ )  $\lambda_{\max}$  (log  $\epsilon$ ): 205 (4.01); IR  $\nu_{\max}$  (thin film)  $\text{cm}^{-1}$ : 3446, 2925, 2838, 1450, 1385;  $^1\text{H}$  NMR and  $^{13}\text{C}$  NMR ( $\text{CDCl}_3$ ): see Table 16.

#### Properties of **WS-08**

Pale yellow oil;  $[\alpha]_D^{22}$   $0^\circ$  (*c* 0.19,  $\text{CHCl}_3$ ); UV ( $\text{CHCl}_3$ )  $\lambda_{\max}$  (log  $\epsilon$ ): 240 (3.87) nm; IR  $\nu_{\max}$  (thin film)  $\text{cm}^{-1}$ : 3412, 1504, 1472, 1264, 1208, 1155;  $^1\text{H}$  NMR and  $^{13}\text{C}$  NMR ( $\text{CDCl}_3$ ): see Table 17; HR ESI-MS (*m/z*): 273.0763  $[\text{M-H}]^-$  (calc. for  $\text{C}_{15}\text{H}_{14}\text{O}_5$ , 273.0768).

#### Properties of **WS-09**

Pale yellow oil;  $[\alpha]_D^{22}$   $+6.0^\circ$  (*c* 0.25,  $\text{CHCl}_3$ ); UV ( $\text{CHCl}_3$ )  $\lambda_{\max}$  (log  $\epsilon$ ): 240 (4.05), 289 (4.35) nm; IR  $\nu_{\max}$  (thin film)  $\text{cm}^{-1}$ : 3348, 2968, 2931, 1624, 1593, 1448, 1377, 1216, 1162, 1099, 826;  $^1\text{H}$  NMR and  $^{13}\text{C}$  NMR ( $\text{CDCl}_3$ ): see Table 18; HR ES-MS (*m/z*): 345.2056  $[\text{M-H}]^-$  (calc. for  $\text{C}_{21}\text{H}_{30}\text{O}_4$ , 345.2071).

### Properties of **WS-10**

Pale yellow oil;  $[\alpha]_D^{22} +5.8^\circ$  (*c* 0.12, CHCl<sub>3</sub>); UV (CHCl<sub>3</sub>)  $\lambda_{\max}$  (log  $\epsilon$ ): 240 (4.26), 290 (3.62) nm; IR  $\nu_{\max}$  (thin film) cm<sup>-1</sup>: 3338, 2967, 2934, 2873, 1620, 1594, 1448, 1217; <sup>1</sup>H NMR and <sup>13</sup>C NMR (CDCl<sub>3</sub>): see Table 19; HR ESI-MS (*m/z*): 363.2168 [M+H]<sup>+</sup> (calc. for C<sub>21</sub>H<sub>30</sub>O<sub>5</sub>, 363.2172).

### Properties of **WS-11**

Pale yellow oil;  $[\alpha]_D^{22} +2.5^\circ$  (*c* 0.41, CHCl<sub>3</sub>); UV (CHCl<sub>3</sub>)  $\lambda_{\max}$  (log  $\epsilon$ ): 240 (4.44), 288 (4.90) nm; IR  $\nu_{\max}$  (thin film) cm<sup>-1</sup>: 3357, 1734, 1653, 1558, 1540, 1506, 1457; <sup>1</sup>H NMR and <sup>13</sup>C NMR (CDCl<sub>3</sub>): see Table 20; HR ESI-MS (*m/z*): 363.2163 [M+H]<sup>+</sup> (calc. for C<sub>21</sub>H<sub>30</sub>O<sub>5</sub>, 363.2172).

### Properties of **WS-12**

Pale yellow oil;  $[\alpha]_D^{22} +2.7^\circ$  (*c* 0.32, CHCl<sub>3</sub>); UV (CHCl<sub>3</sub>)  $\lambda_{\max}$  (log  $\epsilon$ ): 240 (4.05), 289 (4.35) nm; IR  $\nu_{\max}$  (thin film) cm<sup>-1</sup>: 3397, 2970, 2928, 1622, 1594, 1456, 1217; <sup>1</sup>H NMR and <sup>13</sup>C NMR (CDCl<sub>3</sub>): see Table 21; HR ESI-MS (*m/z*): 379.2120 [M+H]<sup>+</sup> (calc. for C<sub>21</sub>H<sub>30</sub>O<sub>6</sub>, 379.2121).

### Properties of **WS-13**

Pale yellow oil;  $[\alpha]_D^{22} +2.6^\circ$  (*c* 0.19, CHCl<sub>3</sub>); UV (CHCl<sub>3</sub>)  $\lambda_{\max}$  (log  $\epsilon$ ): 240 (4.05), 289 (3.68) nm; IR  $\nu_{\max}$  (thin film) cm<sup>-1</sup>: 3376, 2970, 2934, 1622, 1593, 1447, 1217; <sup>1</sup>H NMR and <sup>13</sup>C NMR (CDCl<sub>3</sub>): see Table 22; HR ESI-MS (*m/z*): 363.2181 [M+H]<sup>+</sup> (calc. for C<sub>21</sub>H<sub>30</sub>O<sub>5</sub>, 363.2166).

### Properties of **WS-14**

Yellow oil;  $[\alpha]_D^{22} 0^\circ$  (*c* 0.24, CHCl<sub>3</sub>); UV (CHCl<sub>3</sub>)  $\lambda_{\max}$  (log  $\epsilon$ ): 242 (4.03), 255 (3.98), 374 (3.82) nm; IR  $\nu_{\max}$  (thin film) cm<sup>-1</sup>: 1717, 1700, 1696, 1653, 1616, 1558, 1506; <sup>1</sup>H NMR and <sup>13</sup>C NMR (CDCl<sub>3</sub>): see Table 23; HR ES-MS (*m/z*): 255.1021 [M+H]<sup>+</sup> (calc. for C<sub>16</sub>H<sub>14</sub>O<sub>3</sub>, 255.1016).

#### Properties of **WS-15**

White solid;  $[\alpha]_D^{22} +10.8^\circ$  (*c* 0.37, CHCl<sub>3</sub>); UV (CHCl<sub>3</sub>)  $\lambda_{\max}$  (log  $\epsilon$ ): 240 (3.98) nm; IR  $\nu_{\max}$  (thin film) cm<sup>-1</sup>: 3675, 2943, 2853, 1734, 1558, 1458; <sup>1</sup>H NMR and <sup>13</sup>C NMR (CDCl<sub>3</sub>): see Table 24.

#### Properties of **WS-S-01**

Colourless liquid;  $[\alpha]_D^{22} +10.1^\circ$  (*c* 0.54, CHCl<sub>3</sub>); b.p. 119-120 °C; <sup>1</sup>H NMR and <sup>13</sup>C NMR (CDCl<sub>3</sub>): see Table 26.

#### Properties of **WS-S-02**

Pale yellow oil;  $[\alpha]_D^{22} +8.5^\circ$  (*c* 0.35, CHCl<sub>3</sub>); UV (CHCl<sub>3</sub>)  $\lambda_{\max}$  (log  $\epsilon$ ): 240 (4.17), 290 (3.97) nm; IR  $\nu_{\max}$  (thin film) cm<sup>-1</sup>: 3297, 1628, 1602, 1222; <sup>1</sup>H NMR and <sup>13</sup>C NMR (CDCl<sub>3</sub>): see Table 27; HR ESI-MS (*m/z*): 209.0813 [M-H]<sup>-</sup> (calc. for C<sub>11</sub>H<sub>14</sub>O<sub>4</sub>, 209.0814).

#### Properties of **WS-S-03**

Pale yellow oil;  $[\alpha]_D^{22} +0.7^\circ$  (*c* 0.43, CHCl<sub>3</sub>); UV (CHCl<sub>3</sub>)  $\lambda_{\max}$  (log  $\epsilon$ ): 241 (3.36), 283 (3.66) nm; IR  $\nu_{\max}$  (thin film) cm<sup>-1</sup>: 3618, 1632, 1589, 1500, 1149, 1113, 1073, 1059; <sup>1</sup>H NMR and <sup>13</sup>C NMR (CDCl<sub>3</sub>): see Table 28; HR ESI-MS (*m/z*): 229.1502 [M+H]<sup>+</sup> (calc. for C<sub>15</sub>H<sub>22</sub>O<sub>6</sub>, 229.1495).

#### Properties of **WS-S-04**

Pale yellow oil;  $[\alpha]_D^{22} +4.9^\circ$  (*c* 0.39, CHCl<sub>3</sub>); UV (CHCl<sub>3</sub>)  $\lambda_{\max}$  (log  $\epsilon$ ): 239 (4.26), 290 (4.23) nm; IR  $\nu_{\max}$  (thin film) cm<sup>-1</sup>: 3276, 2973, 1688, 1572, 1531, 1256, 1131, 1072, 850; <sup>1</sup>H NMR and <sup>13</sup>C NMR (CDCl<sub>3</sub>): see Table 29; HR ESI-MS (*m/z*): 437.2554 [M-H]<sup>-</sup> (calc. for C<sub>23</sub>H<sub>42</sub>O<sub>4</sub>Si<sub>2</sub>, 437.2549).

#### Properties of **WS-S-05**

Pale yellow oil;  $[\alpha]_D^{22} +0.3^\circ$  (*c* 0.58, CHCl<sub>3</sub>); UV (CHCl<sub>3</sub>)  $\lambda_{\max}$  (log  $\epsilon$ ): 240 (4.19), 285 (4.23) nm; IR  $\nu_{\max}$  (thin film) cm<sup>-1</sup>: 1689, 1625, 1567, 1212, 1149,

1118, 1072;  $^1\text{H}$  NMR and  $^{13}\text{C}$  NMR ( $\text{CDCl}_3$ ): see Table 30; HR ESI-MS ( $m/z$ ): 435.2756  $[\text{M}+\text{H}]^+$  (calc. for  $\text{C}_{25}\text{H}_{38}\text{O}_6$ , 435.2747).

#### Properties of **WS-S-06**

Pale yellow oil;  $[\alpha]_D^{22} +5.2^\circ$  ( $c$  0.33, MeOH); UV (MeOH)  $\lambda_{\text{max}}$  ( $\log \epsilon$ ): 239 (4.36), 290 (3.97) nm; IR  $\nu_{\text{max}}$  (thin film)  $\text{cm}^{-1}$ : 3423, 2968, 2914, 1630, 1595, 1560, 1420, 1350, 1200;  $^1\text{H}$  NMR and  $^{13}\text{C}$  NMR ( $\text{CDCl}_3$ ): see Table 31; HR ESI-MS ( $m/z$ ): 277.1453  $[\text{M}-\text{H}]^-$  (calc. for  $\text{C}_{16}\text{H}_{22}\text{O}_4$ , 277.1445).

#### Properties of **WS-S-07**

Yellow oil;  $[\alpha]_D^{22} +6.0^\circ$  ( $c$  0.30,  $\text{CHCl}_3$ ); UV ( $\text{CHCl}_3$ )  $\lambda_{\text{max}}$  ( $\log \epsilon$ ): 239 (4.06), 240 (4.23) nm; IR  $\nu_{\text{max}}$  (thin film)  $\text{cm}^{-1}$ : 3357, 2965, 2931, 1623, 1589, 1458, 1212, 1165, 1087, 825;  $^1\text{H}$  NMR and  $^{13}\text{C}$  NMR ( $\text{CDCl}_3$ ): see Table 33; HR ESI-MS ( $m/z$ ): 345.2067  $[\text{M}-\text{H}]^-$  (calc. for  $\text{C}_{21}\text{H}_{30}\text{O}_4$ , 345.2071).

#### Properties of **WS-S-08**

Yellow oil;  $[\alpha]_D^{22} 0^\circ$  ( $c$  0.29,  $\text{CHCl}_3$ ); UV ( $\text{CHCl}_3$ )  $\lambda_{\text{max}}$  ( $\log \epsilon$ ): 240 (4.10), 290 (4.09) nm; IR  $\nu_{\text{max}}$  (thin film)  $\text{cm}^{-1}$ : 3352, 2969, 2933, 1625, 1592, 1463, 1222, 1167, 1092, 831;  $^1\text{H}$  NMR and  $^{13}\text{C}$  NMR ( $\text{CDCl}_3$ ): see Table 34; HR ESI-MS ( $m/z$ ): 345.2069  $[\text{M}-\text{H}]^-$  (calc. for  $\text{C}_{21}\text{H}_{30}\text{O}_4$ , 345.2071).

#### Properties of **WS-S-09**

Yellow oil;  $[\alpha]_D^{22} +6.7^\circ$  ( $c$  0.51,  $\text{CHCl}_3$ ); UV ( $\text{CHCl}_3$ )  $\lambda_{\text{max}}$  ( $\log \epsilon$ ): 239 (4.09), 285 (4.22) nm; IR  $\nu_{\text{max}}$  (thin film)  $\text{cm}^{-1}$ : 3140, 2960, 2921, 1640, 1588, 1529, 1442, 1292, 1166, 1074, 821;  $^1\text{H}$  NMR and  $^{13}\text{C}$  NMR ( $\text{CDCl}_3$ ): see Table 35; HR ESI-MS ( $m/z$ ): 413.2697  $[\text{M}-\text{H}]^-$  (calc. for  $\text{C}_{26}\text{H}_{38}\text{O}_4$ , 413.2698).

#### Properties of **WS-S-10**

White solid;  $[\alpha]_D^{22} +3.5^\circ$  ( $c$  0.34,  $\text{CHCl}_3$ ); UV ( $\text{CHCl}_3$ )  $\lambda_{\text{max}}$  ( $\log \epsilon$ ): 242 (4.39), 288 (4.09) nm; IR  $\nu_{\text{max}}$  (thin film)  $\text{cm}^{-1}$ : 3340, 2936, 2899, 1643, 1631, 1593,

1258, 1110;  $^1\text{H}$  NMR and  $^{13}\text{C}$  NMR ( $\text{CDCl}_3$ ): see Table 36; HR ESI-MS ( $m/z$ ): 279.1598  $[\text{M-H}]^-$  (calc. for  $\text{C}_{16}\text{H}_{24}\text{O}_4$ , 279.1602).

#### Properties of **WS-S-11**

White solid;  $[\alpha]_D^{22} +4.4^\circ$  ( $c$  0.40,  $\text{CHCl}_3$ ); UV ( $\text{CHCl}_3$ )  $\lambda_{\text{max}}$  ( $\log \epsilon$ ): 239 (3.99), 290 (4.21) nm; IR  $\nu_{\text{max}}$  (thin film)  $\text{cm}^{-1}$ : 3233, 2964, 2921, 1661, 1583, 1432, 1241, 1103, 1057;  $^1\text{H}$  NMR and  $^{13}\text{C}$  NMR ( $\text{DMSO}-d_6$ ): see Table 37; HR ESI-MS ( $m/z$ ): 351.2529  $[\text{M+H}]^+$  (calc. for  $\text{C}_{21}\text{H}_{34}\text{O}_4$ , 351.2531).

#### Properties of **WS-S-12**

Pale yellow oil;  $[\alpha]_D^{22} +2.6^\circ$  ( $c$  0.39,  $\text{CHCl}_3$ ); UV ( $\text{CHCl}_3$ )  $\lambda_{\text{max}}$  ( $\log \epsilon$ ): 239 (4.32), 289 (3.79) nm; IR  $\nu_{\text{max}}$  (thin film)  $\text{cm}^{-1}$ : 3300, 2938, 1625, 1225, 1147;  $^1\text{H}$  NMR and  $^{13}\text{C}$  NMR ( $\text{CDCl}_3$ ): see Table 40; HR ESI-MS ( $m/z$ ): 235.0969  $[\text{M-H}]^-$  (calc. for  $\text{C}_{13}\text{H}_{16}\text{O}_4$ , 235.0975).

#### Properties of **WS-S-13**

White solid;  $[\alpha]_D^{22} +2.6^\circ$  ( $c$  0.41,  $\text{CHCl}_3$ ); UV ( $\text{CHCl}_3$ )  $\lambda_{\text{max}}$  ( $\log \epsilon$ ): 240 (4.03), 289 (4.09) nm; IR  $\nu_{\text{max}}$  (thin film)  $\text{cm}^{-1}$ : 3261, 2970, 1622, 1229, 1150;  $^1\text{H}$  NMR and  $^{13}\text{C}$  NMR ( $\text{CDCl}_3$ ): see Table 40; HR ESI-MS ( $m/z$ ): 235.0973  $[\text{M-H}]^-$  (calc. for  $\text{C}_{13}\text{H}_{16}\text{O}_4$ , 235.0975).

#### Properties of **WS-S-14**

Pale yellow oil;  $[\alpha]_D^{22} +2.8^\circ$  ( $c$  0.41,  $\text{CHCl}_3$ ); UV ( $\text{CHCl}_3$ )  $\lambda_{\text{max}}$  ( $\log \epsilon$ ): 240 (4.17), 290 (3.97) nm; IR  $\nu_{\text{max}}$  (thin film)  $\text{cm}^{-1}$ : 3198, 1655, 1623, 1561, 1289;  $^1\text{H}$  NMR and  $^{13}\text{C}$  NMR ( $\text{CDCl}_3$ ): see Table 39; HR ESI-MS ( $m/z$ ): 303.1611  $[\text{M-H}]^-$  (calc. for  $\text{C}_{18}\text{H}_{24}\text{O}_4$ , 303.1602).

#### Properties of **WS-S-15**

White solid;  $[\alpha]_D^{22} +2.7^\circ$  ( $c$  0.41,  $\text{CHCl}_3$ ); UV ( $\text{CHCl}_3$ )  $\lambda_{\text{max}}$  ( $\log \epsilon$ ): 238 (3.57), 290 (4.26) nm; IR  $\nu_{\text{max}}$  (thin film)  $\text{cm}^{-1}$ : 3176, 1656, 1630, 1549, 1293;  $^1\text{H}$  NMR

and  $^{13}\text{C}$  NMR ( $\text{CDCl}_3$ ): see Table 39; HR ESI-MS ( $m/z$ ): 303.1608  $[\text{M-H}]^-$  (calc. for  $\text{C}_{18}\text{H}_{24}\text{O}_4$ , 303.1602).

#### Properties of **WS-S-16**

White solid;  $[\alpha]_D^{22} +2.9^\circ$  ( $c$  0.57,  $\text{CHCl}_3$ ); UV ( $\text{CHCl}_3$ )  $\lambda_{\text{max}}$  ( $\log \epsilon$ ): 239 (4.28), 289 (4.28) nm; IR  $\nu_{\text{max}}$  (thin film)  $\text{cm}^{-1}$ : 3233, 2968, 2926, 1627, 1587, 1478, 1285, 1164, 1069, 824;  $^1\text{H}$  NMR and  $^{13}\text{C}$  NMR ( $\text{CDCl}_3$ ): see Table 41; HR ESI-MS ( $m/z$ ): 371.2235  $[\text{M-H}]^-$  (calc. for  $\text{C}_{23}\text{H}_{32}\text{O}_4$ , 371.2228).

#### Properties of **WS-S-17**

White solid;  $[\alpha]_D^{22} +2.9^\circ$  ( $c$  0.58,  $\text{CHCl}_3$ ); UV ( $\text{CHCl}_3$ )  $\lambda_{\text{max}}$  ( $\log \epsilon$ ): 239 (4.26), 290 (4.23) nm; IR  $\nu_{\text{max}}$  (thin film)  $\text{cm}^{-1}$ : 3150, 2964, 2926, 1623, 1558, 1501, 1287, 1258, 1165, 1104, 1072, 798;  $^1\text{H}$  NMR and  $^{13}\text{C}$  NMR ( $\text{CDCl}_3$ ): see Table 41; HR ESI-MS ( $m/z$ ): 371.2227  $[\text{M-H}]^-$  (calc. for  $\text{C}_{23}\text{H}_{32}\text{O}_4$ , 371.2228).

#### Properties of **WS-S-18**

White solid; UV (MeOH)  $\lambda_{\text{max}}$  ( $\log \epsilon$ ): 240 (3.82), 293 (4.11) nm; IR  $\nu_{\text{max}}$  (thin film)  $\text{cm}^{-1}$ : 3230, 2961, 2910, 1634, 1546, 1258, 1096;  $^1\text{H}$  NMR and  $^{13}\text{C}$  NMR (MeOD): see Table 42; HR ESI-MS ( $m/z$ ): 237.1133  $[\text{M-H}]^-$  (calc. for  $\text{C}_{13}\text{H}_{18}\text{O}_4$ , 237.1132).

#### Properties of **WS-S-19**

White solid; UV (MeOH)  $\lambda_{\text{max}}$  ( $\log \epsilon$ ): 237 (4.09), 291 (4.05) nm; IR  $\nu_{\text{max}}$  (thin film)  $\text{cm}^{-1}$ : 3226, 2960, 1629, 1553, 1521, 1249, 1034;  $^1\text{H}$  NMR and  $^{13}\text{C}$  NMR (MeOD): see Table 42; HR ESI-MS ( $m/z$ ): 237.1129  $[\text{M-H}]^-$  (calc. for  $\text{C}_{21}\text{H}_{30}\text{O}_5$ , 237.1132).

#### Properties of **WS-S-20**

White solid; UV ( $\text{CHCl}_3$ )  $\lambda_{\text{max}}$  ( $\log \epsilon$ ): 242 (3.98), 292 (4.15) nm; IR  $\nu_{\text{max}}$  (thin film)  $\text{cm}^{-1}$ : 3189, 2947, 2910, 1634, 1598, 1537, 1298, 1276, 1097, 1043;  $^1\text{H}$

NMR and  $^{13}\text{C}$  NMR ( $\text{CDCl}_3$ ): see Table 43; HR ESI-MS ( $m/z$ ): 307.1926  $[\text{M-H}]^-$  (calc. for  $\text{C}_{18}\text{H}_{28}\text{O}_4$ , 307.1915).

#### Properties of **WS-S-21**

White solid; UV ( $\text{CHCl}_3$ )  $\lambda_{\text{max}}$  ( $\log \epsilon$ ): 242 (4.00), 292 (4.08) nm; IR  $\nu_{\text{max}}$  (thin film)  $\text{cm}^{-1}$ : 3159, 2929, 2896, 1669, 1538, 1431, 1246, 1219, 1065, 1039;  $^1\text{H}$  NMR and  $^{13}\text{C}$  NMR ( $\text{CDCl}_3$ ): see Table 43; HR ESI-MS ( $m/z$ ): 307.1923  $[\text{M-H}]^-$  (calc. for  $\text{C}_{18}\text{H}_{28}\text{O}_4$ , 307.1915).

#### Properties of **WS-S-22**

White solid; UV ( $\text{CHCl}_3$ )  $\lambda_{\text{max}}$  ( $\log \epsilon$ ): 240 (4.01), 290 (4.19) nm; IR  $\nu_{\text{max}}$  (thin film)  $\text{cm}^{-1}$ : 3260, 2958, 2931, 1651, 1585, 1558, 1530, 1296, 1257, 1168, 1070, 800;  $^1\text{H}$  NMR and  $^{13}\text{C}$  NMR ( $\text{CDCl}_3$ ): see Table 44; HR ESI-MS ( $m/z$ ): 239.1286  $[\text{M+H}]^+$  (calc. for  $\text{C}_{13}\text{H}_{18}\text{O}_4$ , 239.1278).

#### Properties of **WS-S-23**

White solid; UV ( $\text{CHCl}_3$ )  $\lambda_{\text{max}}$  ( $\log \epsilon$ ): 240 (3.36), 288 (4.08) nm; IR  $\nu_{\text{max}}$  (thin film)  $\text{cm}^{-1}$ : 3174, 2939, 1627, 1558, 1463, 1284, 1262, 1164, 1107, 821, 790;  $^1\text{H}$  NMR and  $^{13}\text{C}$  NMR ( $\text{CDCl}_3$ ): see Table 44; HR ESI-MS ( $m/z$ ): 239.1277  $[\text{M+H}]^+$  (calc. for  $\text{C}_{13}\text{H}_{18}\text{O}_4$ , 239.1278).

#### Properties of **WS-S-24**

White solid; UV ( $\text{CHCl}_3$ )  $\lambda_{\text{max}}$  ( $\log \epsilon$ ): 239 (4.51), 288 (4.21) nm; IR  $\nu_{\text{max}}$  (thin film)  $\text{cm}^{-1}$ : 3219, 2853, 1653, 1585, 1559, 1298, 1258, 1169, 1071, 819, 790;  $^1\text{H}$  NMR and  $^{13}\text{C}$  NMR ( $\text{CDCl}_3$ ): see Table 45; HR ESI-MS ( $m/z$ ): 309.2056  $[\text{M+H}]^+$  (calc. for  $\text{C}_{18}\text{H}_{28}\text{O}_4$ , 309.2061).

#### Properties of **WS-S-25**

White solid; UV ( $\text{CHCl}_3$ )  $\lambda_{\text{max}}$  ( $\log \epsilon$ ): 239 (4.22), 290 (4.00) nm; IR  $\nu_{\text{max}}$  (thin film)  $\text{cm}^{-1}$ : 3157, 2917, 2852, 1628, 1558, 1465, 1285, 1258, 1165, 1108, 822, 791;  $^1\text{H}$  NMR and  $^{13}\text{C}$  NMR ( $\text{CDCl}_3$ ): see Table 45; HR ESI-MS ( $m/z$ ): 309.2065  $[\text{M+H}]^+$  (calc. for  $\text{C}_{18}\text{H}_{28}\text{O}_4$ , 309.2061).

### 3.5 Antibacterial activity of natural products

It can be seen from the introduction that many classes of metabolites produced by the *Hypericum* genus have varying degrees of antibacterial activity. The antibacterial activity of the *Hypericum* extracts and the natural products isolated is summarized in Tables 46 and 47.

Table 46. Antibacterial activity of *Hypericum* extracts against SA-1199B. Control in MIC assay: norfloxacin, MIC = 32 µg/ml. Control in disk diffusion assay: vancomycin, 5 µg/disc, zone of inhibition = 20 mm.

Species	MIC (µg/ml) / Zone of inhibition (mm)		
	Hexane	DCM	Methanol
<i>H. forrestii</i>	512 / 13	256 / 13	>512 / 0
<i>H. moserianum</i>	256 / 14	256 / 12	>512 / 0
<i>H. beanii</i>	16 / 17	64 / 15	512 / 9
<i>H. revolutum</i>	256 / 13	256 / 12	>512 / 6
<i>spp. revolutum</i>			
<i>H. olympicum L.</i>	32 / 22	16 / 22	512 / 8
<i>cf. uniflorum</i>			
<i>H. choisianum</i>	32 / 14	128 / 12	>512 / 6

#### 3.5.1 Antibacterial activity of extracts

The antibacterial activity of extracts was determined by both MIC and disk diffusion assay. All hexane and DCM extracts showed activity against SA-1199B in the MIC assay, with *H. beanii* and *H. olympicum L. cf. uniflorum* being the most active (MIC = 16 - 64 µg/ml). The hexane extract of *H. choisianum* also showed good activity at 32 µg/ml, and is comparable to that of norfloxacin (MIC = 32 µg/ml). In the disk diffusion assay, the hexane and DCM extracts of *H. olympicum L. cf. uniflorum* showed large zones of inhibition of 22 mm and were more active than the control (vancomycin, 20 mm). The hexane and DCM extracts of *H. forrestii*, *H. moserianum* and *H. revolutum ssp. revolutum* showed

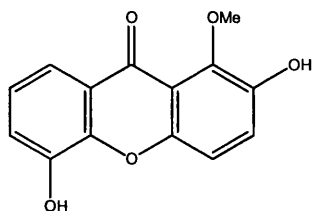
weak antibacterial activity with MIC values ranging from 256 to 512 µg/ml. Only the methanol extracts of *H. beanii* and *H. olympicum L. cf. uniflorum* were active (MIC = 512 µg/ml). In the disk diffusion assay, the methanol extracts of *H. forrestii* and *H. moserianum* did not show any zones of inhibition. The methanol extracts of the other four plants showed inhibition zones ranging from 6 to 9 mm.

Table 47. MICs (µg/ml) of compounds isolated in this study. Abbreviations: N: norfloxacin; T: tetracycline; E: erythromycin; O: oxacillin.

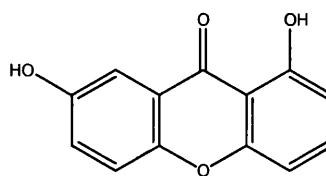
Plant	Compound	MIC (µg/ml)					
		SA-1199B	XU212	RN4220	ATCC 25923	EMRSA-15	EMRSA-16
-	Control	32 (N)	128 (T)	256 (E)	1 (N)	32 (O)	512 (O)
<i>H. forrestii</i>	WS-01	128	256	128	256	256	256
<i>H. moserianum</i>	WS-02	256	256	128	256	128	256
<i>H. beanii</i>	WS-02	256	256	128	256	128	256
	WS-03	>512	NT	NT	NT	NT	NT
	WS-04	32	32	16	32	NT	NT
	WS-05	>512	NT	NT	NT	NT	NT
	WS-06	>512	NT	NT	NT	NT	NT
<i>H. revolutum</i> <i>ssp. revolutum</i>	WS-07	>512	NT	NT	NT	NT	NT
	WS-08	256	256	256	256	256	256
<i>H. olympicum</i>	WS-07	>512	NT	NT	NT	NT	NT
<i>L. cf. uniflorum</i>	WS-09	1	1	1	1	0.5	1
	WS-10	128	128	64	128	128	128
	WS-11	64	64	64	64	64	32
	WS-12	64	64	64	64	64	64
	WS-13	64	64	128	64	64	64
<i>H. choisianum</i>	WS-14	>512	NT	NT	NT	NT	NT
	WS-15	>512	NT	NT	NT	NT	NT

### 3.5.2 Antibacterial activity of the compound isolated from *H. forrestii*

**WS-01**, a xanthone, was isolated from the DCM extract of *H. forrestii*. It was weakly active against the six *S. aureus* strains with MIC values ranging from 128 to 256  $\mu\text{g/ml}$ . It was more active than the control antibiotics against RN4220 (MIC = 256  $\mu\text{g/ml}$ ) and EMRSA-16 (MIC = 512  $\mu\text{g/ml}$ ), but less active than the control antibiotics against SA-1199B (MIC = 32  $\mu\text{g/ml}$ ), XU212 (MIC = 128  $\mu\text{g/ml}$ ), ATCC 25923 (MIC = 1  $\mu\text{g/ml}$ ) and EMRSA-15 (MIC = 256  $\mu\text{g/ml}$ ). Xanthones have been shown to have antibacterial activities (Pinto and Nascimento, 2005). Unlike the control antibiotics, the antibacterial activity of **WS-01** was relatively constant against all the tested strains. This might imply that the mechanism of action of **WS-01** was not affected by the multi-drug resistant mechanisms in these strains.



**WS-01**



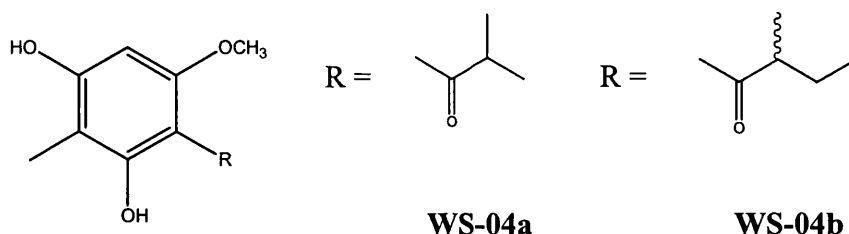
**WS-02**

### 3.5.3 Antibacterial activity of the compound isolated from *H. moserianum*

The xanthone, **WS-02**, was isolated from DCM extract of *H. moserianum*. Like **WS-01**, this compound displayed weak antibacterial activity against the tested *S. aureus* strains with MIC values ranging from 128 to 256  $\mu\text{g/ml}$ . It was only more active than the control against RN4220 and EMRSA-16.

### 3.5.4 Antibacterial activity of the compounds isolated from *H. beanii*

Fractionation of the extracts of *H. beanii* yielded **WS-02**, **WS-03** (stigmasterol), **WS-04** (a mixture of acylphloroglucinols), **WS-05** ((-)-shikimic acid) and **WS-06** ((+)-catechin). Of these compounds, only **WS-02** and **WS-04** showed antibacterial activity. The activity of **WS-02** has already been described in the previous section. **WS-04** was characterized to be a mixture of two acylphloroglucinols, **WS-04a** and **WS-04b**, in a ratio of 5:2. The MIC values of the mixture ranged from 16 to 32 µg/ml against the tested strains. Due to the small amount of material isolated, **WS-04** was only tested against SA-1199B, RN4220, XU212 and ATCC 25923. Since the two compounds could not be separated, the MIC values of the individual compound could not be determined.

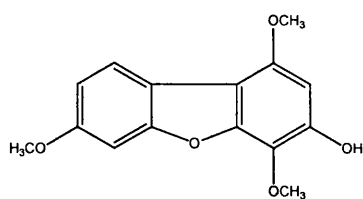


As already mentioned in the introduction, many acylphloroglucinols are known to have antibacterial activity. However, the antibacterial mechanism of action of acylphloroglucinols is still unknown to date. The latest study showed that various acylphloroglucinol derivatives isolated from *Dryopteris crassirhizoma* displayed inhibitory effect on fatty acid synthase (FAS) (Na *et al.*, 2006). By inhibiting FAS, lipid synthesis is therefore disrupted and ultimately lead to cell death. It is a possible mechanism of action of the antibacterial effect in these

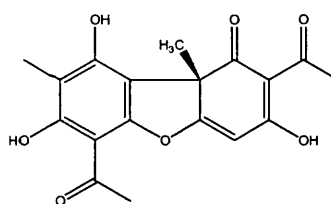
acylphloroglucinols. However, the specific target in FAS has yet to be determined. Because FAS in bacteria (Type II) is structurally different from mammalian FAS (Type I), it is a very attractive target for development of new antibiotics due to specificity.

### **3.5.5 Antibacterial activity of the compounds isolated from *H. revolutum ssp. revolutum ssp. revolutum***

Fractionation of the DCM extracts of *H. revolutum ssp. revolutum* yielded **WS-07** and **WS-08**. **WS-07** was identified as  $\beta$ -sitosterol, which was not active against SA-1199B at 512  $\mu\text{g/ml}$ . **WS-08**, a dibenzofuran, was active against all the tested strains at an MIC value of 256  $\mu\text{g/ml}$ . A series of structurally similar dibenzofurans have been isolated from the sapwood of *Mespilus germanica* when challenged by *Nectria cinnabarina*, a coral spot fungus (Kokubun *et al.*, 1995). The authors found that these dibenzofurans acted as the major phytoalexins and showed antifungal activity, with  $\text{ED}_{50}$ s in the range of 12 to 100 ppm. However, these compounds were not tested for antibacterial activity. Usnic acid is a dibenzofuran lichen substance which has been widely studied. The antibacterial activity of (+) and (-)-usnic acid against a panel of Gram-positive bacteria, anaerobic bacteria and *Mycobacterium* has been documented in a review with MICs ranging from 2 to 120  $\mu\text{g/ml}$  (Ingolfsson, 2002). As part of my research project, (+)-usnic acid was tested at Centre for Pharmacognosy and Phytotherapy, School of Pharmacy. Its MIC values ranged from 8 to 16  $\mu\text{g/ml}$  against the six *S. aureus* strains used in this study (Kokubun *et al.*, 2007).



**WS-08**



**(+)-Usnic acid**

### 3.5.6 Antibacterial activity of the compounds isolated from *H. olympicum L. cf. uniflorum*

Six compounds were isolated from *H. olympicum L. cf. uniflorum*, including  $\beta$ -sitosterol (**WS-07**) and five acylphloroglucinols (**WS-09** to **WS-13**). All the acylphloroglucinol derivatives showed antibacterial activity. **WS-09** showed exceptional activity against the tested strains with MIC values ranging from 0.5 to 1  $\mu\text{g/ml}$ . It was more active than the control antibiotics against the MDR and epidemic strains, and as active as norfloxacin in the standard strain (ATCC 25923). Its activity seemed to be unaffected by the MDR mechanisms, as shown by the fairly consistent MIC values against the different strains. Its antibacterial activity was investigated further and was tested against a panel of *Mycobacterium* strains and the Gram-negative bacteria *Pseudomonas aeruginosa* and *Salmonella typhimurium*. The MIC values of **WS-09** against these bacteria are shown in Table 48. It was active against the four tested *Mycobacterium* strains at MIC values ranging from 4 to 8  $\mu\text{g/ml}$ , but was not as active as the control antibiotics (isoniazid and ethambutol). It was not active against any of the Gram-negative bacteria at 512  $\mu\text{g/ml}$ . This may result from the impermeability of the outer membrane of the Gram-negative bacteria, which prevents the influx of chemicals from the surrounding environment into the cells. Whether **WS-09** is bactericidal or bacteriostatic has not been determined in the

study due to time limitation. As future work, the nature of antibacterial activity of this compound can be determined.

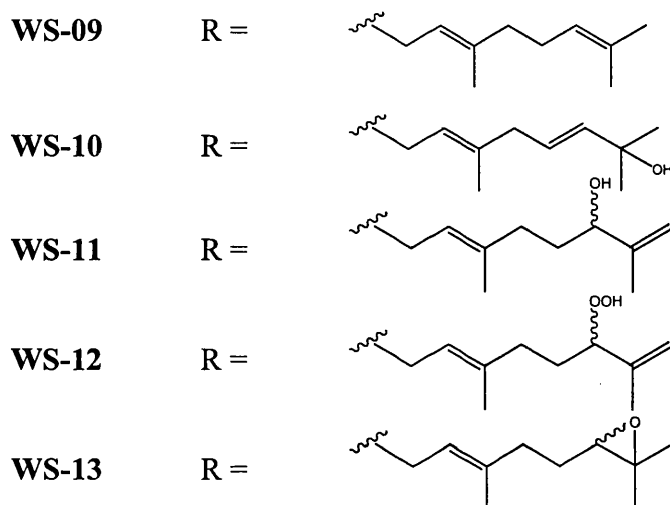
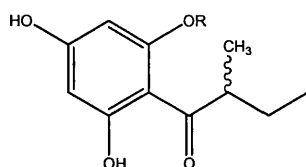


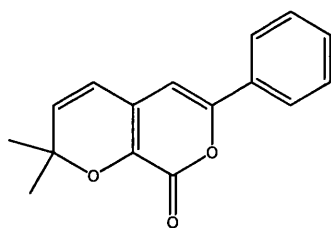
Table 48. MICs ( $\mu\text{g/ml}$ ) of **WS-09** and control antibiotics against *Mycobacterium* strains, *P. aeruginosa* and *S. typhimurium*.

<i>Strain</i>	Control	Control ( $\mu\text{g/ml}$ )	<b>WS-09</b> ( $\mu\text{g/ml}$ )
<b><i>Mycobacterium</i></b>			
<i>M. smegmatis</i> ATCC 14468	Isoniazid; ethambutol	2; 0.5	4
<i>M. fortuitum</i> ATCC 6841	Isoniazid; ethambutol	4; 0.5	8
<i>M. smegmatis</i> MC <sup>2</sup> 2700	Isoniazid; ethambutol	2; 0.5	4
<i>M. phlei</i> ATCC 11758	Isoniazid; ethambutol	2; 0.5	4
<b><i>P. aeruginosa</i></b>			
K 1119	Norfloxacin	2	> 512
K 767	Norfloxacin	2	> 512
<b><i>S. typhimurium</i></b>			
L 354	Tetracycline	1	> 512
L 10	Tetracycline	1	> 512

**WS-10** was active against RN4220 at 64  $\mu\text{g/ml}$  and the other five strains at 128  $\mu\text{g/ml}$ . **WS-11** was active against EMRSA-16 at 32  $\mu\text{g/ml}$  and the other five strains at 64  $\mu\text{g/ml}$ . **WS-12** was active against all *S. aureus* strains at 64  $\mu\text{g/ml}$ . **WS-13** was active against RN4220 at 128  $\mu\text{g/ml}$  and the other tested strains at 64  $\mu\text{g/ml}$ . It was very interesting to note these four acylphloroglucinol derivatives, which differed structurally from **WS-09** in C-5'' to C-8'' of the geranyl side-chain, displayed much weaker activity than **WS-09**. These results might suggest that the double bond between C-6'' and C-7'', a geminal methyl group at C-7'' and/or an intact geranyl side-chain was important for activity.

### 3.5.7 Antibacterial activity of the compounds isolated from *H. choisianum*

Two compounds were isolated from *H. choisianum*, **WS-14** and **WS-15**. **WS-14** was characterized as a pyranone, which did not show any antibacterial activity at a concentration of 512  $\mu\text{g/ml}$ . **WS-15** was identified as lupeol, which was not active at a concentration of 512  $\mu\text{g/ml}$ . Since the hexane and DCM extracts showed antibacterial activity against SA-1199B with MIC values of 32  $\mu\text{g/ml}$  and 128  $\mu\text{g/ml}$ , collection of more plant material and further bioassay-guided fractionation of the extracts is needed to isolate and characterize the antibacterial constituents of this plant.



**WS-14**

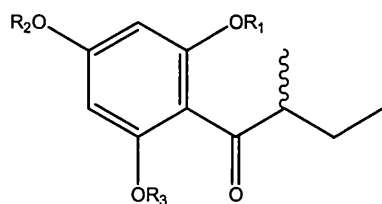
### 3.6 Structure-activity relationship of synthetic derivatives

#### 3.6.1. Acylphloroglucinol derivatives synthesized using protecting groups

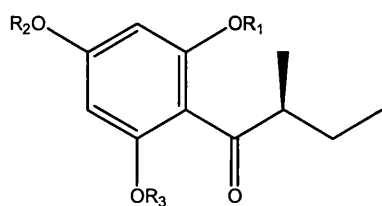
The natural product, **WS-09**, was synthesized together with a series of derivatives in order to investigate the structure-activity relationship of these acylphloroglucinols. They were evaluated for antibacterial activity against a panel of *S. aureus* strains. The antibacterial activity of 2-methylbutanoyl phloroglucinol derivatives is summarized in Table 49.

Table 49. MICs ( $\mu\text{g/ml}$ ) of 2-methylbutanoyl phloroglucinol derivatives  
Abbreviations: N: norfloxacin, T: tetracycline, E: erythromycin, O: oxacillin.

	SA-1199B	XU212	RN4220	ATCC 25923	EMRSA-15	EMRSA-16
Control	32 (N)	128 (T)	256 (E)	1 (N)	32 (O)	512 (O)
<b>WS-S-02</b>	32	32	32	32	32	32
<b>WS-S-03</b>	256	NT	NT	NT	NT	NT
<b>WS-S-04</b>	256	NT	NT	NT	NT	NT
<b>WS-S-05</b>	>256	NT	NT	NT	NT	NT
<b>WS-S-06</b>	2	2	2	1	2	2
<b>WS-S-07</b>	1	1	1	1	1	1
<b>WS-S-08</b>	1	1	1	1	1	1
<b>WS-S-09</b>	>512	>512	>512	>512	>512	>512
<b>WS-S-10</b>	2	2	2	2	2	2
<b>WS-S-11</b>	1	1	1	1	1	1



	R <sub>1</sub>	R <sub>2</sub>	R <sub>3</sub>
<b>WS-S-03</b>	H	MOM	MOM
<b>WS-S-05</b>	Geranyl	MOM	MOM
<b>WS-S-08</b>	Geranyl	H	H



	R <sub>1</sub>	R <sub>2</sub>	R <sub>3</sub>
<b>WS-S-02</b>	H	H	H
<b>WS-S-04</b>	H	TBDMS	TBDMS
<b>WS-S-06</b>	Prenyl	H	H
<b>WS-S-07</b>	Geranyl	H	H
<b>WS-S-09</b>	Farnesyl	H	H
<b>WS-S-10</b>	3-Methylbutyl	H	H
<b>WS-S-11</b>	3,7-Dimethyloctyl	H	H

Among all the synthetic derivatives with the 2-methylbutanoyl side-chain, derivatives with a geranyl (**WS-S-07** and **WS-S-08**) and a 3,7-dimethyloctyl substituent (**WS-S-11**) at the *ortho*- position were found to be the most active, with an MIC value of 1 µg/ml against all tested strains. The synthetic racemic mixture (**WS-S-08**) and the *S*-isomer (**WS-S-07**) of the natural product, **WS-09**, displayed the same level of activity as the natural product, with an MIC of 1 µg/ml. **WS-09** was found to be the *S*-isomer by the comparison of its specific rotation with that of the synthetic product (**WS-S-07**) synthesized with *S*-2-methylbutyryl chloride as the starting material. Since the specific rotation of **WS-S-08** was found to be 0°, the racemic mixture must contain *R*- and *S*-isomers in the ratio of 1:1. The antibacterial activity of the *R*-isomer has not been investigated, however.

The effect of substituting the geranyl side-chain with prenyl (**WS-S-06**), farnesyl (**WS-S-09**), 3-methylbutyl (**WS-S-10**) and 3,7-dimethyloctyl (**WS-S-11**) was investigated. It was found that by increasing the chain length from geranyl to farnesyl, a dramatic loss of activity was observed (not active at 512 µg/ml against all tested strains). On the other hand, by decreasing the chain length from geranyl (C<sub>10</sub>) to prenyl (C<sub>5</sub>), a two-fold reduction in activity was seen (MIC of 1 to 2 µg/ml). The data might imply that an optimum chain length existed in the test compounds and that the farnesyl group exceeded the maximum, or that steric crowding caused by the farnesyl group prevented the effective binding of the acyl group to the target site. In addition, the 3-methylbutyl and 3,7-dimethyloctyl derivatives were as active as the prenyl and geranyl derivatives

respectively, suggesting that the double bonds in the isoprene units might not be important for activity.

**WS-S-03** and **WS-S-04** were acylphloroglucinols with an *ortho*- and a *para*-hydroxyl group protected with MOM and TBDMS respectively. Both compounds were weakly active against SA-1199B at 256 µg/ml. **WS-S-05**, which was synthesized by alkylation of **WS-S-03** with geranyl bromide, did not show any antibacterial activity at 256 µg/ml. This might imply that at least one free hydroxyl group was necessary for the acylphloroglucinol derivative to be active.

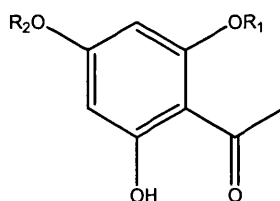
### **3.6.2. Acylphloroglucinol derivatives synthesized without using a protecting group**

Fourteen acetyl-phloroglucinol derivatives were synthesized from seven reactions without the use of a protecting group. Their MIC values against a panel of *S. aureus* strains are shown in Table 50. Among the acetyl-phloroglucinol derivatives, **WS-S-24**, which has a decyl substituent at the *para*-position, was the most active, with an MIC value of 1 to 2 µg/ml. The commercially available phloroglucinol and acetylphloroglucinol were also tested. Acetylphloroglucinol was active against SA-1199B at 512 µg/ml, whereas phloroglucinol was not active at 512 µg/ml. Acetylphloroglucinol was much less active than 2-methylbutanoyl phloroglucinol (**WS-S-03**), which was active at 32 µg/ml against SA-1199B, suggesting that the 2-methylbutanoyl group contributed significantly to the antibacterial activity of the compound.

Table 50. MICs ( $\mu\text{g/ml}$ ) of acetylphloroglucinol derivatives.

Abbreviations: PG: phloroglucinol, N: norfloxacin, T: tetracycline, E: erythromycin, O: oxacillin

	SA-1199B	XU212	RN4220	ATCC 25923	EMRSA-15	EMRSA-16
Control	32 (N)	128 (T)	256 (E)	1 (N)	32 (O)	512 (O)
PG	>512	NT	NT	NT	NT	NT
Acetyl-PG	512	NT	NT	NT	NT	NT
WS-S-12	4	4	8	8	8	8
WS-S-13	2	2	2	4	4	4
WS-S-14	256	256	128	256	256	128
WS-S-15	4	4	4	4	8	4
WS-S-16	>512	>512	>512	>512	>512	>512
WS-S-17	4	4	4	4	4	4
WS-S-18	8	8	8	8	4	8
WS-S-19	8	8	4	8	8	8
WS-S-20	2	2	4	2	2	4
WS-S-21	8	4	8	8	8	8
WS-S-22	16	16	8	16	8	16
WS-S-23	16	8	16	8	16	16
WS-S-24	4	4	4	8	8	4
WS-S-25	1	1	1	2	1	2



	R <sub>1</sub>	R <sub>2</sub>		R <sub>1</sub>	R <sub>2</sub>
Acetyl-PG	H	H	WS-S-18	3-methylbutyl	H
WS-S-12	Prenyl	H	WS-S-19	H	3-methylbutyl
WS-S-13	H	Prenyl	WS-S-20	3,7-dimethyloctyl	H
WS-S-14	Geranyl	H	WS-S-21	H	3,7-dimethyloctyl
WS-S-15	H	Geranyl	WS-S-22	Pentyl	H
WS-S-16	Farnesyl	H	WS-S-23	H	Pentyl
WS-S-17	H	Farnesyl	WS-S-24	Decyl	H
			WS-S-25	H	Decyl

### 3.6.2.1 Acetylphloroglucinol derivatives with an *ortho*- substituent

Among the prenyl (WS-S-12, MIC = 4 to 8  $\mu\text{g/ml}$ ), geranyl (WS-S-14, MIC = 128 to 256  $\mu\text{g/ml}$ ) and farnesyl (WS-S-16, not active at 512  $\mu\text{g/ml}$ ) derivatives, the prenyl derivative was the most active. Like the farnesyl derivative with a 2-

methylbutanoyl side-chain, **WS-S-16** was not active at the tested concentration (i.e. 512 µg/ml). However, by changing the acyl chain from 2-methylbutanoyl to acetyl, the geranyl derivative showed a significant loss of activity. This might indicate that the 2-methylbutanoyl side-chain is important for antibacterial activity.

The effect of the presence of double bond(s) in the side-chain was also studied. **WS-S-18** (3-methylbutyl; MIC = 4 to 8 µg/ml) was as active as **WS-S-12** (prenyl). This observation was also seen in 2-methylbutanoyl derivatives and it was thought that the double bond was not important in contributing to the antibacterial activity. However, the 3,7-dimethyloctyl derivative (**WS-S-20**; MIC = 2 to 4 µg/ml) showed an enhanced activity compared with **WS-S-14** (geranyl; 128 to 256 µg/ml). This finding was not consistent with that in the 2-methylbutanoyl derivatives and the reason for this was unknown.

The antibacterial activity of derivatives with straight alkyl chains was studied. Investigation of the activity of **WS-S-22** (pentyl; MIC = 8 to 16 µg/ml) and **WS-S-24** (decyl; MIC = 4 to 8 µg/ml) showed that derivatives with straight alkyl chains were also active. Studies have shown that the antibacterial activity of various triketone derivatives increased with the length of straight alkyl chain and reached a maximum at C<sub>12</sub> (van Klink *et al.*, 2005). This was due to the hydrophobic interaction between the alkyl chain and the cytoplasmic membrane of the bacterial cells, thereby interfering with cell respiration and ATP synthesis (Kopecky, 1996). This phenomenon was also observed in this study, with **WS-S-24** being two times more active than **WS-S-22**. However, derivatives with a

wider range of straight alkyl chains need to be synthesized and tested in order to fully investigate the effect of chain length on antibacterial activity.

### 3.6.2.2 Acetylphloroglucinol derivatives with a *para*- substituent

The antibacterial activity of derivatives with *ortho*- and the corresponding *para*-substituents was compared. Generally, derivatives alkylated at the *para*-hydroxyl group were found to be more active than the corresponding derivatives at the *ortho*- position. This effect was the most significant in the geranyl and farnesyl derivatives. With the geranyl side-chain at the *para*- position (**WS-S-15**), the MIC was reduced from 128 to 256  $\mu\text{g/ml}$  (*ortho*; **WS-S-14**) to 4 to 8  $\mu\text{g/ml}$ . By substituting the farnesyl side-chain at the *para*- position, the derivative (**WS-S-17**) was active with an MIC of 4  $\mu\text{g/ml}$  while the derivative with an *ortho*- substitution was not active at 512  $\mu\text{g/ml}$ . However, this effect was less significant in prenyl (**WS-S-13**) and decyl (**WS-S-25**) derivatives, where only a 2 to 4 fold reduction was observed. In addition, the *ortho*- and *para*- derivatives substituted with 3-methylbutyl (**WS-S-18**, **WS-S-19**) and pentyl (**WS-S-22**, **WS-S-23**) side-chains showed similar antibacterial activity at 4 to 8  $\mu\text{g/ml}$  and 8 to 16  $\mu\text{g/ml}$  respectively. For derivatives with a 3,7-dimethyloctyl side-chain, the *ortho*- derivative (**WS-S-20**, MIC = 2 to 4  $\text{mg/ml}$ ) was more active than the *para*- derivative (**WS-S-21**; MIC = 4 to 8  $\mu\text{g/ml}$ ).

To sum up, the main observations made in the structure-activity relationship study include:

1. (*S*)-2-*O*-geranyl-2'-methylbutanoyl phloroglucinol (**WS-S-07**), ( $\pm$ )-2-*O*-geranyl-2'-methylbutanoyl phloroglucinol (**WS-S-08**) and (*S*)-2-*O*-(3'',7''-dimethyloctyl)-2'-methylbutanoyl phloroglucinol (**WS-S-11**) were the most active, with an MIC value of 1  $\mu$ g/ml against all tested strains.
2. All 2-methylbutanoyl phloroglucinol derivatives were more active than the corresponding derivatives with an acetyl side-chain.
3. In phloroglucinol derivatives substituted at the *ortho*- position, the geranyl derivative was the most active, followed by the prenyl derivative. The farnesyl derivative was, however, not active at an MIC of 512  $\mu$ g/ml.
4. Most derivatives with substituents at the *para*- position in acetylphloroglucinol derivatives were more active than the corresponding *ortho*- substituted derivatives.
5. Acylphloroglucinol derivatives substituted with straight alkyl chains (**WS-S-22** to **WS-S-25**) were shown to possess antibacterial activity.

Obviously, the study described in this thesis is a preliminary study on the structure-activity relationship of acylphloroglucinol derivatives structurally similar to the bioactive natural product, **WS-09**. There is a need to synthesize and test a larger library of a wider range of acylphloroglucinol derivatives based on this compound to investigate which functional groups are important in

contributing towards the antibacterial activity. This will also be necessary in identifying derivatives which display a greater antibacterial potency than **WS-09**.

Plant extracts from the *Hypericum* genus have been shown to demonstrate anti-staphylococcal activity (Gibbons *et al.*, 2002) and numerous pure compounds isolated from this genus have been shown to be antibacterial with varying degrees of potency. Despite the advances in the development of new antibiotics in the past decade, antibiotic resistance in MRSA remains to be a concern as strains showing resistance to the newer antibiotics (e.g. vancomycin and linezolid) started to emerge. Therefore, there is a need to discover and develop new classes of compounds to combat this problem.

As part of an ongoing project to investigate the phytochemistry and antibacterial properties of the *Hypericum* genus, the phytochemistry of six different species was studied using a bioassay-guided fractionation approach. Fifteen compounds were isolated in this study, of which eight compounds were new. The new compounds included a dibenzofuran isolated from the DCM extract of *H. revolutum ssp. revolutum* (MIC = 256 µg/ml), a pyranone isolated from the hexane extract of *H. choisianum* (not active at a concentration of 512 µg/ml), a mixture of two closely related acylphloroglucinols isolated from the DCM extract of *H. beanii* (MIC = 16 - 32 µg/ml), and a series of five closely related acylphloroglucinols isolated from the hexane and DCM extracts of *H. olympicum L. cf. uniflorum* (MIC = 0.5 - 128 µg/ml).

**WS-09**, an acylphloroglucinol derivative isolated from *H. olympicum L. cf. uniflorum*, exhibited excellent antibacterial activity against a panel of *S. aureus*

strains, with MIC values in the range of 0.5 to 1 µg/ml. This compound, together with a 4-step synthesis method, has been patented for its potential application as an antibacterial agent. Twenty-five compounds were synthesized in this study and the structure-activity relationship of various acylphloroglucinol derivatives was investigated. The most active synthetic analogues were found to be (*S*)-2-*O*-geranyl-2'-methylbutanoyl phloroglucinol (the natural product) and (*S*)-2-*O*-(3'',7''-dimethyloctyl)-2'-methylbutanoyl phloroglucinol, which differed only in the absence of double bonds. Both compounds were active against a panel of *S. aureus* strains with an MIC of 1 µg/ml. The data also suggested that:

- (1) analogues with a 2-methylbutanoyl side-chain were more active than the corresponding derivative with an acetyl side-chain;
- (2) analogues alkylated at the hydroxyl group *para*- to the acyl side-chain were generally more active than the corresponding derivative with a side-chain at the *ortho*- position.

These results highlighted the potential of the *Hypericum* genus as a valuable source of anti-staphylococcal agents. More phytochemical and antibacterial research on this genus is required in the future to explore the potential of other *Hypericum* species. A larger library of acylphloroglucinol analogues needs to be synthesized in order to fully investigate the structure-activity relationship of these compounds and to discover compounds with more potent antibacterial activity. A toxicity profile and the mechanism of action of the active acylphloroglucinol will also need to be established.

Abreu IN, Porto ALM, Marsaioli AJ *et al.*, 2004. Distribution of bioactive substances from *Hypericum brasiliense* during plant growth. *Plant Science*, 167, 949-954.

Alcaráz LE, Blanco SE, Puig ON *et al.*, 2000. Antibacterial activity of flavonoids against methicillin-resistant *Staphylococcus aureus* strains. *Journal of Theoretical Biology*, 205, 231-240.

Allen NE and Nicas TI, 2003. Mechanism of action of oritavancin and related glycopeptide antibiotics. *FEMS Microbiology Reviews*, 26, 511-532.

Andes D and Craig WA, 2006. Pharmacodynamics of a new cephalosporin, PPI-0903 (TAK-599), active against methicillin-resistant *Staphylococcus aureus* in murine thigh and lung infection models: identification of an *in vivo* pharmacokinetic-pharmacodynamic target. *Antimicrobial Agents and Chemotherapy*, 50, 1376-1383.

Appendino G, Bianchi F, Minassi A *et al.*, 2001. Oligomeric acylphloroglucinols from Myrtle (*Myrtus communis*). *Journal of Natural Products*, 65, 334-338.

Aratanechemuge Y, Hibasami H, Sanpin K *et al.*, 2004. Induction of apoptosis by lupeol isolated from mokumen (*Gossampinus malabarica L. Merr*) in human promyelotic leukemia HL-60 cells. *Oncology Reports*, 11, 289-292.

Ashan M, Gray AI and Waterman PG, 1994. Farnesyl acetophenone and flavanone compounds from the aerial parts of *Boronia ramosa*. *Journal of Natural Products*, 57, 673-676.

Aucken HM, Ganner, M, Murchan S *et al.*, 2002. A new UK strain of epidemic methicillin-resistant *Staphylococcus aureus* (EMRSA-17) resistant to multiple antibiotics. *Journal of Antimicrobial Chemotherapy*, 50, 171-175.

Barber M and Rozwadowska-Dowzenko M, 1948. Infection by penicillin-resistant *Staphylococci*. *Lancet*, 2, 641-644.

Barg N, Chambers H and Kernodle D, 1991. Borderline susceptibility to antistaphylococcal penicillins is not conferred exclusively by the hyperproduction of beta-lactamase. *Antimicrobial Agents and Chemotherapy*, 35, 1975-1979.

Barna JCJ and Williams DH, 1984. The structure and mode of action of glycopeptide antibiotics. *Annual Review of Microbiology*, 38, 339-357.

Barnes J, Anderson LA and Phillipson JD, 2001. St John's wort (*Hypericum perforatum L.*): a review of its chemistry, pharmacology and clinical properties. *Journal of Pharmacy and Pharmacology*, 2001, 53, 583-600.

Basile A, Sorbo S, Giordana S *et al.*, 2000. Antibacterial and allelopathic activity of extract from *Castanea sativa* leaves. *Fitoterapia*, 71, S110-116.

Beerhues L, 2006. Hyperforin. *Phytochemistry*, 67, 2201-2207.

Begley MJ, Crombie L, Jones RCF *et al.*, 1987. Synthesis of the *Mammea Coumarins*. Part 4. Stereochemical and regiochemical studies, and synthesis of (-)-Mammea B/BB. *Journal of the Chemical Society, Perkin Transaction I*, 353-357.

Bennett GJ and Lee HH, 1989. Xanthones from Guttiferae. *Phytochemistry*, 28, 967-998.

Berger-Bächi B, 1994. Expression of resistance to methicillin. *Trends in Microbiology*, 2, 389-393.

Bismuth R, Zilhao R, Sakamoto H *et al.*, 1990. Gene heterogeneity for tetracycline resistance in *Staphylococcus* species. *Antimicrobial Agents and Chemotherapy*, 34, 1611-1614.

Bohr G, Gerhäuser C, Knauft J *et al.*, 2005. Anti-inflammatory acylphloroglucinol derivatives from Hops (*Humulus lupulus*). *Journal of Natural Products*, 68, 1545-1548.

Brevoort P, 1998. The booming US botanical market. A new overview. *HerbalGram*, 44, 33-48.

British National Formulary, 2007, 54<sup>th</sup> Edition. <http://www.bnf.org>

Bystrov NS, Chernov BK, Dobrynin VN *et al.*, 1975. The structure of hyperforin. *Tetrahedron Letters*, 32, 2791-2794.

Caccia S, 2005. Antidepressant-like components of *Hypericum perforatum* extracts: an overview of their pharmacokinetics and metabolism. *Current Drug Metabolism*, 6, 531-543.

Canepari P, Boaretti M, del Mar Lleo M *et al.*, 1990. Lipoteichoic acid as a new target for activity of antibiotics: mode of action of daptomycin (LY146032). *Antimicrobial Agents and Chemotherapy*, 34, 1220-1226.

Cannell RJP, 1998. *Natural products isolation*. Humana Press Inc., Totowa, NJ.

Cardona ML, Pedro JR, Seoane E *et al.*, 1985. Xanthone constituents of *Hypericum canariensis*. *Journal of Natural Products*, 48, 467-469.

Chou CJ and Lin LC, 1992. Novel acetophenones from fruits of *Evodia merrillii*. *Journal of Natural Products*, 55, 795-799.

Cox RA, Conquest C, Mallaghan C *et al.*, 1995. A major outbreak of methicillin-resistant *Staphylococcus aureus* caused by a new phage-type (EMRSA-16). *Journal of Hospital Infection*, 29, 87-106.

Cragg GM, Newman DJ and Snader KM, 1997. Natural products in drug discovery and development. *Journal of Natural Products*, 60, 52-60.

Crockett SL, Schaneberg B and Khan IA, 2005. Phytochemical profiling of new and old world *Hypericum* (St John's Wort) species. *Phytochemical Analysis*, 16, 479-485.

Crombie L, Jones RCF and Palmer CJ, 1987. Synthesis of the Mamea Coumarins. Part 1. The coumarins of the Mamea A, B and C series. *Journal of the Chemical Society, Perkin Transaction I*, 317-331.

Dall'Agnol R, Ferraz A, Bernardi AP *et al.*, 2003. Antimicrobial activity of some *Hypericum* species. *Phytomedicine*, 10, 511-516.

Dar A, Faizi S, Naqvi S *et al.*, 2005. Analgesic and antioxidant activity of mangiferin and its derivatives: the structure activity relationship. *Biological and Pharmaceutical Bulletin*, 28, 596-600.

Décosterd L, Stoeckli-Evans H, Msonthi JD *et al.*, 1986. A new antifungal chromene and a related di-chromene from *Hypericum revolutum*. *Planta Medica*, 52, 429.

Dharmaratne HRW, Nanayakkara NPD and Khan IA, 2002. Kavalactones from *Piper methysticum*, and their <sup>13</sup>C NMR spectroscopic analyses. *Phytochemistry*, 59, 429-433.

Dixon RA, Dey PM and Lamb CJ, 1983. Phytoalexins: enzymology and molecular biology. *Advances in Enzymology*, 55, 1-69.

Duke JA, 1985. *Handbook of medicinal herbs*. CRC Press.

Edzard E, 2003. The genus *Hypericum*. *Medicinal and aromatic plants – industrial profiles 30*. Taylor & Francis Inc. New York.

Feher M and Schmidt JM, 2003. Property distributions: Differences between drugs, natural products, and molecules from combinatorial chemistry. *Journal of Chemical Information and Computer Sciences*, 43, 218-227.

Ferrero L, Cameron B, Manse B *et al.*, 1994. Cloning and primary structure of *Staphylococcus aureus* DNA topoisomerase IV: a primary target of fluoroquinolones. *Molecular Microbiology*, 13, 641-653.

Fluit ADC, Visser MR and Schmitz F, 2001. Molecular detection of antimicrobial resistance. *Clinical Microbiology Review*, 14, 836-871.

Foo LY, Lu Y, McNabb WC *et al.*, 1997. Proanthocyanidins from *Lotus pedunculatus*. *Phytochemistry*, 45, 1689-1696.

Forgo P and Kövér KE, 2004. Gradient enhanced selective experiments in the <sup>1</sup>H NMR chemical shift assignment of the skeleton and side-chain resonances of stigmasterol, a phytosterol derivative. *Steroids*, 69, 43-50.

Fotsis T, Pepper MS, Aktas E *et al.*, 1997. Flavonoids, dietary-derived inhibitors of cell proliferation and invitro angiogenesis. *Cancer Research*, 57, 2916-2921.

Gaind KN and Ganjoo TN, 1959. Antibacterial principle of *Hypericum perforatum* L. *Indian Journal of Pharmacy*, 21, 172-175.

Garrido G, González D, Lemus Y *et al.*, 2004. *In vivo* and *in vitro* anti-inflammatory activity of *Mangifera indica* L. extract (VIMANG®). *Pharmacological Research*, 50, 143-149.

Gartner M, Müller T, Simon JC *et al.*, 2005. Aristoforin, a novel stable derivative of hyperforin, is a potent anticancer agent. *Chembiochem*, 6, 171-177.

Ghisalberti EL, 1996. Bioactive acylphloroglucinol derivatives from *Eucalyptus* species. *Phytochemistry*, 41, 7-22.

Gibbons S and Udo EE, 2000. The effect of reserpine, a modulator of multidrug efflux pumps, on the *in vitro* activity of tetracycline against clinical isolates of methicillin-resistant *Staphylococcus aureus* (MRSA) possessing the tet(K) determinant. *Phytotherapy Research*, 14, 139-140.

Gibbons S, Ohlendorf B and Johnsen I, 2002. The genus *Hypericum* – a valuable resource of anti-staphylococcal leads. *Fitoterapia*, 73, 300-304.

Gibbons S, 2004. Anti-staphylococcal plant natural products. *Natural Product Reports*, 21, 263-277.

Gibbons S, Moser E, Hausmann S *et al.*, 2005. An anti-staphylococcal acylphloroglucinol from *Hypericum foliosum*. *Phytochemistry*, 66, 1472-1475.

Giese AC, 1980. Hypericism. *Photochemical and Photobiological Reviews*, 5, 971-977.

Greene T, 1981. *Protective groups in organic synthesis*. John Wiley & Sons, Inc. Hoboken, New Jersey.

Greeson JM, Sanford B and Monti DA, 2001. St John's wort (*Hypericum perforatum*): a review of the current pharmacological, toxicological and clinical literature. *Psychopharmacology*, 153, 402-414.

Grieco PA and Markworth CJ, 1999. Selective deprotection of alkyl t-butyldimethylsilyl ethers in the presence of aryl t-butyldimethylsilyl ethers. *Tetrahedron Letters*, 40, 665-666.

Griesgraber G, Or SY, Chu DTW *et al.*, 1996. 3-keto-11,12-carbazate derivatives of 6-O-methylerythromycin A. Synthesis and *in vitro* activity. *Journal of Antibiotics*, 49, 465-477.

Gryglewski RJ, Korbut R, Robak J *et al.*, 1987. On the mechanism of antithrombotic action of flavonoids. *Biochemical Pharmacology*, 36, 317-322.

Guay GG, Khan SA and Rothstein DM, 1993. The tet(K) gene of plasmid pT181 of *Staphylococcus aureus* encodes an efflux protein that contains 14 transmembrane helices. *Plasmid*, 30, 163-166.

Guha S, Ghosal S and Chattopadhyay U, 1996. Antitumour, immunomodulatory and anti-HIV effect of mangiferin, a naturally occurring glucosylxanthone. *Chemotherapy*, 42, 443-451.

Hamed W, Brajeul S, Mahuteau-Betzer F *et al.*, 2006. Oblongifolins A-D, polyprenylated benzoylphloroglucinol derivatives from *Garcinia oblongifolia*. *Journal of Natural Products*, 69, 774-777.

Haslam E, 1996. Natural polyphenols (vegetable tannins) as drugs: possible mode of action. *Journal of Natural Products*, 59, 205-215.

Health Protection Agency, 2008. <http://www.hpa.org.uk/>

Hebeisen P, Heinze-Krauss I, Anehrn P *et al.*, 2005. *In vitro* and *in vivo* properties of Ro 63-9141, a novel broad-spectrum cephalosporin with activity against methicillin-resistant *Staphylococci*. *Antimicrobial Agents and Chemotherapy*, 49, 4210-4219.

Henwood CJ, Livermore DM, Johnson AP *et al.*, 2000. Susceptibility of Gram-positive cocci from 25 UK hospitals to antimicrobial agents including linezolid. *Journal of Antimicrobial Chemotherapy*, 46, 931-940.

Hiramatsu K, 1998. Vancomycin resistance in *Staphylococci*. *Drug Research Updates*, 1, 135-150.

Hiramatsu K, Hanaki H, Ino T *et al.*, 1997. Methicillin-resistant *Staphylococcus aureus* clinical strain with reduced vancomycin susceptibility. *Journal of Antimicrobial Chemotherapy*, 40, 135-136.

Hiramatsu K, Ito K and Hanaki H, 1999. Mechanisms of methicillin and vancomycin resistance in *Staphylococcus aureus*. *Ballieres Clinical Infectious Diseases*, 5, 221-242.

Hotta K, Sunada A, Ikeda Y *et al.*, 2000. Double stage activity in aminoglycoside antibiotics. *Journal of Antibiotics*, 53, 1168-1174.

Hu LH and Sim KY, 1998. Complex caged polyisoprenylated benzophenone derivatives, sampsoniones A and B, from *Hypericum sampsonii*. *Tetrahedron Letters*, 39, 7999-8002.

Hu LH and Sim KY, 1999. Sampsoniones C-H, a unique family of polyprenylated benzophenone derivatives with the novel tetracyclo-[7.3.1.1<sup>3,11</sup>.0<sup>3,7</sup>]tetradecane-2,12,14-trione skeleton, from *Hypericum sampsonii* (Guttiferae). *Tetrahedron Letters*, 40, 759-762.

Hu LH, Yip SC and Sim KY, 1999. Xanthones from *Hypericum ascyron*. *Phytochemistry*, 52, 1371-1373.

Hu LH and Sim KY, 2000. Sampsoniones A – M, a unique family of caged polyprenylated benzoylphloroglucinol derivatives from *Hypericum sampsonii*. *Tetrahedron*, 56, 1379-1386.

Hu LH, Khoo CW, Vittal JJ *et al.*, 2000. Phloroglucinol derivatives from *Hypericum japonicum*. *Phytochemistry*, 53, 705-709.

Huang C, Zhang Z, Li S *et al.*, 1999. Facile total syntheses of two novel 4-alkenyloxy-2,6-dihydroxyacetophenones. *Journal of Chemical Research*, 148-149.

Ingolfssdottir K, 2002. Usnic acid. *Phytochemistry*, 61, 729-736.

Ishiguro K, Yamaki M, Kashihara M *et al.*, 1986. Sarothralen A and B, new antibiotic compounds from *Hypericum japonicum*. *Planta Medica*, 52, 288-290.

Ishiguro K, Yamaki M, Kashihara M *et al.*, 1987. Saroaspidin A, B and C: additional antibiotic compounds from *Hypericum japonicum*. *Planta Medica*, 53, 415-417.

Ishiguro K, Nagata S, Fukumoto H *et al.*, 1994. Phloroglucinol derivatives from *Hypericum japonicum*. *Phytochemistry*, 35, 469-471.

Ishiguro K, Nakajima M, Fukumoto H *et al.*, 1995. A xanthone substituted with an irregular monoterpene in cell suspension cultures of *Hypericum patulum*. *Phytochemistry*, 39, 903-905.

Ishiguro K, Fukumoto H, Suitani A *et al.*, 1996. Prenylated xanthones from cell suspension cultures of *Hypericum patulum*. *Phytochemistry*, 42, 435-437.

Ishiguro K, Nagareya N, Suitani A *et al.*, 1997. A prenylated xanthone from cell suspension cultures of *Hypericum patulum*. *Phytochemistry*, 44, 1065-1066.

Jakupovic J, Zdero C, Grenz M *et al.*, 1989. Twenty-one acylphloroglucinol derivatives and further constituents from South African *Helichrysum* species. *Phytochemistry*, 28, 1119-1131.

Jayasuriya H and McChesney JD, 1989. Antimicrobial and cytotoxic activity of rottlerin-type compounds from *Hypericum drummondii*. *Journal of Natural Products*, 52, 325-331.

Jayasuriya H, Clark AM and McChesney JD, 1991. New antimicrobial filicinic acid derivatives from *Hypericum drummondii*. *Journal of Natural Products*, 54, 1314-1320.

Jevons MP, 1961. 'Celbenin'-resistant Staphylococci. *British Medical Journal*, 1, 124-125.

Johnson AP, Aucken HM, Cavendish S *et al.*, 2001. Dominance of EMRSA-15 and 16 among MRSA causing nosocomial bacteraemia in the UK: analysis of isolates from the European Antimicrobial Resistance Surveillance System (EARSS). *Journal of Antimicrobial Chemotherapy*, 48, 141-156.

Johnston NH, Mukhtar TA and Wright GD, 2002. Streptogramin antibiotics: mode of action and resistance. *Current Drug Targets*, 3, 335-344.

Kaatz GW, Seo SM and Ruble CA, 1993. Efflux-mediated fluoroquinolone resistance in *Staphylococcus aureus*. *Antimicrobial Agents and Chemotherapy*, 37, 1086-1094.

Kawamoto I, Shimoji Y, Kanno O *et al.*, 2003. Synthesis and structure-activity relationships of novel parenteral carbapenems, CS-023 (R-115685) and related compounds containing an amidine moiety. *Journal of Antibiotics*, 56, 565-579.

Kitanov GM and Nedialkov PT, 1998. Mangiferin and isomangiferin in some *Hypericum* species. *Biochemical Systematics and Ecology*, 26, 647-653.

Kitanov GM, 2001. Hypericin and pseudohypericin in some *Hypericum* species. *Biochemical Systematics and Ecology*, 29, 171-178.

Kobayashi Y, Uchida H and Kawakami Y, 1995. Arbekacin. *International Journal of Antimicrobial Agents*, 5, 227-230.

Kokubun T, Harborne JB, Eagles J *et al.*, 1995. Dibenzofuran phytoalexins from the sapwood tissue of *Photinia*, *Pyracantha* and *Crataegus* species. *Phytochemistry*, 39, 1033-1037.

Kokubun T, Harborne, JB, Eagles J *et al.*, 1995a. Four dibenzofuran phytoalexins from the sapwood from *Mespilus germanica*. *Phytochemistry*, 39, 1039-1042.

Kokubun T, Shiu WKP and Gibbons S, 2007. Inhibitory activities of lichen-derived compounds against methicillin and multidrug-resistant *Staphylococcus aureus*. *Planta Medica*, 73, 176-179.

Kondo S, Iinuma K, Yamamoto H, *et al.*, 1984. Synthesis of 1-N-((S)-4-amino-2-hydroxybutyryl)-kanamycin B and 3',4'-dideoxykanamycin B active against kanamycin resistant bacteria. *Journal of Antibiotics*, 26, 412-415.

Kubin A, Wierrani F, Burner U *et al.*, 2005. Hypericin – the facts about a controversial agent. *Current Pharmaceutical Design*, 11, 233-253.

Kumazawa T, Minatogawa T, Matsuba S *et al.*, 2000. An effective synthesis of isoorientin: the regioselective synthesis of a 6-C-glucosylflavone. *Carbohydrate Research*, 329, 507-513.

Laakmann G, Schüle C, Baghai T *et al.*, 1998. St. John's wort in mild to moderate depression: the relevance of hyperforin for the clinical efficacy. *Pharmacopsychiatry*, 31, S1, 54-59.

Laughton MJ, Evans PJ, Moroney MA *et al.*, 1991. Inhibition of mammalian 5-lipoxygenase and cyclo-oxygenase by flavonoids and phenolic dietary additives. Relationship to antioxidant activity and to iron ion-reducing ability. *Biochemical Pharmacology*, 42, 1673-1681.

Lavie G, Mazur Y, Lavie D *et al.*, 1995. The chemical and biological properties of hypericin – a compound with a broad spectrum of biological activities. *Medicinal Research Reviews*, 15, 111-119.

Leclercq R and Courvalin P, 1991. Bacterial resistance to macrolide, lincosamide and streptogramin antibiotics by target modification. *Antimicrobial Agents and Chemotherapy*, 35, 1267-1272.

Lee JY, Duke RY, Tran VH *et al.*, 2006. Hyperforin and its analogues inhibit CYP3A4 enzyme activity. *Phytochemistry*, 67, 2550-2560.

Li W, Chan C, Leung H *et al.*, 1998. Xanthenes and flavonoids of *Polygala caudata*. *Pharmacy and Pharmacology Communications*, 4, 415-417.

Liu A, Dillon K, Campbell RM *et al.*, 1996. Synthesis of E-selectin inhibitors: use of an aryl-cyclohexyl ether as a disaccharide scaffold. *Tetrahedron Letters*, 22, 3785-3788.

Livermore DM and Williams JD, 1996.  $\beta$ -Lactams: mode of action and mechanisms of bacterial resistance. In: *Antibiotics in laboratory medicine*. Lorian V, Baltimore, MD: Williams and Wilkins, 502-578.

Llano-Sotelo B, Azucena EF Jr, Kotra LP *et al.*, 2002. Aminoglycosides modified by resistance enzymes display diminished binding to the bacterial ribosomal aminoacyl-tRNA site. *Chemistry and Biology*, 9, 455-463.

Maisenbacher P and Kovar KA, 1992. Adhyperforin: A homologue of hyperforin from *Hypericum perforatum*. *Planta Medica*, 58, 291-293.

Makare N, Bodhankar S and Rangari V, 2001. Immunomodulatory activity of alcoholic extract of *Mangifera indica* L. in mice. *Journal of Ethnopharmacology*, 78, 133-137.

Markham PN, Westhaus E, Klyachko K *et al.*, 1999. Multiple novel inhibitors of the NorA multidrug transporter of *Staphylococcus aureus*. *Antimicrobial Agents and Chemotherapy*, 43: 2404-2408.

Marples RR, Richardson JF and De Saxe MJ, 1986. Bacteriological characters of strains of *Staphylococcus aureus* submitted to a reference laboratory related to methicillin resistance. *Journal of Hygiene*, 96, 217-223.

Marty FM, Yeh WW, Wennersten CB *et al.*, 2006. Emergence of a clinical daptomycin-resistant *Staphylococcus aureus* isolate during treatment of methicillin-resistant *Staphylococcus aureus* bacteremia and osteomyelitis. *Journal of Clinical Microbiology*, 44, 595-597.

Medina MA, Martinez-Poveda B, Amores-Sanchez MI *et al.*, 2006. Hyperforin: more than an antidepressant bioactive compound? *Life Science*, 79, 105-111.

Meruelo D, Lavie G and Lavie D, 1988. Therapeutic agents with dramatic antiretroviral activity and little toxicity at effective doses: aromatic polycyclic diones hypericin and pseudohypericin. The Proceedings of the National Academy of Sciences USA, 85, 5230-5234.

Minami H, Takahashi E, Kodama M *et al.*, 1996. Three xanthenes from *Garcinia subelliptica*. Phytochemistry, 41, 629-633.

Miura T, Ichiki H, Hashimoto I *et al.*, 2001. Antidiabetic activity of a xanthone compound, mangiferin. Phytomedicine, 8, 85-87.

Morbidity Mortality Weekly Report, 2002, 51, 902. Vancomycin-resistant: *Staphylococcus aureus* - Pennsylvania.

Morbidity Mortality Weekly Report, 2002a, 565-567. *Staphylococcus aureus* resistant to vancomycin.

Nakamura S, 1997. Mechanisms of quinolone-resistance. Journal of Infection and Chemotherapy, 3, 128-138.

NCCLS – National Committee for Clinical Laboratory Standards, 1997. Methods for dilution antimicrobial susceptibility tests for bacteria that grow aerobically. 3<sup>rd</sup> Edition. Approved Standard. Document M7-A4. Wayne, PA.

Newall CA, Anderson LA and Phillipson JD, 1996. Herbal Medicines. A guide for healthcare professionals. 1<sup>st</sup> Edition. London: Pharmaceutical Press.

Neyfakh AA, Borsch CM and Kaatz GW, 1993. Fluoroquinolone resistance protein NorA of *Staphylococcus aureus* is a multidrug efflux transporter. Antimicrobial Agents and Chemotherapy, 37, 128-129.

Ngugen LHD and Harrison LJ, 1999. Triterpenoid and xanthone constituents of *Cratoxylum cochinchinense*. Phytochemistry, 50, 471-476.

Nielsen H and Arends P, 1979. Xanthone constituents of *Hypericum androsaemum*. *Journal of Natural Products*, 42, 301-304.

O'Grady F, Lambert HP, Finch RG *et al.*, 1997. In: *Antibiotic and Chemotherapy: Anti-infective agents and their use in therapy*. Edinburgh: Churchill Livingstone.

Otsuka M, Sawahata T, Nakai T *et al.*, 1994. Efficacy of combination therapy against MRSA in Ibaraki Prefecture. *Japanese Journal of Antibiotic*, 47, 781-789.

Page MGP, 2006. Anti-MRSA  $\beta$ -lactams in development. *Current Opinion in Pharmacology*, 6, 480-485.

Pao SS, Paulsen IT and Saier MH Jr, 1998. Major facilitator superfamily. *Microbiology and Molecular Biology Review*, 62, 1-34.

Parker WL and Johnson F, 1968. The structure determination of antibiotic compounds from *Hypericum uliginosum*. *Journal of the American Chemical Society*, 90, 4716-4723.

Peeters MJ and Sarria JC, 2005. Clinical characteristics of linezolid-resistant *Staphylococcus aureus* infections. *The American Journal of Medical Sciences*, 330, 102-104.

Peres V and Nagem TJ, 1997. Trioxxygenated naturally occurring xanthenes. *Phytochemistry*, 44, 191-214.

Peres V, Nagem TJ and de Oliveira FF, 2000. Tetraoxxygenated naturally occurring xanthenes. *Phytochemistry*, 55, 683-710.

Physicians' Desk Reference, 2006. Thomson PDR.

Piddock LJV, 1998. Antibacterials - mechanisms of action. *Current Opinion in Microbiology*, 1, 502-508.

Pinto MMM, Sousa ME and Nascimento MSJ, 2005. Xanthone derivatives: new insights in biological activities. *Current Medicinal Chemistry*, 12, 2517-2538.

Ploss O, Petereit F and Nahrstedt A, 2001. Procyanidins from the herb of *Hypericum perforatum*. *Pharmazie*, 56, 509-511.

Rauter AP, Filipe MM, Prata C *et al.*, 2005. A new dihydroxysterol from the marine phytoplankton *Diacronema* sp. *Fitoterapia*, 76, 433-438.

Reacher MH, Shah A, Livermore DM *et al.*, 2000. Bacteraemia and antibiotic resistance of its pathogens reported in England and Wales between 1990 and 1998: trend analysis. *British Medical Journal*, 320, 213-216.

Řezanka T and Sigler K, 2007. Sinaicinone, a complex adamantanyl derivative from *Hypericum sinaicum*. *Phytochemistry*, 68, 1272-1276.

Richardson JF and Reith S, 1993. Characterization of a strain of methicillin-resistant *Staphylococcus aureus* (EMRSA-15) by conventional and molecular methods. *Journal of Hospital Infection*, 25, 45-52.

Robson NKB, 1977. Studies in the genus *Hypericum* L. (Guttiferae). 1. Infrageneric classification. *Bulletin of British Museum Natural History (Botany)*, 5, 291-355.

Robson NKB, 2003. In: *The genus Hypericum. Medicinal and aromatic plants - industrial profiles 30*. Taylor & Francis Inc. New York.

Rocha L, Marston A, Potterat O *et al.*, 1995. Antibacterial phloroglucinols and flavonoids from *Hypericum brasiliense*. *Phytochemistry*, 40, 1447-1452.

Rocha L, Marston A, Potterat O *et al.*, 1996. More phloroglucinols from *Hypericum brasiliense*. *Phytochemistry*, 42, 185-188.

Ross JI, Farrell AM, Eady EA *et al.*, 1989. Characterisation and molecular cloning of the novel macrolide-streptogramin B resistance determinant from *Staphylococcus epidermidis*. *Journal of Antimicrobial Chemotherapy*, 24, 851-862.

Row EC, Brown SA, Stachulski AV *et al.*, 2006. Synthesis of 8-geranyloxypsoralen analogues and their evaluation as inhibitors of CYP3A4. *Bioorganic and Medicinal Chemistry*, 14, 3865-3871.

Russell AD and Chopra I. In: *Understanding Antibacterial Action and Resistance*. 2<sup>nd</sup> Edition, London, Ellis Horwood. 1996.

Sato Y, Suzaki S, Nishikawa T *et al.*, 2000. Phytochemical flavones isolated from *Scutellaria barbata* and antibacterial activity against methicillin-resistant *Staphylococcus aureus*. *Journal of Ethnopharmacology*, 72, 483-488.

Scalbert A, 1991. Antimicrobial properties of tannins. *Phytochemistry*, 30, 3875-3883.

Schempp CM, Pelz K, Wittmer A *et al.*, 1999. Antibacterial activity of hyperforin from St John's wort against multiresistant *Staphylococcus aureus* and Gram-positive bacteria. *The Lancet*, 353, 2129.

Seo EK, Huang L, Wall ME *et al.*, 1999. New biphenyl compounds with DNA strand-scission activity from *Clusia paralicola*. *Journal of Natural Products*, 62, 1484-1487.

Shinabarger DL, Marotti KR, Murray RW *et al.*, 1997. Mechanism of action of oxazolidinones: effects of linezolid and eperzolid on translation reactions. *Antimicrobial Agents and Chemotherapy*, 41, 2132-2136.

Shiu WKP and Gibbons S, 2006. Anti-staphylococcal acylphloroglucinols from *Hypericum beanii*. *Phytochemistry*, 67, 2568-2572.

Škerget M, Kotnik P, Hadolin M *et al.*, 2005. Phenols, proanthocyanidins, flavones and flavonols in some plant materials and their antioxidant activities. *Food Chemistry*, 89, 191-198.

Skiest DJ, 2006. Treatment failure resulting from resistance of *Staphylococcus aureus* to daptomycin. *Journal of Clinical Microbiology*, 44, 655-656.

Sultanbawa MUS, 1980. Xanthonoids of tropical plants. *Tetrahedron*, 36, 1465-1506.

Trifunovic S, Vajs V, Macura S *et al.*, 1998. Oxidation products of hyperforin from *Hypericum perforatum*. *Phytochemistry*, 49, 1305-1310.

Trovato A, Raneri E, Kouladis M *et al.*, 2001. Anti-inflammatory and analgesic activity of *Hypericum empetrifolium* (Guttiferae). *Farmaco*, 56, 455-457.

Ubukata K, Yamashita N, Gotoh A *et al.*, 1984. Purification and characterization of aminoglycoside-modifying enzymes from *Staphylococcus aureus* and *Staphylococcus epidermidis*. *Antimicrobial Agents and Chemotherapy*, 25, 754-759.

UK National Statistics, 2005. <http://www.statistics.gov.uk/>

Vajs V, Vugdelija S, Trifunovic S *et al.*, 2003. Further degradation product of hyperforin from *Hypericum perforatum* (St John's wort). *Fitoterapia*, 74, 439-444.

Van Bambeke F, 2004. Glycopeptides in clinical development: pharmacological profile and clinical perspectives. *Current Opinion in Pharmacology*, 4, 471-478.

Van Klink JW, Brophy JJ, Perry NB *et al.*, 1999.  $\beta$ -Triketones from *Myrtaceae*: isoleptospermone from *Leptospermum scoparium* and papuanone from *Corymbia dallachiana*. *Journal of Natural Products*, 62, 487-489.

Vanhaelen M and Vanhaelen-Fastre R, 1983. Quantitative determination of biologically active constituents in medicinal plant crude extracts by thin-layer chromatography. *Journal of Chromatography A*, 281, 263-271.

Verotta L, Appendino G, Belloro E *et al.*, 1999. Furohyperforin, a prenylated phloroglucinol from St. John's wort (*Hypericum perforatum*). *Journal of Natural Products*, 62, 770-772.

Verotta L, Appendino G, Jakupovic J *et al.*, 2000. Hyperforin analogues from St. John's wort (*Hypericum perforatum*). *Journal of Natural Products*, 63, 412-415.

Want HK, Xia Y, Yang ZY *et al.*, 1998. Recent advances in the discovery and development of flavonoids and their analogues as antitumour and anti-HIV agents. *Advances in Experimental Medicine and Biology*, 439, 191-225.

Weber ND, Murray BK, North JA *et al.*, 1994. The antiviral agent hypericin has in vitro activity against HSV-1 through non-specific association with viral and cellular membranes. *Antiviral Chemistry and Chemotherapy*, 5, 83-90.

Weng JR, Tsao LT, Wang JP *et al.*, 2004. Anti-inflammatory phloroglucinols and terpenoids from *Garcinia subelliptica*. *Journal of Natural Products*, 67, 1796-1799.

Williams D and Fleming I, 1995. *Spectroscopic methods in organic chemistry*, 5<sup>th</sup> Edition. McGraw-Hill Higher Companies.

Winkelmann K, Zerbe HJ, Rali O *et al.*, 2000. New phloroglucinol derivatives from *Hypericum papuanum*. *Journal of Natural Products*, 63, 104-108.

Wondrack L and Sutcliffe J, 1996. A clinical strain of *Staphylococcus aureus* inactivates and effluxes macrolides. *Antimicrobial Agents and Chemotherapy*, 40, 992-998.

Wright GD, 1999. Aminoglycoside-modifying enzymes. *Current Opinion in Microbiology*, 2, 499-503.

Wu QL, Wang SP, Du LJ *et al.*, 1998. Xanthenes from *Hypericum japonicum* and *Hypericum henryi*. *Phytochemistry*, 49, 1395-1402.

Xiao ZY, Mu Q, Shiu WK *et al.*, 2007. Polyisoprenylated benzoylphloroglucinol derivatives from *Hypericum sampsonii*. *Journal of Natural Products*, 70, 1779-1782.

Yamaki M, Miwa M, Ishiguro K *et al.*, 1994. Antimicrobial activity of naturally occurring and synthetic phloroglucinols against *Staphylococcus aureus*. *Phytotherapy research*, 8, 112-114.

Yoshida H, Nakamura M, Bogaki M *et al.*, 1993. Mechanism of action of quinolones against *Escherichia coli* DNA gyrase. *Antimicrobial Agents and Chemotherapy*, 37, 839-845.

Zimhony O, Vilcheze C and Jacobs WR, 2004. Characterization of *Mycobacterium smegmatis* expressing the *Mycobacterium tuberculosis* fatty acid synthase I (fasI) gene. *Journal of Bacteriology*, 186, 4051-4055.

## 6 LIST OF PUBLICATIONS

Shiu WKP and Gibbons S, 2006. Anti-staphylococcal acylphloroglucinols from *Hypericum beanii*. *Phytochemistry*, 67, 2568-2572.

Sharma R, Negi DS, Shiu WKP and Gibbons S, 2006. Characterization of an insecticidal coumarin from *Boenninghausenia albiflora*. *Phytotherapy Research*, 20, 607-609.

Kokubun T, Shiu WKP and Gibbons S, 2007. Inhibitory activities of lichen-derived compounds against methicillin and multidrug-resistant *Staphylococcus aureus*. *Planta Medica*, 73, 176-179.

Xiao ZY, Mu Q, Shiu WKP, Zeng YH and Gibbons S, 2007. Polyisoprenylated benzoyl-phloroglucinol derivatives from *Hypericum sampsonii*. *Journal of Natural Products*, 70, 1779-1782.

### **Publications in preparation**

Shiu WKP and Gibbons S. Phytochemistry of *Hypericum* species. *Phytochemistry*.

**Poster presentations**

Best poster presentation award: Shiu WKP and Gibbons S. Anti-staphylococcal activity of *Hypericum beanii*. ULSOP Research Day, April 2006.

Shiu WKP and Gibbons S. The anti-staphylococcal activity of *Hypericum* species. 55<sup>th</sup> International Congress and Annual Meeting of the Society for Medicinal Plant Research (GA), 2-6 September 2007. Graz, Austria.

Shiu WKP and Gibbons S. Isolation and characterization of a new dibenzofuran from *Hypericum revolutum* ssp. *revolutum* Vahl. 55<sup>th</sup> International Congress and Annual Meeting of the Society for Medicinal Plant Research (GA), 2-6 September 2007. Graz, Austria.

**Oral presentation**

Shiu WKP and Gibbons S. Anti-staphylococcal activity of *Hypericum beanii*. ULSOP Research Day, April 2007.